



JAGIELLONIAN UNIVERSITY
IN KRAKÓW

Faculty of Physics, Astronomy and Applied Computer Science

**Study of the emission of organic material
from a free-standing graphene substrate
by keV cluster bombardment**

Doctoral dissertation by

Mikołaj Gołuński

Under the supervision of

Prof. dr hab. Zbigniew Postawa

Kraków, May 2021

Wydział Fizyki, Astronomii i Informatyki Stosowanej
Uniwersytet Jagielloński

Oświadczenie

Ja niżej podpisany *Mikołaj Gołuński* (nr indeksu: 1039635) doktorant Wydziału Fizyki, Astronomii i Informatyki Stosowanej Uniwersytetu Jagiellońskiego oświadczam, że przedłożona przeze mnie rozprawa doktorska pt. „*Study of the emission of organic material from a free-standing graphene substrate by keV cluster bombardment*” jest oryginalna i przedstawia wyniki badań wykonanych przeze mnie osobiście, pod kierunkiem *prof. dr hab. Zbigniewa Postawy*. Pracę napisałem samodzielnie.

Oświadczam, że moja rozprawa doktorska została opracowana zgodnie z Ustawą o prawie autorskim i prawach pokrewnych z dnia 4 lutego 1994 r. (Dziennik Ustaw 1994 nr 24 poz. 83 wraz z późniejszymi zmianami).

Jestem świadomy, że niezgodność niniejszego oświadczenia z prawdą ujawniona w dowolnym czasie, niezależnie od skutków prawnych wynikających z ww. ustawy, może spowodować unieważnienie stopnia nabytego na podstawie tej rozprawy.

Kraków, dnia 12.05.2021 r.

.....

podpis doktoranta

ABSTRACT

In this dissertation, I investigate processes of emission from free-standing graphene and look at their differences to the emission from bulk materials. Furthermore, I postulate that graphene can be used as an innovative substrate in an investigation of materials via Secondary Ion Mass Spectrometry (SIMS) and Secondary Neutral Mass Spectrometry (SNMS). To achieve a thorough understanding of the topic, I describe the emission of molecules from free-standing graphene irradiated by keV energy cluster projectiles. My research leads through investigation of emission from sole graphene substrates using fullerene and argon-cluster projectiles, processes leading to uplifting of individual phenylalanine molecules, and thorough description of sputtering from the thin layer of organic molecules deposited on free-standing graphene both in a regular SIMS setup as well as the “transmission direction”. All results provide evidence on processes of emission that are unique to the graphene substrate. Knowledge gathered in this dissertation – starting from graphene having not enough atoms for the traditional models to be employed, through unusually high rates of deformation and energy absorption, and ending up with the separation of organic layer from graphene membrane and occurrence of trampolining action – gives a clear notion of new and exciting phenomena present in this field.

STRESZCZENIE

W poniższej rozprawie doktorskiej zajmuję się badaniem procesów emisji z zawieszzonego grafenu przy użyciu pocisków klastrowych o energii rzędu keV oraz różnicami tego układu w stosunku do emisji z grubego podłoża. Dodatkowo stawiam tezę, że grafen może zostać użyty jako innowacyjne podłoże do badania materiałów z użyciem spektrometrii mas jonów wtórnych SIMS oraz spektrometrii mas wtórnych cząstek neutralnych SNMS. W rozprawie opisuję szereg badań: od emisji z samego podłoża grafenowego z użyciem pocisków fulerenowych oraz klastrów argonowych, poprzez zjawisko unoszenia pojedynczych molekuł fenyloalaniny z powierzchni grafenu, aż do szczegółowego opisu rozpylania z cienkiej warstwy molekuł organicznych osadzonych na grafenie w ujęciu tradycyjnej geometrii SIMS a także geometrii „transmisyjnej”. Wszystkie wyniki wskazują na występowanie w badanych układach nietypowych procesów emisji mających miejsce jedynie dla podłoży grafenowych. Przedstawione w rozprawie informacje jasno wskazują na nowe, ekscytujące zjawiska: od stwierdzenia, że w grafenie jest niewystarczająca liczba atomów, żeby tradycyjne modele rozpylania miały dla niego zastosowanie, przez nadzwyczaj duże odkształcenia i absorpcję energii przez grafen, po zjawisko oddzielania się warstwy organicznej od grafenowej membrany i występowanie „efektu trampoliny”.

ACKNOWLEDGEMENTS

First and foremost, I would like to thank my supervisor, prof. dr hab. Zbigniew Postawa for all knowledge he passed to me and all opportunities he gave to me. I would also like to thank Professor Schweikert's group from Texas A&M University, especially Dr Stanislav V. Verkhoturov, for the inspiring collaboration that led to the creation of this dissertation.

Big thanks are due to my colleagues: Michał Kański and Dawid Maciążek. Without insightful discussions during work-time, lunch-time, and free-time, I would struggle much more and achieve much less. During my years at the Physics Department, I met too many people that shaped me in one way or the other to list them all. Nevertheless, I need to mention at least two of them. My great friend that pushes me in often strange directions that still mostly lead to unexpectedly positive results, Piotr Ciochoń, and my old friend that for many years made the perils of studying physics much more enjoyable, Dariusz Kotas.

Life is not only about the Department, and I am lucky to have many friends outside of “the world of physics”. Let me mention just two memorable groups that always helped me regain my sanity. My superb friends from Czupakabra provide a sense of long-lasting friendship and deep understanding possible to achieve only after uncountable hours spent together. Also, a much newer group but already having humongous impact on my life – Dinozaury – a bit crazy bunch that keeps good company in all terrain, urban and wilderness.

Last but not least, I want to thank my family for their never-ending support and love. Ania for walking through our lives together at a surprisingly harmonious pace, my Mom for keeping with my temper and always giving me all the best she has, my Dad for on-point advice and discussions bursting in knowledge, Ija for unconditional love and always making my ego rise through the roof, Pikuś for being so positive and loving, supporting me in all of my endeavours, and sharing his deep knowledge and fascinations with fields I sometimes know something and sometimes I know nothing about, and Tytus who is showing me that you can do anything and become anyone if you work hard and be brave enough. Finally, I wanted to appreciate my beloved cats, Iskierka and Filuś, as well as Milka, who is watching us from the skies above. They are my sunshine, constantly purring and meowing calmly and providing a tiny bit of insight into the actual necessities of life.

TABLE OF CONTENTS

Structure of the dissertation	ix
1 Introduction	1
1.1 Cluster bombardment.....	1
1.2 Molecular dynamics simulations	4
2 Bombardment of free-standing graphene	9
2.1 Fullerene projectile	9
2.2 Argon cluster projectile	14
3 Uplifting individual organic molecules	17
4 Sputtering from an organic monolayer.....	21
4.1 Collaboration with Professor Schweikert's team	21
4.2 Further investigation.....	24
5 Summary	29
Bibliography	31
Appendices	35
Reprints of publications	37
Acta Physica Polonica A 132, 222-224 (2017).....	39
Nuclear Instruments and Methods B 393, 13-16 (2017).....	45
Journal of Vacuum Science & Technology B 36, 03F112 (2018)	51
Journal of Chemical Physics 148, 144309 (2018).....	61
Journal of Chemical Physics 150, 160901 (2019).....	75
Surface and Coatings Technology 391, 125683 (2020)	93
Applied Surface Science 539, 148259 (2021).....	103
Additional achievements	117
Licenses and permissions	119

STRUCTURE OF THE DISSERTATION

This doctoral dissertation focuses on a thesis that the process of emission from graphene differs from the mechanism of emission described for bulk materials. Furthermore, I postulate that graphene can be used as an innovative substrate in an investigation of materials via Secondary Ion Mass Spectrometry and Secondary Neutral Mass Spectrometry. To achieve a thorough understanding of the topic, I describe the emission of molecules from free-standing graphene irradiated by keV energy cluster projectiles. The dissertation is based on the following seven scientific publications published in international journals and listed in the bibliography of the dissertation in the first seven positions [1-7]:

1. Goluński M. & Postawa Z. *Effect of Sample Thickness on Carbon Ejection from Ultrathin Graphite Bombarded by keV C₆₀*. Acta Physica Polonica A 132, 222-224 (2017), doi:[10.12693/APhysPolA.132.222](https://doi.org/10.12693/APhysPolA.132.222),
2. Goluński M., Verkhoturov S. V., Verkhoturov D. S., Schweikert E. A. & Postawa Z. *Effect of substrate thickness on ejection of phenylalanine molecules adsorbed on free-standing graphene bombarded by 10 keV C₆₀*. Nuclear Instruments and Methods in Physics Research Section B: Beam Interactions with Materials and Atoms 393, 13-16 (2017), doi:[10.1016/j.nimb.2016.09.006](https://doi.org/10.1016/j.nimb.2016.09.006),
3. Goluński M. & Postawa Z. *Effect of kinetic energy and impact angle on carbon ejection from a free-standing graphene bombarded by kilo-electron-volt C₆₀*. Journal of Vacuum Science & Technology B, Nanotechnology and Microelectronics: Materials, Processing, Measurement, and Phenomena 36, 03F112 (2018), doi:[10.1116/1.5019732](https://doi.org/10.1116/1.5019732),
4. Verkhoturov S. V., Goluński M., Verkhoturov D. S., Geng S., Postawa Z. & Schweikert E. A. *“Trampoline” ejection of organic molecules from graphene and graphite via keV cluster ions impacts*. Journal of Chemical Physics 148, 144309 (2018), doi:[10.1063/1.5021352](https://doi.org/10.1063/1.5021352),
5. Verkhoturov S. V., Goluński M., Verkhoturov D. S., Czerwinski B., Eller M. J., Geng S., Postawa Z. & Schweikert E. A. *Hypervelocity cluster ion impacts on free standing graphene: Experiment, theory, and applications*. Journal of Chemical Physics 150, 160901 (2019), doi:[10.1063/1.5080606](https://doi.org/10.1063/1.5080606),

6. Goluński M., Hrabar S. & Postawa Z. *Mechanisms of particle ejection from free-standing two-layered graphene stimulated by keV argon gas cluster projectile bombardment – Molecular dynamics study*. Surface and Coatings Technology 391, 125683 (2020), doi:[10.1016/j.surfcoat.2020.125683](https://doi.org/10.1016/j.surfcoat.2020.125683),
7. Goluński M., Hrabar S. & Postawa Z. *Mechanisms of Molecular Emission from Phenylalanine Monolayer Deposited on Free-standing Graphene Bombarded by C₆₀ Projectiles*. Applied Surface Science 539, 148259 (2021), doi:[10.1016/j.apsusc.2020.148259](https://doi.org/10.1016/j.apsusc.2020.148259).

The dissertation consists of three parts, the introduction, the description of my work, divided into five chapters, and appendices. In the first chapter I describe the importance of this work and the methods I use. Three following chapters are devoted to my research. In each of them, I shortly describe the most important aspects of the topics of the chapters. Articles the chapters are based on provide an in-depth report on the matters. The fifth chapter presents the conclusions of the dissertation, followed by a bibliography. The last part of the dissertation is a set of appendices in which I present reprints of articles this dissertation is based on, a list of my additional achievements, and a section on copyrights permissions.

I chose not to present my research chronologically but rather to cluster it into separate topics. In my opinion, such an approach provides a clearer view of my train of thought. Additionally, publishing schedules sometimes result in publications getting mixed up from a chronological point of view; hence sorting them by topics rather than the time of publication prevents an inevitable confusion.

1 INTRODUCTION

1.1 CLUSTER BOMBARDMENT

This dissertation focuses on the bombardment of material with cluster projectiles. Bombardment refers to the process of hitting a sample with a stream of energetic ions. Those ions, hitting the surface of a material, induce a number of effects, including but not limited to, implantation, material mixing, and emission of radiation and various types of particles. [8] These processes are widely used, e.g., in doping of semiconductors in electronics (implantation), or chemical analysis of materials (emission). The chemical analysis is the central area of Secondary Ion Mass Spectrometry (SIMS) and Secondary Neutral Mass Spectrometry (SNMS) techniques. [9] The dissertation provides information that could be used particularly in the advancement of these analysis methods.

Both SIMS and SNMS work similarly. A sample is irradiated with a stream of ions, leading to the emission of material from it. Ejected atoms, fragments, molecules, and clusters are detected in a mass spectrometer. The difference between those methods is that in SIMS we are detecting only material that got ionised during irradiation, while SNMS is sensitive to neutral particles. Detection in both cases is carried out using mass spectrometry but in SNMS neutral elements go through a process of post-ionisation, meaning artificial ionisation of material that has been already emitted from the sample. [9] SIMS method is less complicated but is limited by ionisation processes leading to ionisation of only a tiny fraction of the ejected material. [9] SNMS allows for the acquisition of a much higher signal but requires a complicated post-ionisation setup, making it much less accessible. Nevertheless, geometrically both methods are similar. Usually, the detector is placed on the same side of the target as the ion gun, and the sample consists of a metal or semiconductor support with a relatively thick layer of investigated material deposited on it.

The team of Professor Emile A. Schweikert from A&M Texas University has recently proposed a novel transmission configuration. [10,11] The analysed material is placed on one side of an ultrathin substrate (few-layered free-standing graphene is an ideal substrate of that kind), while the other side is bombarded with an ion beam. The detector is on the other side of the sample than the ion gun, as shown in Fig. 1. I collaborated with Prof. Schweikert's team

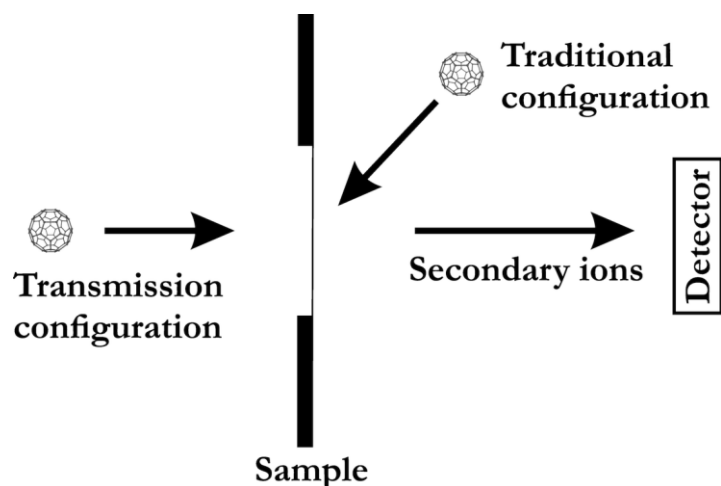


Fig. 1: Regular and transmission SIMS setups.

to investigate the possibilities of using a unique transmission geometry in SIMS. This dissertation provides information on the usefulness of this new approach and physicochemical processes leading to particle emission in this system.

There are four main types of projectile ions used in the ion bombardment: individual atoms, small clusters consisting of a few atoms, medium-sized clusters such as C₆₀, and large clusters having many hundreds or thousands of atoms or molecules. [8,9,12] Cluster projectiles are of high interest as they proved to enhance the ejection of large intact organic molecules and reduce ion-induced damage building up in the analysed organic material. [13,14] As the emission of organic material is a substantial part of this dissertation, cluster projectiles were a natural choice.

Processes leading to the emission of material from the bulk surface bombarded with ions are well-described. In short, there are two main paths of emission. [12] The first one is a linear collision cascade, depicted in Fig. 2a. [8,9,12] An atomic projectile collides with one of the sample atoms, which gets knocked out of its position. This atom collides with a subsequent atom which collides with yet another atom, forming a cascade of collisions. The cascade may ultimately result in a collision with an atom on the surface, leading to its ejection. However, cluster projectile's impact leads to another process of emission. [9,12] In this process, it is not possible to discern individual collision cascades, but rather the material is relocated in a concerted, mesoscopic fashion. Additionally, the energetic pressure pulses develop and propagate into the sample after impact, which is not present during the atomic projectile impact. The impact of cluster projectile deposits energy in a volume much bigger but closer to the

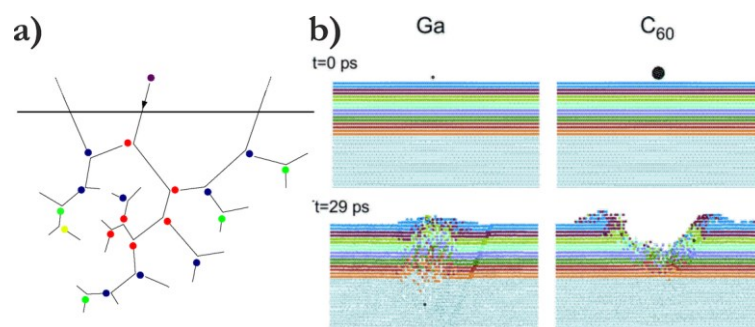


Fig. 2: a) Schematics of collision cascade process. Coloured dots represent colliding atoms. The incoming atom is purple, primary recoil atoms are red, secondary recoils are blue, and tertiary recoils are green. b) Simulations showing difference between single-atom impact (to the left) and cluster impact (to the right) on the silver sample. Colours denote atoms from different initial depths of the sample.

Images copyright: a) Wikimedia commons public domain, b) Reprinted with permission from J. Phys. Chem. B 2004, 108, 23, 7831-7838. Copyright 2004 American Chemical Society.

surface, creating a shallower disturbance in the sample and providing more opportunities for the gentle uplifting of molecules. [12] Fig. 2b presents differences in craters and mixing of sample layers after both types of impact. Nevertheless, neither of these descriptions can be used in ultrathin systems. There is simply not enough material and volume present for collision cascade or pressure pulses to develop. The following research focuses on finding the processes leading to particle emission from samples a few nanometres thick.

As mentioned earlier, only ionised species can be detected in SIMS. In fact, only a small fraction of sputtered material leaves a sample in an ionised state. [9] Raising the ionisation rate could be one of the more potent ways of getting higher sputtering signal. Unfortunately, ionisation processes during bombardment are still not well-known, especially when dealing with organic materials. Several models of ionisation exist, but none of them describes this process thoroughly. They all have one characteristic in common, though – the requirement of the to-be-ionised particle to be in an energetically excited state. [9] This means that without delivering significant energy to the system, there will be probably little to no ionisation of ejecta. This is especially important when regarding slow projectiles as they provide lower amount of energy and may not be suitable for SIMS experiments, even if processes leading to the ejection are scientifically interesting.

At the beginning of my work, and at the time I was conducting my research, there were very few theoretical publications available describing the cluster ion

bombardment on graphene. Several simulations have been performed on the C_{60} bombardment of graphene in the context of defect creation and evolution [15-20]. Additionally, some works showed that ion impact could cause vibrations of a graphite's membrane-like structure that could also be present in graphene. It was suggested that the interaction of these waves with molecules adsorbed on graphene could stimulate the ejection of small, weakly bound molecules. [11,21-24] A few experimental papers were published as well. Eller et al. showed an emission of carbon from graphene in transmission direction using gold nanoparticles as projectiles [10] while Verkhoturov et al. looked into emission of carbon in transmission direction from graphene bombarded with fullerenes [11]. They both stressed a high probability of carbon ionisation when using their unusual experimental setup. Up to this day, several new articles regarding simulations of ion irradiation of graphene were published [25-31], but this topic is still highly underrepresented.

1.2 MOLECULAR DYNAMICS SIMULATIONS

Molecular dynamics (MD) is one of many techniques used to simulate the movement and interactions of atoms. It can describe systems of sizes up to a few million atoms. We can think of MD as a method in middle grounds between ab initio methods such as DFT, which is much more accurate but can only deal with small systems, and statistical methods such as Monte Carlo simulations, that can work with much larger systems but represent reality with lower precision. [32,33]

Atoms in the MD technique are defined as point particles, each having three main properties: position, velocity and mass. Their movement is described by classical Newtonian dynamics. [12,13,32] It means that to find the movement of atoms, the solving of the following system of equations of motion is required:

$$m_i \frac{d^2 \vec{r}_i}{dt^2} = \sum_{i < j} \vec{F}_{ij}, \text{ for } i, j = 1, \dots, N \quad (1)$$

where N is a number of modelled atoms, m_i is a mass of atom i , \vec{r}_i is a vector describing the position of atom i , t is time, and \vec{F}_{ij} is a force vector between atoms i and j . The sum presented in the equation above can be understood simply as a net force acting on an atom i .

The main challenge is finding forces that act between atoms. In MD we do this using so-called potentials. There are many potentials developed in the field of computer simulations, each of them taking a slightly different approach, making it useful in different situations. Additionally, potentials are constructed in such way that they can be used with different parametrisations making it possible to perform simulations of various groups of atoms in various conditions. As molecular dynamics is a mature scientific method, there is a considerable number of parametrisations for many different potentials already developed that can be reliably used. The most notable potentials I used during my research are as follows:

- Ziegler-Biersack-Littmark (ZBL) [34] – purely repulsive pair-wise potential used in the description of short-distance interactions present during keV bombardment,
- Lennard-Jones (LJ) [35] – classical 6-12 potential useful for simulations involving noble gasses,
- ReaxFF [36,37] – advanced many-body reactive potential allowing formation and breaking of covalent bonds between atoms, used mainly in simulations of organic molecules and graphene.

I should also mention another noteworthy many-body reactive potential – AIREBO. [38] It is on par with ReaxFF when regarding hydrocarbon systems, including graphene, while providing better performance. [39] Unfortunately, AIREBO cannot be used with atoms other than carbon and hydrogen. As my goal was to observe the behaviour of biologically relevant organic molecules composed of carbon, hydrogen, oxygen, and nitrogen atoms, I chose to use ReaxFF in all my simulations. Because it is one of the more advanced potentials, it has the significant drawback of being very taxing on computer processors. Its computational complexity is several times higher than for most of the other many-body potentials. [32,33] Nevertheless, the possibility of a direct description of molecules' and clusters' fragmentation and formation during bombardment as well as the availability of a wide range of elements, such as hydrogen, carbon, nitrogen, and oxygen, is of much higher importance. Therefore, it could be said that I sacrificed speed in favour of versatility and accuracy.

As the molecular dynamics method treats atoms as the basic particles, it does not describe any electronic phenomena natively. It is essential to remember this drawback when describing effects seen during SIMS experiments as MD cannot simulate ionisation processes. All particles in the MD simulations are neutrals, and we cannot distinguish between real neutrals and particles that would get ionised. Some methods try to combine molecular dynamics with electron calculations, for example, Ab Initio Molecular Dynamics [40], but their computational cost is much higher. Even with the said flaw, classical molecular dynamics can still provide much insight into processes happening during a surface bombardment.

MD simulation itself consists of three main steps [12,32]:

1. The initialisation of a system by setting positions, masses, and initial velocities of atoms.
2. Calculation of forces acting on atoms based on their positions and potentials used.
3. Calculation of atoms' movement by a numerical solution of Newton's equations (1) during a set timestep followed by updating their positions and velocities.

Steps 2 and 3 are repeated until the stopping condition is met. The value of a timestep used in step 3 has a significant impact on simulation precision and the amount of time needed to finish it. The smaller the timestep, the more precise the simulation is, but it also takes longer. The stopping condition most often is chosen to be the specific simulation time (counted as from the point of view of simulated atoms).

Even though the MD algorithm is straightforward, its technical implementation can be challenging. Creating proper software could be especially tricky when one takes into account all needs related to the speed, efficiency, and parallelisation of computation. I decided to use a freely available specialistic programme called Large-scale Atomic/Molecular Massively Parallel Simulator (LAMMPS). [41,42] It is an open-source MD software that has been actively developed for more than 25 years, implements a multitude of potentials, and has excellent multi-processor computations possibilities making it highly viable in a super-computer environment. Our group has modified this program to describe a sputtering process better.

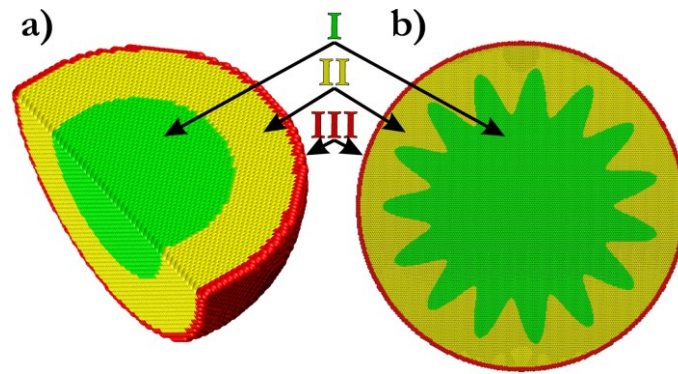


Fig. 3: a) A cross-section through a hemispherical sample with typical rigid-stochastic encapsulation. b) Breakwater-like design of a stochastic region used in simulations of ultrathin graphene samples. In both pictures regions of a sample are marked as following: I free-moving atoms, II stochastic region, III rigid region. Slight changes in colours are artefacts from the rendering software.

Before starting an MD simulation, one has to create a sample that will represent the real world. MD capabilities are limited to a few million atoms which allow the creation of nanometre-sized samples. There are many possible ways of defining the boundaries of the simulated sample. [12,43] The approach proven to be well suited for bombardment with cluster projectiles, called rigid-stochastic encapsulation, incorporates a division of a sample into three main regions. [12,43] The central region consists of moving atoms that accurately describe the evolution of a system. Around the centre there is a stochastic layer that absorbs energy transferred to the sides of the sample, acting as an energy sink and therefore allowing to mimic a real-scale system where this energy would dissipate further along the material. On the outside of the sample, there is a thin skin-like layer of rigid atoms that holds all atoms together in a specified shape. When investigating cluster bombardment processes, the usual way is to create a hemispherical sample with simple rigid-stochastic encapsulation type boundaries (Fig. 3a). [12] However, ultrathin systems behave differently from bulk ones, hence there is a need for alteration of a standard setup. I have chosen a cylindrical sample with a very distinct design of the stochastic region. As energy can be transferred very efficiently in the plane of graphene's surface [44,45], this leads to problems with creating an absorption layer that would dampen this energy without raising reflections and therefore changing the results of the simulation. I found out that using a breakwater-like design of the stochastic region (as shown in Fig. 3b) eliminates the probability of the occurrence of constructive interference from backscattered energy waves.

2 BOMBARDMENT OF FREE-STANDING GRAPHENE

The first step in the evaluation of a system consisting of a substrate and organic layer is to look at the substrate alone. Without knowing how the substrate behaves, it is difficult to say anything about the complex sample. Therefore I devoted three articles to studies of the bombardment of free-standing graphene alone.

2.1 FULLERENE PROJECTILE

Section based on *Act. Phys. Pol. A* (2017) [1] and *J. Vac. Sc. & Tech. B* (2018) [3]

To fully describe the interactions between graphene and fullerene projectile, I performed a number of simulations on systems with varying graphene thickness (number of graphene layers), the projectile's kinetic energy, and its impact angle (measured as an angle between normal to the surface and a direction of impact). As the graphene under consideration is free-standing, there might be an ejection from both of its sides (contrary to the bulk sample where atoms pushed into the sample would be buried inside it and stopped there with no chance of ejection from the other side). Hence, I monitored ejection in both transmission and sputtering direction, as depicted in Fig. 4.

C_{60} projectile's atoms lose integrity very fast after initial impact with graphene. Even during the bombardment of merely one graphene layer, the fullerene shatters into individual atoms just after passing through the sample¹. Still though, the projectile's atoms interact collectively with the sample during the impact.

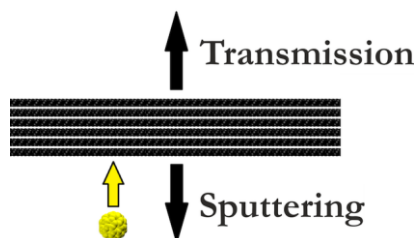


Fig. 4: Transmission and sputtering directions during bombardment of free-standing graphene.

Image copyright: As stated in the permission granted for reuse of the article [3].

¹ See [1] Fig. 1 and [3] Fig. 4

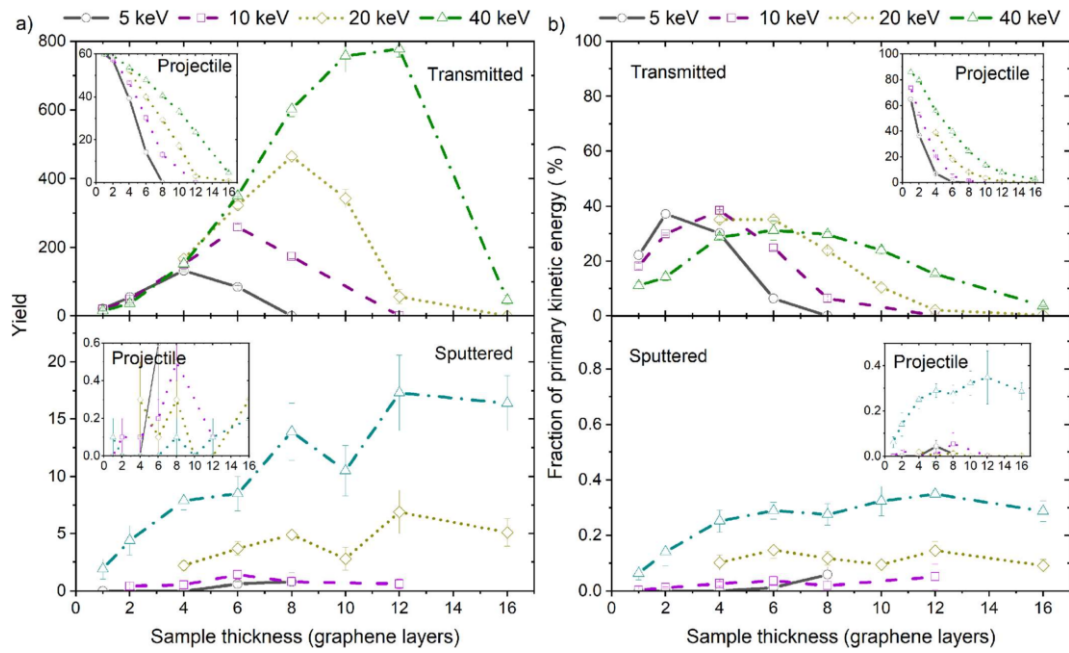


Fig. 5: Dependence of (a) the ejection yield and (b) the fraction of primary kinetic energy carried away by particles emitted in the transmission (top) and sputtering (bottom) directions on the thickness of the sample bombarded by 5, 10, 20, and 40 keV C_{60} projectiles at normal incidence. Main graphs represent the atoms ejected from the sample, while the insets depict projectile atoms. Fig. 2 in [3] and its discussion provides more details.

Image copyright: As stated in the permission granted for reuse of the article [3].

Surprisingly, graphene absorbs a high amount of projectile's kinetic energy. Part of this energy is taken away by atoms emitted from the graphene, and a fraction is absorbed by the graphene sheet and conveyed out of the impact point through graphene acoustic oscillations. Just one layer of graphene can absorb even 35% of the impact energy (for 5 keV 0-degree impact angle), out of which around 20% is reemitted with substrate atoms, and 15% is accumulated in the graphene sheet, as shown in Fig. 5^{II}. The amount of energy absorbed by graphene changes with the primary kinetic energy of the projectile. As the fullerene energy increases, the absolute amount of energy absorbed rises as well, but the absorption percentage lowers. Compared to the previous example, one layer of graphene, when bombarded with 40 keV projectile, absorbs around 15% (6 keV) of its energy compared to 35% (1.75 keV) for 5 keV impact. What is also worthy of note, the amount of energy absorbed by the sample rises rapidly with the number of graphene sheets. 8 layers of graphene absorb around

^{II} See [3] Fig. 2b

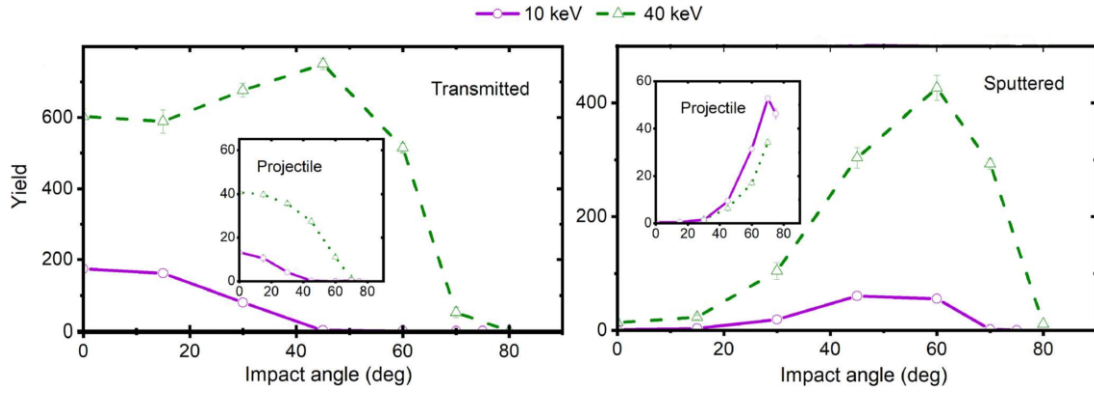


Fig. 6: Example of dependence of the yields of carbon atoms ejected in the transmission (left) and sputtering (right) directions from the 8-layers system bombarded by 10 keV (solid line) and 40 keV (dashed line) C_{60} projectiles on the projectile impact angle. Main graphs represent the atoms originating from the sample, while the insets depict projectile's atoms. Fig. 3 in [3] provides more details.

Image copyright: As stated in the permission granted for reuse of the article [3].

90% (18 keV) of 20 keV of projectile's energy, out of which 13 keV stays within the sample (is not emitted with ejected sample atoms). In the case of 40 keV impact, around 75% of its energy (30 keV) is absorbed by graphene, out of which 18 keV dissipates in the graphene. These are remarkably vast amounts of absorbed energy for such thin material.

If the projectile has enough energy to pierce the set number of graphene layers, the system presents a substantial emission of the sample's atoms in the transmission direction. Its exact value depends on the impact conditions but always displays a peak during a specific set of conditions. On the other hand, the emission in the sputtering direction is minuscule, often more than an order of magnitude lower than in transmission direction^{III}. The sputtering emission rises with raising the impact angle (Fig. 6), reaching its peak at high impact angles and plummeting afterward. When near its peak value, the sputtering direction emission can be comparable to the transmission direction emission detected in the same conditions. Nevertheless, even in conditions highly favourable for the sputtering, it still emits less material than is emitted in the transmission direction^{IV}.

All observations lead to the conclusion that the substrate atoms' yield is determined by two factors: the amount of material available for ejection and the

^{III} See [1] inset to Fig. 2a

^{IV} See [3] Fig. 3

amount of the energy stored near the surface from which the ejection occurs. The first factor increases with the thickness of the sample and with the impact angle as projectile can travel through a larger volume of graphene. The second factor behaves differently for each surface. For emission in transmission direction, one should look at the energy stored near the “top” of the sample. This energy rises with the projectile’s primary kinetic energy but diminishes with the increase of the thickness of the sample and with the impact angle, as the projectile loses more energy to travel through the sample to its “top” surface. For emission in a sputtering direction, the “bottom” surface is essential. The energy stored near this surface will rise with the sample’s thickness until we reach the thickness equal to the depth of a volume from which atoms are ejected. With further thickening of the sample, some of the energy is stored in deeper layers, not contributing to an ejection in a sputtering direction, and the yield saturates. Increasing the impact angle leads to a downwards shift of the energy deposition profile providing more energy near the “bottom” surface but, simultaneously, gives more opportunities for the back-reflection of the projectile’s atoms. The latter process leads to the lowering of the energy transfer into the sample as more energy is carried away by backreflected atoms leading ultimately to a signal decrease.

Furthermore, the dynamics of the impact display interesting properties. During the bombardment, graphene shows a great deal of vertical movement. Layers in multi-layered graphene move in respect to each other getting closer and further away from each other, allowing parts of the layers to bend. “Top” surface bulges before breaking and further orchestrates the creation of surface waves propagating outside from the point of impact. Top layers move in a catapult-like fashion during the creation of the rim near the point of rupture, as shown in Fig. 7. The exact evolution of graphene’s topography depends on the impact conditions^v. Nevertheless, all kinds of movements are especially interesting in the context of the potential emission of molecules deposited on the graphene surface.

Last but not least, I should briefly discuss the energetics of the emission. As I described earlier, graphene absorbs vast amounts of energy from the projectile. However, for thin systems, carbon atoms coming from fullerene that

^v The in-depth description is provided in discussion of Fig. 1 in [1] and in Fig. 4 and Fig. 5 in [3].

puncture the sample are still very energetic, as shown in Fig. 5. In the case of 2-layered graphene, each transmitted atom has, on average, the kinetic energy of 70 eV for 5 keV impact and 100 eV for 10 keV impact. Likewise, the atoms emitted from the sample carry a considerable part of the energy initially absorbed by graphene. Considering the same example of 2-layered free-standing graphene, each emitted atom has, on average, the kinetic energy of 14 eV for 5 keV impact and 60 eV for 10 keV impact. All these atoms, both coming from the projectile and emitted from the sample, have energies that are several times larger than average bond energy in an organic molecule. [46] By raising the thickness of graphene (adding more graphene layers), we can lower the kinetic energy of emitted and transmitted atoms. 10 keV impact onto 4-layered graphene results in transmitted projectile atoms having, on average, 44.5 eV and atoms emitted from the sample having 25 eV. Adding additional two layers of graphene lowers the energies of the transmitted and emitted atoms to 13 eV and 9 eV, respectively. Even though lowering the kinetic energy of transmitted and emitted atoms is possible, these energies are still too high to collide with organic molecules without breaking their bonds. For very thick graphene, it is possible to achieve low enough emission energies. However, the number of atoms emitted also becomes very low, meaning fewer possibilities of colliding with investigated molecules and a lower probability of ejecting any material from the sample. If our goal is to desorb intact molecules from the graphene surface efficiently, it seems that the more promising are processes involving the movement of its surface, as mentioned above, rather than a direct impact with carbon atoms.

Accordingly, we can infer that graphene is a viable option as a substrate for the analysis of ultrathin organic samples in SIMS experiments. Primarily, graphene is extremely thin, so only a small number of atoms is available to be sputtered from the substrate. It means that tiny amounts of material deposited on the graphene should be detected as there will be little to no interference from the substrate signal. Unfortunately, direct collisions with projectile atoms and atoms emitted from the graphene might be too energetic for the intact molecules uplifting. On the other hand, the collective movement of top layers of the graphene in a catapult-like fashion or the movement present during bulging of the topmost layer can provide high amounts of energy and pass it gently to the molecules deposited on graphene. This process can provide means

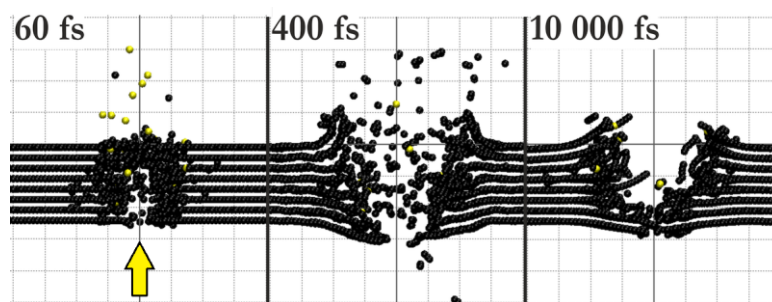


Fig. 7: Example of a dynamics of a C_{60} projectile's impact at a few-layered graphene sample. Graphene atoms are depicted in black, projectile atoms are yellow. Yellow arrow shows the direction of impact. A 1 nm slice through the system centred at the point of impact is shown. Dashed lines in the back are spaced by 1 nm. Fig. 1 in [1] and Fig. 4 and Fig. 5 in [3] provide more details into the process.

Image copyright: As stated in the permission granted for reuse of the article [3].

of emission of intact, organic molecules, especially in the transmission direction. As mentioned in the introduction section, it has also been proposed that circular acoustic waves generated during bombardment could lead to the ejection of weakly bound molecules from the graphene. [11,23,24] In my research such waves are also present, though their amplitudes are relatively small. Nevertheless, they are still another possible option leading to ejection of adsorbed molecules.

2.2 ARGON CLUSTER PROJECTILE

Section based on *Surf. & Coat. Tech.* (2020) [6]

As there are already experimental results available for C_{60} bombardment of organic material deposited on free-standing graphene, which means I can check and correlate my theoretical simulations with real-world data, the main projectile I am considering in this work is C_{60} fullerene. Nevertheless, it is beneficial to get a glimpse of the substrate's behaviour under bombardment with other projectiles. That way it is possible to check if these projectiles could be useful for more complicated setups or do the fullerene projectiles have just the needed properties that they are required specifically and no other projectiles are viable. I chose to look at the interactions of argon clusters of different sizes as there is considerable interest in large cluster projectiles consisting of hundreds or even thousands of atoms. [47-49] Impacts of such projectiles lead to the gentler, collective movement of the substrate and analysed material favouring intact molecules' emission even more than C_{60} projectiles.

Additionally, at the time of writing the dissertation, there was no research available in the literature on the emission from graphene stimulated by argon clusters' impacts. Most, if not all, works focused on the investigation of defects and not on emission. [18,19]

I investigated different sizes and kinetic energies of projectiles impacting 2-layered graphene at the 0-degree impact angle. There are several similarities between C_{60} and argon cluster projectiles. In both situations, graphene absorbs a lot of projectiles' energy, at least around 40% for 40 keV Ar_{60} and even more for lower initial projectile's energies or larger projectiles^{VI}. As I showed in [3], C_{60} projectiles at 40 keV lose 20% of their energy. Similarly, the argon cluster's impact leads to the accumulation of a high amount of energy in the sample, the creation of significant deformation of graphene, and substantial movement of its topmost layer (I present an example in Fig. 8 where 10 keV Ar_{1000} impacts at graphene). All these processes could result in the uplifting of large intact organic molecules from its surface.^{VII} The difference between C_{60} and Ar_{60} projectiles in energy absorbed by graphene could result from the difference in their sizes. Ar_{60} is around two times larger than C_{60} , which means its energy is distributed on the larger area of graphene, and, in consequence, more graphene atoms take part in the absorption of the projectile's energy.

Although the system with the argon cluster projectile is similar in many ways to the one with the fullerene projectile, I discovered additional features worth mentioning. I found that there are three categories of impacts based on the kinetic energy per atom of the projectile^{VIII}. This metric has been proposed earlier as a universal metric describing ejection phenomena during interactions of 3D systems with cluster projectiles. [50,51] Impacts in each of the categories lead to ejection through different processes, therefore resulting in different characteristics of the ejecta. An especially interesting situation is visible during low energy impacts of large projectiles, which have sufficient momentum to break through the graphene sheets but not enough energy to eject any carbon atoms from it. Under such conditions, petal-like structures are formed through the rapture of graphene, as shown in Fig. 8^{IX}. Lookalike structures have been

^{VI} See [6] inset to Fig. 1b

^{VII} Examples of graphene movement are shown in [6] Figures 4-8

^{VIII} In-depth discussion is presented in [6], in the text above Fig. 2

^{IX} See also [6] Fig. 8

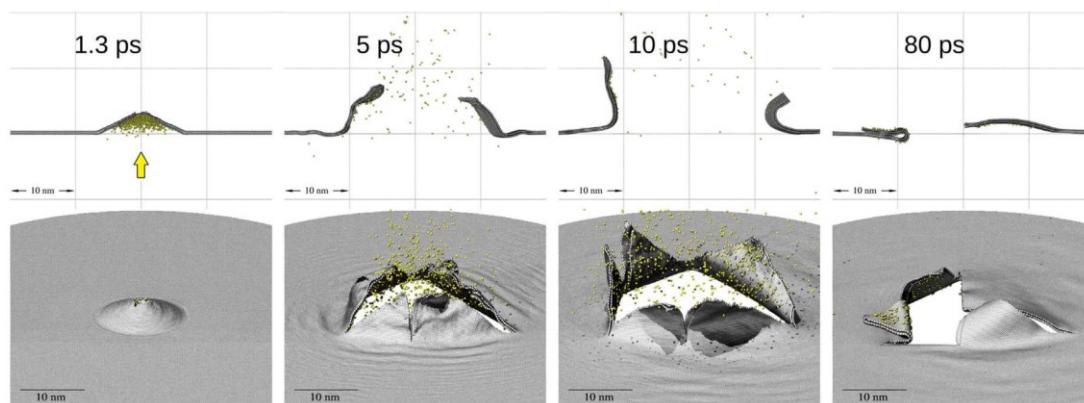


Fig. 8: Example of a dynamics of the 10 keV Ar_{1000} projectile's impact at a two-layered graphene sample. Graphene atoms are depicted in grey, projectile atoms are yellow. The top row contains side views of the system obtained at various moments given by the values at the top left corners. The lower row contains perspective view of the same system. For a side view a 2 nm thick slice through the centre of the sample is shown. Thin lines in the background denote the distance of 10 nm. Yellow arrow indicates the direction of an incoming projectile. Figures 4-8 in [6] provide more details including dynamics of impacts with other projectile's sizes and other primary kinetic energies.

Image copyright: As stated in the permission granted for reuse of the article [6].

observed experimentally after the bombardment of multilayer graphene with micro-scale projectiles. [52] Remarkably, we can observe similar shapes forming during experiments in size scales that differ by several orders of magnitude.

My investigation of the argon cluster bombardment of graphene showed that large argon clusters might be another interesting candidate for a projectile when regarding desorption of large intact organic molecules. In some ways, argon clusters are more suitable than fullerene. There is more energy accumulated in the movement of the topmost graphene layer, the deformation of the graphene sheet is more prominent, and the movement extends to a much higher lateral distance from the point of impact. On the other hand, it is currently impossible to make an ion beam composed of single-sized argon clusters. Argon cluster beams are much less controllable than C_{60} sources, and there is always a distribution of cluster sizes impacting the sample. [48,53] Furthermore, as I mentioned earlier, there are already experimental results available for C_{60} projectile, while no similar results exist for Ar_n projectiles. Therefore I chose to use C_{60} projectiles in my further research.

3 UPLIFTING INDIVIDUAL ORGANIC MOLECULES

Section based on *Nucl. Inst. & Meth. B* (2017) [2]

Having an insight into the graphene substrate's behaviour under bombardment and having confirmation that the system has potential for the uplifting of deposited organic material, I began an investigation of the processes stimulated by cluster projectile impact at the sample with organic molecules deposited on graphene. I chose phenylalanine molecules as they are small enough to be feasible for computer simulations but, at the same time, big enough as a proof-of-concept molecules for other, bigger compounds. Additionally, experimental results are available for systems with thin layers of phenylalanine on free-standing graphene [4,5], meaning I could compare my theoretical results with reality.

Guided by the spirit of my workflow, which is taking one step at a time, I firstly considered a graphene sample with only a few organic molecules deposited on it. In this research, there are ten molecules placed on graphene at a growing distance from the point of impact, as depicted in Fig. 9^x. I performed simulations with C₆₀ projectile, the initial kinetic energy of 10 keV, and 0-degree impact angle. Graphene substrate had a 2 to 16 layers thickness.

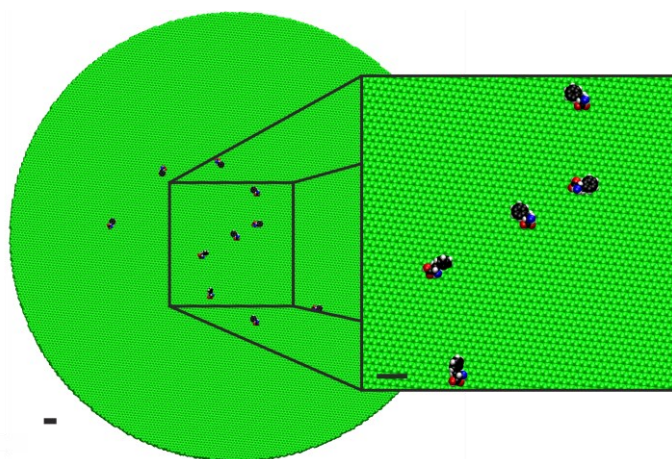


Fig. 9: Placement of phenylalanine molecules on graphene in a 10-molecules' sample. Black bars denote distance of 1 nm.

Image copyright: As stated in the permission granted for reuse of the article [2].

^x See also Fig. 1 in [2]

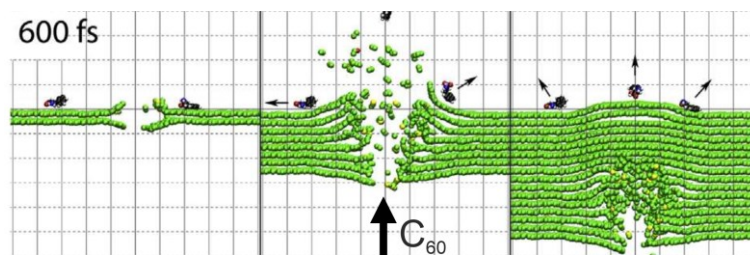


Fig. 10: Example of three regimes of a C_{60} projectile's impact at a few-layered graphene sample with phenylalanine molecules deposited on it. Graphene atoms are depicted in green, projectile atoms are yellow, phenylalanine atoms have colours depending on the atoms' type. A 1.5 nm slice through the system centred at the point of impact is shown. Dashed lines in the back are spaced by 1 nm. Big arrow shows the direction of impact and small arrows depict movement directions of phenylalanine molecules in later stages of the process. Fig. 2 in [2] and its discussion provide more details.

Image copyright: As stated in the permission granted for reuse of the article [2].

I have found that there are three regimes leading to the ejection of organic molecules (Fig. 10 shows example of their dynamics)^{XI}:

1. The first one is present when considering a thin substrate, so when relatively low amounts of energy are dispersed into graphene. In this regime, the molecule at the point of impact gets shattered, which is understandable, considering the energetics of such collisions discussed on page 12 of this dissertation. We can also observe small acoustic waves (amplitude of 1 Å) forming on graphene, but they are not energetic enough to uplift any molecule. As a result, no other molecule is emitted.
2. We can talk about the second regime for thicker samples but still thin enough for the projectile to pierce it. In this situation, the molecule at the point of impact still gets atomised, but the topmost graphene layer shows much more movement. The molecule closest to the centre of the impact, placed 22 Å from the point of impact, is desorbed through catapult-like movement. Molecules placed further away are displaced by the wave on graphene, but the wave's energy diminishes too fast to provide enough movement for the uplifting of any other molecules.
3. The third regime is present when the sample is thick enough, so the projectile does not penetrate it. In this case, graphene's deformation is the most substantial and, simultaneously, the most gentle. All molecules stay intact, and three of them are uplifted. The first molecule, at the centre of the

^{XI} For more details see Fig. 2 in [2] and its discussion

sample, the second one, placed 22 Å from the centre, and even the third one, placed 33 Å from the point of impact. All of them get desorbed through a concerted motion of the graphene membrane deforming under the force of decelerating cluster projectile.

These results suggest that uplifting of intact organic molecules from graphene in transmission direction is possible indeed. For most cases, the desorption of intact molecules may occur from places located at a certain distance from the point of impact, through the direct deformation of graphene. Such behaviour was observed for metal substrates as well but for much smaller lateral distances. [54] I observed circular acoustic waves, but their energy was never high enough to uplift any molecule.

These results are intriguing in one additional aspect. The possibility of the efficient desorption of intact molecules deposited so sparsely without additional solvents could be an interesting approach to the matrix effect in SIMS. In short, the chemical environment of the analysed material can have a drastic influence on the intensities of detected ejecta. [55] There are several methods of lowering the impact of this effect, mostly by diluting the analyte to the point that each molecule is spatially separated from other molecules. The idea is simple: by reducing the chemical environment, we could diminish the matrix effect as well. [56,57] Free-standing graphene in a transmission SIMS geometry could be a suitable substrate for such extremely diluted samples. It provides an efficient way of desorbing intact molecules positioned very far from other molecules, giving minimal signal from the substrate itself.

I should also note that the presented results relate to the sputtering of neutral molecules while the SIMS method records ions. As described in section 1.2, classical molecular dynamics is incapable of describing ionisation and neutralisation processes. However, the description of structural modifications of the system applies to both ions and neutrals. Having that in mind, we can try some fortune-telling. Based on the energetics of the system, I predict that even though third regime emission (no projectile penetration, emission only through graphene movement) is the most efficient one, it will not lead to ionisation of emitted organic molecules. As described in section 1.1, the ionisation process requires particles to be in an energised state while third regime provides a low amount of energy to the ejected molecules. This regime would be of much

interest for the SNMS experiments but with little use for the SIMS methodology. On the other hand, second regime impacts could result in the emission of ions, especially negative ions. As described by Verkhoturov et al. [5,11], as well as in the references in these articles, there is high emission of electrons present while breaking graphene sheets. Electrons emitted from the graphene can attach to fragments and molecules ejected from the graphene's surface, creating negative ions. This would make such conditions much more compelling for the SIMS community.

4 SPUTTERING FROM AN ORGANIC MONOLAYER

4.1 COLLABORATION WITH PROFESSOR SCHWEIKERT'S TEAM

Section based on *J. Chem. Phys.* (2018) [4] and *J. Chem. Phys.* (2019) [5]

Knowing how substrate behaves and if the uplifting of intact molecules is possible, I started to look into the irradiation with C_{60} projectile of a thin layer of organic material deposited on free-standing graphene. In this research, I used the sample with one layer of phenylalanine molecules, which is around 1.1 nm thick, deposited on 2-layered graphene. To further elucidate the mechanism present during the bombardment of such a system, I compared it with a bulk phenylalanine sample (represented by 10 layers of phenylalanine placed on 2-layered graphene) and a single layer of phenylalanine on graphite (computer sample of one layer of phenylalanine on 30 layers of graphene), shown in Fig. 11.

As mentioned in the introductory section, this research was performed in collaboration with a team from the Texas A&M University in the USA, led by Professor Emile A. Schweikert, especially with Dr Stanislav V. Verkhoturov. This group constructed a unique transmission SIMS system that can operate both in traditional and transmission geometry, simultaneously, in a single impact mode (they can detect ejecta from each C_{60} impact separately). [10,11] To my knowledge, there was no other SIMS apparatus in the world with such capabilities at the time of writing this dissertation. Thanks to this collaboration we could pair up experimental results with computer simulations and provide an extensive description of impacts on free-standing graphene. The articles [4,5] resulting from this collaboration are much broader in their scope than this

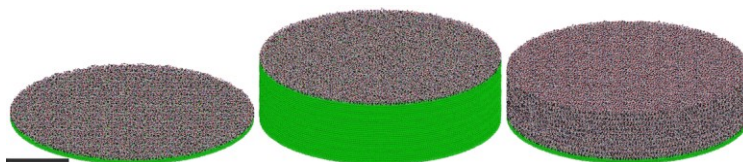


Fig. 11: Samples used in the comparison of emission from thin layer of organic molecules. From the left: one layer of phenylalanine on two layers of graphene, one layer of phenylalanine on 30 layers of graphene, and 10 layers of phenylalanine on two layers of graphene. Substrate atoms are green, organic layers are represented by dark mix of colours. Black bar denotes distance of 10 nm.

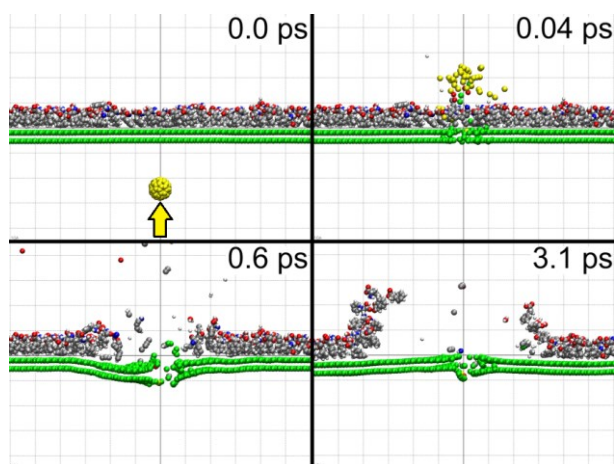


Fig. 12: Snapshots of the model system consisting of the single layer of phenylalanine molecules deposited on two-layer graphene taken at various moments after 50 keV C_{60} impact (cross-sectional view). The grey lines in the background are separated by 1 nm. Graphene atoms are green, projectile atoms are yellow, organic layer is represented by darker mix of colours. Yellow arrow depicts direction of projectile's movement. Fig. 7 and Fig. 8 in [4], and Fig. 10 and Fig. 11 in [5] provide more details.

Image copyright: As stated in the permission granted for reuse of the article [5].

dissertation hence I will shortly describe only parts regarding simulations which I performed, with a little bit of experimental background mentioned when needed.

Both simulations and experimental results show that intact molecules are being emitted from a single layer of phenylalanine. Interestingly, the experimental yields of *intact molecular ions* ejected from a single layer and bulk organic samples are comparable^{XII}. It is even more exciting as simulations showed at least 18-times higher emission of neutral molecules from the bulk sample. This result indicates that bombardment of extremely thin sample on free-standing graphene results in two orders of magnitude higher ionisation rates as compared to emission from a bulk sample, and is viable for use in various experiments requiring minuscule amounts of sample material.

Of most interest to my work are the processes which lead to the emission of intact molecules. Firstly, let us talk about the monolayer of phenylalanine on graphene (Fig. 12 shows an example dynamics of such system). Projectile impacts at the bottom of graphene pierces through it, and, similarly to the

^{XII} Further discussion in [4] at the beginning of part “Phenylalanine monolayer on graphene” and in [5] at the beginning of part “III. Ejection and ionization of molecules via 50 keV C_{60}^{2+} impacts on thin molecular layers deposited on free standing graphene”

graphene-only system described earlier, loses its integrity just after passing graphene atoms. Despite losing structural integrity, fullerene atoms are still acting on the organic layer together in a correlated manner. Molecules at the point of impact become fragmented by collisions with high energy atoms. Nevertheless, the phenylalanine layer is pushed to the sides, compressing radially around the point of impact. This compression pushes the graphene membrane down, which results in a separation between graphene and the molecular layer. This step is crucial as the separation of layers causes the weakening of organic molecules' bonds to the substrate, making it easier to uplift intact molecules. While separating from each other, the graphene membrane bends and stretches when the organic layer keeps compressing and starts forming a rim. After a few picoseconds, graphene starts to move upward again, converting accumulated potential energy into kinetic energy of its movement. This correlated movement provides additional energy to the organic layer supporting the emission of intact molecules from the rim around the impact site. The graphene acts like a trampoline for the organic molecules.^{XIII}

Interestingly, phenylalanine on the graphite sample provides a comparable experimental yield of intact negative molecular ions as phenylalanine on graphene (0.1 ions/impact and 0.15 ions/impact, respectively). The process of emission is similar though slightly different. Fullerene deposits its energy around 5 nm deep into the graphite, leaving the organic layer at the surface relatively intact. Graphite expands radially from the inside, pushing the topmost layer upwards. Through this movement, graphite provides trampolining action to the organic layer stimulating the emission of intact molecules.^{XIV}

Experimental emission of 0.13 ions/impact from the bulk sample is comparable to phenylalanine on graphene as well. The sputtering process, in this case of weakly bounded molecular solid, is already extensively described. [12,58,59] In short, there are two distinct ways of emission of intact molecules from such system. Firstly, a cluster's collision leads to the creation of a highly energised region that expands and stimulates high energy emission at off-normal angles

^{XIII} See [4] Fig. 7 and Fig. 8, and [5] Fig. 10 and Fig. 11

^{XIV} See [4] Fig. 10 and Fig. 11

through fluid flow. Secondly, effusive-type motions in the later stages of crater's forming lead to the emission of low energy molecules over all angles.^{xv}

The comparison of all three samples gives a clear notion that the graphene system is unique and could be used to uplift intact molecules from extremely thin organic layers. Trampoline-like movement after ion irradiation of graphene has not been described earlier, even though it is a crucial element of efficient emission from such a thin sample. Moreover, a very high ionisation rate and almost no interference from the substrate's atoms (as mentioned in section 3) make this setup highly promising in specialised detection techniques. Although the graphite sample provides similar yields and ionisation rates, it emits much higher number of substrate's atoms together with the organic material leading to high noise.

4.2 FURTHER INVESTIGATION

Section based on *App. Surf. Sci.* (2020) [7]

As computer simulations allow for a much broader set of initial conditions than experimental setups, I was able to test phenylalanine on graphene setup further. In article [7] I employed various kinetic energies of the projectile and impact angles. In addition, I evaluated the difference in behaviour between impacts onto the graphene side of the sample and the side where organic material was deposited, as shown in Fig. 13.

Based on the investigation of ejecta metrics, such as yields of intact molecules and organic fragments, their mass spectra, angular distributions, as well as direct analysis of impacts' kinetics, I proposed a differentiation between two regimes of impacts characterised by distinct mechanisms of ejection. The more frequently observed regime is present during all impacts in sputtering geometry,

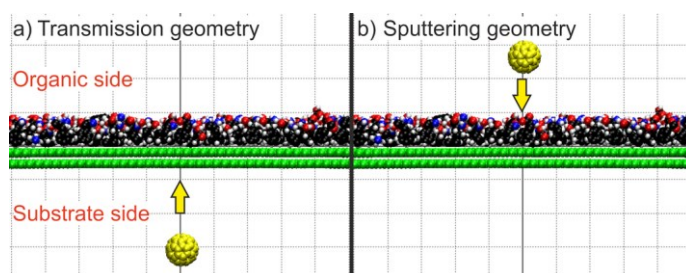


Fig. 13: Impact directions in a) transmission and b) sputtering geometries.

^{xv} More detailed description available in [4], in section "Bulk phenylalanine"

as shown in Fig. 13b, and during impacts that can pierce through the sample in transmission geometry, as depicted in Fig. 13a. The second regime can be observed in transmission geometry when the projectile does not perforate the sample. Fig. 14 provides example snapshots of the two regimes based on four arrangements between bombardment direction and energy.

In the latter scenario, the projectile collides directly only with the graphene substrate. Graphene sheets bulge out along the direction of the primary beam, pushing organic molecules up. The process is delicate and spatially correlated. A short time after impact, graphene begins to return to its original position, but energised molecules continue to move. As they are bound only by intermolecular forces that are too weak to stop them, molecules continue their movement out from the sample in directions close to the normal to the surface.^{XVI}

In contrast, the process of emission of intact molecules during regime present in the sputtering direction and piercing transmission direction is more convoluted. Even though details of the interaction differ slightly between those two situations, the essential process is the same as described earlier in the part of section 4.1 devoted to irradiation of thin phenylalanine layer on graphene as part of publications with S. V. Verkhoturov [4,5].^{XVII}

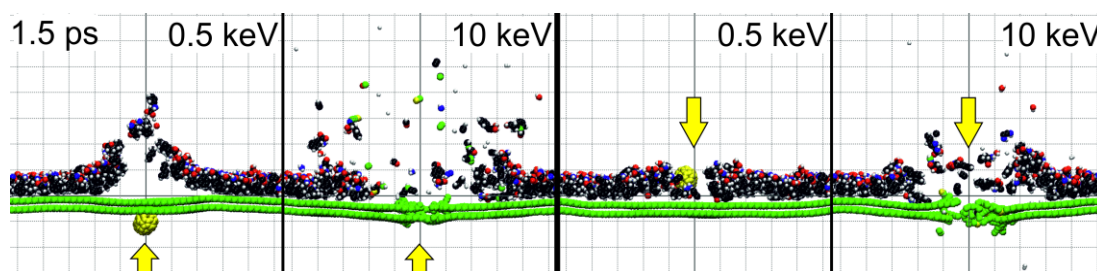


Fig. 14: Example snapshots from the simulation of 0.5 keV and 10 keV C_{60} impacts along the surface normal at phenylalanine monolayer deposited on free-standing graphene. Only 2 nm wide cross-section through the centre of the sample is shown. Thin lines in the background denote the distance of 1 nm. The yellow arrows indicate directions of the projectile impact. Graphene atoms are green, projectile atoms are yellow, organic layer is represented by dark mix of colours. Fig. 6 in [7] provides more details.

Image copyright: As stated in the permission granted for reuse of the article [7].

^{XVI} Described in more details in [7] Fig. 6a and c, and its discussion

^{XVII} Detailed description in discussion of Fig. 6b and d in [7]

What is especially surprising is that the molecules' fragmentation is more frequent in transmission than in sputtering geometry. The basic process of fragmentation is due to direct collisions with projectile atoms. For this reason, I would assume that the more energetic collisions occurring in sputtering geometry, where the projectile collides with an organic overlayer still having its original kinetic energy, will lead to higher fragmentation. For transmission geometry, on the other hand, a significant part of the kinetic energy is lost during graphene perforation, as shown in section 2.1. Contrary to my earlier beliefs, transmission geometry results in more fragmentation than sputtering geometry.^{XVIII} The explanation is that in transmission geometry, C₆₀ projectile breaks down when it collides with graphene. It is no longer a single object. Instead, it creates a conglomerate of smaller, high energy particles moving independently. They shatter all organic molecules on their path, acting in a bigger radius than the intact fullerene would have. Additionally, in the sputtering geometry, the collisions between projectile and organic molecules are spatially and temporally correlated. As a result, they are more gentle, and fewer molecules are destroyed.^{XIX}

Last but not least, I have found out that to describe changes in molecular emission due to the change of the angle of incidence, three factors should be considered: 1. area of the sample excited by the projectile, 2. the component of the projectile momentum perpendicular to the sample and the projectile back-reflection process, and 3. molecular fragmentation. Firstly, as the angle of incidence increases, the projectile can move a longer path inside the organic layer. As a consequence, it can collide with more molecules. The second factor is reducing molecular emission. For off-normal impacts, the component of the projectile momentum perpendicular to the sample is reduced. Moreover, an increasing part of the projectile kinetic energy is carried by back-reflected projectile atoms. Therefore less energy is available to stimulate molecular emissions. The third factor is straightforward. If a collision is less energetic because of an increase in the angle of incidence, fewer molecules become fragmented and, subsequently, the yield of intact molecules increases at the

^{XVIII} See Fig 4b and d in [7]

^{XIX} In-depth discussion available in [7] as a discussion to Fig. 6

expense of the yield of molecular fragments. The interplay of these three processes determines the shape of the yield versus impact angle dependence.^{xx}

To summarise, I showed that emission of intact phenylalanine molecules from extremely thin molecular layer deposited on free-standing graphene is possible in a wide range of conditions. Simulations suggest that the most preferred configuration for SIMS is a high-energy C₆₀ bombardment at off-normal angles regardless of the impact's geometry (transmission or sputtering). It provides high yields of intact molecules, and we can assume that high energy impacts will provide decent ionisation rates, especially when taking into account the results described in section 4.1. On the other hand, if one would be interested in achieving strong emission of intact neutral molecules, such as in Secondary Neutral Mass Spectrometry (SNMS), the best choice should be the transmission geometry in combination with fullerene impacts that do not lead to sample perforation. These conditions give a very clear signal of intact molecules with next to no fragmentation, but it is perhaps less probable for molecules to get ionised. As molecular dynamics does not model ionisation processes, the question of which regime is suitable for SIMS and which for SNMS cannot be answered with certainty in this dissertation.

^{xx} More details are available in discussion to Fig. 7 in [7]

5 SUMMARY

In this dissertation, I provided a comprehensive investigation of processes leading to the emission of organic material from a free-standing graphene substrate irradiated by keV clusters.

I started my research by describing in detail the interactions of cluster projectile with free-standing graphene alone. The research provided insight into the astounding ability of graphene to absorb energy as well as unveiled the substantial movement of the graphene layers. The graphene system also served as an opportunity for comparing C₆₀ fullerene projectile and various sizes of argon cluster projectiles. Large argon clusters appear to be better suited for gentle interaction with organic molecules deposited on the graphene. Nevertheless, considering the availability of experimental data and properties of currently developed argon clusters' sources, I chose to focus on C₆₀ projectiles.

As a next step, I described the behaviour of individual phenylalanine molecules placed on free-standing graphene that get targeted by fullerene projectile. I showed that uplifting of intact organic molecules in such system is possible and, in the right circumstances, the area of interaction leading to such uplifting could be considerable. I also discussed briefly the possibility of using such a setup as a method of mitigating the matrix effect in SIMS briefly.

Earlier parts lead to the analysis of fullerene projectile's impact onto the sample with a thin organic layer deposited on graphene. I confirmed that it is possible to uplift intact phenylalanine molecules from its thin layer placed on free-standing graphene. A significant component of this section comes from the collaboration with Texas A&M University. We discovered that using graphene as a substrate leads to the substantial enhancement of ionisation probability of intact molecules and that the transmission SIMS could be an exciting choice for detecting minuscule amounts of material in the sample.

I also described in detail the whole process of emission from the sample in a much broader range of conditions than experimentally available. The most important aspect is the trampolining action of graphene layers on phenylalanine. The additional energy provided to the organic layer together with separation between both types of layers provides a gentle and efficient way of

desorption of intact molecules. What is also interesting, there is no apparent advantage, from the point of view of molecular dynamics, of employing transmission geometry over traditional sputtering geometry of impact.

All results provide evidence on processes of emission that are unique to the graphene substrate. Knowledge gathered in this dissertation – starting from graphene having not enough atoms for the traditional models to be employed, through unusually high rates of deformation and energy absorption, and ending up with the separation of organic layer from graphene membrane and occurrence of trampolining action – gives a clear notion of new and exciting phenomena. Therefore, my thesis that the process of emission from graphene differs from the paths of emission described for bulk materials is confirmed.

BIBLIOGRAPHY

- 1 Goluński M. & Postawa Z. Effect of Sample Thickness on Carbon Ejection from Ultrathin Graphite Bombarded by keV C₆₀. *Acta Physica Polonica A* **132**, 222-224, doi:10.12693/APhysPolA.132.222 (2017).
- 2 Goluński M., Verkhoturov S. V., Verkhoturov D. S., Schweikert E. A. & Postawa Z. Effect of substrate thickness on ejection of phenylalanine molecules adsorbed on free-standing graphene bombarded by 10 keV C₆₀. *Nuclear Instruments and Methods in Physics Research Section B: Beam Interactions with Materials and Atoms* **393**, 13-16, doi:10.1016/j.nimb.2016.09.006 (2017).
- 3 Goluński M. & Postawa Z. Effect of kinetic energy and impact angle on carbon ejection from a free-standing graphene bombarded by kilo-electron-volt C₆₀. *Journal of Vacuum Science & Technology B, Nanotechnology and Microelectronics: Materials, Processing, Measurement, and Phenomena* **36**, 03F112, doi:10.1116/1.5019732 (2018).
- 4 Verkhoturov S. V., Goluński M., Verkhoturov D. S., Geng S., Postawa Z. & Schweikert E. A. “Trampoline” ejection of organic molecules from graphene and graphite via keV cluster ions impacts. *The Journal of Chemical Physics* **148**, 144309, doi:10.1063/1.5021352 (2018).
- 5 Verkhoturov S. V., Goluński M., Verkhoturov D. S., Czerwinski B., Eller M. J., Geng S., Postawa Z. & Schweikert E. A. Hypervelocity cluster ion impacts on free standing graphene: Experiment, theory, and applications. *The Journal of Chemical Physics* **150**, 160901, doi:10.1063/1.5080606 (2019) and references therein.
- 6 Goluński M., Hrabar S. & Postawa Z. Mechanisms of particle ejection from free-standing two-layered graphene stimulated by keV argon gas cluster projectile bombardment – Molecular dynamics study. *Surface and Coatings Technology* **391**, 125683, doi:10.1016/j.surfcoat.2020.125683 (2020).
- 7 Goluński M., Hrabar S. & Postawa Z. Mechanisms of molecular emission from phenylalanine monolayer deposited on free-standing graphene bombarded by C₆₀ projectiles. *Applied Surface Science* **539**, 148259, doi:10.1016/j.apsusc.2020.148259 (2021).
- 8 Urbassek H. M. “Status of cascade theory” in *ToF-SIMS: Materials Analysis by Mass Spectrometry* (eds J. C. Vickerman & D. Briggs) (IM Publications, 2013) and references therein.
- 9 Vickerman J. C. “Prologue: ToF SIMS - An evolving mass spectrometry of materials” in *ToF-SIMS: Materials Analysis by Mass Spectrometry* (eds J. C. Vickerman & D. Briggs) (IM Publications, 2013) and references therein.
- 10 Eller M. J., Liang C.-K., Della-Negra S., Clubb A. B., Kim H., Young A. E. & Schweikert E. A. Hypervelocity nanoparticle impacts on free-standing graphene: a sui generis mode of sputtering. *The Journal of Chemical Physics* **142**, 044308, doi:10.1063/1.4906343 (2015).
- 11 Verkhoturov S. V., Geng S., Czerwinski B., Young A. E., Delcorte A. & Schweikert E. A. Single impacts of keV fullerene ions on free standing graphene: Emission of ions and electrons from confined volume. *The Journal of Chemical Physics* **143**, 164302, doi:10.1063/1.4933310 (2015).
- 12 Garrison B. J. & Postawa Z. “Molecular Dynamics Simulations, the Theoretical Partner to dynamic cluster SIMS Experiments” in *ToF-SIMS: Materials Analysis by Mass Spectrometry* (eds J. C. Vickerman & D. Briggs) (IM Publications, 2013) and references therein.
- 13 Garrison B. J. & Postawa Z. Computational view of surface based organic mass spectrometry. *Mass Spectrometry Reviews* **27**, 289-315, doi:10.1002/mas.20165 (2008).

- 14 Winograd N. The Magic of Cluster SIMS. *Analytical Chemistry* **77**, 142 A-149 A, doi:10.1021/ac053355f (2005) and references therein.
- 15 Zhao S., Xue J., Liang L., Wang Y. & Yan S. Drilling Nanopores in Graphene with Clusters: A Molecular Dynamics Study. *The Journal of Physical Chemistry C* **116**, 11776-11782, doi:10.1021/jp3023293 (2012).
- 16 Zan R., Ramasse Q. M., Bangert U. & Novoselov K. S. Graphene reknits its holes. *Nano Letters* **12**, 3936-3940, doi:10.1021/nl300985q (2012).
- 17 Xu Z.-C. & Zhong W.-R. Probability of self-healing in damaged graphene bombarded by fullerene. *Applied Physics Letters* **104**, 261907, doi:10.1063/1.4886580 (2014).
- 18 Lehtinen O., Kotakoski J., Krasheninnikov A. V., Tolvanen A., Nordlund K. & Keinonen J. Effects of ion bombardment on a two-dimensional target: Atomistic simulations of graphene irradiation. *Physical Review B* **81**, doi:10.1103/PhysRevB.81.153401 (2010).
- 19 Lehtinen O., Kotakoski J., Krasheninnikov A. V. & Keinonen J. Cutting and controlled modification of graphene with ion beams. *Nanotechnology* **22**, 175306, doi:10.1088/0957-4484/22/17/175306 (2011).
- 20 Bellido E. P. & Seminario J. M. Molecular Dynamics Simulations of Ion-Bombarded Graphene. *The Journal of Physical Chemistry C* **116**, 4044-4049, doi:10.1021/jp208049t (2012).
- 21 Dong Y., He Y., Wang Y. & Li H. A theoretical study of ripple propagation in defective graphene. *Carbon* **68**, 742-747, doi:10.1016/j.carbon.2013.11.060 (2014).
- 22 He Y. Z., Li H., Si P. C., Li Y. F., Yu H. Q., Zhang X. Q., Ding F., Liew K. M. & Liu X. F. Dynamic ripples in single layer graphene. *Applied Physics Letters* **98**, 063101, doi:10.1063/1.3551574 (2011).
- 23 Webb R. P. The computer simulation of energetic cluster–solid interactions. *Radiation Effects and Defects in Solids* **162**, 567-572, doi:10.1080/10420150701564936 (2007).
- 24 Kerford M. & Webb R. P. Desorption of molecules by cluster impact: A preliminary molecular dynamics study. *Nuclear Instruments and Methods in Physics Research Section B: Beam Interactions with Materials and Atoms* **180**, 44-52, doi:10.1016/s0168-583x(01)00395-0 (2001).
- 25 Wu X., Mu F., Wang Y. & Zhao H. Application of atomic simulation methods on the study of graphene nanostructure fabrication by particle beam irradiation: A review. *Computational Materials Science* **149**, 98-106, doi:10.1016/j.commatsci.2018.03.022 (2018).
- 26 Bai Z., Zhang L., Li H. & Liu L. Nanopore Creation in Graphene by Ion Beam Irradiation: Geometry, Quality, and Efficiency. *ACS Applied Materials & Interfaces* **8**, 24803-24809, doi:10.1021/acsami.6b06220 (2016).
- 27 Luo J., Gao T., Li L., Xie Q., Tian Z., Chen Q. & Liang Y. Formation of defects during fullerene bombardment and repair of vacancy defects in graphene. *Journal of Materials Science* **54**, 14431-14439, doi:10.1007/s10853-019-03938-2 (2019).
- 28 Qin X., Yan W., Guo X., Gao T. & Xie Q. Molecular Dynamics Simulations of Si ion Substituted Graphene by Bombardment. *IOP Conference Series: Materials Science and Engineering* **394**, 022020, doi:10.1088/1757-899x/394/2/022020 (2018).
- 29 Hosseini-Hashemi S., Sepahi-Boroujeni A. & Sepahi-Boroujeni S. Analytical and molecular dynamics studies on the impact loading of single-layered graphene sheet by fullerene. *Applied Surface Science* **437**, 366-374, doi:10.1016/j.apsusc.2017.12.141 (2018).
- 30 Martinez-Asencio J., Ruestes C. J., Bringa E. M. & Caturla M. J. Controlled rippling of graphene via irradiation and applied strain modify its mechanical properties:

- a nanoindentation simulation study. *Physical Chemistry Chemical Physics* **18**, 13897-13903, doi:10.1039/c6cp01487a (2016).
- 31 Yoon K., Rahnamoun A., Swett J. L., Iberi V., Cullen D. A., Vlassioux I. V., Belianinov A., Jesse S., Sang X., Ovchinnikova O. S., Rondinone A. J., Unocic R. R. & van Duin A. C. T. Atomistic-Scale Simulations of Defect Formation in Graphene under Noble Gas Ion Irradiation. *ACS Nano* **10**, 8376-8384, doi:10.1021/acsnano.6b03036 (2016).
- 32 Yip S. *Handbook of Materials Modeling*. (Springer, Dordrecht, 2005).
- 33 Akimov A. V. & Prezhdo O. V. Large-Scale Computations in Chemistry: A Bird's Eye View of a Vibrant Field. *Chemical Reviews* **115**, 5797-5890, doi:10.1021/cr500524c (2015).
- 34 Ziegler J. F. & Biersack J. P. "The Stopping and Range of Ions in Matter" in *Treatise on Heavy-Ion Science* (ed D.A. Bromley) (Springer, Boston, MA, 1985).
- 35 Aziz R. A. & Slaman M. J. The argon and krypton interatomic potentials revisited. *Molecular Physics* **58**, 679-697, doi:10.1080/00268978600101501 (1986).
- 36 Kański M., Maciążek D., Postawa Z., Ashraf C. M., van Duin A. C. T. & Garrison B. J. Development of a Charge-Implicit ReaxFF Potential for Hydrocarbon Systems. *The Journal of Physical Chemistry Letters* **9**, 359-363, doi:10.1021/acs.jpcclett.7b03155 (2018).
- 37 Liu L., Liu Y., Zybin S. V., Sun H. & Goddard W. A., 3rd. ReaxFF-lg: correction of the ReaxFF reactive force field for London dispersion, with applications to the equations of state for energetic materials. *The Journal of Physical Chemistry A* **115**, 11016-11022, doi:10.1021/jp201599t (2011).
- 38 Stuart S. J., Tutein A. B. & Harrison J. A. A reactive potential for hydrocarbons with intermolecular interactions. *The Journal of Chemical Physics* **112**, 6472-6486, doi:10.1063/1.481208 (2000).
- 39 Kański M., Maciążek D., Goluński M. & Postawa Z. Sputtering of octatetraene by 15 keV C₆₀ projectiles: Comparison of reactive interatomic potentials. *Nuclear Instruments and Methods in Physics Research Section B: Beam Interactions with Materials and Atoms* **393**, 29-33, doi:10.1016/j.nimb.2016.10.023 (2017).
- 40 Iftimie R., Minary P. & Tuckerman M. E. Ab initio molecular dynamics: concepts, recent developments, and future trends. *Proceedings of the National Academy of Sciences of the United States of America* **102**, 6654-6659, doi:10.1073/pnas.0500193102 (2005).
- 41 Plimpton S. Fast Parallel Algorithms for Short-Range Molecular Dynamics. *Journal of Computational Physics* **117**, 1-19, doi:10.1006/jcph.1995.1039 (1995).
- 42 Aktulga H. M., Fogarty J. C., Pandit S. A. & Grama A. Y. Parallel reactive molecular dynamics: Numerical methods and algorithmic techniques. *Parallel Computing* **38**, 245-259, doi:10.1016/j.parco.2011.08.005 (2012).
- 43 Postawa Z., Czerwinski B., Szewczyk M., Smiley E. J., Winograd N. & Garrison B. J. Enhancement of sputtering yields due to C₆₀ versus Ga bombardment of Ag[111] as explored by molecular dynamics simulations. *Analytical Chemistry* **75**, 4402-4407, doi:10.1021/ac034387a (2003).
- 44 Haque B. Z., Chowdhury S. C. & Gillespie J. W. Molecular simulations of stress wave propagation and perforation of graphene sheets under transverse impact. *Carbon* **102**, 126-140, doi:10.1016/j.carbon.2016.02.033 (2016).
- 45 Pribat D., Balandin A. A., Lee Y.-H. & Razeghi M. In-plane and cross-plane thermal conductivity of graphene: applications in thermal interface materials. *SPIE NanoScience + Engineering Proceedings* **8101**, 810107, doi:10.1117/12.894455 (2011).
- 46 Blanksby S. J. & Ellison G. B. Bond dissociation energies of organic molecules. *Accounts of Chemical Research* **36**, 255-263, doi:10.1021/ar020230d (2003).

- 47 Rabbani S., Barber A. M., Fletcher J. S., Lockyer N. P. & Vickerman J. C. TOF-SIMS with argon gas cluster ion beams: a comparison with C_{60}^+ . *Analytical Chemistry* **83**, 3793-3800, doi:10.1021/ac200288v (2011).
- 48 Lee S. J., Choi C. M., Min B. K., Baek J. Y., Eo J. Y. & Choi M. C. Development of an Argon Gas Cluster Ion Beam for ToF-SIMS Analysis. *Bulletin of the Korean Chemical Society* **40**, 877-881, doi:10.1002/bkcs.11840 (2019).
- 49 Angerer T. B., Blenkinsopp P. & Fletcher J. S. High energy gas cluster ions for organic and biological analysis by time-of-flight secondary ion mass spectrometry. *International Journal of Mass Spectrometry* **377**, 591-598, doi:10.1016/j.ijms.2014.05.015 (2015).
- 50 Anders C., Urbassek H. M. & Johnson R. E. Linearity and additivity in cluster-induced sputtering: A molecular-dynamics study of van der Waals bonded systems. *Physical Review B* **70**, doi:10.1103/PhysRevB.70.155404 (2004).
- 51 Delcorte A., Garrison B. J. & Hamraoui K. Dynamics of molecular impacts on soft materials: from fullerenes to organic nanodrops. *Analytical Chemistry* **81**, 6676-6686, doi:10.1021/ac900746x (2009).
- 52 Lee J.-H., Loya P. E., Lou J. & Thomas E. L. Dynamic mechanical behavior of multilayer graphene via supersonic projectile penetration. *Science* **346**, 1092-1096, doi:10.1126/science.1258544 (2014).
- 53 Winograd N. Gas Cluster Ion Beams for Secondary Ion Mass Spectrometry. *Annual Review of Analytical Chemistry* **11**, 29-48, doi:10.1146/annurev-anchem-061516-045249 (2018).
- 54 Postawa Z. Sputtering simulations of organic overlayers on metal substrates by monoatomic and clusters projectiles. *Applied Surface Science* **231-232**, 22-28, doi:10.1016/j.apsusc.2004.03.019 (2004).
- 55 Briggs D. "Information from SSIMS" in *Surface Analysis of Polymers by XPS and Static SIMS* (Cambridge University Press, 1998).
- 56 Wirtz T. & Migeon H. N. Storing Matter: A new quantitative and sensitive analytical technique. *Applied Surface Science* **255**, 1498-1500, doi:10.1016/j.apsusc.2008.05.109 (2008).
- 57 Wirtz T., Mansilla C., Verdeil C. & Migeon H. N. Storing Matter: A new quantitative and sensitive analytical technique based on sputtering and collection of sample material. *Nuclear Instruments and Methods in Physics Research Section B: Beam Interactions with Materials and Atoms* **267**, 2586-2588, doi:10.1016/j.nimb.2009.05.044 (2009).
- 58 Garrison B. J., Postawa Z., Ryan K. E., Vickerman J. C., Webb R. P. & Winograd N. Internal energy of molecules ejected due to energetic C_{60} bombardment. *Analytical Chemistry* **81**, 2260-2267, doi:10.1021/ac802399m (2009).
- 59 Sheraz née Rabbani S., Razo I. B., Kohn T., Lockyer N. P. & Vickerman J. C. Enhancing ion yields in time-of-flight-secondary ion mass spectrometry: a comparative study of argon and water cluster primary beams. *Analytical Chemistry* **87**, 2367-2374, doi:10.1021/ac504191m (2015).

APPENDICES

REPRINTS OF PUBLICATIONS

In this section I present publications that the thesis is based on in the respective formats of the journals in which they originally appeared.

Article 1

Effect of Sample Thickness on Carbon Ejection from Ultrathin Graphite Bombarded by keV C₆₀

Goluński M. & Postawa Z.

Acta Physica Polonica A 132, 222-224 (2017)

doi:[10.12693/APhysPolA.132.222](https://doi.org/10.12693/APhysPolA.132.222)

Reproduced with no permission required from Acta Physica Polonica.

Effect of Sample Thickness on Carbon Ejection from Ultrathin Graphite Bombarded by keV C₆₀

M. GOLUNSKI AND Z. POSTAWA*

Institute of Physics, Jagiellonian University, S. Łojasiewicza 11, 30-348 Kraków, Poland

Molecular dynamics computer simulations are employed to investigate the effect of a sample thickness on the ejection process from ultrathin graphite. The thickness of graphite varies from 2 to 16 graphene layers and the system is bombarded by 10 keV C₆₀ projectiles at normal incidence. The ejection yield and the kinetic energy of emitted atoms are monitored. The implications of the results to a novel analytical approach in secondary ion mass spectrometry based on the ultrathin free-standing graphene substrates and transmission geometry are discussed.

DOI: [10.12693/APhysPolA.132.222](https://doi.org/10.12693/APhysPolA.132.222)

PACS/topics: Computer simulations, sputtering, graphene

1. Introduction

In recent years cluster ion beams have attracted increasing experimental and theoretical attention due to their capacity to enhance the ejection of large intact organic molecules in secondary ion mass spectrometry (SIMS) [1, 2]. One of the most successful clusters used in organic SIMS is C₆₀ fullerene [3]. In the typical SIMS geometry the detector is located at the same side of the target as the ion gun. Usually metal or semiconductor supports are used to deposit the investigated material. A novel SIMS configuration, using transmission orientation, has been proposed recently by a group from Texas A&M University [4]. In this orientation, the analysed organic material is deposited at one side of the ultrathin substrate, while another side is bombarded by cluster projectiles. It is argued that such geometry can be particularly attractive for the analysis of small amounts of organic material, molecular nano-objects and supramolecular assemblies.

So far only one simulation has been done for C₆₀ bombardment of graphene system [4]. Most of the existing simulations are performed on thick graphite [5–11]. Moreover, many of these studies concentrate on defect creation in the bombarded system rather than on material ejection. Theoretical studies of graphite sputtering by keV C₆₀ projectiles show that the sputtering yield is unexpectedly low [5, 6]. Krantzman et al. attribute this fact to a low atomic density of graphite [5] while the effect of layered structure of graphite was emphasised by Tian et al. [6]. It has been also shown that the membrane-like structure of graphite can be made to vibrate as a result of a low-energy cluster impact [4, 9]. The mesoscopic motion of created low-energy circular acoustic waves can stimulate ejection of small weakly bound organic molecules adsorbed at graphite. It has been found that large molecules can be ejected from metal or semiconductor substrates by simultaneous and correlated collisions with

ejecting substrate atoms [12, 13] or by energetic deformations occurring during crater unfolding [1, 14, 15]. We would like to test if a similar phenomenon can be observed at the ultrathin graphite.

The goal of this paper is, therefore, to supply theoretical description of processes that occur in the ultrathin graphite systems of various thickness bombarded by the keV C₆₀ projectile. We will concentrate on monitoring ejection of projectile and substrate atoms, testing viability of ultrathin graphite as a substrate for organic analysis.

2. Computer model

A detailed description of the molecular dynamics computer simulations used to model cluster bombardment can be found elsewhere [1]. Briefly, the motion of particles is determined by integrating the Hamilton equations of motion. The forces among carbon atoms in our system are described by a Reax-FF force field [16] splined at short distances with a Ziegler–Biersack–Littmark (ZBL) potential to properly describe high energy collisions. The shape and size of the samples are chosen based on visual observations of energy transfer pathways stimulated by impacts of C₆₀ projectiles. As a result, cylindrical samples with a radius of 200 Å are used. Samples with a thickness between 2 and 16 graphene layers with a high oriented pyrolytic graphite (HOPG) structure are bombarded by 10 keV C₆₀ projectiles that are directed at the bottom of the sample. Rigid and stochastic regions are used to simulate the thermal bath that keeps the sample at required temperature, to prevent reflection of pressure waves from the boundaries of the system, and to maintain the shape of the sample [1, 17]. The simulations are run at 0 K target and extend up to 4 ps, which is long enough to achieve saturation in the sputtering yield vs. time dependence. Sixty four randomly selected impact points located near the center of the sample are chosen to achieve statistically reliable data.

3. Results and discussion

Cross sectional views of the temporal evolution of 2, 8, and 16-layer systems bombarded by 10 keV C₆₀ projectiles are shown in Fig. 1. It is evident that C₆₀ clusters

*corresponding author; e-mail: zbigniew.postawa@uj.edu.pl

fragment into smaller pieces, almost immediately after the impact. At the 2-layer (2L) sample almost all projectile atoms penetrate through the substrate, as shown in Fig. 2a. Nevertheless, already a half of the primary kinetic energy is transferred to the sample, as shown in Fig. 2b. Most of this energy is carried away by the substrate particles emitted in the transmission direction. No sample atoms are sputtered. The projectile impact leads to a creation of cylindrical acoustic waves that propagate outward from the point of impact with a maximum amplitude of 1 Å.

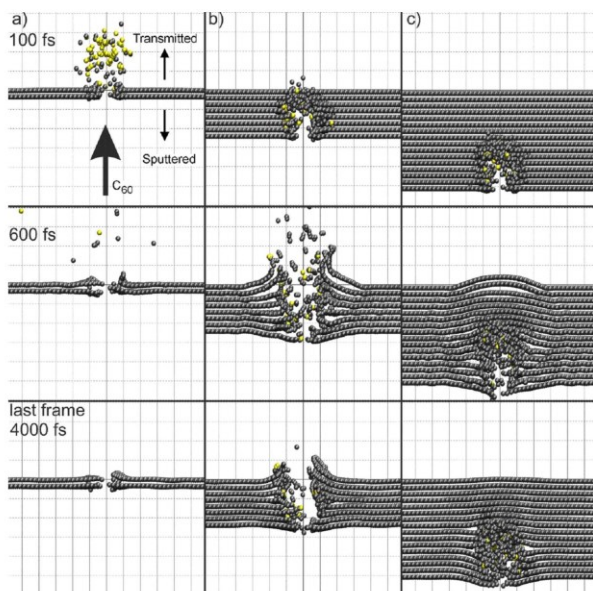


Fig. 1. Cross-sectional view of the temporal evolution of a typical collision event leading to ejection of atoms due to 10 keV C_{60} bombardment of a system composed of (a) 2, (b) 8, and (c) 16 graphene layers. Bright (yellow) spheres indicate the projectile atoms. A 1.5 nm wide slice of the system centred at the impact point is shown. The dashed lines in the background are separated by 10 Å. The arrows indicate directions of the primary beam, transmitted and sputtered atoms.

Much more dramatic alteration is observed for the 8L system. Projectile is more efficiently decelerated, depositing almost all its kinetic energy into the sample. As a result, the energized cylindrical volume is created along the projectile path. Bonds of many carbon atoms located in this volume are broken which means that these atoms are highly reactive. Soon after the projectile impact sample integrity is compromised. Graphene sheets are bent up in the direction of moving projectile and, for a few hundred fs, they are even separated from each other near the point of impact. Finally, cylindrical opening is formed in the sample. It is surrounded by an elevated rim at the top surface of the sample. No rim is formed at the bottom surface. The wall of the opening is hardened by interlayer new bonds that form between under-coordinated carbon atoms.

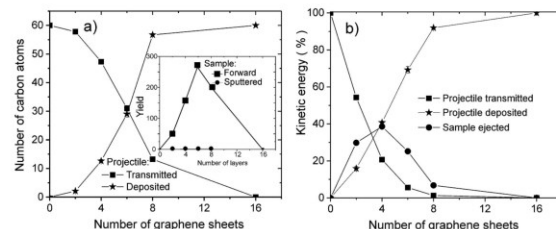


Fig. 2. Dependence of (a) the number of transmitted and sample-deposited projectile atoms and (b) the percentage of the primary kinetic energy carried by the transmitted projectile atoms, ejected sample atoms, as well as the energy deposited in the sample (projectile deposited) on the number of graphene sheets for 10 keV C_{60} projectiles at normal incidence. Inset to part (a) shows dependence of a number of sample atoms ejected in the forward and sputtered directions on the sample thickness.

All bombarded systems, except for 16-layer graphite, are perforated by a C_{60} projectile. The number of projectile atoms penetrating the substrate decreases with a thickness of the sample, as indicated in Fig. 2a. At the same time, the number of projectile atoms getting implanted in the sample increases in the inverse way, as fewer than one projectile atom is backreflected on average. The sputtering yield is almost zero for all investigated systems, as shown in the inset to Fig. 2a. It has been proved that the layered structure of graphite is mostly responsible for a lack of sputtering [6]. Computer simulations indicate that the energy transfer in graphite is highly anisotropic and occurs predominantly along graphene sheets. Not much energy is transferred in the vertical direction. Consequently, energy that normally would be directed towards the surface is now laterally channelled and does not contribute to particle ejection.

Despite a very low sputtering yield, the ejection of substrate atoms in the transmission direction can be quite significant. These particles are ejected by collisions with the projectile atoms very soon after the projectile impact before the deposited energy is effectively drained out of the altered volume. As shown in the inset of Fig. 2a, the dependence of the ejection yield on the substrate thickness is non-monotonic. At first, the signal increases as more carbon atoms become available for ejection when the sample is getting thicker. However, at the same time more primary kinetic energy has to be sacrificed to penetrate through a thicker solid. As a result, less energy is available near the surface from where the ejection occurs and ultimately the overall signal decreases.

Our results indicate that such ultrathin graphite substrates supports can have several advantages over the traditional metal or semiconductor substrates for analysis of small amounts of organic material. Firstly, the extremely small thickness of the support results in small amounts of emitted substrate material. As a result, there is a minimal interference between the substrate and the analyzed signal. From this point of view the 2L system is the most optimal. In this system also a large portion of the

primary kinetic energy can be transmitted to the organic overlayer in the direction towards the detector, increasing a chance that a small amount of analyte can be recorded. However, the energetics of this transfer is also important. In a 2L system both projectile and sample atoms ejected in the transmission direction have high kinetic energies. A rough estimate based on the data presented in Fig. 2 implies that the average kinetic energy of these atoms is around 100 eV (≈ 5500 eV/58 atoms) for the projectile and 60 eV (≈ 3000 eV/50 atoms) for the sample atoms. These values are several times larger than a bond energy in organic molecules. As a result, the molecules that will be hit by these atoms will be fragmented. Apart from ejection of atoms, there is not much movement present in the 2L system. The energy of acoustic waves is admittedly sufficient to eject small molecules but will not be sufficient to eject a massive particle. All these arguments indicate that 2L systems may not be the best choice.

Much more promising is the 8L system. As shown in Fig. 1b, unfolding of the topmost graphene sheet can work as a catapult that will hurl large molecules adsorbed in this region into the vacuum. Such phenomenon is one of the processes responsible for ejection of large molecules from the metal substrates where unfolding of the crater rims serves as a catapult [1, 14, 15]. There is a considerable amount of energy associated with this movement which means that even very large molecules can be uplifted. However, in graphite this movement extends to a much larger lateral distance from the point of impact as compared to the analogous phenomenon present in metals [1, 14, 17]. As a result, this mechanism will be more effective in ultrathin graphite. A larger number of adsorbed molecules can be ejected by a single projectile impact making analysis of small amounts of organic material viable. Catapult-like ejection of organic molecules can be additionally enhanced by correlated collisions with ejecting substrate atoms [12, 13]. As can be deduced for Fig. 2 many substrate atoms are ejected with the average kinetic energy of 3 eV which is low enough not to fragment molecules. As shown in Fig. 1c, perforation of ultrathin graphite is not necessary to stimulate molecular emission. The upper surface of the 16L substrate buckles up during the projectile deceleration. This motion potentially can also cause ejection of large molecules that are physisorbed at the upper surface.

4. Conclusions

Molecular dynamics computer simulations have been performed to study the effect of the sample thickness on the ejection efficiency of particles emitted from the ultrathin graphene layers bombarded by 10 keV C_{60} projectiles. The number of transmitted projectile atoms decreases with the thickness of the sample. All atoms that are not transmitted are being implanted in the sample as almost no backreflection is present due to a lack of vertical motion in the system and strong covalent C–C bonds. The dependence of a number of sample atoms ejected in the transmission direction on the layer thickness has a

maximum at a four layer system. Such behavior can be explained by an interplay between the amount of material available for ejection and the energy available near the surface from where ejection occurs. No sputtering is observed which is attributed to a lower atomic density and the layered structure of graphite. It has been shown that ultrathin graphite can be an interesting support for organic SIMS where a small amount of organic material is probed.

Acknowledgments

The authors gratefully acknowledge financial support from the Polish National Science Center, Program No. 2013/09/B/ST4/00094 and 2015/19/B/ST4/01892.

References

- [1] B.J. Garrison, Z. Postawa, *Mass Spectrom. Rev.* **27**, 289 (2008).
- [2] N. Winograd, *Anal. Chem.* **77**, 142A (2005).
- [3] D. Weibel, S. Wong, N. Lockyer, P. Blenkinsopp, R. Hill, J.C. Vickerman, *Anal. Chem.* **75**, 1754 (2003).
- [4] S.V. Verkhoturov, S. Geng, B. Czerwinski, A.E. Young, A. Delcorte, E.A. Schweikert, *J. Chem. Phys.* **143**, 164302 (2015).
- [5] K.D. Krantzman, R.P. Webb, B.J. Garrison, *Appl. Surf. Sci.* **255**, 837 (2008).
- [6] J.T. Tian, T. Zheng, J.Y. Yang, S.Y. Kong, J.M. Xue, Y.G. Wang, K. Nordlund, *Appl. Surf. Sci.* **337**, 6 (2015).
- [7] M. Kerford, R.P. Webb, *Nucl. Instrum. Methods Phys. Res. B* **153**, 270 (1999).
- [8] M. Kerford, R.P. Webb, *Nucl. Instrum. Methods Phys. Res. B* **180**, 44 (2001).
- [9] R.P. Webb, *Radiat. Eff. Def. Solids* **162**, 567 (2007).
- [10] R.P. Webb, M. Kerford, M. Kappes, G. Brauchle, *Radiat. Eff. Def. Solids* **142**, 23 (1997).
- [11] C. Anders, H. Kirihaata, Y. Yamaguchi, H.M. Urbassek, *Nucl. Instrum. Methods Phys. Res. B* **255**, 247 (2007).
- [12] B.J. Garrison, A. Delcorte, K.D. Krantzman, *Acc. Chem. Res.* **33**, 69 (2000).
- [13] R. Chatterjee, Z. Postawa, N. Winograd, B.J. Garrison, *J. Phys. Chem. B* **103**, 151 (1999).
- [14] Z. Postawa, *Appl. Surf. Sci.* **231**, 22 (2004).
- [15] B. Czerwinski, R. Samson, B.J. Garrison, N. Winograd, Z. Postawa, *Vacuum* **81**, 167 (2006).
- [16] L.C. Liu, Y. Liu, S.V. Zybin, H. Sun, W.A. Goddard, *J. Phys. Chem. A* **115**, 11016 (2011).
- [17] Z. Postawa, B. Czerwinski, M. Szewczyk, E.J. Smiley, N. Winograd, B.J. Garrison, *Anal. Chem.* **75**, 4402 (2003).

Article 2

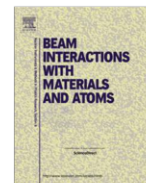
Effect of substrate thickness on ejection of phenylalanine molecules adsorbed on free-standing graphene bombarded by 10 keV C₆₀

Goluński M., Verkhoturov S. V., Verkhoturov D. S., Schweikert E. A. & Postawa Z.

Nuclear Instruments and Methods B 393, 13-16 (2017)

doi:[10.1016/j.nimb.2016.09.006](https://doi.org/10.1016/j.nimb.2016.09.006)

Reproduced with permission of Elsevier.



Effect of substrate thickness on ejection of phenylalanine molecules adsorbed on free-standing graphene bombarded by 10 keV C₆₀

M. Golunski^a, S.V. Verkhoturov^b, D.S. Verkhoturov^b, E.A. Schweikert^b, Z. Postawa^{a,*}

^a Institute of Physics, Jagiellonian University, ul. Lojasiewicza 11, 30-348 Krakow, Poland

^b Department of Chemistry, Texas A&M University, College Station, TX 77840, USA

ARTICLE INFO

Article history:

Received 31 July 2016

Received in revised form 17 August 2016

Accepted 2 September 2016

Available online 1 October 2016

Keywords:

Computer simulations

Sputtering

Cluster projectiles

Graphene

Organic overlayers

ABSTRACT

Molecular dynamics computer simulations have been employed to investigate the effect of substrate thickness on the ejection mechanism of phenylalanine molecules deposited on free-standing graphene. The system is bombarded from the graphene side by 10 keV C₆₀ projectiles at normal incidence and the ejected particles are collected both in transmission and reflection directions. It has been found that the ejection mechanism depends on the substrate thickness. At thin substrates mostly organic fragments are ejected by direct collisions between projectile atoms and adsorbed molecules. At thicker substrates interaction between deforming topmost graphene sheet and adsorbed molecules becomes more important. As this process is gentle and directionally correlated, it leads predominantly to ejection of intact molecules. The implications of the results to a novel analytical approach in Secondary Ion Mass Spectrometry based on ultrathin free-standing graphene substrates and a transmission geometry are discussed.

© 2016 Elsevier B.V. All rights reserved.

1. Introduction

In recent years, cluster ion beams have attracted increasing experimental and theoretical attention due to their capacity to enhance ejection of large intact organic molecules in Secondary Ion Mass Spectrometry (SIMS) [1,2]. One of the most successful clusters used in organic SIMS is C₆₀ fullerene [3]. In a typical SIMS geometry the detector is located on the same side of the target as the ion gun. Usually metal or semiconductor supports are used to deposit the investigated material. A novel SIMS configuration, using transmission orientation, has been proposed recently [4,5]. In this orientation, the analysed organic material is deposited on one side of the ultrathin substrate, while another side is bombarded by cluster projectiles. It is argued that such geometry can be particularly attractive for analysis of small amounts of organic material, molecular nano-objects and supramolecular assemblies [5].

There are several simulations performed on C₆₀ bombardment of graphene and graphite [4,6–13]. However, most of these studies concentrate on defect creation in the bombarded system rather than on material ejection. Theoretical studies of sputtering of graphite by keV C₆₀ projectiles show that the sputtering yield is low

[11,13]. Krantzman et al. have attributed this fact to a low atomic density of graphite [11], while the effect of the layered structure of graphite was emphasised by Tian et al. [13]. It also has been shown that the membrane-like structure of graphite can be made to vibrate as a result of a cluster impact [4,8,9]. The mesoscopic motion of created circular acoustic waves can stimulate ejection of small weakly bound molecules [8,9]. Although this mechanism may not be efficient for uplifting heavier molecules as it may not provide enough energy, it has been postulated that vibrational energy can be utilized to stimulate ionization [4]. Computer simulations of bombardment of organic molecules deposited on metal substrates show that intact molecules are emitted by low-energy collisions with ejecting substrate or projectile atoms [14], and/or by surface deformations occurring during crater formation [15]. As sputtering of graphite is different from sputtering of metals [13,16] we would like to check if similar phenomena are present for the ultrathin graphite. Furthermore, the only theoretical study performed so far with C₆₀ impacts in transmission geometry was done on a system of a constant thickness [4]. The goal of this paper is, therefore, to investigate processes that lead to ejection of organic molecules deposited on ultrathin free-standing graphene of various thickness bombarded by 10 keV C₆₀ projectiles in a transmission orientation.

* Corresponding author.

E-mail address: zbigniew.postawa@uj.edu.pl (Z. Postawa).

2. Computer model

A detailed description of the molecular dynamics computer simulations used to model cluster bombardment can be found elsewhere [1]. Briefly, the motion of particles is determined by integrating Hamilton's equations of motion. The forces among atoms in the system are described by a Reax-FF force field [17] splined at short distances with a ZBL potential to properly describe high energy collisions. The shape and size of the samples are chosen based on a visual observation of energy transfer pathways stimulated by impact of C_{60} projectiles. As a result, cylindrical samples with a diameter of 400 Å are used. Substrates with a thickness ranging from 2 to 16 graphene layers with a HOPG structure are bombarded by 10 keV C_{60} projectiles that are directed at the bottom of the sample. Ten phenylalanine molecules are deposited on the top of the graphene substrate, as shown in Fig. 1. Molecules are placed away from each other to mimic submonolayer coverage. They are also located at different distance from the impact zone to probe the influence of this parameter on the mechanism of ejection. Phenylalanine molecules are selected as they are important amino acids, they are simple, yet consist of most elements that are present in biomaterials. Particles ejected both in direction of the primary beam (transmission direction) and in the opposite direction (reflection direction) are collected. Rigid and stochastic regions are used to simulate the thermal bath and to prevent reflection of pressure waves from the boundaries of the system [1,18]. The simulations are run at 0 K target temperature in an NVE ensemble and extend up to 10 ps, which is long enough to achieve saturation in the ejection yield vs time dependence. Eight impact points within the linear impact zone represented by white line in Fig. 1 are chosen to achieve statistically more reliable data.

3. Results and discussion

Numbers of particles ejected from systems of various thickness by 10 keV C_{60} impacts are given in Table 1. While it is evident that the yields depend on substrate thickness, the actual dependence is different for different particles. The number of projectile atoms penetrating the sample decreases with a thickness of the substrate. Interestingly, almost no projectile atoms are backscattered even from the thickest system, which means that non-ejected atoms are implanted into the sample. The ejection yield of substrate

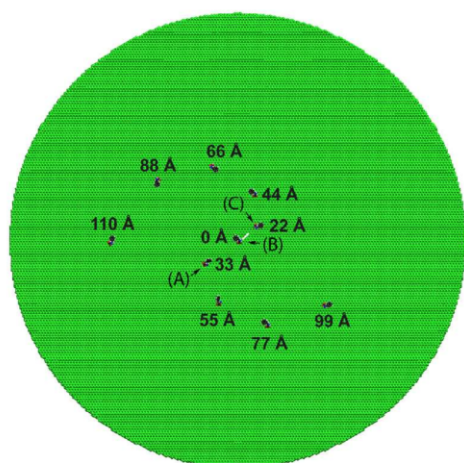


Fig. 1. The model system used to study ejection processes of phenylalanine molecules deposited on free-standing graphene. Numbers indicate distance from the centre of the system. The white line depicts impact points.

atoms in the transmission direction depends non-monotonically on the substrate thickness. At first, the signal increases as more carbon atoms become available for ejection when the sample is getting thicker. However, with the increase of the substrate thickness more primary kinetic energy is sacrificed to penetrate through a thicker solid. As a result, less energy is available near the surface from where the ejection occurs, and, ultimately, the signal decreases. Atoms originally located in all layers are recorded in the ejected flux, although ejection from the topmost layer is dominant. A similar dependence on the substrate thickness occurs for atoms originating from phenylalanine molecules, however, the reason of such behavior has to be different than for substrate atoms as the number of molecules available for ejection is constant. For substrates composed of up to 6 graphene layers predominantly molecular fragments are ejected. For thick substrates ($\geq 12L$) the ejected flux is composed entirely from intact molecules.

Cross sectional views of the temporal evolution of 2, 8 and 16-layer systems are shown in Fig. 2 to identify processes responsible for molecular ejection. In all systems C_{60} projectiles decompose into smaller pieces almost immediately after the impact. As indicated in Table 1 at the 2-layer (2L) sample almost all projectile atoms penetrate through the substrate. Nevertheless, even in this system a projectile-graphene interaction is surprisingly strong, as already a half of the primary kinetic energy is transferred to the substrate. Most of this energy is carried away by ejected substrate particles. Ejection of both projectile and substrate atoms is forward directed. Ejecting atoms can collide with organic molecules causing their ejection. However, the average kinetic energy of ejected projectile and substrate atoms is high. As a result, such collisions lead to molecular fragmentation, as seen for molecule B in Fig. 2a. The projectile impact also leads to a creation of cylindrical acoustic waves that propagate in the graphene outward from the point of impact with a maximum amplitude of 1 Å. It was reported that these waves are capable to uplift benzene and cumene molecules [8,9]. However, no similar phenomenon has been observed in our study.

A dramatic alteration of a substrate structure caused by C_{60} impact is observed at thicker systems, as shown in Fig. 2b for the 8L graphene. The projectile is more efficiently decelerated, depositing almost all of its primary kinetic energy into the substrate. Part of this energy is used to eject substrate atoms in the forward direction. The remaining part is used to deform the substrate. Soon after the projectile impact substrate integrity is compromised. Near the point of impact graphene sheets become separated from each other and bend up in a direction parallel to the movement of incoming projectile. Finally, a cylindrical opening is formed surrounded by elevated rim at the top surface of the sample.

While the average kinetic energy of ejected projectile and substrate atoms is smaller than in the 2L system, it is still high enough to fragment molecule B. However, the unfolding of graphene sheets, which works like a catapult can also eject other molecules, as visible for molecule C. As the process is gentle and occurs in a coordinated fashion, the ejected molecules are not fragmented. This process supplements molecular ejection by collisions leading to an increase of the organic signal and to the appearance of intact molecules in the sputtered flux. A similar mechanism was observed during crater formation at the metal surfaces bombarded by cluster projectiles [15]. However, surface deformation observed in graphene extends to a much larger lateral distance making this process much more efficient than in metals. It is also worth mentioning that catapult-like sheets movement is almost absent at the surface directly hit by a projectile. This observation indicates that a transmission geometry is a better choice for efficient ejection of adsorbed molecules, at least, for ultra-small coverages.

Table 1

The total number of atoms ejected in transmission (Ejected) and reflection (Sputtered/Reflected) directions, and the average kinetic energy KE_{ave} of atoms ejected from a free-standing graphene of various thickness bombarded by 10 keV C_{60} projectiles. The term “organic atoms” relates to atoms of phenylalanine molecules. The numbers in round brackets depict relative contribution of intact phenylalanine molecules in the ejected flux.

Number of substrate layers	Projectile atoms			Substrate atoms			“Organic atoms”
	Ejected	Reflected	KE_{ave} [eV]	Ejected	Sputtered	KE_{ave} [eV]	Ejected
2	57 ± 1	0.0	89	49 ± 2	0.13 ± 0.1	59	21 ± 4 (0%)
4	46 ± 1	0.2	44	155 ± 4	1.1 ± 0.5	24	39 ± 5 (7%)
6	32 ± 2	0.2	16	259 ± 5	0.9 ± 0.6	10	49 ± 4 (23%)
8	12 ± 1	0.3	13	205 ± 13	3.3 ± 1.0	3	60 ± 4 (62%)
12	0.2 ± 0.2	0.5	5	0.3 ± 0.2	5 ± 2	2	81 ± 5 (100%)
16	0.0	1.2	0	0.0	9 ± 3	0	64 ± 5 (100%)

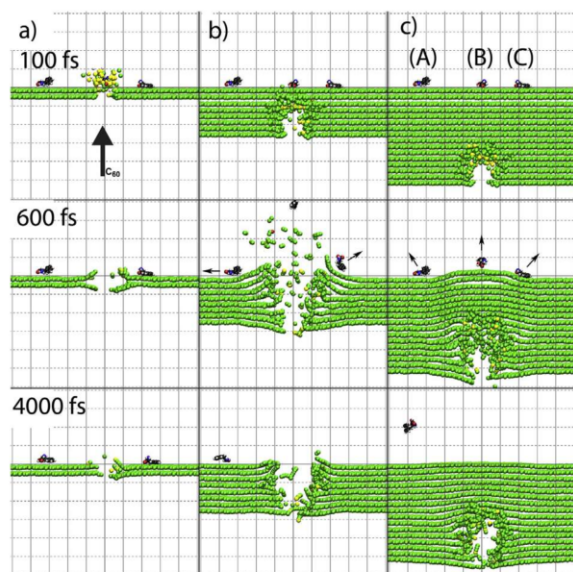


Fig. 2. Cross-sectional view of the temporal evolution of a typical collision event leading to ejection of atoms due to 10 keV C_{60} bombardment of a system composed from phenylalanine molecules deposited on (a) 2, (b) 8 and (c) 16 graphene layers. A slice 15 Å wide of the system centred at the impact point is shown. The dashed lines in the background are separated by 10 Å.

The process of graphene unfolding becomes less efficient with a further increase of a substrate thickness. As shown in Fig. 2c, the 16L substrate is too thick to be perforated by a 10 keV C_{60} projectile. In this case no unfolding is present. It is interesting to note that all projectile atoms become implanted inside the substrate. Such behavior is different than observed during C_{60} bombardment of metals, where almost all projectile atoms are backscattered into the vacuum [16,18]. There is also a big difference in sputtering yields recorded from these two materials. The sputtering yield is large for metals and low for graphite. For instance, a sputtering yield of 41 ± 3 was reported for 20 keV C_{60} impact on graphite [13], while ejection of almost 500 atoms was observed from Ag (111) at the same impact conditions [16]. Barely 9 carbon atoms are sputtered on average, i.e. ejected in reflection direction, from our thickest system bombarded by 10 keV C_{60} . The different behavior of implantation and sputtering processes is a consequence of a different redistribution of the deposited energy in these two systems. In metals, C_{60} is quickly decelerated depositing its kinetic energy close to the bombarded surface [1,16]. The density of deposited energy is high and the energy is redistributed initially by spherical pressure pulses. Atoms are relocated and a crater is formed. Substrate atoms are ejected from the corona of the crater by a fluid flow motion, which is supplemented at later time by atom effusion from the inside of a formed crater [15,16,19]. Most

of impinging projectile atoms either immediately rebound into the vacuum when colliding with heavier Ag surface atoms, or are implanted inside the volume, where the crater will be formed, and will be ejected during this process.

The behavior of graphite is different. Firstly, graphite has a low number density which leads to a lower density of deposited energy. As a result, both the number of carbon atoms taking place in the flow and the strength of the outward pressure pulse is reduced [11,19]. However, the most critical factor for sputtering is the layered structure of graphite [13]. Computer simulations show that the energy transfer is more efficient along the graphene sheets than in the vertical direction [9,13]. Consequently, energy that normally would be directed towards the surface and contribute to particle ejection, is now laterally channeled away. Finally, the binding between carbon atoms in graphite is stronger than binding between C and Ag atoms. A stronger binding combined with a lower efficiency of vertical movement is responsible for the absence of backreflection of projectile atoms in graphite.

Although projectile atoms are not penetrating through the substrate, the upper surface of the 16L system bulges outward during projectile deceleration as shown in Fig. 2c. This motion is energetic enough to stimulate ejection of physisorbed phenylalanine molecules, as shown at the bottom panel. The efficiency of this process depends on the substrate thickness. One may expect it to be the most efficient for substrates where the largest fraction of the primary kinetic energy is delivered to the largest area of the topmost graphene sheet. As the bulging process is gentle and no energetic projectile or substrate atoms are ejected, only intact molecules are emitted. The simulations presented here are done for a single projectile kinetic energy. It would be interesting to verify how the primary kinetic energy influences ejection processes. For instance, is there a scaling effect of energy versus number of layers for the cases shown in Fig. 2? This topic is currently investigated and will be published elsewhere.

4. Conclusions

Molecular dynamics computer simulations have been performed to study the effect of the sample thickness on the ejection mechanism of phenylalanine molecules deposited on free-standing graphene bombarded by 10 keV C_{60} . The mechanism of molecular ejection depends on the substrate thickness. For thin substrates, which are perforated by projectile atoms, collisions between projectile/substrate atoms and adsorbed molecules is the main mechanism of molecular ejection. At thicker substrates the catapult-like action of the unfolding graphene sheets becomes important. The efficiency of this process depends on the substrate thickness reaching the maximum for 8-layer system, at least, for 10 keV C_{60} projectiles. When the graphite layer becomes too thick to be perforated, the ejection of adsorbed molecules occurs due to a bulging out of the surface. Although acoustic waves are created by the C_{60} impact, interaction with these waves does not lead to ejection of phenylalanine molecules.

Based on our results a few comments can be made about applicability of ultrathin graphite substrates for SIMS. Before doing this it should be pointed out, however, that the data presented in this paper relate to the sputtering of neutral organic molecules while ions are recorded in SIMS. To simulate ion emission, ionization and neutralization processes should be included into the model calculations, which is still an unresolved problem. One should refrain, therefore, from quantitative comparisons between emission enhancements of ions and neutrals. However, analysis of the structural modifications of the bombarded system and its influence on particle emission is applicable to the study of both ions and neutrals. Our study confirms that graphene supports have several advantages, as compared to traditional metal or semiconductor substrates especially for analysis of sub-monolayer amounts of analyte. Firstly, the extremely small thickness of the support results in a small amount of emitted substrate material especially for 2L or 4L systems. As a result, there is a minimal interference between substrate and analyzed signal. Furthermore, the emission processes favor ejection of molecules towards the detector improving detection efficiency.

Finally, it also should be stressed that our findings are valid for sub-monolayer coverages. For thicker organic overlayers, a significant portion of the primary kinetic energy will be directly deposited inside the organic layer. The propagation of this energy within the overlayer will lead to molecular ejection and, most probably, will dominate ejection process. However, this phenomenon will be examined in future work.

Acknowledgments

The authors gratefully acknowledge financial support from the Polish National Science Center, Program No. 2013/09/B/ST4/00094,

2015/19/B/ST4/01892 and from the US National Science Foundation grant CHE-1308312.

References

- [1] B.J. Garrison, Z. Postawa, *Mass Spectrom. Rev.* 27 (2008) 289–315 (and references therein).
- [2] N. Winograd, *Anal. Chem.* 77 (2005) 142A–149A (and references therein).
- [3] D. Weibel, S. Wong, N. Lockyer, P. Blenkinsopp, R. Hill, J.C. Vickerman, *Anal. Chem.* 75 (2003) 1754–1764.
- [4] S.V. Verkhoturov, S. Geng, B. Czerwinski, A.E. Young, A. Delcorte, E.A. Schweikert, *J. Chem. Phys.* 143 (2015) 164302-1.
- [5] M.J. Eller, C.K. Liang, S. Della-Negra, A.B. Clubb, H. Kim, A.E. Young, E.A. Schweikert, *J. Chem. Phys.* 142 (2015) 044308.
- [6] R. Smith, R.P. Webb, *Proc. R. Soc. London, Ser. A* 441 (1993) 495–499.
- [7] M. Kerford, R.P. Webb, *Nucl. Instrum. Methods Phys. Res., Sect. B* 153 (1999) 270–274.
- [8] M. Kerford, R.P. Webb, *Nucl. Instrum. Methods Phys. Res., Sect. B* 180 (2001) 44–52.
- [9] R.P. Webb, *Radiat. Eff. Defects Solids* 162 (2007) 567–572.
- [10] C. Anders, H. Kirihata, Y. Yamaguchi, H.M. Urbassek, *Nucl. Instrum. Methods Phys. Res., Sect. B* 255 (2007) 247–252.
- [11] K.D. Krantzman, R.P. Webb, B.J. Garrison, *Appl. Surf. Sci.* 255 (2008) 837–840.
- [12] S.J. Zhao, J.M. Xue, L. Liang, Y.G. Wang, S. Yan, *J. Phys. Chem. C* 116 (2012) 11776–11782.
- [13] J.T. Tian, T. Zheng, J.Y. Yang, S.Y. Kong, J.M. Xue, Y.G. Wang, K. Nordlund, *Appl. Surf. Sci.* 337 (2015) 6–11.
- [14] B.J. Garrison, A. Delcorte, K.D. Krantzman, *Acc. Chem. Res.* 33 (2000) 69–77.
- [15] Z. Postawa, *Appl. Surf. Sci.* 231 (2004) 22–28.
- [16] Z. Postawa, B. Czerwinski, M. Szewczyk, E.J. Smiley, N. Winograd, B.J. Garrison, *J. Phys. Chem. B* 108 (2004) 7831–7838.
- [17] L.C. Liu, Y. Liu, S.V. Zybin, H. Sun, W.A. Goddard, *J. Phys. Chem. A* 115 (2011) 11016.
- [18] Z. Postawa, B. Czerwinski, M. Szewczyk, E.J. Smiley, N. Winograd, B.J. Garrison, *Anal. Chem.* 75 (2003) 4402–4407.
- [19] M.F. Russo, B.J. Garrison, *Anal. Chem.* 78 (2006) 7206–7210.

Article 3

Effect of kinetic energy and impact angle on carbon ejection from a free-standing graphene bombarded by kilo-electron-volt C₆₀

Goluński M. & Postawa Z.

Journal of Vacuum Science & Technology B 36, 03F112 (2018)

doi:[10.1116/1.5019732](https://doi.org/10.1116/1.5019732)

Reprinted with permission from J. Vac. Sc. & Tech. B 2018, 36, 03F112. Copyright 2018, American Vacuum Society.

Effect of kinetic energy and impact angle on carbon ejection from a free-standing graphene bombarded by kilo-electron-volt C₆₀

Mikolaj Golunski and Zbigniew Postawa^{a)}

Institute of Physics, Jagiellonian University, ul. Lojasiewicza 11, 30-348 Kraków, Poland

(Received 15 December 2017; accepted 1 February 2018; published 16 February 2018)

Molecular dynamics computer simulations are employed to investigate the effect of the kinetic energy and impact angle on the ejection process from a free-standing graphene of thickness between 1 and 16 layers. The target is bombarded by C₆₀ projectiles with kinetic energy between 5 and 40 keV and the impact angle ranging between 0° and 80°. The yields, kinetic energies, and ejection directions of atoms are monitored. Computer simulations are used to point to optimal conditions when a soft ejection of unfragmented molecules may occur, which may be invaluable information for the development of secondary ion mass spectrometry based on a transmission geometry.

Published by the AVS. <https://doi.org/10.1116/1.5019732>

I. INTRODUCTION

In recent years, cluster ion beams have attracted increasing experimental and theoretical attention due to their capacity to enhance the ejection of large intact organic molecules in secondary ion mass spectrometry (SIMS).^{1,2} One of the most successful clusters used in organic SIMS is C₆₀ fullerene.³ In a typical SIMS geometry, the detector is located on the same side of the target as the ion gun. Usually, metal or semiconductor supports are used to deposit the analyzed material. A novel SIMS configuration, based on ultrathin free-standing graphene substrates and a transmission geometry, was proposed recently by a group from Texas A&M University.^{4,5} In this approach, the analyzed organic material is deposited at one side of the ultrathin substrate, while another side is bombarded by cluster projectiles. It is argued that such geometry can be particularly attractive for analysis of small amounts of organic material, molecular nano-objects, and supramolecular assemblies. It has also been reported that the formation of negative ions emitted from ultrathin organic films deposited on a free-standing graphene⁴ or covered by a graphene sheet⁶ is enhanced.

While the experimental data showing the advantages of graphene application to SIMS are convincing, much less is known about the processes leading to material ejection from this system. Only a few simulations have been performed so far for C₆₀ bombardment of a free-standing graphene.^{4,5,7–10} Most of the existing simulations modeled projectile impact at graphite.^{11–18} Moreover, many of these studies concentrate on defect creation in the bombarded system rather than on material ejection. Theoretical studies of sputtering of graphite by kilo-electron-volt C₆₀ projectiles show that the sputtering yield is unexpectedly low.^{17,18} Krantzman *et al.* attributed this fact to a low atomic density of graphite,¹⁷ while the effect of the layered structure of graphite was emphasized by Tian *et al.*¹⁸ It has also been shown that the membranelike structure of graphite can vibrate after a low-energy cluster impact.^{4,16} Similar vibrations have been

observed in a single layer of graphene.^{19,20} It has been argued that the energy stored in this process can be sufficient to uplift molecules adsorbed on a graphite.^{14,16}

The effect of the graphene substrate thickness on the ejection process has been recently investigated for a single primary kinetic energy and a single impact angle.⁸ In that study, free-standing graphene substrates, 2–16 layer thick, were bombarded by 10 keV C₆₀ projectiles at normal incidence. It has been shown that the yield depends on the sample thickness in a nonmonotonic way and the shape of this dependence is a consequence of an interplay between the amount of material available for ejection and the energy deposited in the subsurface regions by impinging projectiles. The goal of this paper is to investigate the effect of the kinetic energy and the impact angle on the ejection processes.

II. COMPUTER MODEL

The molecular dynamics (MD) computer simulations were used to model cluster bombardment. Briefly, the movement of particles is determined by integrating Hamilton's equations of motion. The forces among carbon atoms in the system are described by the ReaxFF-Ig force field,²¹ which allows for the creation and breaking of covalent bonds. This potential is splined at short distances with a Ziegler-Biersack-Littmark potential²² to properly describe high energy collisions. A detailed description of the MD method can be found elsewhere.¹ The shape and size of the samples are chosen based on visual observations of energy transfer pathways stimulated by impacts of C₆₀ projectiles.⁸ As a result, cylindrical samples with a diameter of 40 nm are used. Samples with a thickness between 1 (1L) and 16 (16L) graphene layers with a highly oriented pyrolytic graphite structure are bombarded by C₆₀ directed at the bottom of the sample. The kinetic energy and the impact angle of the projectile are changed to investigate the effect of these parameters on the particle ejection process. Particles ejected both in the direction of the primary beam (transmission direction) and in the opposite direction (sputtering direction) are collected, as shown schematically in Fig. 1. Rigid and stochastic regions are used to simulate the thermal bath that keeps the sample at required temperature, to prevent

^{a)} Author to whom correspondence should be addressed; electronic mail: zbigniew.postawa@uj.edu.pl

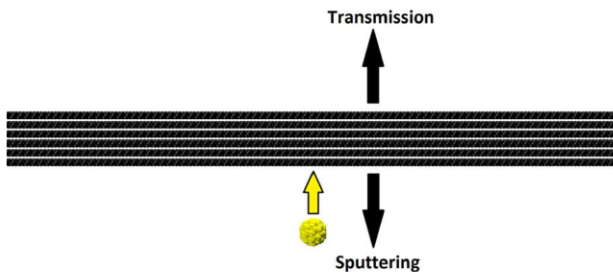


FIG. 1. (Color online) Schematic side view of the modeled system. The bright (yellow) arrow indicates the impact direction. Black arrows show the transmission and sputtering directions mentioned throughout this paper.

reflection of pressure waves from the boundaries of the system, and to maintain the shape of the sample.^{1,23} The simulations are run at a target temperature of 0 K in an NVE ensemble and extend up to 10 ps, which is long enough to achieve saturation in the ejection yield versus time dependence. Between 8 and 32 randomly selected impact points located near the center of the sample are chosen to achieve statistically reliable data. Simulations are performed with the large-scale atomic/molecular massively parallel simulator code²⁴ which was modified to better describe sputtering conditions.

III. RESULTS AND DISCUSSION

The effect of the substrate thickness and primary kinetic energy on the yield of carbon atoms ejected from free-

standing graphene systems bombarded by C_{60} projectiles at normal incidence is shown in Fig. 2(a). The yield initially increases with the increase in the surface thickness for substrate atoms ejecting in both transmission and sputtering directions. Subsequently, the yield decreases for atoms ejected in the transmission direction and it saturates for sputtered atoms. The primary kinetic energy does not influence the shape of the yield versus thickness dependence. However, bombardment by a more energetic projectile leads to a stronger emission and shifts the position of the maximum in the yield versus thickness dependence to thicker systems. Our results demonstrate a direct proportionality between the position of the maximum and the projectile kinetic energy.

Variation of the substrate thickness has a different impact on ejection of projectile atoms. The yield decreases monotonically with the sample thickness for atoms ejected in the transmission direction. The yield of backscattered projectile atoms is very low and does not exhibit a consistent dependence on the substrate thickness. These observations indicate that projectile atoms are being trapped inside the graphene substrate. The magnitude of this process increases with the sample thickness. More energetic projectiles are able to perforate thicker substrates. As a result, the yield versus thickness dependence broadens for more energetic projectiles.

Almost all projectile atoms penetrate through a thin substrate, as shown in the inset of Fig. 2(a). However, even in this case, the projectile-graphene interaction is significant, especially for low-energy projectiles. For instance, for 5 keV C_{60} ,

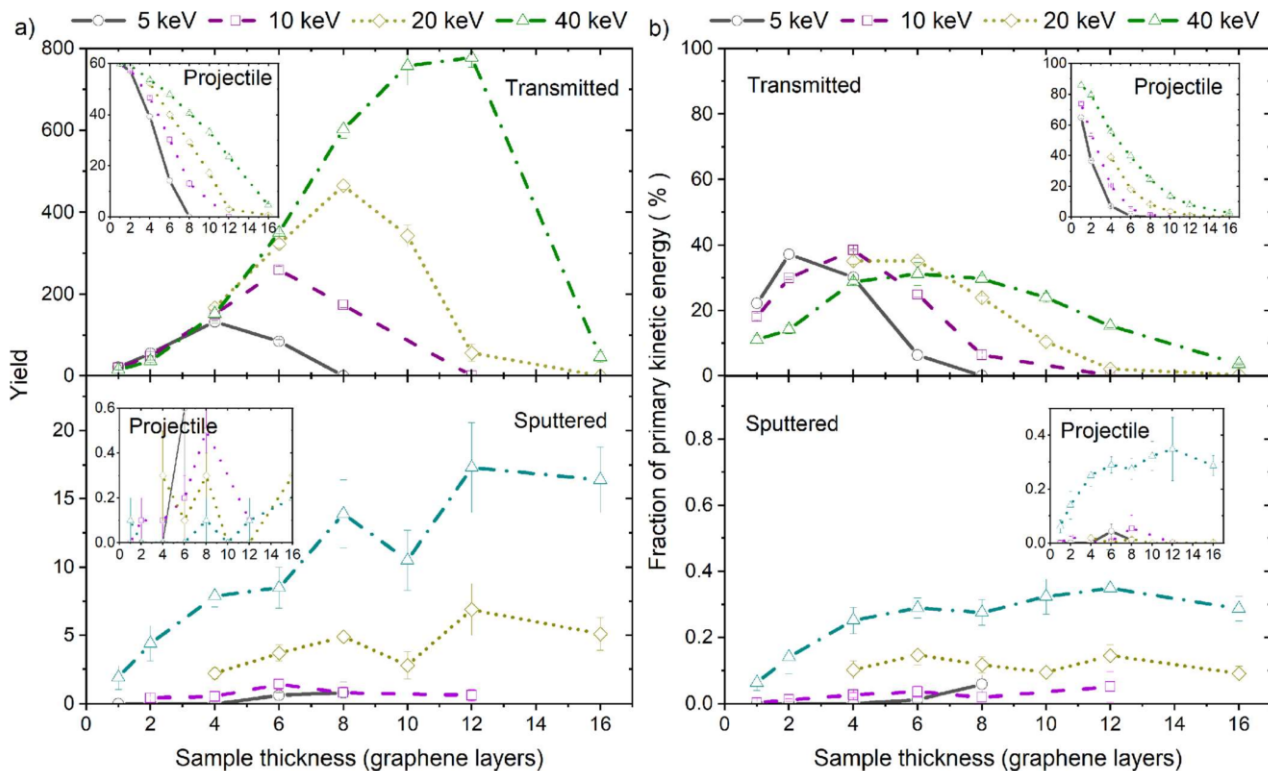


FIG. 2. (Color online) Dependence of (a) the ejection yield and (b) the fraction of primary kinetic energy carried away by particles emitted in the transmission (top) and sputtering (bottom) directions on the thickness of the sample bombarded by 5, 10, 20, and 40 keV C_{60} projectiles at normal incidence. Main graphs represent the atoms ejected from the sample, while the insets depict projectile atoms.

almost 40% of the primary kinetic energy is deposited into the one layer (1L) sample, as shown in the inset of Fig. 2(b). Almost 70% of impact energy is deposited in the 2L system. These numbers drop to 15% and 20% for analogous systems bombarded by 40 keV projectiles. Most of the deposited energy is carried away by substrate atoms emitted in the transmission direction. The energy carried away by sputtered atoms is small and does not exceed 0.5% of the initial kinetic energy. For a given primary kinetic energy, the amount of deposited energy increases with the sample thickness. Nevertheless, there is always an optimum thickness when the largest portion of the primary kinetic energy is carried away by ejecting atoms. This optimum thickness is not equal to the thickness yielding the largest particle emission. For instance, the largest fraction of primary kinetic energy is carried away from a 2L system for 5 keV C_{60} projectiles, whereas the most efficient ejection occurs from the 4L system at this impact energy. The increase in the primary kinetic energy shifts this optimal thickness to a higher value. Interestingly, the maximum fraction of the primary energy carried away by substrate atoms does not depend on the kinetic energy of a projectile. It is approximately 40% regardless of the value of this parameter.

The effect of the impact angle on the ejection yield from the 2L and 8L systems bombarded by 10 and 40 keV C_{60} projectiles is shown in Fig. 3. The impact angle has a similar influence on the yield of substrate atoms emitted in the transmission and sputtering directions for both these systems.

First, the yield increases with the impact angle, and then, it decreases. The position of a maximum shifts to a larger impact angle and becomes more pronounced for more energetic projectiles.

The impact angle also has a significant influence on a number of ejected projectile atoms. The functional form of this influence is, however, different from the one observed for substrate atoms. The number of projectile atoms penetrating through the sample decreases monotonically with the impact angle, whereas the yield of backreflected atoms increases for more oblique impacts. For the 2L system, these yields are almost complementary, which indicates that projectile atoms can be either transmitted or backreflected. In other words, projectile atoms cannot be trapped inside such a thin system. The situation is different for the 8L system, especially when it is bombarded by low-energy projectiles. In this case, many projectile atoms are trapped inside the sample.

Cross-sectional views of the temporal evolution of the bombarded systems can be used to gain insight into the mechanism of particle ejection. As SIMS analysis with graphene substrates is performed at high kinetic energy,^{4,5} we limit our discussion to a 40 keV bombardment. Cross-sectional views of the 2L and 8L systems bombarded by 40 keV C_{60} projectiles are shown in Figs. 4 and 5, respectively. See supplementary material for animations of the impacts.²⁹ The plots are made for impact angles which correspond to a normal incidence, the incidence when ejection of substrate atoms is the most efficient, and the impact angle

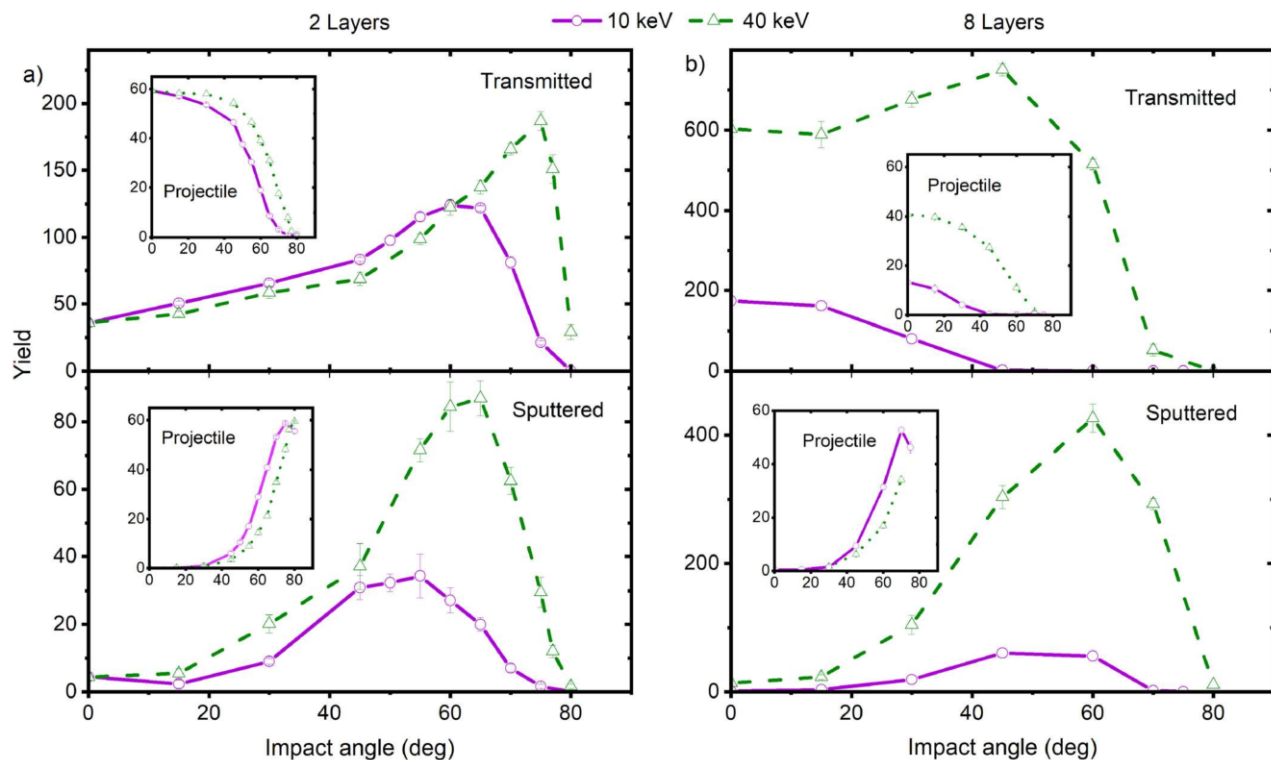


FIG. 3. (Color online) Dependence of the yields of carbon atoms ejected in the transmission (top) and sputtering (bottom) directions from the (a) two and (b) eight layer systems bombarded by ten (solid line) and 40 keV C_{60} (dashed line) projectiles on the impact angle. Main graphs represent the atoms originating from the sample, while the insets depict projectile's atoms.

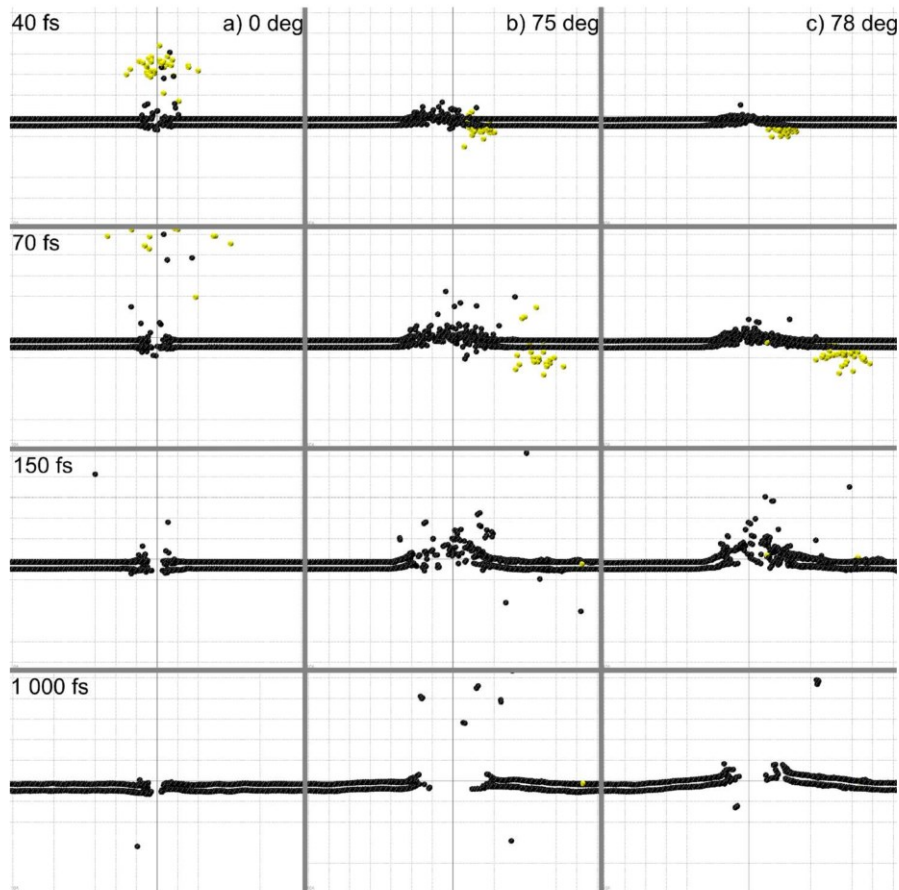


FIG. 4. (Color online) Cross-sectional view of the temporal evolution of a typical collision event leading to ejection of atoms due to 40 keV C_{60} bombardment of a system composed of two graphene layers. Bright (yellow) spheres indicate projectile atoms. A 1 nm slice of the system centered at the impact point is shown. The plots are made for impact angles, which correspond to a normal incidence, the incidence when ejection of substrate atoms is the most efficient, and the impact angle when the yield of these atoms decreases. The dashed lines in the background are separated by 1 nm.

when the yield of these atoms decreases. These impacts should lead to the widest range of phenomena stimulated by projectile impact. From Figs. 4 and 5, it is evident that the integrity of the C_{60} projectile is compromised almost immediately after the impact. However, the projectile atoms remain together and interact collectively with the sample.

For the 2L sample bombarded at normal incidence, all projectile atoms penetrate through the substrate and an almost circular nanopore is created, as shown in Fig. 6. Zhao *et al.* have found that energetic clusters can be used to fabricate nanopores in graphene in a controlled way by varying the properties of the incident projectile.⁷ They have found that an impact energy of 11.4 eV/atom is needed to create a nanopore in a single layer of graphene when bombarded with C_{60} projectile at normal incidence.⁷ This energy corresponds to approximately 0.68 keV for the entire C_{60} projectile. Assuming that the same energy is necessary to perforate additional layers, one can predict that approximately 5.4 keV is needed to perforate the 8L system. This value is close to the threshold energy observed in our simulations [see the top inset of Fig. 2(a)]. The ejection process is very fast, and most of the atoms are emitted within 200 fs after the projectile impact. Regardless of a high projectile kinetic energy,

most of the substrate atoms are ejected from the topmost layer in the transmission direction. In fact, approximately 75% from 42 atoms ejected in the transmission direction originate from the topmost layer. The trend is opposite for substrate atoms ejected in the sputtering direction. In this case, ejection from the bottom layer dominates. Most projectile and substrate atoms emitted in the transmission direction are ejected at off normal angles. With the increase in the impact angle, the nanopore becomes larger. However, its size increases almost entirely along the impact azimuth. As a result, it becomes ellipsoidal. The size of the nanopore increases as the projectile impinging at the off normal angle travels a longer path inside the layer and consequently can interact with the larger amount of substrate material. However, simultaneously, the normal component of the projectile momentum decreases, and it becomes more difficult to perforate the substrate. As a result, a larger number of projectile atoms are backreflected from the sample and less energy becomes available to stimulate ejection of substrate atoms. At a certain moment, this process begins to dominate over the increase in the substrate material excited by the projectile, and both the sputtering yield and the nanopore size decrease. The projectile impact leads to the creation of

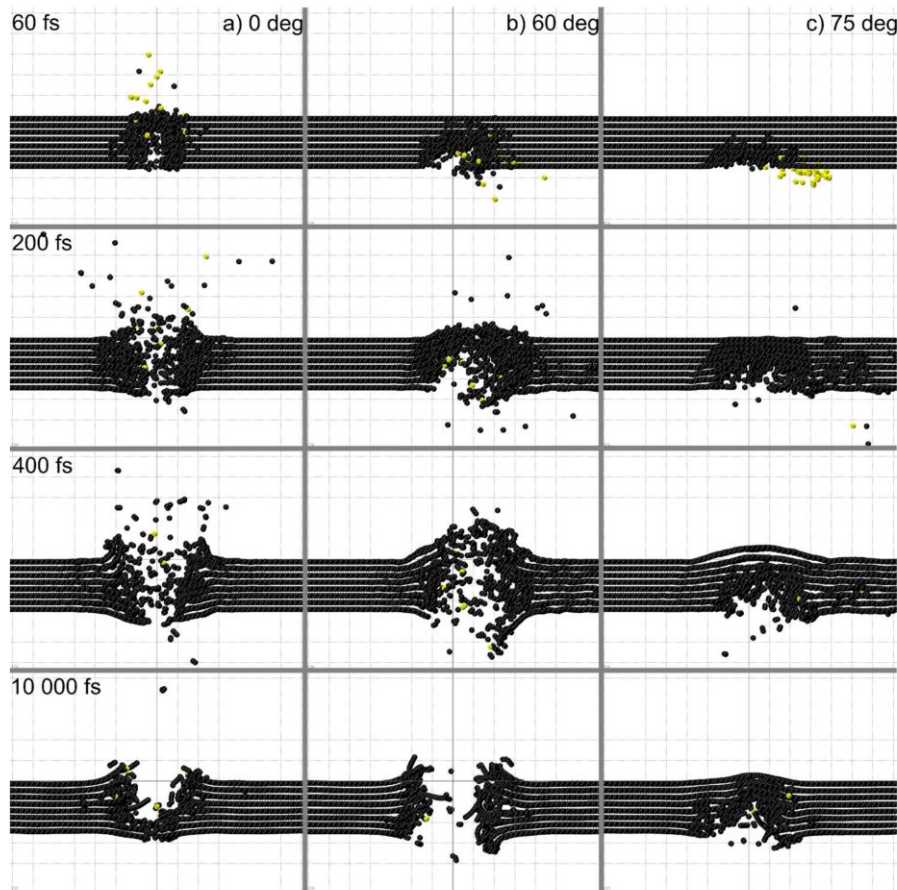


FIG. 5. (Color online) Cross-sectional view of the temporal evolution of a typical collision event leading to ejection of atoms due to 40 keV C_{60} bombardment of a system composed of eight graphene layers. Bright (yellow) spheres indicate projectile atoms. A 1 nm slice of the system centered at the impact point is shown. The plots are made for impact angles, which correspond to a normal incidence, the incidence when ejection of substrate atoms is the most efficient, and the impact angle when the yield of these atoms decreases. The dashed lines in the background are separated by 1 nm.

cylindrical acoustic waves that propagate outward from the point of impact with a maximum amplitude of approximately 0.1 nm.

More dramatic alteration is observed in the 8L system. In this case, the ejection process requires more time to complete. The projectile is more efficiently decelerated, depositing almost all its kinetic energy into the sample. Ejection of substrate atoms in the transmission direction is the main channel of material removal. The original location of ejected substrate atoms is not restricted to the top layers, but it extends deep into the sample. For instance, approximately 40%, 25%, 16%, 10%, and 5% of 603 atoms ejected in the transmission direction originate from the first (topmost), second, third, fourth, and fifth layers, respectively, which explains a conical shape of the evacuated volume. The remaining part of deposited energy is used to deform the substrate. Near the point of impact, for a short time, graphene sheets become separated from each other and bend up in a direction parallel to the movement of incoming projectile. Finally, a circular opening is formed surrounded by the elevated rim at the top surface of the sample. No rim is formed at the bottom surface. Bonds of many carbon atoms located in the energized volume are broken, which means

that these atoms become highly reactive. Many of the decelerated projectile atoms bound with these atoms.

The evolution of a system bombarded at an impact angle corresponding to the most efficient ejection of substrate atoms is shown in the second column of Figs. 4 and 5. For a 2L system, this angle is approximately 75° , while an angle of 60° is the most optimal for an 8L system. The 2L system is perforated within 70 fs. The projectile integrity is compromised again, but most of the projectile atoms preserve their original movement direction. There is a lot of movement at the edges of the created nanopore which now is elongated along the impact azimuthal direction, as shown in Fig. 6. Because the movement trajectory is now oblique, a larger volume of the sample is energized. However, the component of the projectile momentum perpendicular to the surface is reduced. As a result, it is easier to reflect projectile atoms.

Again, a more dramatic action is observed for an 8L system. The projectile atoms penetrate along the initial direction, but soon they become decelerated by collisions with substrate atoms. Most of these atoms become trapped inside the sample. First, the opening at a bottom surface is created and the substrate atoms are sputtered at oblique angles. Approximately 400 fs after the projectile impact, the integrity of the upper

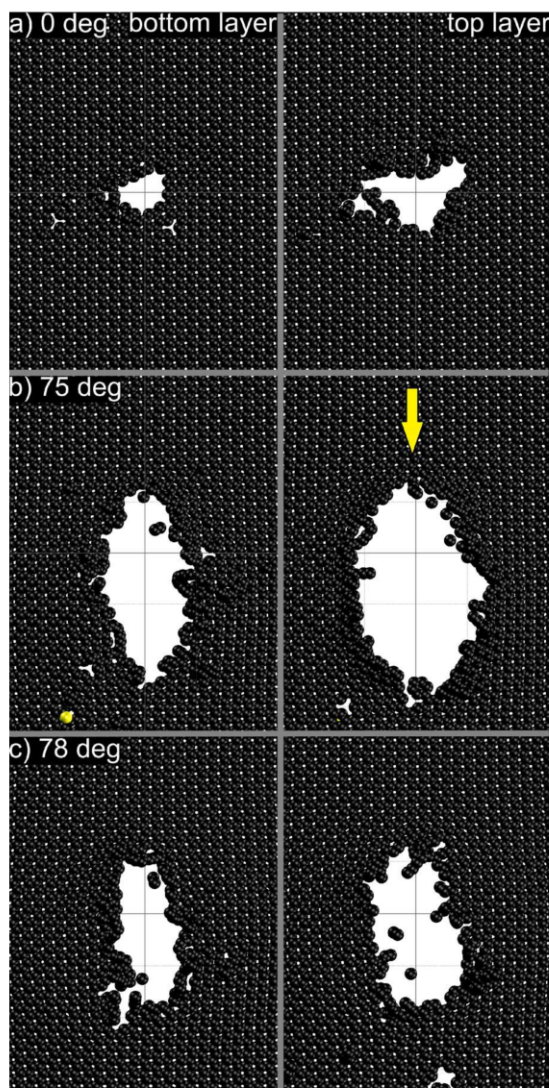


FIG. 6. (Color online) Top view of the 2L system bombarded by 40 keV projectiles at several impact angles. Bright (yellow) balls depict projectile atoms. The image is collected 1 ps after the projectile impact. The dashed lines in the background are separated by 1 nm. Arrow indicates azimuthal direction of the impacting projectile.

part of the sample is compromised, and the sample atoms start to eject in the transmission direction. It is interesting to note that regardless of a very large impact angle, most of these atoms eject in directions close to the surface normal. Finally, a cylindrical nanopore is created with openings of similar dimensions. Strong deformations are observed near the point of impact, which results in a graphene layer unfolding over a larger area.

A further increase in the impact angle leads to a signal decrease as shown in the third column of Figs. 4 and 5 for bombardment at the 78° and 75° impact angles of the 2L and 8L systems, respectively. The normal component of the projectile momentum is now so low that it becomes difficult to perforate even a 2L system. The 8L system is not perforated. Almost all projectile atoms backreflect from the 2L sample, while some of these atoms are trapped inside the 8L system.

Although the projectile atoms are not penetrating through the 8L substrate, its upper surface bulges outward during projectile deceleration.

Based on all observations, it can be concluded that the yield of substrate atoms is determined by two factors. The first factor is the amount of material available for sputtering. This quantity will increase with the sample thickness and with the impact angle, as projectile will travel a longer path inside the layer. The second factor is the amount of energy stored near the surface from where the ejection occurs. For ejection in the transmission direction, the upper surface is important. The energy stored near this surface will decrease with the sample thickness and the impact angle as projectile atoms have to sacrifice more energy to penetrate through the layer. For conditions where the substrate is perforated, an increase in the material available for ejection dominates and the yield increases with the substrate thickness or impact angle. However, ultimately less energy becomes available near the upper surface and the yield drops. For ejection in the sputtering direction, a bottom surface is important. The energy deposited near this surface increases with the sample thickness until the layer becomes thicker than a depth of a volume from where particles are ejected. Subsequently, the yield will saturate. The increase in the impact angle has also a positive effect on the amount of energy stored near the bottom surface, as the energy deposition profile is shifted downward. However, the increase in the impact angle also reduces the projectile momentum component perpendicular to the surface. It becomes easier to backreflect the projectile atoms, and more energy is carried away by these particles. As a result, less energy is deposited near the bottom surface and the yield decreases for too oblique impacts.

The yield of the projectile atoms ejected in the transmission direction is determined only by the capability of projectile atoms to perforate the sample. This capability decreases with the increase in both the layer thickness and the impact angle. The yield of the projectile atoms ejected in the sputtering direction will be determined by the capability of the sample to backreflect the projectile atoms. As already discussed, this capability increases with the impact angle.

The increase in the primary kinetic energy leads to the deposition of a larger amount of this energy in the sample and to a larger projectile range. Both these factors lead to a stronger ejection of substrate atoms. A larger penetration range increases the substrate thickness which can be perforated by the projectile. This factor leads to a shift of the emission maximum toward thicker samples for a constant impact angle or toward larger impact angles for a constant thickness when the projectile kinetic energy is increased. The increase in the primary kinetic energy also results in a broader distribution for projectile atoms.

Finally, a few comments can be made about the applicability of ultrathin graphene substrates for SIMS analysis of organic overlayers. It is known that for a standard sputtering geometry, collisions of adsorbed molecules with ejecting substrate atoms or a concerted action of the unfolding of the crater rim are the main processes leading to molecular emission from ultrathin organic layers deposited on solid substrates

bombarded by atomic and cluster projectiles, respectively.^{1,25–28} Direct collisions between projectile atoms and adsorbed molecules lead to molecular fragmentation.^{27,28} From this point of view, strong ejection of substrate atoms is a preferred experimental condition. The application of a transmission geometry allows us to satisfy this requirement. As shown in Fig. 2(a), ejection in the transmission direction is much stronger than that in the sputtering direction. However, the energetics of collisions between ejecting substrate atoms and the adsorbed molecules is also important. From the point of view of this factor, the application of a transmission geometry is less beneficial, as the energy of substrate atoms ejecting in the transmission direction is higher than the energy of a typical bond. For instance, in a 2L system bombarded by 5 keV projectile at normal incidence, the molecules located immediately above the point of projectile impact will collide with projectile atoms moving with the average kinetic energy of almost 70 eV per atom. Even for substrate atoms, the average kinetic energy will be close to 14 eV per atom. Collisions with such atoms will certainly lead to molecular fragmentation. Much more promising is a process of unfolding of the topmost graphene layer. In this case, the graphene sheet acts as a catapult that can gently hurl molecules into the vacuum. There is a considerable amount of energy associated with this movement, which means that even very large molecules can be uplifted. In the transmission geometry, this movement extends to a much larger lateral distance from the point of impact, as compared to a similar process present in metals or semiconductors.^{23,26} As shown in Figs. 4 and 5, it may be even more advantageous to bombard thicker samples and use the off-normal impact angle to enhance the catapult action. Consequently, a larger number of adsorbed molecules could be ejected by a single projectile impact, making analysis of small amounts of organic material viable. However, it should also be kept in mind that ejection of electrons is necessary to stimulate formation of negative ions,^{4–6} which means that a certain amount of kinetic energy must be present near the area of molecular ejection to emit such electrons. From this point of view, the application of thick substrates or bombardment at large impact angles may not be optimal.

IV. SUMMARY

Processes responsible for particle ejection from graphene substrates of various thicknesses bombarded by C₆₀ projectiles in a wide range of primary kinetic energies and impact angles were investigated. It has been observed that these quantities have a significant influence on the yield and the dynamics of particle ejection. For a given impact angle and primary kinetic energy, the yield of the substrate atoms ejected in the transmission direction has a nonmonotonic dependence on the sample thickness, with a pronounced maximum. A similar shape of dependence is observed if the impact angle is changed, while the primary kinetic energy and the sample thickness are kept constant. The position of the maximum in these dependencies shifts to thicker samples for a constant impact angle and to a larger impact angle for a

constant thickness, if the kinetic energy of a projectile is increased. The yield of sample atoms ejected in the sputtering direction saturates with the sample thickness for a given kinetic energy and impact angle. The number of projectile atoms ejected in the transmission direction decreases monotonically with the increase in the sample thickness and impact angle or with the decrease in the primary kinetic energy. All these changes result in a decrease in energy deposited in the top subsurface region. The yield of projectile atoms backreflected from the sample does not have a visible dependence on the sample thickness, but it increases for more oblique impacts, as it is easier to reflect atoms with a small component of momentum perpendicular to the surface. The width of these dependencies broadens with the increase in a primary kinetic energy. All observed trends can be explained by an interplay between the amount of material available for ejection and the amount of primary kinetic energy being deposited in the top and bottom subsurface regions of the sample.

Our study confirms that graphene supports and a transmission geometry have advantages over traditional metal or semiconductor substrates for analysis of ultrathin materials. First, the extremely small thickness of the support results in small amounts of emitted substrate material. As a result, there is a minimal interference between the substrate and the analyzed signal. A large portion of the primary kinetic energy can be transmitted to the organic overlayer in the direction toward the detector by the collective movement of the topmost layer, increasing a chance that a small amount of analyte can be recorded. Our results confirm that the graphene sheet can act as a catapult, leading to efficient soft ejection of adsorbed organic molecules. However, ejection of secondary electrons is also necessary to stimulate efficient ionization.

ACKNOWLEDGMENTS

The authors gratefully acknowledge financial support from the Polish National Science Centre, Programs Nos. 2016/23/N/ST4/00971 and 2015/19/B/ST4/01892.

¹B. J. Garrison and Z. Postawa, *Mass Spectrom. Rev.* **27**, 289 (2008).

²N. Winograd, *Anal. Chem.* **77**, 142A (2005).

³D. Weibel, S. Wong, N. Lockyer, P. Blenkinsopp, R. Hill, and J. C. Vickerman, *Anal. Chem.* **75**, 1754 (2003).

⁴S. V. Verkhoturov, S. Geng, B. Czerwinski, A. E. Young, A. Delcorte, and E. A. Schweikert, *J. Chem. Phys.* **143**, 164302 (2015).

⁵S. Geng, S. V. Verkhoturov, M. J. Eller, S. Della-Negra, and E. A. Schweikert, *J. Chem. Phys.* **146**, 054305 (2017).

⁶P. P. Michalowski, W. Kaszub, I. Pasternak, and W. Strupinski, *Sci. Rep.* **7**, 7479 (2017).

⁷S. J. Zhao, J. M. Xue, L. Liang, Y. G. Wang, and S. Yan, *J. Phys. Chem. C* **116**, 11776 (2012).

⁸M. Golunski and Z. Postawa, *Acta Phys. Pol., A* **132**, 222 (2017).

⁹M. Golunski, S. V. Verkhoturov, D. S. Verkhoturov, E. A. Schweikert, and Z. Postawa, *Nucl. Instrum. Methods, B* **393**, 13 (2017).

¹⁰Z. C. Xu and W. R. Zhong, *Appl. Phys. Lett.* **104**, 261907 (2014).

¹¹R. Smith and R. P. Webb, *Proc. R. Soc. London, Ser. A* **441**, 495 (1993).

¹²R. P. Webb, M. Kerford, M. Kappes, and G. Brauchle, *Nucl. Instrum. Methods, B* **122**, 318 (1997).

¹³M. Kerford and R. P. Webb, *Nucl. Instrum. Methods, B* **153**, 270 (1999).

¹⁴M. Kerford and R. P. Webb, *Nucl. Instrum. Methods, B* **180**, 44 (2001).

¹⁵C. Anders, H. Kirihata, Y. Yamaguchi, and H. M. Urbassek, *Nucl. Instrum. Methods, B* **255**, 247 (2007).

¹⁶R. P. Webb, *Radiat. Eff. Defect. Syst.* **162**, 567 (2007).

- ¹⁷K. D. Krantzman, R. P. Webb, and B. J. Garrison, *Appl. Surf. Sci.* **255**, 837 (2008).
- ¹⁸J. T. Tian, T. Zheng, J. Y. Yang, S. Y. Kong, J. M. Xue, Y. G. Wang, and K. Nordlund, *Appl. Surf. Sci.* **337**, 6 (2015).
- ¹⁹Y. N. Dong, Y. Z. He, Y. Wang, and H. Li, *Carbon* **68**, 742 (2014).
- ²⁰Y. Z. He, H. Li, P. C. Si, Y. F. Li, H. Q. Yu, X. Q. Zhang, F. Ding, K. M. Liew, and X. F. Liu, *Appl. Phys. Lett.* **98**, 063101 (2011).
- ²¹L. C. Liu, Y. Liu, S. V. Zybin, H. Sun, and W. A. Goddard, *J. Phys. Chem. A* **115**, 11016 (2011).
- ²²J. F. Ziegler, J. P. Biersack, and U. Littmark, *The Stopping and Range of Ions in Matter* (Pergamon, New York, 1985).
- ²³Z. Postawa, B. Czerwinski, M. Szewczyk, E. J. Smiley, N. Winograd, and B. J. Garrison, *Anal. Chem.* **75**, 4402 (2003).
- ²⁴S. Plimpton, *J. Comput. Phys.* **117**, 1 (1995).
- ²⁵B. J. Garrison, A. Delcorte, and K. D. Krantzman, *Acc. Chem. Res.* **33**, 69 (2000).
- ²⁶Z. Postawa, B. Czerwinski, M. Szewczyk, E. J. Smiley, N. Winograd, and B. J. Garrison, *J. Phys. Chem. B* **108**, 7831 (2004).
- ²⁷A. Delcorte and B. J. Garrison, *J. Phys. Chem. B* **108**, 15652 (2004).
- ²⁸Z. Postawa, B. Czerwinski, N. Winograd, and B. J. Garrison, *J. Phys. Chem. B* **109**, 11973 (2005).
- ²⁹See supplementary material at <https://doi.org/10.1116/1.5019732> for animations of 40 keV C60 impacts at 2 L and 8 L graphene at impact angles corresponding to a normal incidence, the incidence when ejection of substrate atoms is the most efficient, and the impact angle when the yield of these atoms is decreasing.

Article 4

*“Trampoline” ejection of organic molecules from graphene and graphite
via keV cluster ions impacts*

Verkhoturov S. V., Goluński M., Verkhoturov D. S., Geng S., Postawa Z. &
Schweikert E. A.

Journal of Chemical Physics 148, 144309 (2018)

doi:[10.1063/1.5021352](https://doi.org/10.1063/1.5021352)

Reprinted from J. Chem. Phys. 2018, 148, 144309, with the permission of AIP
Publishing.

“Trampoline” ejection of organic molecules from graphene and graphite via keV cluster ions impacts

Stanislav V. Verkhoturov,¹ Mikołaj Gołuński,² Dmitriy S. Verkhoturov,¹ Sheng Geng,¹ Zbigniew Postawa,² and Emile A. Schweikert^{1,a)}

¹Department of Chemistry, Texas A&M University, College Station, Texas 77843-3144, USA

²Department of Physics, Jagiellonian University, Kraków, Poland

(Received 3 January 2018; accepted 27 March 2018; published online 12 April 2018)

We present the data on ejection of molecules and emission of molecular ions caused by single impacts of 50 keV C_{60}^{2+} on a molecular layer of deuterated phenylalanine (D8Phe) deposited on free standing, 2-layer graphene. The projectile impacts on the graphene side stimulate the abundant ejection of intact molecules and the emission of molecular ions in the transmission direction. To gain insight into the mechanism of ejection, Molecular Dynamic simulations were performed. It was found that the projectile penetrates the thin layer of graphene, partially depositing the projectile's kinetic energy, and molecules are ejected from the hot area around the hole that is made by the projectile. The yield, Y , of negative ions of deprotonated phenylalanine, $(D8Phe-H)^-$, emitted in the transmission direction is 0.1 ions per projectile impact. To characterize the ejection and ionization of molecules, we have performed the experiments on emission of $(D8Phe-H)^-$ from the surface of bulk D8Phe ($Y = 0.13$) and from the single molecular layer of D8Phe deposited on bulk pyrolytic graphite ($Y = 0.15$). We show that, despite the similar yields of molecular ions, the scenario of the energy deposition and ejection of molecules is different for the case of graphene due to the confined volume of projectile-analyte interaction. The projectile impact on the graphene-D8Phe sample stimulates the collective radial movement of analyte atoms, which compresses the D8Phe layer radially from the hole. At the same time, this compression bends and stretches the graphene membrane around the hole thus accumulating potential energy. The accumulated potential energy is transformed into the kinetic energy of correlated movement upward for membrane atoms, thus the membrane acts as a trampoline for the molecules. The ejected molecules are effectively ionized; the ionization probability is $\sim 30\times$ higher compared to that obtained for the bulk D8Phe target. The proposed mechanism of ionization involves tunneling of electrons from the vibrationally excited area around the hole to the molecules. Another proposed mechanism is a direct proton transfer exchange, which is suitable for a bulk target: ions of molecular fragments (i.e., CN^-) generated in the impact area interact with intact molecules from the rim of this area. There is a direct proton exchange process for the system D8Phe molecule + CN^- . *Published by AIP Publishing.* <https://doi.org/10.1063/1.5021352>

INTRODUCTION

Secondary ion mass spectrometry, SIMS, is well recognized as a highly sensitive surface analysis technique.¹ The secondary ion, SI, emission process is explained as the result of the dissipation of the projectile kinetic energy via linear collision cascades (atomic projectiles) or high density collision cascades in the case of cluster impacts.² The high density cascades in turn generate correlated pulses toward the surface around the impact crater promoting the sputtering of neutral and emission of ionized species as atoms, molecules and molecular fragments. The full development of the collision cascades assumes a solid of at least 100 nm in thickness. However, in a departure from the conventional SIMS experiment, we have observed abundant emission of small carbon clusters, when bombarding free-standing graphene with C_{60}^{2+}

or Au_{400}^{4+} at hypervelocities.^{3,4} The emissions referred to here are in a transmission (forward) direction. Further experiments, where a single layer of C_{60} deposited on free-standing graphene was bombarded with 50 keV C_{60}^{2+} , showed that the yield of C_{60}^- emitted in the transmission direction is comparable to that obtained from a monolayer of C_{60} on pyrolytic graphite, and even comparable to that from a bulk C_{60} deposit.⁵ In the latter cases, bombardment was also with 50 keV C_{60}^{2+} , but the C_{60}^- emission was measured in the conventional reflection direction. Clearly, the C_{60} on the 2D substrate is ejected and ionized with high efficiency, in a mode that differs from the conventional SIMS process. Molecular dynamics (MD) simulations of C_{60} bombarding a monolayer of C_{60} deposited on two layers of free standing graphene show that intact C_{60} is ejected within a few ps from a “hot” vibrationally excited rim around the impact rupture.⁵ The proposed mechanism of ejection involves a combination of an “evaporation” process from the vibrationally excited area, with a kinetic repulsion process due to the graphene membrane oscillating around the

^{a)}Electronic mail: schweikert@tamu.edu

impact hole. The high degree of ionization of the ejected C_{60} may be explained as due to electron tunneling between the hot graphene and the ejecta.

The question now arises if the efficient ejection-ionization observed for C_{60} occurs also for organic molecules in monolayer deposit on graphene. We address this issue here with a study on SI emission from monolayer deposits of phenylalanine on graphene under C_{60} bombardment. The observations are compared with data from monolayer and bulk deposits of the same analyte on bulk graphite. For the additional insight, the findings are compared with MD simulations run on equivalent samples and conditions.

EXPERIMENTAL

Instrumentation

The experiments were run with a custom-built cluster-SIMS instrument consisting of two identical C_{60} effusion sources (Fig. 1). One cluster ion source generates 50 keV C_{60}^{2+} projectiles which impact the back side of a thin target (e.g., graphene) at an angle of incidence of 0° from normal. This setup is used for the detection of secondary ions which are emitted in the transmission direction. Another C_{60} source is used for impacts on the front side of the bulk target at an angle of incidence of 25° from normal. The secondary ions are emitted/detected in the reflection direction. The SIMS instrument is equipped with a 1.2 m linear time-of-flight mass spectrometer, ToF-MS, and an electron emission microscope, EEM.^{6,7} The EEM was used here solely to detect secondary electrons for the ToF start signal. The data were acquired at the level of individual C_{60} impacts with a repetition rate of 1000 impacts/s. This event-by-event bombardment-detection mode allows us to select specific impacts, in the present case those involving free-standing graphene,³ at the exclusion of signals from the target holder and support. A detailed description of the components and data acquisition processing scheme can be found elsewhere.⁷

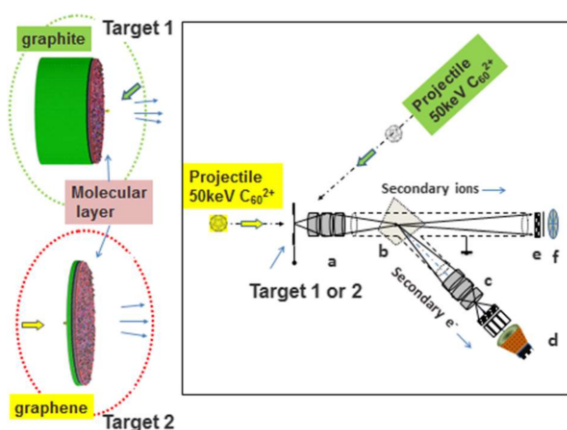


FIG. 1. Schematic of experiment: (a) objective lens for secondary ions and electrons, (b) magnetic prism for the redirection of electrons toward imaging electron optics (c), (d) position sensitive detector consisting of dual microchannel plate, phosphor screen, and CMOS camera, (e) dual microchannel plate, and (f) 8 anode detector.

Samples

A layer of deuterated phenylalanine (D8Phe) molecules (Fig. 1) was vapor deposited on 2-layer graphene or pyrolytic graphite. The graphene was supported by a lacey carbon film on a copper TEM grid with 300 lines/in. (Ted Pella, Inc., Redding, CA). The support was analyzed and the contribution of the observed SIs from the lacey carbon was found to be small.³ The pyrolytic graphite plate of thickness of 0.5 mm (Sigma Aldrich, Inc.) has 99.99% purity.

The deposition of D8Phe was made in high vacuum with a growth rate of the molecular layer of 50 nm/min. The time of deposition was controlled with a shutter placed in front of the sample. A one second exposure time resulted in a single molecular layer of ~ 1 nm thickness.

Homogeneity test

The uniformity of the D8Phe layer was tested using event-by-event bombardment-detection mode.⁶ The method allows us to detect the $(D8Phe-H)^-$ ions that are co-emitted with the D^- ions and compute the correlation coefficients of co-emission⁸

$$K_n = \frac{Y_{D,Phe}}{Y_D Y_{Phe}}, \quad (1)$$

where Y_D and Y_{Phe} are the yields (the number of emitted ions that are detected per projectile impact) of $(D8Phe-H)^-$ ions and D^- ions, respectively, and $Y_{D,Phe}$ is the yield of co-emitted $(D8Phe-H)^-$ and D^- ions.

For the homogeneous surface, the ions are emitted independently from any point of the impacting area.⁸ Thus, for the homogeneous surface, $K_n = 1$.

The measured yields are given by

$$Y_{Phe} = I_{Phe}/N_{eff}, \quad (2)$$

$$Y_D = I_D/N_{eff}, \quad (3)$$

$$Y_{D,Phe} = I_{D,Phe}/N_{eff}, \quad (4)$$

where I_{Phe} is the number of detected $(D8Phe-H)^-$, I_D is the number of detected D^- , $I_{D,Phe}$ is the number of detected co-emitted ions and N_{eff} is the effective number of impacts on the area of the target, which is covered by the molecular layer.

Using the expressions (1)–(4), one can obtain N_{eff} ,

$$N_{eff} = \frac{I_D I_{Phe}}{I_{D,Phe}}. \quad (5)$$

If the molecular coverage of the surface is incomplete, the effective number of impacts is less than the total number of impacts, N_0 ,

$$N_{eff} < N_0. \quad (6)$$

To compare the quality of the D8Phe layers deposited on different substrates, the degree of coverage can be written in the form as

$$\alpha (100\%) = \frac{N_{eff}}{N_0} 100\%. \quad (7)$$

The degree of coverage, α , the yields of $(D8Phe-H)^-$, Y_{Phe} and other measured ions for the different targets are presented in Table I.

The degrees of coverage, presented in Table I, show that the Targets I and II are well covered by D8Phe molecules. The

TABLE I. Degree of coverage, α , yield of (D8Phe-H)⁻, Y_{Phe} , and the yields of some atomic and fragment negative ions measured for different targets. (Target I) 2-layer graphene coated by ~ 1 nm layer of D8Phe. The projectiles impact graphene first; the emitted ions are detected in the transmission direction. (Target II) Bulk pyrolytic graphite coated by ~ 1 nm layer of D8Phe. (Target III) Thick layer (~ 500 nm) of D8Phe deposited on pyrolytic graphite. A thickness of 500 nm is enough to consider this target as bulk D8Phe. For the Targets II and III, the projectiles impact first the D8Phe layer; the emitted ions are detected in the reflection direction. The standard deviation is better than $\pm 5\%$ for all values of the experimental α .

	α (%)	Y_{Phe}	Y_D	Y_{C_1}	Y_{CN}	Y_{CD}	Y_{OD}	Y_O
Target I	89	0.10	0.10	0.15	0.31	0.04	0.02	0.12
Target II	86	0.15	0.06	0.03	0.22	0.02	0.01	0.04
Target III	100	0.13	0.11	0.04	0.23	0.03	0.01	0.04

thickness of the layer is ~ 1 nm (50 nm/min deposition rate with an exposure time of 1 s). The coverages were 89% and 86% for the Targets I and II, respectively.

Molecular dynamics simulations

The molecular dynamics (MD) computer simulations were used to investigate processes leading to material ejection from a graphene substrate covered with a phenylalanine overlayer bombarded by C₆₀ projectiles. Briefly, the movement of particles is determined by integrating Hamilton's equations of motion. Targets consisting of one layer of phenylalanine (Phe) deposited on 2 layers and 30 layers of graphene are shown in Fig. 2. A detailed description of the MD method can be found elsewhere.⁹ The cylindrical samples are selected based on visual observations of energy transfer pathways stimulated by impacts of C₆₀ projectiles. The sample diameter was chosen to minimize edge effects associated with the dynamic events leading to ejection of particles. The graphene substrates had a circular shape with a radius of 20 nm and a thickness of approximately 0.34 nm and 5.1 nm, containing 92 162 and 1 382 430 carbon atoms, respectively. The phenylalanine monolayer, consisting of 5013 molecules or 115 299 atoms, was deposited on graphene and re-equilibrated to achieve

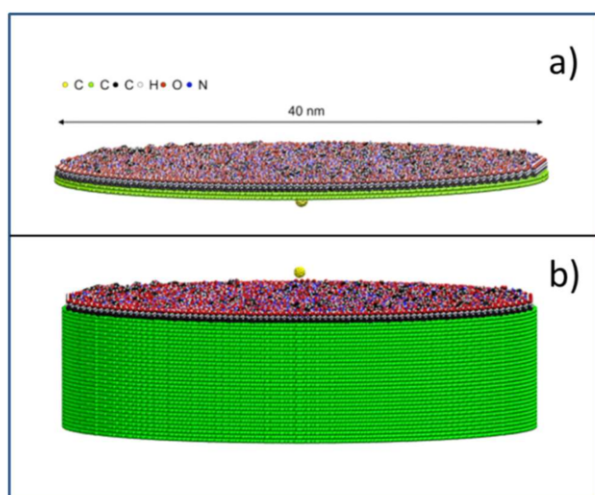


FIG. 2. Visualization of the atomic system used in simulations.

a configuration with minimal potential energy. This procedure resulted in a monolayer approximately 1.11 nm thick. The phenylalanine multilayer was represented by 10 layers of phenylalanine deposited on two layers of graphene. This system consisted of 50 317 molecules or 1 157 291 atoms. One should note that in MD simulations, the Phe molecules are not deuterated. The slight difference in bond strength between D8Phe and Phe is of no concern here. Reactive force field (ReaxFF) potential splined at a short distance with the Ziegler-Biersack-Littmark (ZBL) potential to properly describe high energy collisions was used to describe interactions among all atoms in the system.¹⁰

Rigid and stochastic regions around the edge of the sample were used to preserve sample shape and prevent back reflection of the waves generated by the projectile impact from back reflection from the system boundary.¹¹ We found that the tooth-sawtooth shape of the stochastic zone (like in breakwaters) is more effective for eliminating constructive interference of energy waves that reflect from the boundaries than a simpler cylindrically shaped zone. The C₆₀ projectile is situated “below” the sample in a “transmission” setup for a 2-layer graphene substrate [Fig. 2(a)]. Thus the detected molecules are ejected on the other side of the sample than the side that is hit by a projectile. The projectile is located above the substrate in a “reflection” configuration for a 30-layer graphene system [Fig. 2(b)]. In this case, molecules are emitted in the direction opposite to the initial projectile movement. The atoms in the target have initially zero velocity. The atoms in the C₆₀ projectile have initially no velocity relative to the center of mass motion. The C₆₀ projectiles with a kinetic energy of 50 keV are directed along the surface normal.

The simulations are run in a NVE ensemble and extend up to 60 ps, which is long enough to achieve saturation in the ejection yield vs time dependence. Nine randomly selected impact points located near the center of the sample are chosen to achieve statistically reliable data. Simulations are performed with the Large-scale Atomic/Molecular Massively Parallel Simulator (LAMMPS) code,¹² which was modified to better describe sputtering conditions.

RESULTS AND DISCUSSION

The mass spectra of negative ions emitted from different targets (Targets I-III) are shown in Figs. 3–5, respectively.

All mass spectra of emitted negative ions contain peaks of D8Phe fragment ions of C_n⁻, C_nH⁻, C_nD⁻ ($n \leq 10$), OH⁻, OD⁻, and O⁻ (Figs. 3–5). The presence of O⁻ and C_nH_x⁻ in the spectra also implies that the graphene as well as pyrolytic graphite is partially oxidized and has contaminants due to exposure in air prior to the experiments in a vacuum.³

While the mass spectra of all targets appear to be similar, there are a few notable differences. The first difference is the high yield of C₁⁻ in the transmission experiments (Target I), which is in part attributed to fragmentation and atomization of the projectile after impact followed by the ionization of the projectile's carbon atoms. Indeed, the yields of C₁⁻ measured for the reflection direction (bulk targets II and III) are much lower due to fewer recoiled projectile atoms. For Target I,

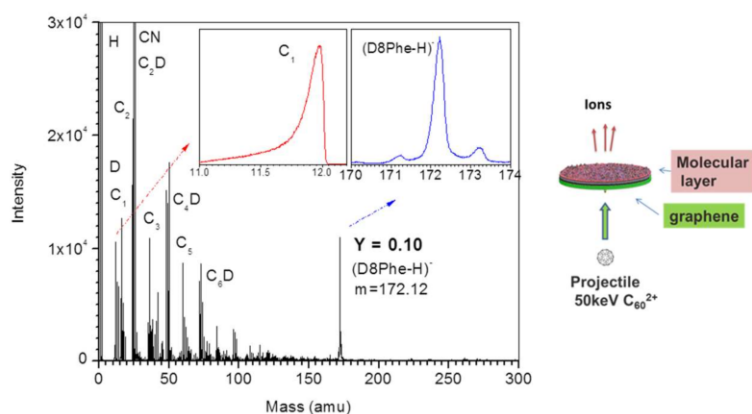


FIG. 3. Mass spectrum of negative ions emitted from the Target I (2-layer graphene coated by the molecular layer of D8Phe). The directions of bombardment and emission are shown in the sketch presented on the right-hand side of the figure.

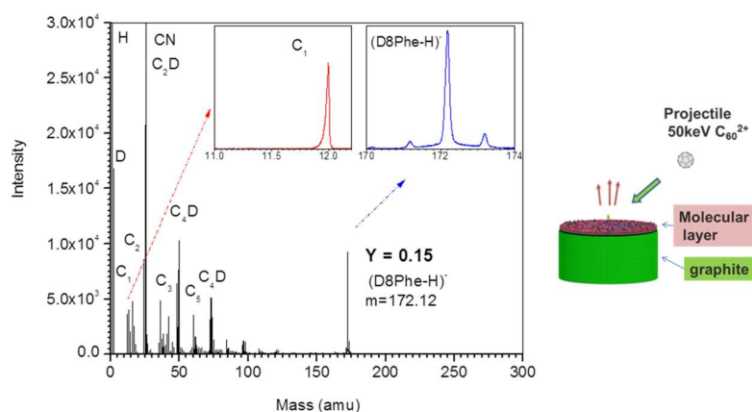


FIG. 4. Mass spectrum of negative ions emitted from the Target II (bulk pyrolytic graphite coated by the molecular layer of D8Phe). The directions of bombardment and emission are shown in the sketch presented on the right-hand side of the figure.

the shape of the C_1^- peak has an extended tail toward the low mass range, which indicates the presence of ions with high kinetic energies (discussed below). A further difference is the shape of the peak of $(D8Phe-H)^-$, which depends on mechanism/s of molecule ejection and ionization (discussed below).

The shape of the C_1^- peak can be converted into the kinetic energy distribution. Details of the measurement of the kinetic energy distributions are given in the supplementary material of Ref. 3.

The kinetic energy distributions of C_1^- are different for transmission and reflection experiments (Fig. 6). For the transmission experiments, the kinetic energies of C_1^- extend up to

1/60 (833 eV) of the projectile energy. This energy corresponds to the energy of projectile C atoms, or to the energy of C atoms, which are knocked on in a direct collision between projectile C atoms and C atoms of the D8Phe+graphene film. For the bulk target, the kinetic energies of C_1^- extend up to ~60–75 eV. These energies correspond to the energies of the C recoils, which are generated via collision cascades.²

Phenylalanine monolayer on graphene

A key finding is the abundant emission of deprotonated molecular ions of D8Phe from the molecular layer of D8Phe deposited on 2-layer graphene. The yield of 0.1 ions/impact

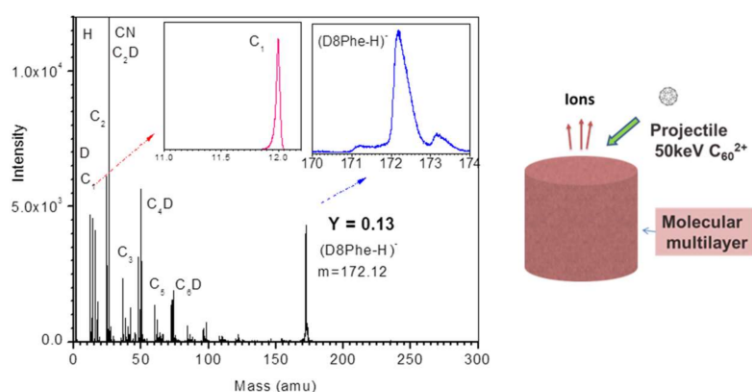


FIG. 5. Mass spectrum of negative ions emitted from the Target III (bulk D8Phe). The directions of bombardment and emission are shown in the sketch presented on the right-hand side of the figure.

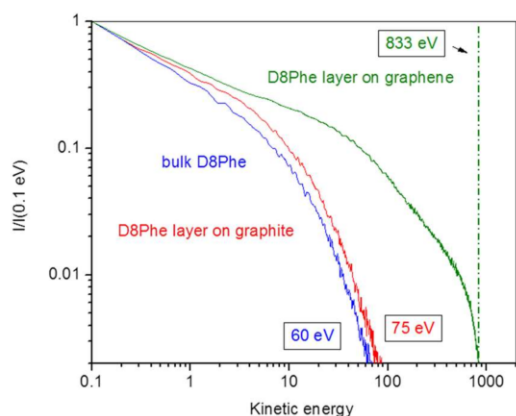


FIG. 6. Kinetic energy distributions measured for the atomic ions C_1^- emitted from the single molecular layer of D8Phe deposited on 2-layer graphene (green color, Target I), the single molecular layer of D8Phe deposited on pyrolytic graphite (red color, Target II) and bulk D8Phe (blue color, Target III).

is comparable with the yield for $(D8Phe-H)^-$ emitted from the bulk target (0.13 ions/impact). As noted earlier, projectile

impacts on bulk matter result in high density collision cascades, which are an efficient source for sputtering of intact molecules.²

In the case of 50 keV C_{60}^{2+} impacts on graphene covered with a monolayer of D8Phe, the C atoms of the projectile collide with those of the target. The knocked-on atoms carry a part of the kinetic energy of the projectile atoms. Another part of the kinetic energy is deposited into the rim around the impact site. MD simulations show that the molecules are ejected from this area (Figs. 7 and 8) (Multimedia view). Figure 7 (Multimedia view) shows the cut view and Fig. 8 (Multimedia view) shows the side view of the processes of Phe+graphene evolution and molecule ejection. The critical process, which regulates the abundance of the ejecta, is the separation of the molecular layer from graphene. The molecular layer evolves as a collective movement of Phe molecules and simultaneously the graphene oscillates downward/upward. The key step of molecule ejection occurs within first 2 ps after impact. The initial atom-atom interactions stimulated by the projectile impact are transformed into a collective radial movement of atoms of Phe molecules, which compresses the molecular layer

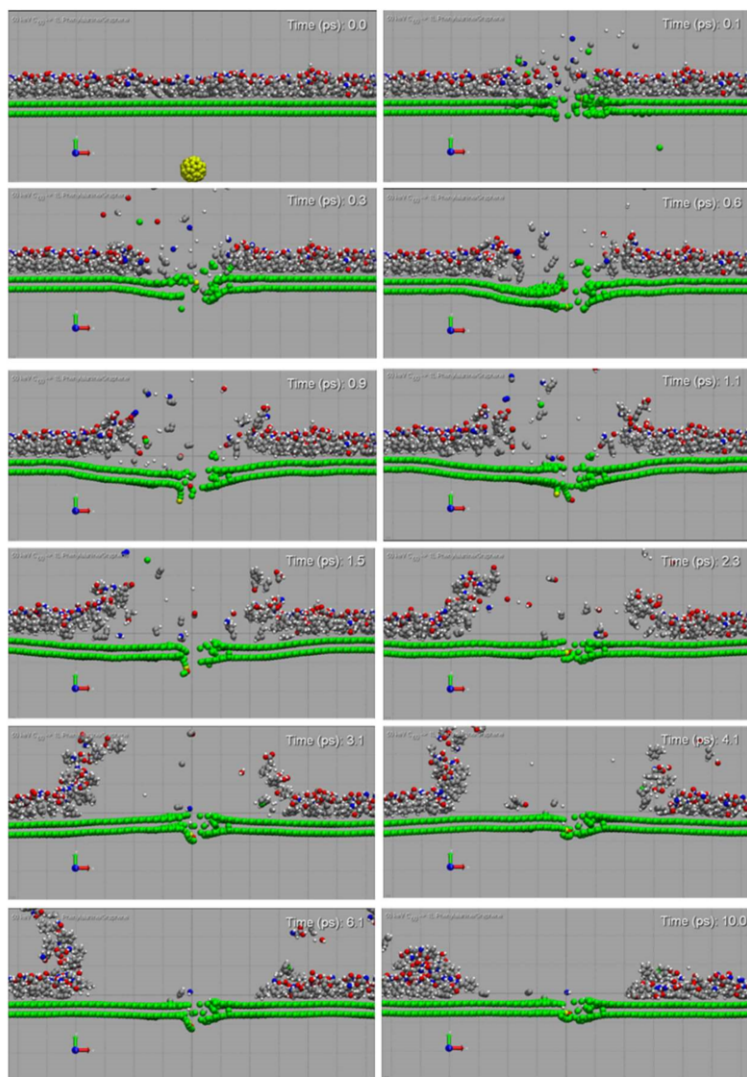


FIG. 7. Snapshots of the model system consisting of the single layer of phenylalanine molecules (1.1 nm) deposited on 2L graphene taken at various moments after 50 keV C_{60} impact—cross-sectional view. The corresponding movie file is here. Multimedia view: <https://doi.org/10.1063/1.5021352.1>

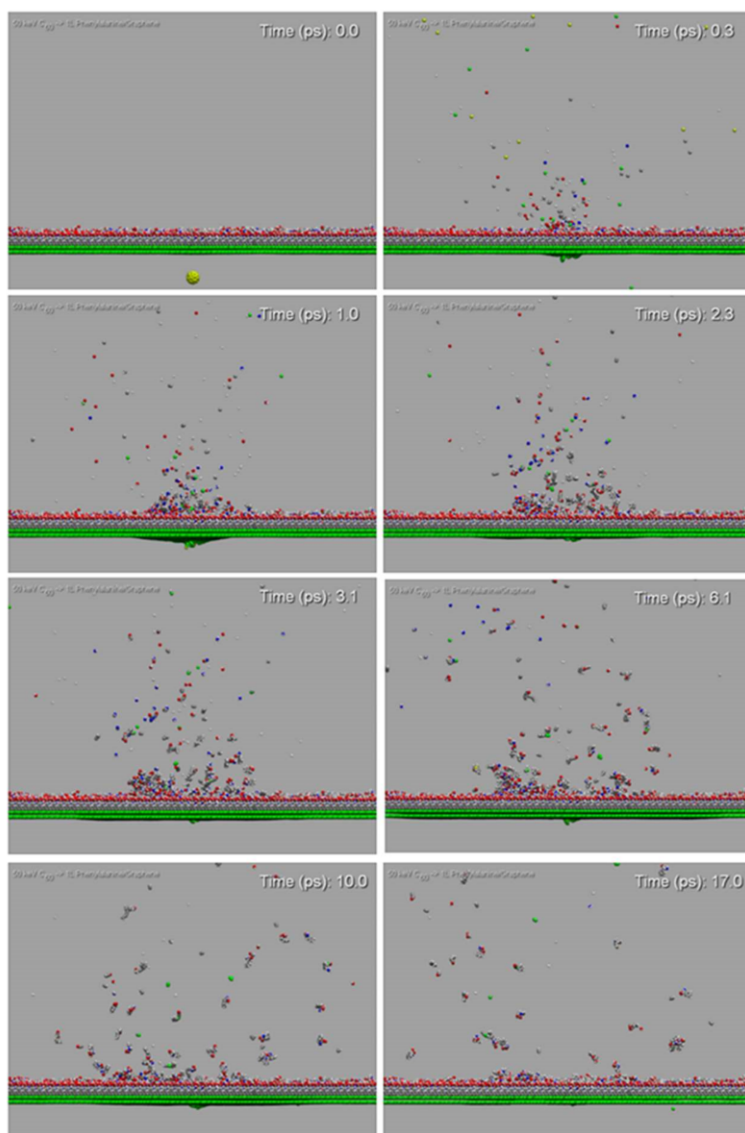


FIG. 8. Snapshots of the model system consisting of the single layer of phenylalanine molecules (1.1 nm) deposited on 2L graphene taken at various moments after 50 keV C_{60} impact—side view. The corresponding movie file is here. Multimedia view: <https://doi.org/10.1063/1.5021352.2>

radially from the hole [Fig. 7 (Multimedia view), screenshots for times 0.1 and 0.3 ps]. At the same time, this compression pushes the graphene membrane down. The molecular layer and graphene membrane are separated [Fig. 7 (Multimedia view), screenshots for times 0.6, 0.9, and 1.1 ps]. The pushed down graphene membrane is bent and stretched around the hole, thus accumulating potential energy. The result of the bending and stretching is an elastic movement of the membrane upward [Fig. 7 (Multimedia view), screenshots for times 1.5, 2.3, and 3.1 ps]. The accumulated potential energy is transformed into the kinetic energy of a correlated movement upward for membrane atoms. The membrane atoms interact with the atoms of Phe molecules and transfer the correlated momenta to them. Thus, the molecules eject without destruction. In other words, the membrane acts as a trampoline for the molecules. The ejection of molecules is clearly observable from the side view [Fig. 8 (Multimedia view)]. The screenshot for the time 1 ps [Fig. 8 (Multimedia view)] shows the strong

bending of the graphene membrane followed by the abundant trampoline ejection (1 ps–10 ps) of molecules and molecular clusters. Note that the emission/ejection of molecules is not effective in the reflection direction (impact on molecules first). This is due to the impact stimulated damage of molecules prior to the radial compression. This effect was investigated in Ref. 3 (MD simulations and experiments) for the single layer of C_{60} deposited on graphene.

A top view of the impact (Fig. 9) shows the evolution of the surface molecules around the impact site. This point evolves into a small graphene rupture of ~ 2 nm (time 0.1 ps after impact). The size of this rupture is reduced (self-healing effect¹³) within ~ 20 ps. The evolution of the area around the rupture shows a clearing of the graphene substrate by the processes of molecule ejection and radial compression. At the end of the ejection/compression, the area of graphene that is cleared of Phe molecules is ~ 6 nm in diameter. That area (at least in theory) corresponds to the

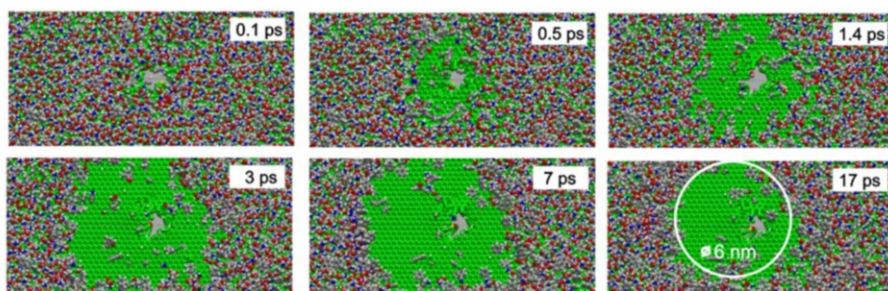


FIG. 9. Snapshots of the model system consisting of phenylalanine molecules deposited on 2L graphene taken at various moments after 50 keV C_{60} impact—top view. White circle marks dimension of the area cleared of organic molecules.

probing surface area for a single impact of 50 keV C_{60} projectile.

Phenylalanine monolayer on graphite

For comparison, we consider now molecule ejection and molecular ion emission from a single molecular layer deposited on pyrolytic graphite (Fig. 4). The yield of

0.15 ions/impact is comparable to the yield of $(D8Phe-H)^-$ emitted from the monolayer deposited on graphene (0.1 ions/impact). The MD simulations show that the critical process, which regulates the abundance of the ejecta, is a correlated upward movement of topmost graphite layers (Figs. 10 and 11) (Multimedia view). Figure 10 (Multimedia view) and the corresponding movie show the cut view, and Fig. 11 (Multimedia view) shows the side view.

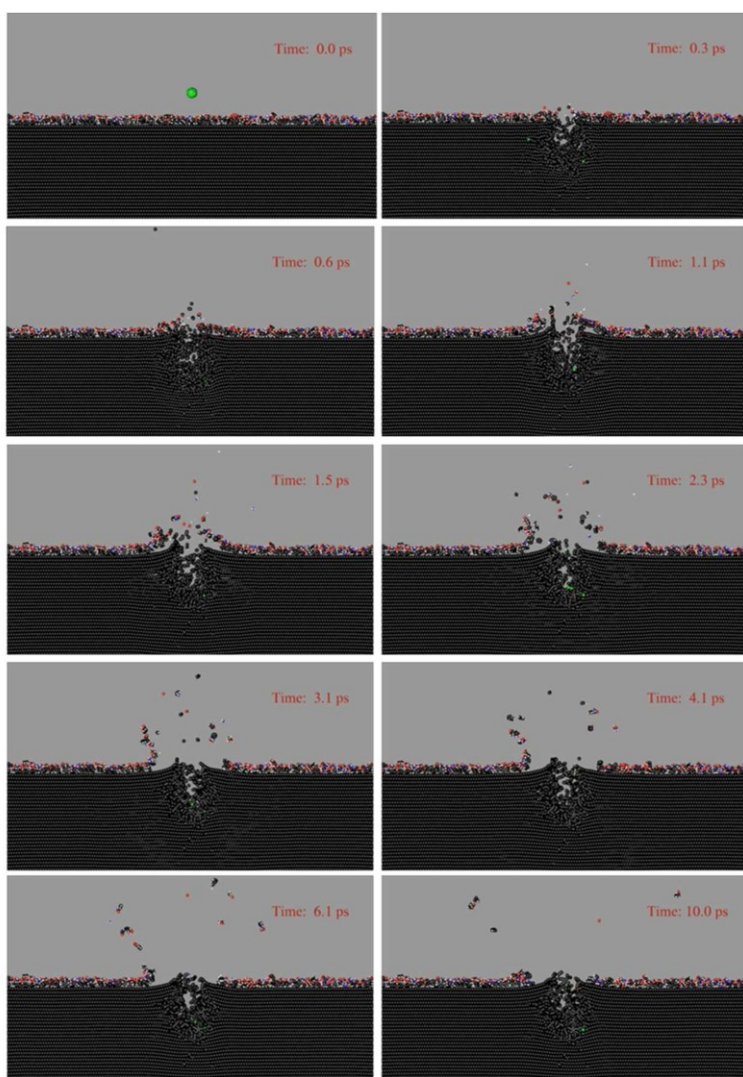


FIG. 10. Snapshots of the model system consisting of the single layer of phenylalanine molecules (1.1 nm) deposited on graphite taken at various moments after 50 keV C_{60} impact—cross-sectional view (slice 10 Å wide centered at the projectile impact point). The corresponding movie file is here. Multimedia view: <https://doi.org/10.1063/1.5021352.3>

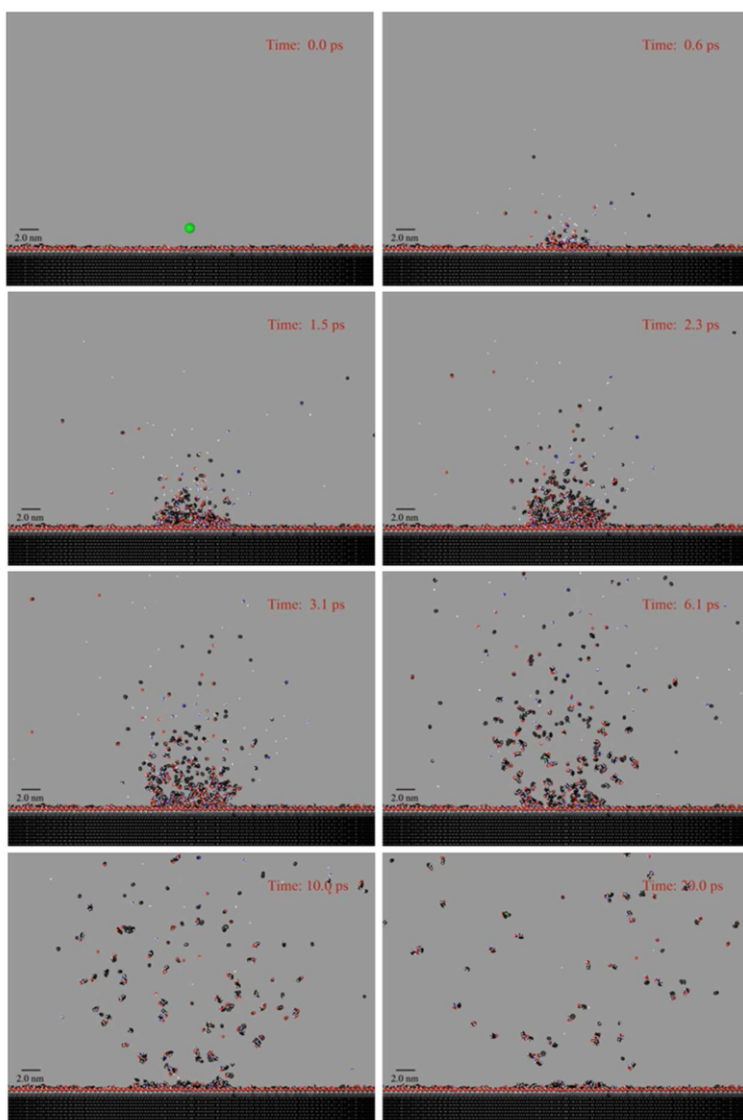


FIG. 11. Snapshots of the model system consisting of the single layer of phenylalanine molecules (1.1 nm) deposited on graphite taken at various moments after 50 keV C_{60} impact—side view. The corresponding movie file is here. Multimedia view: <https://doi.org/10.1063/1.5021352.4>

The detailed scenario is as follows: After impact [Fig. 10 (Multimedia view), screenshots for times 0.3 and 0.6 ps], the projectile atoms and fast recoiling atoms deliver the energy into the depth of graphite without strong damage to the surface layers of the analyte and graphite due to the latter's layer structure.

The result of the energy deposition is a high density collision cascade to a depth of ~ 5 nm (~ 15 graphite layers). The matter at this depth expands radially as seen in the deformation of the periphery graphite layers [Fig. 10 (Multimedia view), screenshots for times 1.1 and 1.5 ps]. At the same time, the expanding volume stimulates the collective movement of the topmost graphite layers upward. This movement transfers the correlated momenta to surface molecules, which eject without destruction [Figs. 10 and 11 (Multimedia view), screenshots for times 1.5, 2.3, and 3.1 ps].

The actual ejection mechanisms are similar for molecular layers on graphite or graphene. The graphene membrane as well as the topmost graphite layer acts as a trampoline for

the Phe molecules. The main difference is the initial projectile energy deposition for graphite and graphene prior to the molecule ejection. In the case of graphite, the high density collision cascade reaching the depth of ~ 5 nm stimulates in-depth radial expansion. The graphene evolution prior to the molecule ejection (more details are given above) does not involve a collision cascade.

In the case of bulk phenylalanine, the yield (0.13) of $(D8Phe-H)^-$ (Target III, Fig. 5) is again similar to the yields measured for ~ 1 nm layer of D8Phe deposited on graphene and graphite substrates (Figs. 3 and 4) despite the very different mechanisms of ejection/sputtering.

Bulk phenylalanine

For the bulk targets of organic molecules (weakly bonded molecular solids),¹⁴ the sputtering process has been extensively investigated.^{2,9,15,16} The abundant sputtering arises from the high density collision cascades that develop a crater in

the weakly bonded solid. The projectile impact at the surface creates an energized region primarily composed of molecular fragments.⁹ Expansion of this region stimulates molecular desorption at off-normal angles and high kinetic energy by means of fluid flow.¹⁵ Upon expansion of the region, molecules with low kinetic energy begin to desorb over all angles due to effusive-type motions.^{9,15} The periphery of the crater is responsible for the abundant sputtering of molecules and molecular clusters.⁹ Indeed, despite the similar yields (Targets I–III, Figs. 3–5), the shapes of the peaks of (D8Phe-H)⁻ are different. The right part of the peak (Fig. 5) has an extended tail, which is due to the fragmentation of molecular cluster ions.¹⁷ The vibrationally excited parent molecular cluster ion of phenylalanine (for instance Phe dimer) undergoes a unimolecular fragmentation¹⁸ into a daughter Phe ion and a neutral molecule.

The fragmentation of the parent molecular cluster ions occurs in the electrostatic field between the target and the extraction electrode and hence leads to a lesser daughter ion acceleration. The deficit in kinetic energy of a daughter ion when apparent as a peak tail indicates that the fragmentation process is a frequent de-excitation pathway for the parent molecular cluster ions.

The situation is different in the case of a monolayer deposited on graphite, here the small number of molecules limits the formation of molecular clusters in the ejection area [Target II, Fig. 4 and Figs. 10 and 11 (Multimedia view)]. Indeed, there is no extended tail (Fig. 4). Interestingly, molecular cluster fragmentation is observed in the peak obtained from a single layer of molecules deposited on graphene (Fig. 3). The effect is due to the radial compression of the molecular layer, when the molecules are agglomerated into the thick rim [Figs. 7 and 8 (Multimedia view)]. The MD simulations of 50 keV C₆₀ impacts on 10 layers of Phe molecules deposited on graphene demonstrate that this system can be considered as an analog of the bulk Phe crystal. The total yield of Phe molecules computed for this case (165 molecules as separate entities, plus 190 molecules as molecular clusters) is significantly larger than the yield of Phe molecules from 1 layer of Phe deposited on graphene (9 molecules/impact).

Kinetic energy distributions

The shape of the low mass side of the (D8Phe-H)⁻ peak corresponds to the initial kinetic energy distribution of ejecta. Using the procedure referred to earlier, the peak shapes were converted into the kinetic energy distribution for all targets (Fig. 12). The distributions show that most of the molecular ions have low kinetic energies (0.01–0.1 eV range). This feature corroborates the mechanisms of a gentle ejection described above. However some molecular ions still have high kinetic energies (~10 eV), which are higher than the bond energies in the organic molecules. The molecular ejecta can acquire high translational velocities and survive, if the atom's momenta are correlated during the ejection. An oscillating membrane experiences up/down movement with frontal acceleration/deceleration, thus the membrane provides the correlated momenta (trampoline mechanism) that give some molecules an energetic push. The number of ejected molecules

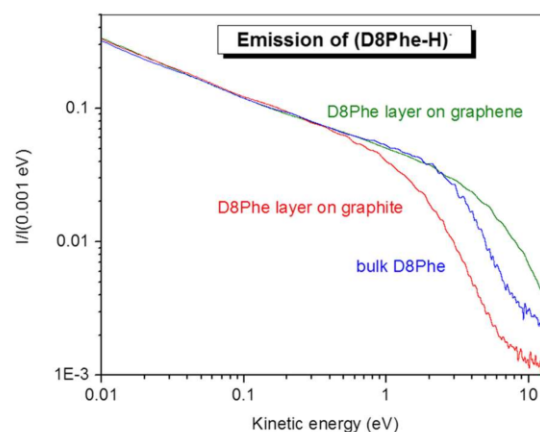


FIG. 12. Kinetic energy distributions measured for the molecular ions (D8Phe-H)⁻ emitted from: the single molecular layer of D8Phe deposited on 2-layer graphene (green color, Target I), the single molecular layer of D8Phe deposited on pyrolytic graphite (red color, Target II) and bulk D8Phe (blue color, Target III). The energy distributions at the high energy tails (>10 eV) are not shown as they are distorted by an overlap with the small peaks of (D7Phe-H)⁻ ions. A small amount of D7Phe molecules are generated during the molecule deposition at the graphene surface.

at the peak velocity of the system molecule/membrane is small. Their probability of ionization though should be high as fast molecular ions pass the critical distance of electron tunneling within shorter time from ejection, thus having a lower probability of neutralization.¹⁹

Again most molecules have low kinetic energy, thus the low translational velocities do not increase the ionization probability. The high ionization probability of these molecules can be explained with the model of thermalized excitation.²⁰

Ionization

The ionization probability of molecules can be estimated from the experimental yields of ions and yields of neutral molecules from MD simulations as follows:

$$P_{Phe}^{(exp)} = \frac{Y_{Phe}^-}{Y_{Phe}^0} \cdot \frac{1}{x}, \quad (8)$$

where Y_{Phe}^- is the yield of emitted (D8Phe-H)⁻ ions (measured experimentally), Y_{Phe}^0 is the yield of ejected Phe molecules (MD simulations) and $x \approx 0.5$ is the transmission/detection efficiency of the mass-spectrometer.

The yield of intact neutral molecules of Phe computed by MD is 9 molecules/impact for the Target I (the molecular layer of D8Phe deposited on graphene). Taking into account that the measured yield of (D8Phe-H)⁻ is 0.1, we infer an ionization probability (PI) of ~0.02. A high PI = 0.2 is observed for the molecular fragment CN⁻. The ionization probability for the Target III (bulk Phe) is significantly smaller. The measured yield of (D8Phe-H)⁻ is 0.13, and the computed by MD total yield of Phe is 355 molecules/impact, thus the PI ~ 7 · 10⁻⁴ only.

We have shown previously that for the emission of carbon cluster ions from 4-layer graphene³ as well as for the emission of C₆₀⁻ from a single layer of C₆₀ deposited on graphene,⁴ the relevant mechanism of ionization is that of electron tunneling. The vibrationally excited graphene has an average electron

temperature of 3700 K at the rim at the time of the tunneling process.³ We can estimate within the framework of the adiabatic limit of the thermalized excitation model,¹⁹ the ionization probability of the Phe molecules

$$P_{Phe}^{(T)} = \left(\frac{Z^-}{Z^0} \right) \exp \left[-\frac{(\varphi - A - \delta_{ic})}{F(kT_e)} \right], \quad (9)$$

where T_e is the average electron temperature of the rim around the graphene hole at the time of the tunneling process, δ_{ic} is the image charge correction factor (set to zero here) and Z^- along with Z^0 are the partition functions of emitted C ions and neutrals at T_e . The work function of the rim is unknown. As an estimate, we can take the value of the work function of the free standing pristine graphene ($\varphi = 4.5$ eV). The electron affinity of the Phe molecule is in a range 3.2–3.5 eV,²⁰ thus taking the value of $T_e = 3700$ K from Ref. 3 one can estimate the ionization probability as $P_{Phe}^{(T)} \sim 0.02 - 0.04$. These values are consistent with the experimental value of 0.02. After ionization, the Phe⁻ molecule experiences a prompt fragmentation into the deprotonated negative ion, (D8Phe-H)⁻,^{21,22} thus the mass spectra contain (D8Phe-H)⁻ only. The formation of deprotonated negatively charged amino acids has previously been observed in the studies on the dissociative electron attachment.^{22–24} The difference with the experiment presented here is the nature of electrons involved in the ionization (free electron capture versus electron tunneling from graphene to Phe). The particular mechanisms of the prompt deprotonation of negatively charged amino acids are under discussion^{22–24} (out of scope of the present study).

Another possible mechanism of ionization is a direct proton transfer exchange: The ions of molecular fragments (i.e., CN⁻) generated in the impact area interact with intact molecules from the rim. The proton exchange for the system, Phe molecule + CN⁻, is energetically favorable (the energy of 15.2 eV for CN⁻ protonation²⁵ toward the energy of 14.75 eV for Phe molecule deprotonation).²⁶ The CN ions themselves are ionized by the tunneling mechanism mentioned above ($EA_{CN} \sim 3.9$ eV), as well as by an electron exchange with interacting molecular fragments within the hot area of the impact, where the density of the fragments is high.

The ionization via proton exchange between Phe molecules and negative ions of small fragments should be relevant for the molecular ion emission from bulk molecular matter. A different path via electron exchange between the sputtered molecules is unlikely given the high activation energy barrier (~ 12 eV—sum of Phe molecule electron affinity²¹ and ionization potential²⁷). One should note that the electron tunneling process between the molecule and the graphene/graphite layer is different due to the metallic bond structure (free electrons in the conduction band) of the graphene/graphite. The barrier for tunneling is only ~ 1 eV [Eq. (9)]. The hypothesis of the proton exchange mechanism for bulk Phe is supported by the evidence of a large number of the daughter molecular ions, which originate via fragmentation of the molecular cluster ions (Fig. 4 and discussion above). The neutral molecular clusters have a large cross section of interaction with CN⁻. The ionized molecular ion clusters (proton exchange with CN⁻) are, at the same time, sufficiently vibrationally excited (low energy bonds between molecules) to

fragment within the short times (ns-ms interval).¹⁷ The daughter molecular ions appear as prominent fragmentation tails of (D8Phe-H)⁻ (Fig. 4).

CONCLUSION

The efficient emission of molecular ions stimulated by impacts of 50 keV C₆₀²⁺ on phenylalanine molecules deposited as a single molecular layer on graphene was investigated experimentally. The abundant ion emission can be explained with insight from MD simulations showing a radial compression of the deposit combined with an oscillating movement of the graphene. The result is a “trampoline-like” ejection of molecules and molecular fragments. MD simulations confirm the experimental observation of emission of high kinetic energy molecular ions via the trampoline effect. We show that graphene enhances a probability of ionization for ejected molecules. We postulate that the high rate of negative ionization is due to electron tunneling from graphene to phenylalanine. A recently developed laser post-ionization, LPI, was applied on organic molecules of guanine and coronene, which were sputtered by 40 keV C₆₀⁺ bombardment from bulk targets^{28,29}. The LPI approach has yielded experimental positive ionization probabilities of $\sim 10^{-3}$ which may be compared with the 7×10^{-4} estimated for the molecules sputtered from bulk phenylalanine reported here. It will be interesting to compare on a broader range of compounds the experimental ionization probability measurements via LPI with the estimate involving data from MD simulations.

The trampoline ejection combined with efficient ionization generates molecular ion yields from monolayers of phenylalanine on graphene or graphite similar to those from a bulk analyte target. The similarity may be a fortuitous outcome of our experimental conditions. To advance our insight into the differences of projectile energy deposition in 2D and 3D targets, we plan experiments with varying projectile impact energies. Our observation shows that the deposition of energy into the 2D-like electron-rich atomic layer enhances the analyte ion yield, a critical issue for secondary ion mass spectrometry. Put differently, the physical properties of the substrate are the key for maximizing ejection-ionization of monolayer deposits of weakly bonded moieties. The prime condition though, is that of the energy density that must be delivered in a sub-ps interval into the 2D solid. Future experiments focusing on projectile energy loss should provide insight into the energetics required for trampolining-ionization.

ACKNOWLEDGMENTS

This work was supported by the National Science Foundation under Grant No. CHE-1308312 and by the Polish National Science Center, Grant No. 2015/19/B/ST4/01892.

¹P. van der Heide, *Secondary Ion Mass Spectrometry: An Introduction to Principles and Practices* (John Wiley & Sons, Inc., Hoboken, New Jersey, 2014).

²R. Behrisch and W. Eckstein, *Sputtering by Particle Bombardment* (Springer-Verlag Berlin Heidelberg, 2007).

³S. V. Verkhoturov, S. Geng, B. Czerwinski, A. E. Young, A. Delcorte, and E. A. Schweikert, “Single impacts of keV fullerene ions on free standing

- graphene: Emission of ions and electrons from confined volume," *J. Chem. Phys.* **143**, 164302 (2015).
- ⁴S. Sheng Geng, V. Verkhoturov, M. J. Eller, S. Della-Negra, and E. A. Schweikert, "The collision of a hypervelocity massive projectile with free-standing graphene: Investigation of secondary ion emission and projectile fragmentation," *J. Chem. Phys.* **146**, 054305 (2017).
- ⁵S. V. Verkhoturov, B. Czerwinski, D. S. Verkhoturov, S. Geng, A. Delcorte, and E. A. Schweikert, "Ejection-ionization of molecules from free standing graphene," *J. Chem. Phys.* **146**, 084308 (2017).
- ⁶S. V. Verkhoturov, M. J. Eller, R. D. Rickman, S. Della-Negra, and E. A. Schweikert, "Single impacts of C₆₀ on solids: Emission of electrons, ions and prospects for surface mapping," *J. Phys. Chem. C* **114**(12), 5637–5644 (2010).
- ⁷M. J. Eller, S. V. Verkhoturov, S. Della-Negra, and E. A. Schweikert, "SIMS instrumentation and methodology for mapping of co-localized molecules," *Rev. Sci. Instrum.* **84**(10), 103706-1–103706-7 (2013).
- ⁸R. D. Rickman, S. V. Verkhoturov, E. S. Parilis, and E. A. Schweikert, "Simultaneous ejection of two molecular ions from keV gold atomic and polyatomic projectile impacts," *Phys. Rev. Lett.* **92**, 047601-1–047601-4 (2004).
- ⁹B. J. Garrison and Z. Postawa, "Molecular dynamics simulations, the theoretical partner to dynamic cluster SIMS experiments," in *ToF-SIMS—Surface Analysis by Mass Spectrometry*, 2nd ed., edited by J. C. Vickerman and D. Briggs (IMP & Surface Spectra, Ltd., Chichester, Manchester, 2013), pp. 151–192, and references therein.
- ¹⁰J. F. Ziegler, J. P. Biersack, and U. Littmark, *The Stopping and Range of Ions in Solids* (Pergamon, New York, 1985).
- ¹¹Z. Postawa, B. Czerwinski, M. Szewczyk, E. J. Smiley, N. Winograd, and B. J. Garrison, "Enhancement of sputtering yields due to C₆₀ versus Ga bombardment of Ag{111} as explored by molecular dynamics simulations," *Anal. Chem.* **75**, 4402–4407 (2003).
- ¹²S. Plimpton, "Fast parallel algorithms for short-range molecular dynamics," *J. Comput. Phys.* **117**, 1 (1995).
- ¹³R. Zan, Q. M. Ramasse, U. Bangert, and K. S. Novoselov, "Graphene reknits its holes," *Nano Lett.* **12**, 3936–3940 (2012).
- ¹⁴M. Schwoerer and H. Ch. Wolf, *Organic Molecular Solids* (Wiley-VCH Verlag GmbH & Co., Weinheim, Germany, 2007).
- ¹⁵B. J. Garrison, Z. Postawa, K. E. Ryan, J. C. Vickerman, R. P. Webb, and N. Winograd, "Internal energy of molecules ejected due to energetic C₆₀ bombardment," *Anal. Chem.* **81**, 2260–2267 (2009).
- ¹⁶S. Sheraz nee Rabbani, I. B. Razo, T. Kohn, N. P. Lockyer, and J. C. Vickerman, "Enhancing ion yields in time-of-flight-secondary ion mass spectrometry: A comparative study of argon and water cluster primary beams," *Anal. Chem.* **87**, 2367–2374 (2015).
- ¹⁷J. D. DeBord, S. V. Verkhoturov, L. M. Perez, S. W. North, M. B. Hall, and E. A. Schweikert, "Measuring the internal energies of species emitted from hypervelocity nanoparticle impacts on surfaces using recalibrated benzylpyridinium probe ions," *J. Chem. Phys.* **138**, 214301 (2013).
- ¹⁸A. Wucher, N. K. Dzhelev, I. V. Veryovkin, and S. V. Verkhoturov, "Fragmentation lifetimes and the internal energy of sputtered clusters," *Nucl. Instrum. Methods Phys. Res., Sect. B* **149**, 285 (1999).
- ¹⁹M. L. Yu and N. D. Lang, "Mechanisms of atomic ion emission during sputtering," *Nucl. Instrum. Methods Phys. Res., Sect. B* **14**(4-6), 403–413 (1986).
- ²⁰Z. Sroubek, X. Chen, and J. A. Yarmoff, "Ion formation and kinetic electron emission during the impact of slow atomic metal particles on metal surfaces," *Phys. Rev. B* **73**(4), 045427-1–045427-8 (2006).
- ²¹Z. G. Keolopile, M. Gutowski, and M. Haranczyk, "Discovery of most stable structures of neutral and anionic phenylalanine through automated scanning of tautomeric and conformational spaces," *J. Chem. Theory Comput.* **9**, 4374–4381 (2013).
- ²²Y. V. Vasil'ev, B. J. Figard, D. F. Barofsky, and M. L. Deinzer, "Resonant electron capture by some amino acids esters," *Int. J. Mass Spectrom.* **268**, 106–121 (2007).
- ²³A. M. Scheer, P. Mozejko, G. A. Gallup, and P. D. Burrow, "Total dissociative electron attachment cross sections of selected amino acids," *J. Chem. Phys.* **126**, 174301 (2007).
- ²⁴S. Denifl, H. D. Flosadóttir, A. Edtbauer, O. Ingólfsson, T. D. Märk, and P. Scheier, "A detailed study on the decomposition pathways of the amino acid valine upon dissociative electron attachment," *Eur. Phys. J. D* **60**, 37–44 (2010).
- ²⁵F. Ahu Akin and K. M. Ervin, "Collision-induced dissociation of HS⁻(HCN): Unsymmetrical hydrogen bonding in a proton-bound dimer anion," *J. Phys. Chem. A* **110**, 1342–1349 (2006).
- ²⁶C. M. Jones, M. Bernier, E. Carson, K. E. Colyer, R. Metz, A. Pawlow, E. D. Wischow, I. Webb, E. J. Andriole, and J. C. Poutsma, "Gas-phase acidities of the 20 protein amino acids," *Int. J. Mass Spectrom.* **267**, 54–62 (2007).
- ²⁷K. T. Lee, J. Sung, K. J. Lee, S. K. Kim, and Y. D. Park, "Conformation-dependent ionization of L-phenylalanine: Structures and energetics of cationic conformers," *Chem. Phys. Lett.* **368**, 262–268 (2003).
- ²⁸N. J. Popczun, L. Breuer, A. Wucher, and N. Winograd, "Ionization probability in molecular secondary ion mass spectrometry: Protonation efficiency of sputtered guanine molecules studied by laser postionization," *J. Phys. Chem. C* **121**, 8931–8937 (2017).
- ²⁹N. J. Popczun, L. Breuer, A. Wucher, and N. Winograd, "On the SIMS ionization probability of organic molecules," *J. Am. Soc. Mass Spectrom.* **28**, 1182 (2017).

Article 5

Hypervelocity cluster ion impacts on free standing graphene:

Experiment, theory, and applications

Verkhoturov S. V., Goluński M., Verkhoturov D. S., Czerwinski B., Eller M.
J., Geng S., Postawa Z. & Schweikert E. A.

Journal of Chemical Physics 150, 160901 (2019)

doi:[10.1063/1.5080606](https://doi.org/10.1063/1.5080606)

Reprinted from J. Chem. Phys. 2019, 150, 160901, with the permission of AIP
Publishing.

Hypervelocity cluster ion impacts on free standing graphene: Experiment, theory, and applications

Cite as: J. Chem. Phys. 150, 160901 (2019); doi: 10.1063/1.5080606

Submitted: 9 November 2018 • Accepted: 11 March 2019 •

Published Online: 24 April 2019



View Online



Export Citation



CrossMark

Stanislav V. Verkhoturov,^{1,a)} Mikołaj Gołuński,^{2,b)}  Dmitriy S. Verkhoturov,^{1,c)} Bartłomiej Czerwinski,^{3,d)} 
Michael J. Eller,^{1,e)}  Sheng Geng,^{1,f)} Zbigniew Postawa,^{2,g)}  and Emile A. Schweikert^{1,h)} 

AFFILIATIONS

¹Department of Chemistry, Texas A&M University, College Station, Texas 77843-3144, USA

²Department of Physics, Jagiellonian University, Kraków, Poland

³Applied Physics, Division of Materials Science, Department of Engineering Sciences and Mathematics, Luleå University of Technology, SE-971 87 Luleå, Sweden

^{a)}verkhoturov@tamu.edu

^{b)}mikolaj.golunski@gmail.com

^{c)}verkhoturovdm@tamu.edu

^{d)}bartlomiej.czerwinski@ltu.se

^{e)}meller@chem.tamu.edu

^{f)}gengsheng@tamu.edu

^{g)}zbigniew.postawa@uj.edu.pl

^{h)}schweikert@chem.tamu.edu

ABSTRACT

We present results from experiments and molecular dynamics (MD) simulations obtained with C_{60} and Au_{400} impacting on free-standing graphene, graphene oxide (GO), and graphene-supported molecular layers. The experiments were run on custom-built ToF reflectron mass spectrometers with C_{60} and Au-LMIS sources with acceleration potentials generating 50 keV C_{60}^{2+} and 440–540 keV Au_{400}^{4+} . Bombardment-detection was in the same mode as MD simulation, i.e., a sequence of individual projectile impacts with separate collection/identification of the ejecta from each impact in either the forward (transmission) or backward (reflection) direction. For C_{60} impacts on single layer graphene, the secondary ion (SI) yields for C_2 and C_4 emitted in transmission are ~ 0.1 (10%). Similar yields were observed for analyte-specific ions from submonolayer deposits of phenylalanine. MD simulations show that graphene acts as a trampoline, i.e., they can be ejected without destruction. Another topic investigated dealt with the chemical composition of free-standing GO. The elemental composition was found to be approximately COH_2 . We have also studied the impact of Au_{400} clusters on graphene. Again SI yields were high (e.g., 1.25 C^- /impact). 90–100 Au atoms evaporate off the exiting projectile which experiences an energy loss of ~ 72 keV. The latter is a summation of energy spent on rupturing the graphene, ejecting carbon atoms and clusters and a dipole projectile/hole interaction. The charge distribution of the exiting projectiles is $\sim 50\%$ neutrals and $\sim 25\%$ either negatively or positively charged. We infer that free-standing graphene enables detection of attomole to zeptomole deposits of analyte via cluster-SI mass spectrometry.

Published under license by AIP Publishing. <https://doi.org/10.1063/1.5080606>

I. INTRODUCTION

A number of studies have dealt with the interaction of energetic ions (mostly atomic ions) with graphene deposited on substrates (e.g., Refs. 1–3). However, the collision of hypervelocity particles

with free-standing graphene has so far received limited attention. Yet, the interaction exhibits many unusual aspects not present in bulk materials. The 2D target material occupies a niche between a gas and a solid, and the collision process occurs under extreme dynamic conditions.

We refer here to experiments and molecular dynamics (MD) simulations detailing graphene's response to impacts of single atomic ions, clusters, or nanoparticles with velocities of 1–30 km s⁻¹.^{4–7} It has been reported that impacts with nanometer diameter particles initiate peculiar track mechanisms that can lead to the formation of nanopores.^{6,8,9} The result is a molecular sieving membrane combining unmatched mechanical strength with a low transport resistance and a high flux rate.¹⁰ Bombardment with larger (\geq micrometer diameter) projectiles has shown that multilayer graphene has spectacular mechanical strength in the ballistic regime due to a highly efficient mode of energy absorption.¹¹ The straining and rupturing of graphene under bombardment are accompanied by ultrafast processes with characteristics modulated by those of the projectiles. For instance, a single highly charged ion passing through free-standing graphene causes within femtoseconds emission of a burst of electrons corresponding to an astounding current density in an excess of 10¹² A cm⁻².¹² This observation opens prospects for graphene-based ultrafast high current-electronic applications. Another intriguing finding is a sizable energy loss experienced by medium and large cluster projectile passing through free-standing graphene.^{5,9} Further, bombardment combined with mass spectrometric identification of the ejecta showed a dramatic increase in the ionization probability of organic molecules deposited on graphene.⁷ Akin to this observation are reports of enhanced ionization in secondary ion mass spectrometry (SIMS) experiments where samples were covered with graphene.¹³

This paper is not a comprehensive review but an introduction to a key aspect of hypervelocity projectile-graphene interactions, namely, the characteristics of the ejecta which in turn should provide insight into the mechanisms of energy dissipation. The focus is on the ejecta from free-standing graphene, graphene oxide (GO), and graphene-supported molecular layers under impact of a 2D (C₆₀) or 3D (Au₄₀₀) massive cluster projectiles at impact velocities of 1–30 km s⁻¹. The directly relevant literature is sparse and consists mainly of MD simulations with attention on defect creation in the graphene rather than on the ejection of matter.⁸ We focus here on observations from experiments and MD simulations run under equivalent conditions on like-targets.

A schematic of the experimental setup is provided in Fig. 1. A detailed description is provided in Refs. 4, 14, and 15. Briefly, the emitted secondary ions and ionized fragments of projectiles are detected as time-of-flight mass spectra.¹⁶ The applied experimental setup allows the separate recording of the emitted ions from each collision. The event-by-event bombardment-detection mode allows for the selection of specific impacts, i.e., those involving free-standing graphene at the exclusion of signals from the target holder and support. The instrument has two ion sources and a single mass spectrometer, allowing a direct comparison of mass spectra measured in either transmission (graphene) or reflection (bulk target) experiments.

The graphene targets referred to herein consist of graphene or graphene oxide layers placed on a lacey carbon structures itself placed on a 300 mesh Cu grid.¹⁷

As noted, we combine experimental observations with molecular dynamics (MD) computer simulations of cluster bombardment. In this approach, the movement of particles is determined by integrating Hamilton's equations of motion. A detailed description of the MD method can be found elsewhere.¹⁸ The forces among atoms

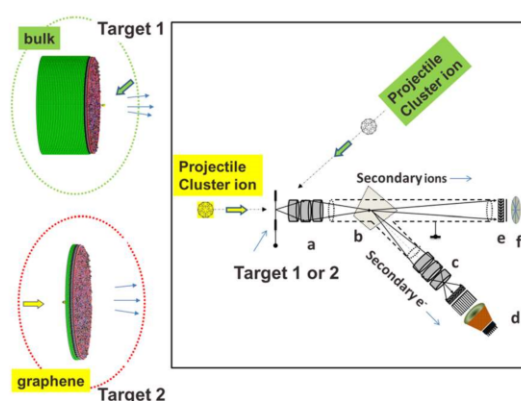


FIG. 1. Schematic of the experimental setup: (a) objective lens for secondary ions and electrons, (b) magnetic prism for redirection of electrons toward imaging electron optics (c), (c) imaging electron optics, (d) position sensitive detector consisting of dual microchannel plate, phosphor screen, and CMOS camera, (e) dual microchannel plate, and (f) 8 anode detector.

in the modeled system are described by the AIREBO¹⁹ (C–C interactions in earlier simulations⁵) or by ReaxFF-Ig force fields.²⁰ Both these potentials allow for the creation and breaking of covalent bonds; however, the ReaxFF-Ig force field is more advanced. It gives predictions that are more accurate and is able to describe interactions between C, H, N, O atoms. The forces between Au atoms are described by the embedded atom model (EAM) potential,²¹ while a purely repulsive Ziegler-Biersack-Littmark (ZBL) potential is used to model Au–C interactions.²² Electronic energy losses are ignored due to a low velocity of moving projectile atoms. The shape and size of the samples are chosen based on visual observations of energy transfer pathways stimulated by impacts of C₆₀ and Au₄₀₀ projectiles. As a result, cylindrical samples with a diameter of 40 nm are used. Rigid and stochastic regions are applied to simulate the thermal bath that keeps the sample at required temperature, to prevent reflection of pressure waves generated by cluster projectile impacts from the boundaries of the system, and to maintain the shape of the sample.^{18,23} Samples with a thickness between 1 (1L) and 16 (16L) graphene layers with a highly oriented pyrolytic graphite structure, a monolayer of phenylalanine (Phe) deposited on a 2L graphene substrate, and a bulk system of Phe molecules are probed. The kinetic energy and the impact angle of the projectile are changed to investigate the effect of these parameters on the particle ejection process. Particles emitted both in the direction of the primary beam (transmission direction) and in the opposite direction (sputtering direction) are collected. The simulations are run at a target temperature of 0 K in an NVE ensemble and extend up to 20 ps for a clean graphene, up to 40 ps for a monolayer of Phe molecules, and up to 80 ps for a bulk Phe system. These values are long enough to achieve saturation in the ejection yield versus time dependence. Between 8 and 32 randomly selected impact points located near the center of the sample are chosen to achieve statistically reliable data.

Returning to the topic of this perspective, the challenge here is to gain insight into the mechanism(s) of ejection and ionization.

Clearly, the sputtering mechanism valid for bulk targets is not applicable. It may be recalled that in a bulk target, sputtering results from the dissipation of the projectile kinetic energy via linear collision cascades (atomic projectiles) or high density collision cascades, or spike, in the case of cluster impacts.^{18,24} It should be mentioned that a spike is also reported for impacts of the atomic projectiles at specific conditions. Such conditions occur during bombardment of weakly bound solids (frozen gases) or when heavy projectiles (Xe) are used.²⁵ There are several differences between ejection stimulated by a linear collision cascade and spike. The presence of the dense collision cascade leads to a more efficient sputtering and emission of less energetic atoms. Cluster projectile impacts are particularly prone to form high-density cascades due to shallow deposition of the primary kinetic energy.^{18,26,27} Impacts of such clusters generate correlated momenta toward the surface around the impact point leading to a formation of almost hemispherical craters.^{26,27} In the case of the bulk molecular target, the projectile impact at the surface initially creates an energized volume primarily composed of molecular fragments.¹⁸ Expansion of this volume stimulates sputtering of energetic molecules at off-normal angles by means of fluid flow.^{18,28} Upon a further expansion of the volume, molecules with low kinetic energy begin to desorb over all angles due to effusive-type motions.^{18,28} The development of the both linear collision cascade and spike requires a 3D medium, which is at least a few tens of nanometers thick. There has to be a certain number of atomic collisions to randomize a linear collision cascade or form a high-density core in spike. For 2D targets, the amount of material is not sufficient and sputtering-ionization does not originate from fully developed collision cascades. We examine four cases below to probe processes taking place in 2D targets: C_{60} impacts on graphene, graphene oxide, molecular layers deposited on graphene, and Au_{400} impacts on graphene. We summarize here the relevant literature describing experiments and MD simulations as well as recent new observations dealing with the characterization of ejecta as well as the evolution of graphene.

II. C_{60} IMPACTS ON FREE STANDING GRAPHENE

Let us consider the interaction of 50 keV C_{60} at normal incidence with graphene step by step.⁴ As shown in Fig. 2 (Multimedia view), even for a monolayer graphene, there is complete atomization of C_{60} projectile. The C atoms of projectile and most of knocked-on atoms of graphene travel in the transmission direction.

In the 1L graphene case, the colliding/atomizing C_{60} projectile (diameter 0.7 nm) spends approximately 10 fs to pass the graphene plane. The presence of a conglomerate of C atoms at a distance of ~ 1.5 nm from the graphene at 30 fs indicates that most of projectile atoms retain high velocity as a consequence of a low collisional energy loss. The latter increases with the thickness of graphene as illustrated with the case of 2L and 4L graphene [Figs. 2(b) and 2(c) (Multimedia view)]. In the 4L graphene case, the 30 fs snapshot shows that the atoms of the projectile barely exit the graphene, which indicates that they efficiently transferred the kinetic energy to the knocked-on atoms of graphene. This aspect will be discussed in more details later.

A second phase of the interaction lasting picoseconds is characterized by an abundant ejection of C atoms and clusters from the rim area around the primary graphene rupture (Fig. 3).⁴

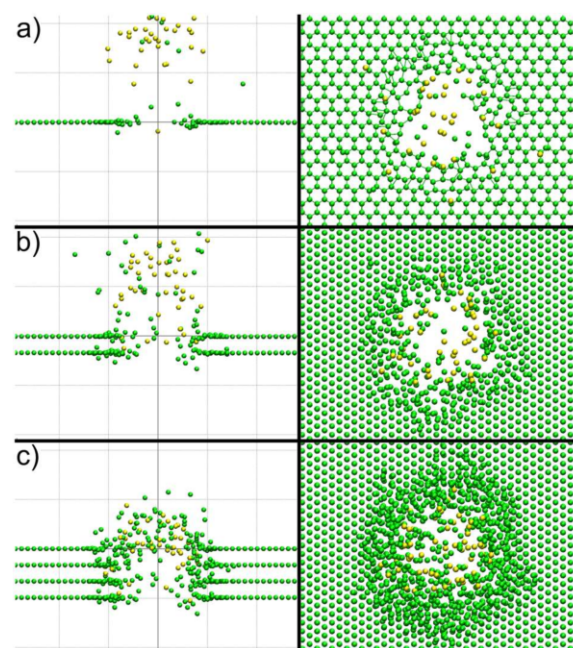


FIG. 2. MD simulation (cut and top view) of 50 keV C_{60} on (a) 1 layer, (b) 2 layer, and (c) 4 layer graphene at a time of 30 fs after impact. A 1 nm slice of the system centered at the impact point is shown. The gray lines in the background are separated by 1 nm. Only fragment of the bombarded system is visualized. The corresponding movie files are here. Multimedia views: (a) <https://doi.org/10.1063/1.5080606.1>; (b) <https://doi.org/10.1063/1.5080606.2>; and (c) <https://doi.org/10.1063/1.5080606.3>

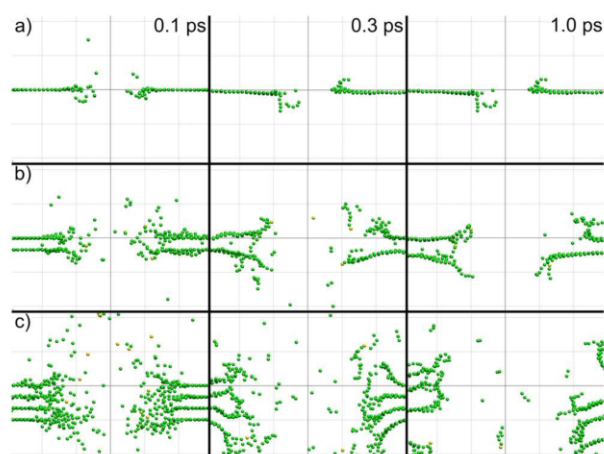


FIG. 3. MD simulation (cut view) of 50 keV C_{60} on (a) 1 layer, (b) 2 layer, and (c) 4 layer graphene at 0.1 ps, 0.3 ps, and 1 ps after impact. A 1 nm slice of the system centered at the impact point is shown. The gray lines in the background are separated by 1 nm. Only fragment of the bombarded system is visualized. The corresponding movie files are as for Figs. 2(a)–2(c).

The radial movement of C atoms around the rupture initiated by the first fast phase is transformed into collective movements, which develop a wavelike vertical oscillations and radial planar compressions. Similar phenomenon also has been observed on a graphite surface bombarded by C_{60} .^{29,30} The vibrationally excited rim is the source of the C ejection (see the movies in the supplementary material of Refs. 4 and 9). One should note that although the energy accumulated around the hole is small (a few percent of the total energy), it is sufficient for the ejection of carbon atoms and clusters due to the confined energy dissipation in the 2D material. This process clearly differs from the sputtering induced by impacts on a bulk material.^{24,28,31}

As visible in Fig. 3, the ejection efficiency depends on the substrate thickness. To probe this phenomena more accurately, the yield of carbon atoms ejected in the transmission and reflection/sputtering directions are plotted as a function of the substrate thickness and primary kinetic energy. The results are shown in Fig. 4(a). For particles ejected in the transmission direction, the yield vs thickness dependence has a maximum, which shifts to thicker systems with the increase in the projectile kinetic energy. For substrate atoms ejected in the sputtering direction, the yield initially increases but ultimately saturates. Variation of the substrate thickness has a different impact on ejection of projectile atoms. The

yield decreases monotonically with the sample thickness for carbon atoms ejected in the transmission direction. The yield of backscattered projectile atoms is very low and does not exhibit a consistent dependence on the substrate thickness. The last two observations indicate that projectile atoms are being trapped inside the graphene substrate due to a strong covalent interaction with the surrounding medium. The occurrence of this process is also seen in Fig. 3. The magnitude of this process increases with the sample thickness. Projectiles that are more energetic are able to perforate thicker systems, which explain broadening of the yield versus thickness dependence with the increase in the primary kinetic energy.

Almost all projectile atoms penetrate through a thin substrate, as shown in the inset of Fig. 4(a). However, even in this case, the projectile-graphene interaction is significant, especially for low-energy projectiles. For instance, for 5 keV C_{60} , almost 40% of the primary kinetic energy is lost during penetration of the one layer (1L) sample, as shown in the inset of Fig. 4(b). Almost 70% of impact energy is lost in the 2L system. These numbers drop to 15% and 20% for analogous systems bombarded by 40 keV projectiles. Substrate atoms emitted in the transmission direction carry most of the deposited energy away. The energy carried away by sputtered atoms is small and does not exceed 0.5% of the initial kinetic energy. For a

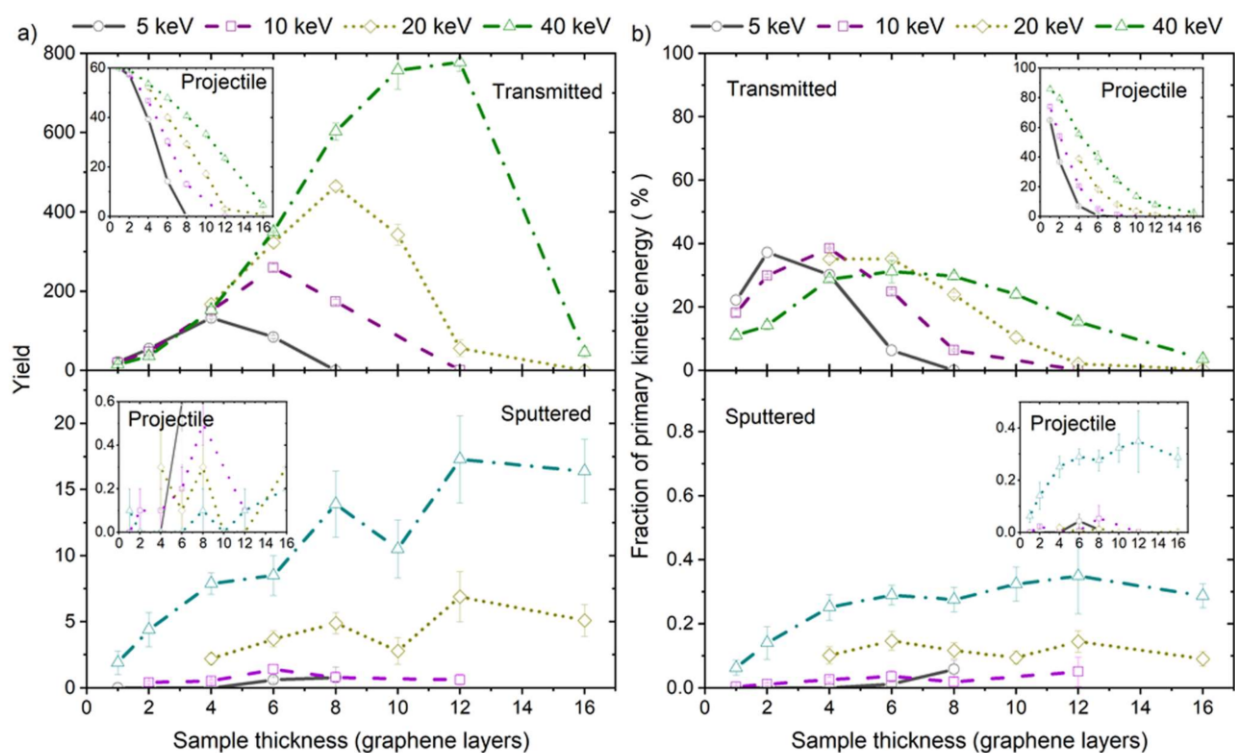


FIG. 4. Dependence of (a) the ejection yield and (b) the fraction of primary kinetic energy carried away by particles emitted in the transmission (top) and sputtering (bottom) directions on the thickness of the sample bombarded by 5, 10, 20, and 40 keV C_{60} projectiles at normal incidence. Main graphs represent the atoms ejected from the sample, while the insets depict projectile atoms. Reprinted with permission from M. Golunski and Z. Postawa, *J. Vac. Sci. Technol. B* **36**, 03F112 (2018).

given primary kinetic energy, the amount of energy deposited in the solid increases with the sample thickness.

The kinetic energy distributions of C ions (Ref. 1, Fig. 5) ejected in the transmission direction obtained experimentally and of C atoms computed by MD simulations⁴ are similar, showing that most atoms/ions have kinetic energies in the eV range. However, some C atoms/ions have much higher kinetic energy. The latter corresponds to atoms originating from the projectile or/and substrate atoms ejected via direct elastic atom-atom collisions. The MD simulations show that some of projectile atoms residing at the front of the impinging cluster gain additional kinetic energy during projectile deceleration and deformation. These atoms gain additional kinetic energy from atoms located at the back of the projectile, when these particles collide. Thus, theoretically, after collision, the kinetic energy of few atoms can be higher than the kinetic energy of projectile atoms (50 keV/60 atoms = 833 eV, Fig. 4).

The evolution of the graphene in the first phase ($t < 10$ fs) is characterized by the generation of a round shaped rupture (diameter ~ 1 nm) and a fast planar wave of collective radial movements of the graphene atoms [Fig. 2 (Multimedia view) and Fig. 3, top view]. The atoms around the rupture (hole) are displaced radially breaking of the atom-atom bonds. This process initiates the formation of a vibrationally exited rim around the rupture.^{4,5,9}

The flux of emitted particles is composed of single atoms and clusters. The experimental yields of the emitted cluster ions (ions/projectile impact) and the yields of the neutral clusters obtained by MD simulations are shown in Fig. 5 for 50 keV C_{60}^{2+} impacts at 4L graphene.⁴

In both cases, ejection of single C atoms is the dominant ejection channel. However, the most interesting observation is an abundant ejection of negative ions. The calculated ionization probabilities are shown in Fig. 6. It is evident that the ionization process is much

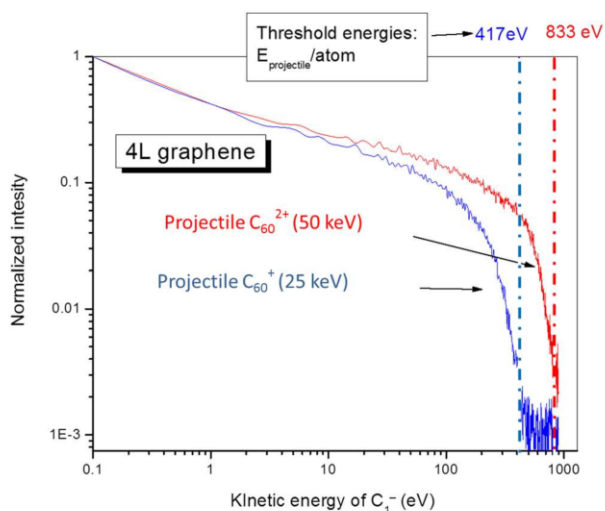


FIG. 5. Kinetic energy distributions of C_1^- emitted by impacts of fullerenes. The distributions show that doubling of the energy of C_{60} projectile from 25 keV to 50 keV doubles the maximum energy of the emitted C_1^- ions.⁴

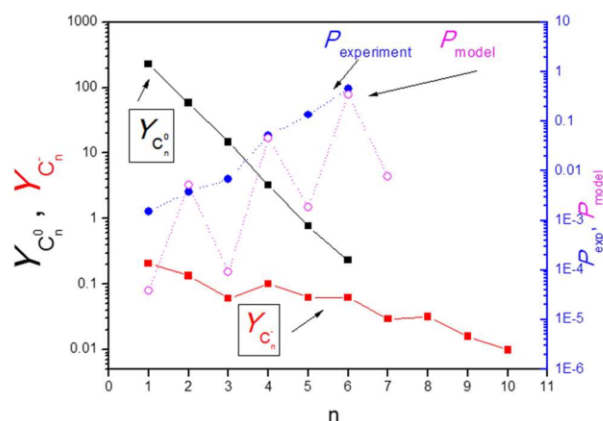


FIG. 6. Yields of neutral (MD) and negatively charged carbon clusters (experiment) emitted via 50 keV C_{60}^{2+} impacts on 4L graphene (left Y axis); ionization probabilities (right Y axis).⁴

more efficient than observed in analogous experiments performed on clean metals, semiconductors and organic samples.^{24,32,33}

The abundant ion emission prompts the issues of ionization mechanism(s). The ionization mechanisms in the case of sputtering of bulk matter have been a subject of extensive investigations over decades.^{32,33} In the case of sputtering of the surface of conductive matter (metal or metal-like materials),³² the main ionization mechanism is that of electron tunneling from a bulk surface to the sputtered species. The relevance of this mode for ion emission from graphene was evaluated in Refs. 4 and 5. Briefly, the following mechanism was proposed: the knocked-on carbon atoms, along with those from the shattered projectile and the ejected clusters from the rim of the hole, undergo of electron exchange processes before they escape beyond the critical distance for electron tunneling (~ 1 nm). The electron tunneling from the vibrationally and electronically exited rim, and, i.e., the ionization probability, P_n , can be explained with the thermalized excitation model.³³ The adiabatic limit of this model can be expressed as

$$P_n^{(T)} = \left(\frac{Z^-}{Z^0} \right) \exp \left[- \frac{(\varphi - EA - \delta_{ic})}{F(kT_e)} \right], \quad (1)$$

where T_e is the average electron temperature of the rim around the graphene hole at the time of the tunneling process, δ_{ic} is the image charge correction factor (set to zero in Refs. 4 and 5), and Z^- and Z^0 are the partition functions of emitted C ions and neutrals at T_e . The work function of the rim is unknown. For estimation, we may take the value of the work function of the free standing pristine graphene, $\varphi = 4.5$ eV. The values obtained for the adiabatic electron affinities of carbon clusters from Ref. 34 are shown in Table I. An approximation of the experimental ionization probabilities by the thermalized excitation model gives an average electron temperature of 3700 °K at the rim at the time of the tunneling process. One should note that the tunneling mechanism is applied here for the negative ionization of ejecta, which involves an electron transfer from graphene to ejecta. It means that the electron must be provided

TABLE I. Yields and experimental ionization probabilities of carbon clusters as a function of cluster size. The data were obtained for 50 keV C_{60}^{2+} impacts on 4L graphene.

Carbon cluster	EA (eV)	Yield of ion, $Y_{C_n^-}$	Yield of neutral, $Y_{C_n^0}$	Experimental ionization probability, $\frac{Y_{C_n^-}}{Y_{C_n^0}} = P_{exp}$
C_1	1.26	0.21	228	0.0015
C_2	2.82	0.13	58.5	0.004
C_3	1.53	0.06	14.8	0.007
C_4	3.52	0.10	3.23	0.052
C_5	2.49	0.062	0.77	0.136
C_6	4.16	0.063	0.23	0.452

by the conductive band of graphene. For the case of emission of positive ions, generally, the electron tunneling is not the only mechanism of ionization. The molecular/cluster ejecta, being vibrationally excited, undergo thermionic emission of electrons.³⁵

All experimental and computational data discussed so far have been obtained at a normal incidence angle. The effect of the impact angle on the ejection yield from the 2L and 8L systems bombarded by 10 and 40 keV C_{60} projectiles is shown in Fig. 7.⁹ The results obtained by MD simulations demonstrate that the impact angle has a similar influence on the yield of substrate atoms emitted in the transmission and sputtering directions for both these systems. As

in the case of substrate thickness, dependence of the yield of emitted substrate atoms has a maximum. The position of this maximum shifts to a larger impact angle and becomes more pronounced for projectiles that are more energetic. The shape of the plot obtained for sputtered atoms is particularly interesting as it is different from the yields reported for bulk solids bombarded by medium cluster projectiles, like C_{60} , where the signal decreases with the impact angle.^{36,37} Such different behavior can be attributed to the limited thickness of the bombarded free-standing graphene.

The impact angle also has a significant influence on a number of ejected projectile atoms. Again, the functional form of this influence

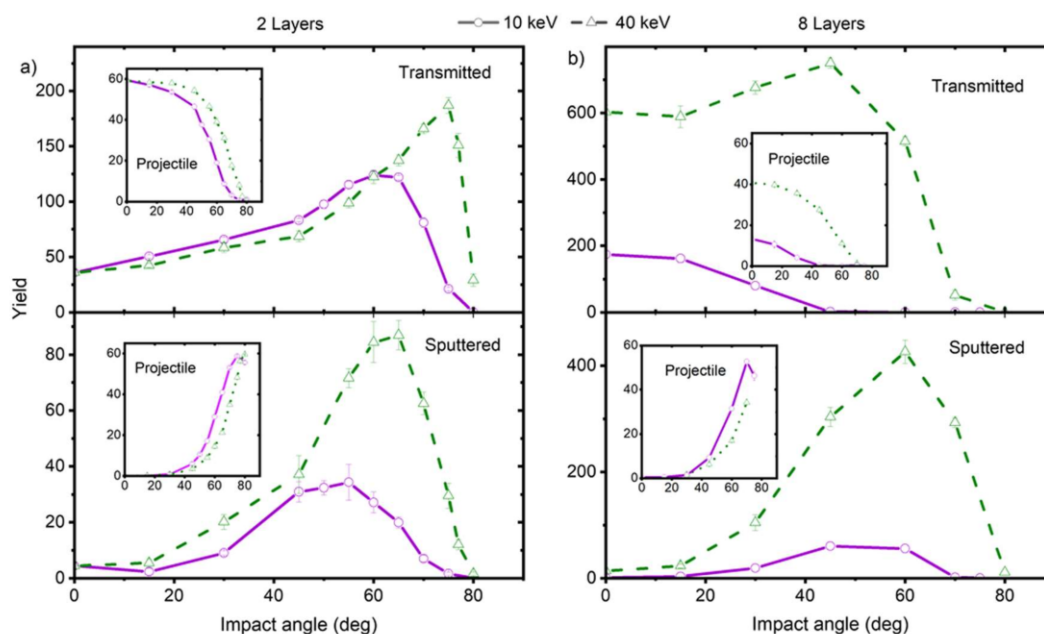


FIG. 7. Dependence of the yields of carbon atoms ejected in the transmission (top) and sputtering (bottom) directions from the (a) two and (b) eight layer systems bombarded by ten (solid line) and 40 keV C_{60} (dashed line) projectiles on the impact angle. Main graphs represent the atoms originating from the sample, while the insets depict projectile's atoms. Reprinted with permission from M. Golunski and Z. Postawa, *J. Vac. Sci. Technol. B* **36**, 03F112 (2018).

is different from the one observed for substrate atoms. The number of projectile atoms penetrating through the sample decreases monotonically with the impact angle, whereas the yield of backreflected atoms increases for more oblique impacts. For the 2L system, these yields are almost complementary, which indicates that projectile atoms can be either transmitted or backreflected. In other words, projectile atoms are not trapped inside such a thin system. The situation is different for the 8L system, especially when it is bombarded by low-energy projectiles. In this case, many projectile atoms are trapped inside the sample. Based on all observations, it can be concluded that the yield of graphene atoms is determined by two factors. The first factor is the amount of material available for ejection. This quantity will increase with the sample thickness and with the impact angle as the projectile will travel a longer path inside the substrate. The second factor is the amount of energy stored near the surface from where the ejection occurs. For ejection in the transmission direction, the upper surface is important. The energy stored near this surface will decrease with the sample thickness and the impact angle as projectile atoms have to sacrifice more energy to penetrate through the layer. For conditions where the substrate is perforated, there is an increase in the material available for ejection, and the yield increases with the substrate thickness or impact angle. However ultimately, less energy becomes available near the upper surface and the yield drops. For ejection in the sputtering direction, a bottom surface is important. Both the amount of material available for emission and the energy deposited near this surface increase with the sample thickness, until the layer becomes thicker than a thickness of a volume from where particles are ejected. Subsequently, the yield saturates because emission does not benefit from further increase in the sample thickness. The increase in the impact angle has also a positive effect on the amount of energy stored near the bottom surface as the energy deposition profile is shifted downward and the projectile can interact with a larger volume of material. However, the increase in the impact angle also reduces the projectile momentum component perpendicular to the surface. It becomes easier to backreflect the projectile atoms, and more energy is carried away by these particles. As a result, less energy is deposited near the bottom surface and the yield decreases for too oblique impacts. The yield of the projectile atoms ejected in the transmission direction is determined only by the capability of projectile atoms to perforate the sample. This capability decreases with the increase in both the layer thickness and the impact angle. The yield of the projectile atoms ejected in the sputtering direction will be determined by the capability of the sample to backreflect the projectile atoms. As already discussed, this capability increases with the impact angle. The increase in the primary kinetic energy leads to the deposition of a larger amount of this energy in the sample and to a larger projectile range. Both these factors lead to a stronger ejection of substrate atoms. A larger penetration range increases the substrate thickness, which can be perforated by the projectile. This factor leads to a shift of the emission maximum toward thicker samples for a constant impact angle or toward larger impact angles for a constant thickness when the projectile kinetic energy is increased. The increase in the primary kinetic energy also results in a broader distribution for projectile atoms.

It is known that for standard sputtering geometry, the substrate plays a major role in the ejection of intact molecules from ultrathin organic layers deposited on solid substrates.¹⁸ Direct

collisions between projectile atoms and adsorbed molecules lead to molecular fragmentation.^{26,43} Collisions of adsorbed molecules with ejecting substrate atoms or a concerted action of the unfolding of the crater rim in the substrate are the main processes leading to molecular emission from systems bombarded by atomic and cluster projectiles, respectively.^{26,38–40} The application of graphene combined with a transmission geometry exhibit a significant contribution from both these processes. For instance, as shown in Fig. 4(a), ejection of substrate atoms in the transmission direction is much stronger than that in the sputtering direction. As visible in Fig. 2, the impact of C_{60} results in a viable collective motion of graphene sheets near the rim area. The effective processes of ejection and ionization of ejecta convey the idea of using of graphene as the support for the small amounts of molecules or nano-objects, which can be ejected/analyzed via cluster projectile impacts. This concept is addressed below.

III. EJECTION AND IONIZATION OF MOLECULES VIA 50 keV C_{60}^{2+} IMPACTS ON THIN MOLECULAR LAYERS DEPOSITED ON FREE STANDING GRAPHENE

To date, there are experimental data and MD simulations for three targets: single layers of molecules of phenylalanine (Phe), single layers of deuterated phenylalanine (D8Phe), and C_{60} molecules deposited on 2L graphene.^{5,7,41} The experiments show emission of molecular ions with yields comparable to the yield of ions emitted from the bulk targets (multilayers of molecules). For instance, the yield of negative ions of deprotonated phenylalanine, $(D8Phe-H)^-$, emitted in the transmission direction is 0.10 ion per projectile impact for the target of 2 layer graphene coated by molecular layer of D8Phe (Fig. 8). This yield is comparable to a yield of 0.13 for a bulk target (Fig. 9) measured for secondary ions emitted in the reflection/sputtering direction.

These results raise the question of the mechanism(s) of organic molecule ejection and ionization from the graphene substrate. As noted earlier, the mechanism of molecule sputtering valid for bulk targets of organic molecules (weakly bonded molecular solids)¹⁸ is not applicable for the target of the molecular layer on graphene.

Indeed, the experimental data show notable differences between ion emission from single molecular layer+2L graphene and bulk D8Phe. The first difference is the high yield of C_1^- for graphene (0.15 ions/impact), which is attributed in part to fragmentation and atomization of the projectile after impact followed by the ionization of the projectile's atoms. The yield of C_1^- measured for the bulk target is much lower (0.04 ions/impact) due to less recoiled projectile atoms. In the case of graphene, the shape of C_1^- peak has an extended tail toward the low mass range. In the experimental range of sensitivity, these ions of high kinetic energies extend up to 1/60 (833 eV) of the projectile energy.⁷ A further difference is the shape of the peak of $(D8Phe-H)^-$, which depends on the mechanism/s of molecule ejection. In the case of emission from graphene, the shape of $(D8Phe-H)^-$ peak has an extended tail toward the high mass range (Fig. 6). This extended tail is due to fragmentation of molecular cluster ions.^{42,43} The vibrationally excited parent molecular cluster ion of phenylalanine (e.g., Phe dimer) undergoes a unimolecular fragmentation⁷ into a daughter Phe ion and a neutral molecule. Indeed, the total yield of Phe molecules computed for this case (165 molecules as separate entities, plus 190 molecules

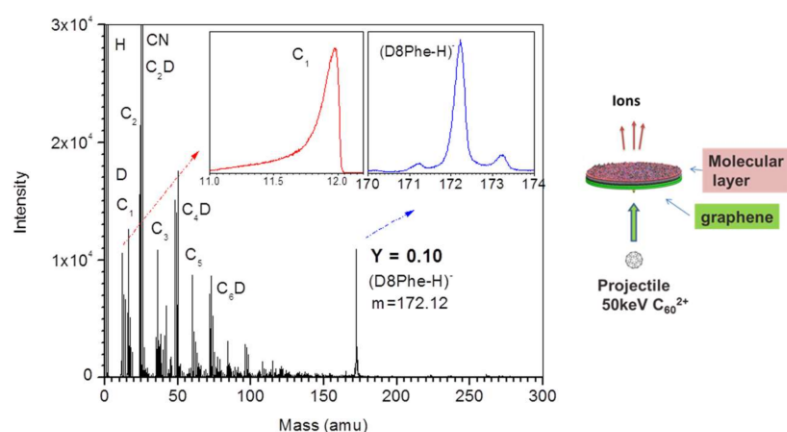


FIG. 8. Mass spectrum of negative ions emitted from the 2-layer graphene coated by the molecular layer of D8Phe. The directions of bombardment and emission are shown in the sketch presented on the right side of the figure. The angle of incidence is 25° from the normal.

as molecular clusters) is significantly larger than the yield of Phe molecules from 1 layer of Phe deposited on graphene (9 molecules per impact).⁴ The MD simulations [Figs. 10 and 11 (Multimedia view)] show that the collision process for the latter case evolves in 2 steps. In a first phase ($t < 50$ fs), there is projectile atomization via atom-atom collisions. Interaction of these energetic atoms with the organic overlayer leads to molecular fragmentation and emission of fragments.^{5,7,41} A second phase (~ 3 ps) is characterized by a post-collision collective process of molecular interaction with the vibrating rim. A notable emission of electrons was also observed (~ 3 electrons/impact).

The critical process, which regulates the abundance of the ejecta, is the separation of the molecular layer from graphene. As a result, the molecules are bound only by weak intermolecular interactions and are easy to eject. The molecular layer evolves as a collective radial movement of Phe molecules, and simultaneously the graphene oscillates downward/upward. The pushed down graphene membrane is bent and stretched around the hole, thus accumulating potential energy. The result of the bending and stretching is an elastic movement of the membrane upward (Fig. 8, screenshot for time 3.1 ps). The accumulated potential

energy is transformed into the kinetic energy of a correlated movement upward for membrane atoms. The membrane atoms interact with the atoms of Phe molecules and gently transfer the correlated momenta to them. Thus, the molecules eject without destruction. In other words, the membrane acts as a trampoline for the molecules. The ejection of molecules is clearly observable from the side view [Fig. 11 (Multimedia view)]. The screenshot for the times 0.6 and 3.1 ps [Figs. 10 and 11 (Multimedia view)] shows the strong bending of the graphene membrane followed by the abundant trampoline ejection of molecules. Graphene not only provides the effective trampoline ejection but also enhances the probability of negative ionization for ejected molecules. We postulate that the high rate of negative ionization is due to electron tunneling from graphene to phenylalanine. The mechanism of ionization is the same as for the emission of C clusters from graphene [Eq. (1) and discussion above]. The yield of intact neutral molecules of Phe computed by MD is 9 molecules/impact for the molecular layer of D8Phe deposited on graphene. Taking in account that the measured yield of $(\text{D8Phe-H})^-$ which is 0.1, the ionization probability (PI) is estimated as ~ 0.02 . The ionization probability of Phe molecules sputtered from a bulk Phe target is $\sim 30\times$ smaller.

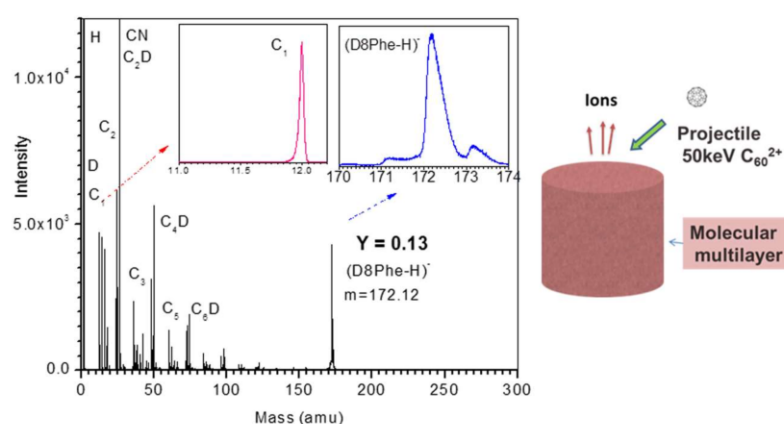


FIG. 9. Mass spectrum of negative ions emitted from the target of bulk D8Phe. The directions of bombardment and emission are shown in the sketch presented on the right side of the figure.

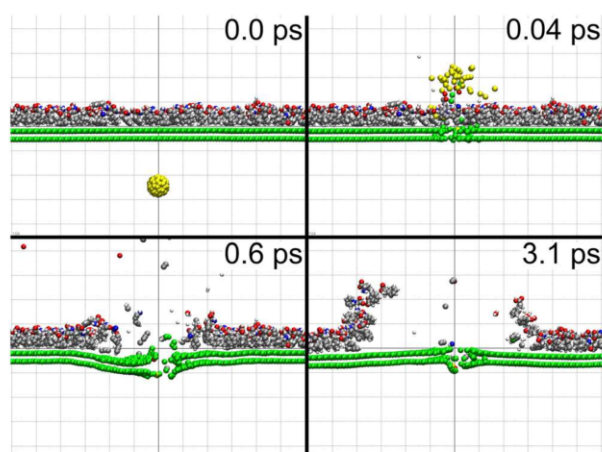


FIG. 10. Snapshots of the model system consisting of the single layer of phenylalanine molecules (1.1 nm thick) deposited on 2L graphene taken at various moments after 50 keV C_{60} impact—cross-sectional view. The gray lines in the background are separated by 1 nm. Only fragment of the bombarded system is visualized. The corresponding movie file is here. Multimedia view: <https://doi.org/10.1063/1.5080606.4>

This difference is due to the distinct mechanism of ionization for emission from a bulk molecular matter. The difference was discussed in Ref. 7. The relevant mechanism is the ionization via proton exchange between Phe molecules and negative ions of small fragments. This is a two-step process, when (a) small molecular fragments (e.g., CN), which have a high electron affinity, capture electrons via interactions in the sputtered volume of exited fragments;

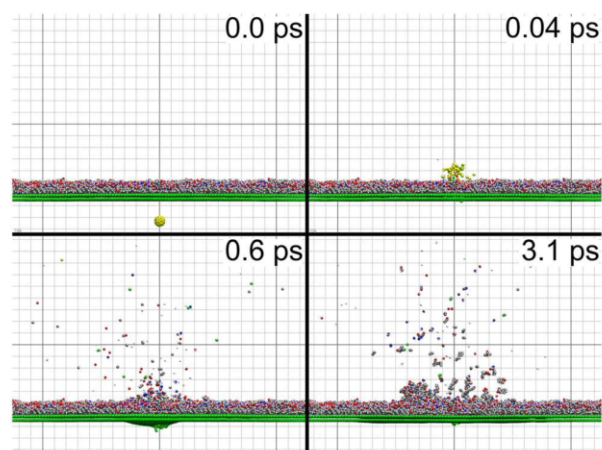


FIG. 11. Snapshots of the model system consisting of the single layer of phenylalanine molecules (1.1 nm) deposited on 2L graphene taken at various moments after 50 keV C_{60} impact—side view. The gray lines in the background are separated by 1 nm. Only fragment of the bombarded system is visualized. The corresponding movie file is here. Multimedia view: <https://doi.org/10.1063/1.5080606.5>

and (b) those negative fragments experience proton exchange with neutral Phe molecules or molecular clusters. The ionization probability depends mostly on the cross section of fragment/fragment and fragment/molecule interaction in the sputtered medium.⁷ The ionization probability is sufficient for the case of bulk molecular matter but $30\times$ smaller than that for electron tunneling from graphene to molecule.

One should note that for the case of “Phe on graphene,” the pre-existing Phe molecules obtain additional kinetic energies via a trampoline effect.⁷ The kinetic energies may result in enhanced ionization probability due to the molecule’s fast escape from the tunneling distance.³²

Thus, the physical properties of the substrate are key for maximizing ejection-ionization of monolayer deposits of weakly bonded moieties. The prime condition, however, is that of the energy density that must be delivered in a subpicosecond interval into the 2D solid in a way to generate collective motion of the substrate atoms. Future studies (experiments and simulations) focusing on projectile energy loss should provide insight into the energetics required for trampolining-ionization.

IV. TEST OF ELEMENTAL AND CHEMICAL COMPOSITION OF FREE STANDING GRAPHENE OXIDE (GO)

We turn now to C_{60} impacts on free standing graphene oxide, GO. GO has promising applications in many fields, including nanoelectronics, nanocomposites, as well as in biotechnology and environmental science.^{44–46} A first issue is the chemical composition of GO. The degree of oxidation (relative elemental concentration of C, O, and H) affects the relative presence of functional groups (epoxy, hydroxyl, and carboxyl). The stoichiometry of GO is a subject of recent investigations.^{45,47} For instance, elemental combustion analysis of oxidized flakes (thickness ~ 1.8 nm) shows a variation of composition from $C_1O_{1.04}H_{0.84}$ for regular GO to $C_1O_{2.54}H_{2.16}$ for a so-called graphene acid (GA) state.⁴⁵ XPS analysis performed on the same GO and GA shows lower O contents due to the possible contribution of adsorbed water in the case of combustion analysis. XPS also showed different C to O ratios for GO samples from different commercial sources.⁴⁶ The accurate elemental composition of GO flakes remains a challenge.⁴⁶ The assay of free standing GO is fraught with further complications. For instance, elemental analysis via XPS is likely impaired due to contributions from the sample support (lacey carbon nets or quantifoil grids).

We show here that the elemental analysis of free standing GO can be performed with the technique of single cluster impacts of keV C_{60}^{2+} , which stimulate the emission/detection of secondary ions from GO in the transmission direction (Fig. 1 and discussion above). The measurements were performed on free standing 2-layer GO film made from a graphene film by a proprietary oxidation process.⁴⁷ Figure 12 shows the mass spectrum of negative secondary ions emitted from this sample via single impacts of 50 keV C_{60}^{2+} . The mass spectrum contains peaks of H_1^- , C_1^- , and O_1^- [Fig. 12(a)].

The relative abundances of these ions (peak areas) do not correspond to the relative atom concentrations due to the different ionization probabilities of H, C, and O. Atomic ions of H_1^- , C_1^- , and O_1^- have long tails on the low mass side. The tails are due

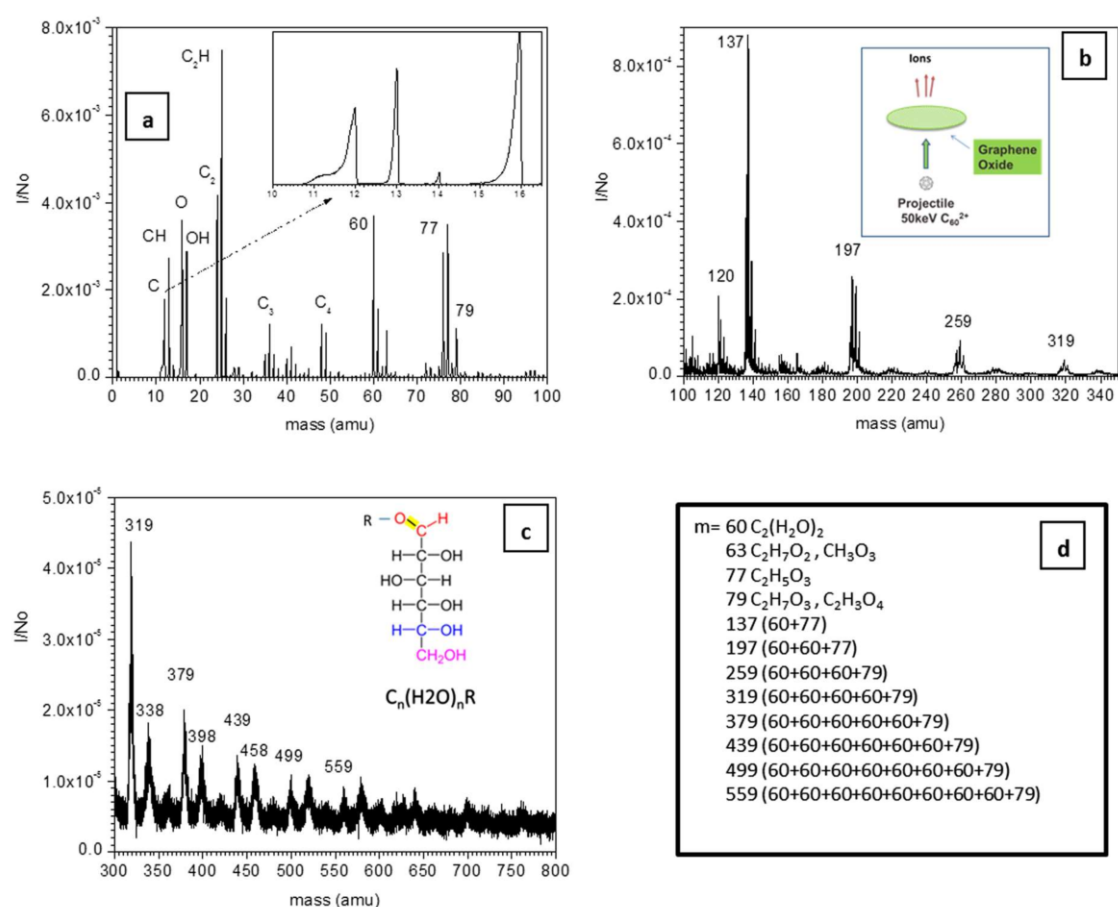


FIG. 12. Mass spectrum of negative ions emitted via impacts of 50 keV C_{60}^{2+} from free standing 2-layer GO film. The relevant data are shown in three mass segments [(a)–(c)]. The assignments of the peaks of molecular clusters are shown in (d).

to high energy knocked-on ions which are ionized by direct atom-atom collisions in the 2D material.⁴ The peak of C_1^- consists also of ions originating from projectile atomization via collisions with C and O atoms of graphene.^{4,5} The low energy ions emitted from the rim around the rupture are, as noted earlier, likely due to electron tunneling from the hot rim.⁴ Thus, the complex picture of the ejection/ionization complicates (even makes impossible) an estimation of the relative concentrations of H, C, and O from abundances of the atomic ions. By contrast, the relative concentrations of H, C, and O can be estimated from the emission of molecular clusters.

The spectrum in the high mass range [Figs. 12(b)–12(d)] consists of molecular cluster ions of the type (a) $[C_{2n}(H_2O)_{2n+1}(CO_3H)]^-$ ($n = 3, \dots, 8$) and (b) $[C_{2n}(H_2O)_{2n}(C_2O_3H_5)]^-$ ($n = 1, 2, \dots, 8$). These ions have as main constituents clusters such as $C_{2n}(H_2O)_{2n+1}$ and $C_{2n}(H_2O)_{2n}$, which are bonded to the moieties CO_3H (mass 61 amu) and $C_2O_3H_5$ (mass 77 amu). These molecules have high electron affinities of 3.68 eV and 4.08 eV, respectively;

thus, the molecular clusters (a) and (b) are efficiently ionized. The core composition of the molecular clusters implies that the relative concentration of H, C, and O is approximately $C_1O_1H_2$ for the free standing 2-layer GO film (PELCO® film from Ted Pella, Inc.). Surprisingly, the main constituent of the cluster is a carbohydrate [Fig. 12(d)]. The presence of carbohydrates indicates that the functional groups for GO are epoxy and hydroxyl and unlikely carboxyl. The absence of carboxylic groups supports data from GO flakes analyzed by Magic Angle Spinning NMR Spectroscopy.⁴⁶

The GO film is hydrophilic and will absorb water when exposed to air prior to insertion into the vacuum chamber of the mass spectrometer. Indeed, some H_2O in (a) and (b) may be water molecules recombined to that molecular cluster ions. To explore the hydration of GO, we tested oxidized carbon nanotubes with the method of single impact SIMS using keV C_{60}^{2+} .¹⁵ The sample was a sponge-like 3D nanostructure made from onionlike carbon nanotubes with a porosity of $\sim 97\%$.⁴⁸ This sponge-like hydrophilic nanostructure was completely filled with deuterated water prior to insertion into

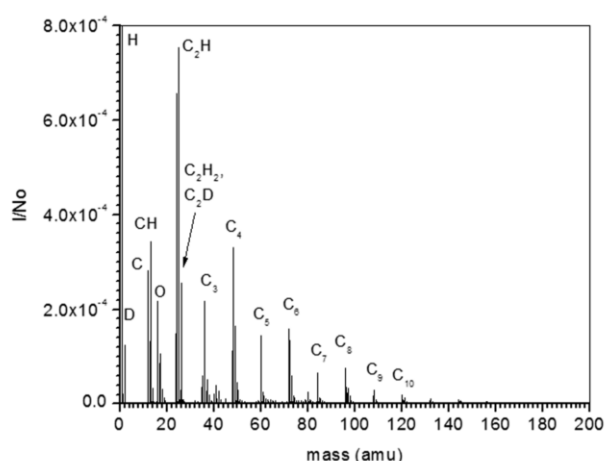


FIG. 13. Mass spectrum of negative ions emitted from hydrophilic spongelike 3D nanostructure made from onionlike carbon nanotubes with a porosity of $\sim 97\%$. The sponge was filled with deuterated water prior to insertion into vacuum.

vacuum for the mass spectrometry experiment. The sample was in high vacuum for ~ 10 min prior to the MS experiment. The mass spectrum of negative ions emitted via 50 keV C_{60}^{2+} impacts (Fig. 13) does not contain water molecules. The only evidence of the presence of water before evaporation is the peak of D^- and probably peak of C_2D^- , which indicate a substitution of hydrogen by deuterium. Thus, under vacuum the water was removed from the carbon nanostructure.

The oxidation process⁴⁹ oxidized only the surface of the nanotubes, without oxidation of the inner shells of the onionlike

nanotubes. As a result, the mass spectrum of the 3D nanotube structure has dominant peaks of C_n and C_nH_m clusters ions. The 2D GO case is different. The concentrations of O and H are high for free standing 2L GO, which as noted earlier as $C_1O_1H_2$. The method demonstrated on 2D GO can be applied for any functionalized graphene films.

V. Au_{400}^{4+} CLUSTERS IMPACTS ON FREE-STANDING GRAPHENE

We contrast now the 2D projectile impacts with 3D ones, specifically Au_{400}^{4+} (of 440–540 keV or 33–36 km/s) again at the level of individual events.⁶ The Au atoms undergo atom-atom collisions, which are different from those occurring with C_{60} . First, Au_{400} projectile is a 3D object composed from atoms filling up the entire volume. C_{60} projectile has a shell 2D structure, in which carbon atoms are located at the surface of the projectile. It will be much easier to disrupt such structure. Second, Au atoms are much heavier than C atoms. The mass difference will result in a less efficient energy transfer in Au–C collisions as compared to C–C interactions present during C_{60} impact. It will be also more difficult to change movement trajectories of the heavy Au atoms. Au_{400} will mostly deform when meeting a network of C atoms in graphene rather than disintegrate as the latter requires efficient trajectory deflection of individual gold atoms. Finally, the 500 keV Au_{400} projectile will have a much larger momentum as compared to 50 keV C_{60} due to larger mass of Au atoms and a larger number of atoms composing Au_{400} cluster. Most of carbon atoms scatter off the surface of Au_{400} , a few may experience collisions in the vicinity of Au_{400} .

Thus, at any moment, each C atom residing in the interaction area experiences a gentle correlated action of many Au atoms. A pressure exerted by a single object rather than by individual collisions punctures the graphene layer. Consequently, the projectile pushes through graphene as a deformed but single entity. Figure 14

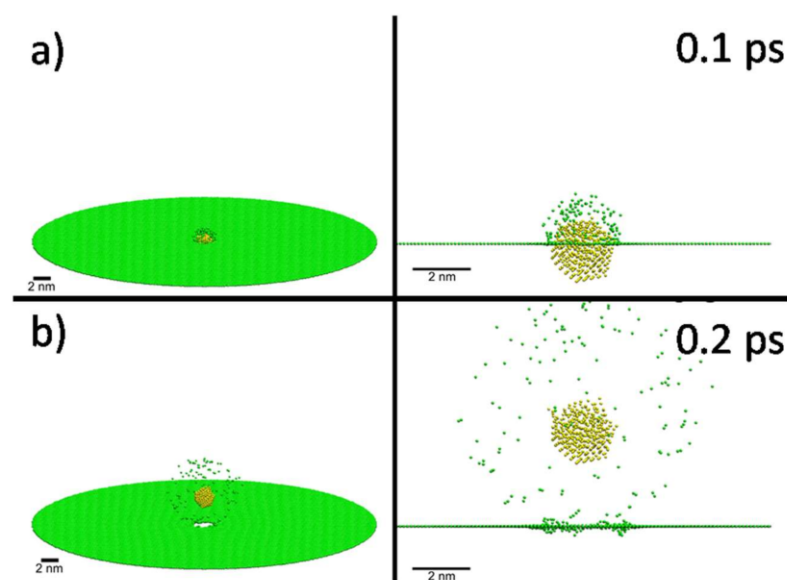


FIG. 14. Snapshot (MD simulations) of the 1 layer graphene taken at (a) 0.1 ps and (b) 0.2 ps after 500 keV Au_{400}^{4+} impact at a monolayer of graphene at normal incidence.

shows the MD simulations of 500 keV Au_{400}^{4+} impacting on 1 layer graphene at first 0.1 ps and 0.2 ps. During the passage through graphene (~ 0.1 ps), the projectile makes a round shaped rupture of ~ 2 nm in diameter. C atoms, which are knocked on from the ruptured area, are spread into the space around the transmitted projectile. The zone raptured by the impinging projectile is much less than the punched area observed experimentally. This discrepancy will be discussed below.

In punching a hole, the projectile experiences a strong asymmetric atomic disorder in its top hemisphere. Thus, a part of the kinetic energy of the projectile is transferred into the excitation of its electronic system.^{50–52} The exited Au_{400} is for a short time (0.2 ps) present in the vicinity of the hole in the graphene, with a rim area which is also electronically excited.⁴ We posit that this excitation in part is spent on electromagnetic interaction between Au_{400} and the graphene hole (discussed below). The remainder of excitation is by electron-phonon coupling,^{51,52} transformed into the vibrational excitation of the isolated Au cluster (time > 0.2 ps after impact). The vibrationally excited clusters undergo fragmentation, as observed

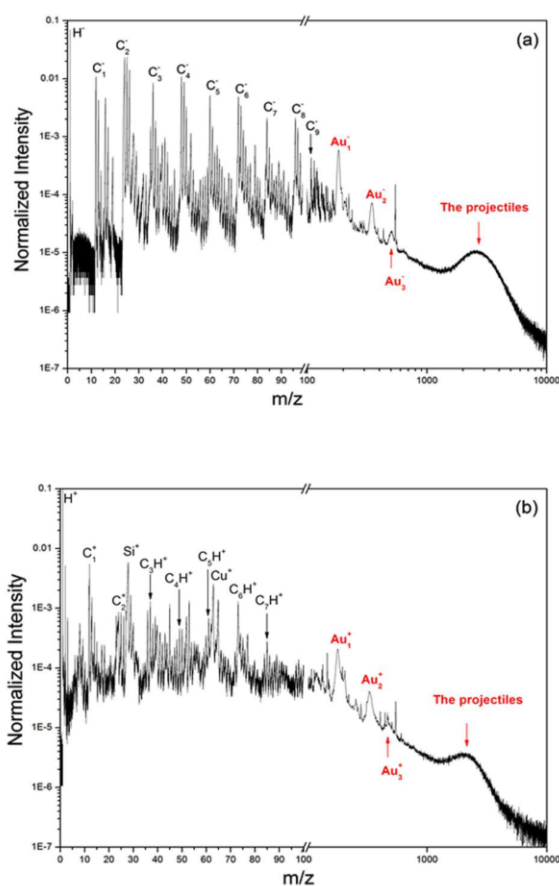


FIG. 15. Negative (a) and positive (b) ion spectra of 540 keV and 440 keV Au_{400}^{4+} projectile impacts (-15 kV and $+10$ kV target bias) on graphene in the transmission direction.

experimentally.^{53,54} The massive emission of atomic and C cluster ions (negative and positive) from the rim of the raptured graphene is also documented.⁶

Figure 15(a) shows the mass spectrum of negative ions detected in the transmission direction.⁶ The mass spectrum was obtained with $\sim 10^6$ impacts of 540 keV Au_{400}^{4+} on 1-layer graphene. The target bias was set to -15 kV. The main features of the mass spectrum are the C_n^- ions ($n = 1-10$) followed by C_nH_m^- ions. These ions have high SI yields (e.g., 1.25 ions per impact for C_2^-). In the higher mass range, there are peaks due to the Au_{400} projectiles and projectile fragments of Au_{1-3}^- ions. These peaks are broad and centered at lower m/z , indicating that these ions have shorter flight times and have initial kinetic energy distributions that come from the hypervelocity Au_{400} projectiles.

When the target bias was set to $+10$ kV, the positive ion mass spectrum consisted of C_n^+ ($n = 1-7$) and C_nH_m^+ ions in the low mass range, and Au_{1-3}^+ and Au_{400} projectile peaks in the high mass range [Fig. 15(b)]. Fragmentation via evaporation of atomic or cluster ions is possible if the parent cluster has a high charge state. The detection of both Au_{1-3}^- and Au_{1-3}^+ verifies that the projectile can indeed be charged negatively or positively after passing the graphene.

As the projectile approaches the graphene at a distance shorter than that of electron tunneling, it is neutralized by electron exchange with the target. At the moment of passage, the projectile and the rim around the hole are electronically excited. Upon exiting, the projectile undergoes electron exchange with the rim. The non-adiabatic interaction allows the projectile to carry a random charge (discussion below).⁵¹ The charge state of Au_{400} regulates the number of Au ions that evaporate.⁵⁵ Approximately 50% of atomic Au is charged positively or negatively. Most evaporated Au is singly or doubly charged with a small number carrying multiple charges. Another 50% of the transmitted projectiles or fragments are neutral.⁶

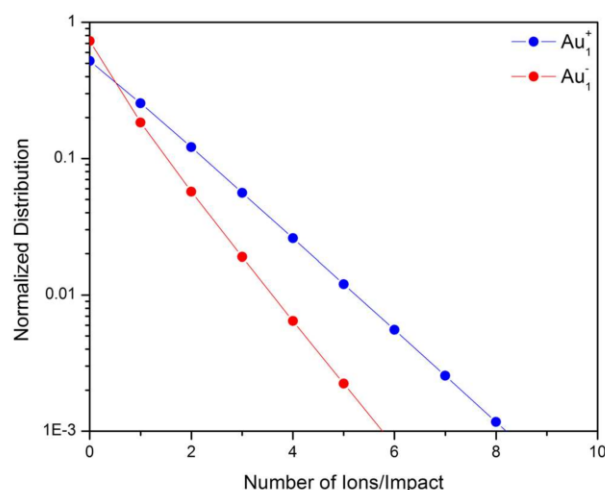


FIG. 16. Normalized (area under distribution is unity) distributions of the number of $\text{Au}_{1\pm}$ ions evaporated from a single Au_{400} . Number of evaporated ions correlate with the charge state (negative-neutral-positive) of Au_{400} passing graphene.

An analysis of the rates of evaporation⁶ shows that A_{400} carries an internal energy of ~ 450 – 500 eV which is dissipated in a multi-fragmentation process resulting on average in the evaporation of ~ 90 – 100 atoms, regardless the charge state of Au_{400} . The internal energy is similar for projectiles with different charge states (positive, negative, or neutral). Figures 16 and 17 illustrate the experimental data on the evaporation process. Mostly, the fragmentation via evaporation takes place after randomization of the excitation energy (>0.2 ps), when the classic statistical approach of internal energy fluctuations among the clusters degrees of freedom applies.^{53,54} The fragmentation was measured in the experimental time range from $t_0 = 0.2$ ps to $t = 0.1$ μ s.

Another important characteristic is the size of the graphene rupture. MD simulations [Fig. 12(b)] show that the diameter of the rupture is comparable with the diameter of the projectile (~ 2 nm). However, the experimental data show larger ruptures.⁵⁶

Impacts of a sequence of single projectiles on single layer graphene are shown in the transmission electron micrograph in Figs. 18(a) and 18(b). Round holes surrounded by an amorphized graphene are evident. They are distinct in size and shape from the significantly larger holes attributed to defects in the graphene film [Fig. 18(b)]. The holes caused by 480 keV Au_{400}^{4+} impacts

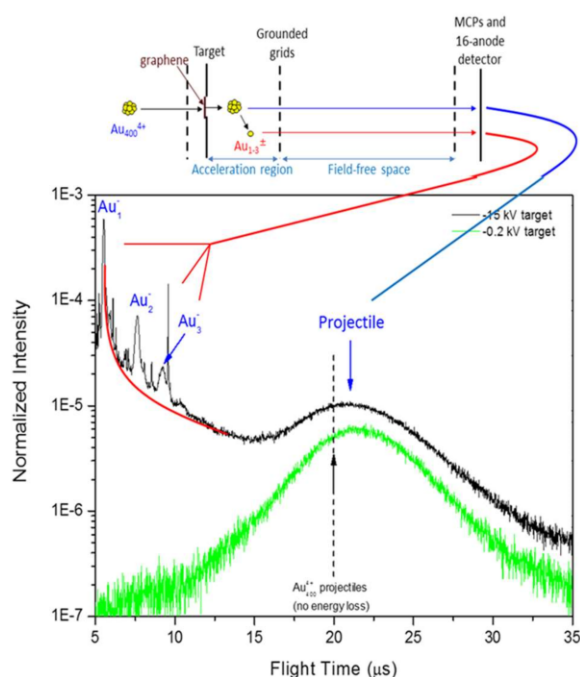


FIG. 17. Sketch of the evaporation of Au fragment ions from the projectiles in acceleration region (top). Negative ion mass spectrum (black) of 540 keV Au_{400}^{4+} projectile (-15 keV target bias) impacting on graphene in the transmission direction. The peaks of $Au_{1,2,3}^-$ have the fragmentation tails, which overlap and extend up to the parent projectile peak. The red line is for guiding the eye. Mass spectrum (green) of 480 keV Au_{400}^{4+} projectile only (-0.2 kV target bias) does not contain the secondary ions and Au fragments due to the low target bias. This spectrum shows clearly the sufficient projectile kinetic energy loss after impact.

on graphene have a size distribution with a mean diameter of 9 ± 2 nm. Interestingly, the mean diameter of the holes is independent of the number of layers of graphene in the sample (1, 2, or 4 layer graphene).⁵⁶

The density of round shaped holes corresponds to the dose of projectiles. The scanning electron microscopy (SEM) micrograph [Fig. 18(c)] shows a large area of the ruptured graphene. The scale of this SEM image is too coarse to show the correct image of the holes; however, the density of the randomly distributed holes ($\sim 120/\mu\text{m}^2$) can be counted. Note, that both micrographs [transmission electron microscopy (TEM) micrograph and SEM] show also the rare mechanical ruptures, which are approximately two times larger than the round shaped holes [Figs. 18(b) and 18(c)]. These ruptures are not round shaped. Graphene is contaminated by CuCl nanoparticles, which are visible in micrograph as black small spots of a size of ~ 2 nm [Figs. 18(a) and 18(b)]. The presence of these particles is due to the process for producing the graphene. The density of CuCl particles is very low. One can speculate that direct impacts on the CuCl nanoparticles are responsible for the generation of large holes. However, their low density and the low probability of direct impacts suggest that the generation of large holes from impacts on the CuCl nanoparticles is negligible.

It must be noted that 50 keV C_{60}^{2+} impacts produced no visible holes suggesting a self-healing process.⁵⁷

To explain the effect of large holes, we postulate that a neutral or charged cluster undergoes a dipole interaction with the rim of the rupture. The A_{400} projectiles, after passing through graphene, are partially neutral ($\sim 50\%$) and partially negatively ($\sim 25\%$) and positively (25%) charged. Charged Au_{400} are not only singly charged; the charge distribution (Fig. 16) shows that high charge states ($8+$ and $5-$) were detected. The charge is distributed evenly over the Au_{400} surface after passing the critical distance for electron tunneling (1 nm, $t > 0.1$ ps). The time evolution of Au_{400} was discussed in detail in Ref. 6. Let us consider first the multicharged Au_{400} , which passed the graphene and is aligned with the rupture at distance >1 nm (critical distance of electron tunneling.³² Charged Au_{400} induces the opposite charge at the surface area around the rupture. The electric field lines between the projectile and the rim of the rupture result in a dipole. The electric field of the dipole is strong due to the short distance and high charge. One can estimate the field of the dipole at the surface of the projectile as follows:

$$E_x = \frac{1}{4\epsilon_0\pi} \frac{Q}{r_0^2} + \frac{x}{2\epsilon_0} \int_{r_0}^{r_{\text{eff}}} \left[\frac{\beta(y)y}{(x^2 + y^2)^{3/2}} \right]' dy, \quad (2)$$

where Q is the charge of the nanoparticle, r_0 is the radius of the nanoparticle and the initial puncture in the graphene, $\beta(y)$ is the radial density of the charge around the primary hole, and x is distance between the surface of nanoparticle and the hole plane. The boundary condition for the charge around the hole is $\int_{r_0}^{r_{\text{eff}}} \beta(y) dy = Q$, where r_{eff} is the effective radius of the charge area around hole. Assuming that $r_{\text{eff}} \approx r_0$, the solution of Eq. (2) for the field strength at the surface of the projectile is

$$E_x = \frac{Q}{4\pi\epsilon_0} \left(\frac{x}{(x^2 + r_0^2)} + \frac{1}{r_0^2} \right). \quad (3)$$

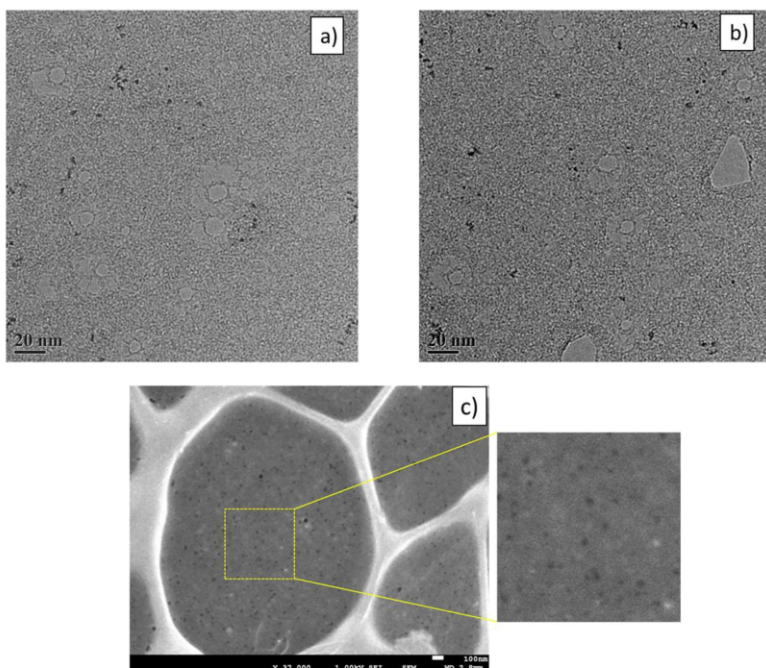


FIG. 18. Transmission electron microscopy image [(a) and (b)] of single layer graphene after irradiating with 480 keV Au₄₀₀⁺ projectiles in a 3 mm diameter area (scale bar 20 nm). The small black particles correspond to copper chloride nanoparticles produced from the manufacturing process as indicated by the manufacturer. Scanning electron microscopy image (c) shows the graphene attached to the lacey carbon frame. The density of the randomly distributed holes is $\sim 120/\mu\text{m}^2$.

Due to the strong bonding of the poles of the dipole (field of $\sim 1 \text{ V/\AA}$), the movement of the multicharged projectile (one side of dipole) will bend and stretch the graphene around the hole. The projectile will experience an energy loss, when a part of projectile kinetic energy is transferred to the rim via the electrostatic interaction of the dipole poles. The graphene membrane accumulates the strain energy very effectively due to its high Young modulus ($\sim 1 \text{ TPa}$). The average energy loss of the projectile of $\sim 72 \text{ keV}$ is higher than the energy, which the projectile spends on rupturing the graphene and on the carbon ejecta ($\sim 53 \text{ keV}$) via atom-atom collisions only.⁶ We infer that part of the additional energy loss is due to the dipole projectile/hole rim interaction, and this energy is accumulated into the stretching of the graphene. The stripping of carbon atomic and cluster ions due to the strong field of the dipole can be considered as a mechanism of the enlargement of the hole size. Thus, the charged nanoparticle-graphene dipole interaction may explain the experimental observations of (a) high kinetic energy loss of the projectiles; (b) charge distribution of projectiles; (c) abundant emission of C_n^\pm ; and (d) large size of holes made by projectile impact, which are $9 \pm 2 \text{ nm}$.

The most intriguing part of A_{400} graphene interaction occurs within $t < 0.1 \text{ ps}$. The Au_{400}^{4+} projectile approaching the graphene surface ($t = 0$) is neutralized by electron tunneling with graphene; thus, the actual impact makes a neutral system of Au_{400} connected to graphene. Indeed, the electronic processes are fast; thus, the system has a joint Fermi level and a small potential gradient due to the different work functions of Au_{400} and graphene (6 eV and 4.5 eV, respectively). After impact, a unique self-organized system is obtained (Fig. 14). MD simulation show that Au_{400} being deformed

via interaction is aligned axially within the hole in graphene made by the Au_{400} . The deformation is observed in the top semi-sphere of A_{400} only, indicating that electrical contact (joint Fermi level) is lost, when the second half of A_{400} passes the hole. The diameter of the hole (Fig. 14) is slightly larger than the diameter of Au_{400} . The difference in the work functions is limited, and the induced charge on Au_{400} cannot be above $+1$.⁵⁸ However, the projectile located in the hole is electronically exited due to deformation via impact.

A correct model of time evolution of the electronically exited nanoparticle located in the graphene hole is a subject for future work, but some important features of the behavior of this system can be already discussed. The case of metallic nanovolume electronically excited via keV cluster impact was theoretically examined in Ref. 51. It was noted that fluctuations of the local electron density should be taken in account to describe the transfer of a kinetic energy of projectile into the electronic subsystem. In this case, fast electron density fluctuations, which are generated and then quenched multiple times, characterized the deformed Au_{400} , where the displaced atoms are reorganized during the time of passage of $\sim 0.1 \text{ ps}$ (Fig. 14).

The fluctuations of the local electron density of Au_{400} within the hole stimulate the production of local random dipoles between Au_{400} and the rim of the hole. The random dipoles are generated by electron density fluctuations and are quenched by electron exchange with graphene during the time of passage. The force of this electrostatic interaction should be always attractive between the A_{400} and the hole, regardless of the dipoles polarities. Moreover, even if the average charge of the projectile is zero, an attractive

force will be generated. As a result, the hole works as a trap for the electronically excited metal cluster. The strength of this force can be described formally by Eq. (2) where instead of the charge of Au_{400} , the fluctuations of local electron density are applied. The non-adiabatic electron exchange between Au_{400} and graphene may describe the exotic charge distribution of the projectile after interaction (~50% of neutrals, ~25% of negatively, and ~25% positively charged Au_{400}). Again, a more detailed model of the electronically excited nanoparticle located in the graphene hole remains to be developed.

VI. CONCLUDING REMARKS

MD simulations of fullerene impacting free standing graphene at ~0.8 keV/atom agree well with the experimental observations. This is not the case for impacts with gold nanoparticles at ~1.2 keV/atom. This interaction has drastic consequences for the emerging projectile in terms of energy loss and evaporation of atoms. Remarkable effects caused by a single layer of graphene!

Setting aside the fate of the projectile, the collision regimes considered here involve distinct ejection-ionization mechanisms. The abundant ionization of atoms, molecular fragments, and entities can be explained with ultrafast cooperative motion and electronic projectile-target interactions. They evolve as the target thickness increases into ultimately the well described process occurring in projectile-bulk matter impact.

We infer from the observations reported here that free-standing graphene is an interesting candidate as a substrate for a chemical analysis of atto/zeptomole samples via cluster-SIMS in the transmission mode. First, the extremely small thickness of the support results in small amounts of emitted substrate material. As a result, there is a minimal interference between the substrate and the analyzed signal. A large portion of the primary kinetic energy can be transmitted to the organic overlayer in the direction toward the detector by gentle, collective movement of the graphene layer. Such concerted action of substrate atoms increases a chance that intact molecules can be recorded. These observations confirm the feasibility of detecting of attomole to zeptomole amounts of analyte. Deposition of such small amounts of material opens the potential capability to perform quantitative analysis by SIMS in the way proposed in the so-called storing matter technique.⁵⁹ In this approach, SIMS analysis is performed on deposit which is sufficiently dilute not to give rise to matrix effects.

The present report focuses on negative ion emission from graphene impacted with 2D and 3D projectiles of comparable velocities. Other target and bombardment conditions remain to be explored for a broader understanding of the effects of projectile characteristics, impact angle/target thickness on the nature, and abundance of the ejecta. A more nuanced insight into fascinating motional and electronic processes will require experiment paralleling MD simulations. In particular, an exploration of lower momentum of impacts should be useful to assess prospects for surface analysis. Here, the observations of ionized ejecta should be complemented with detection of neutrals via postionization. The postionization technique⁶⁰ can potentially explore the very effective “direct trampolining” of large intact molecules from the graphene, in the case when the energy of projectile is not enough for graphene rupturing.

ACKNOWLEDGMENTS

This work is supported by NSF Grant No. CHE-1308312 to E.A.S. M.G. and Z.P. gratefully acknowledge financial support from the Polish National Science Centre, Grant Nos. 2015/19/B/ST4/01892 and 2016/23/N/ST4/00971. MD simulations were performed at the PLGrid Infrastructure.

REFERENCES

- ¹S. Standop, O. Lehtinen, C. Herbig, G. Lewes-Malandrakis, F. Craes, J. Kotakoski, T. Michely, A. V. Krasheninnikov, and C. Busse, “Ion impacts on graphene/Ir(111): Interface channeling, vacancy funnels, and a nanomesh,” *Nano Lett.* **13**(5), 1948–1955 (2013).
- ²C. Herbig and T. Michely, “Graphene: The ultimately thin sputtering shield,” *2D Mater.* **3**, 025032 (2016).
- ³P. P. Michałowski, I. Pasternak, P. Ciepiewski, F. Guinea, and W. Strupiński, “Formation of a highly doped ultra-thin amorphous carbon layer by ion bombardment of graphene,” *Nanotechnology* **29**, 305302 (2018).
- ⁴S. V. Verkhoturov, S. Geng, B. Czerwinski, A. E. Young, A. Delcorte, and E. A. Schweikert, “Single impacts of keV fullerene ions on free standing graphene: Emission of ions and electrons from confined volume,” *J. Chem. Phys.* **143**, 164302 (2015).
- ⁵S. V. Verkhoturov, B. Czerwinski, D. S. Verkhoturov, S. Geng, A. Delcorte, and E. A. Schweikert, “Ejection-ionization of molecules from free standing graphene,” *J. Chem. Phys.* **146**, 084308 (2017).
- ⁶S. Geng, S. V. Verkhoturov, M. J. Eller, S. Della-Negra, and E. A. Schweikert, “The collision of a hypervelocity massive projectile with free-standing graphene: Investigation of secondary ion emission and projectile fragmentation,” *J. Chem. Phys.* **146**, 054305 (2017).
- ⁷S. V. Verkhoturov, M. Golunski, D. S. Verkhoturov, S. Geng, Z. Postawa, and E. A. Schweikert, “‘Trampoline’ ejection of organic molecules from graphene and graphite via keV cluster ions impacts,” *J. Chem. Phys.* **148**, 1443091 (2018).
- ⁸Z. Bai, L. Zhang, H. Li, and L. Liu, “Nanopore creation in graphene by ion beam irradiation: Geometry, quality, and efficiency,” *Appl. Mater. Interfaces* **8**(37), 24803–24809 (2016).
- ⁹M. Golunski and Z. Postawa, “Effect of kinetic energy and impact angle on carbon ejection from a free-standing graphene bombarded by kilo-electron-volt C_{60} ,” *J. Vac. Sci. Technol., B* **36**, 03F112 (2018).
- ¹⁰S. Zhao, J. Xue, L. Liang, Y. Wang, and J. Sha Yan, “Drilling nanopores in graphene with clusters: A molecular dynamics,” *J. Phys. Chem. C* **116**, 11776–11782 (2012).
- ¹¹J.-H. Lee, P. E. Loya, J. Lou, and E. L. Thomas, “Dynamic mechanical behavior of multilayer graphene via supersonic projectile penetration,” *Science* **346**(6213), 1092–1096 (2014).
- ¹²E. Gruber, R. A. Wilhelm, R. Pétuya, V. Smejkal, R. Kozubek, A. Hierzenberger, B. C. Bayer, I. Aldazabal, A. K. Kazansky, F. Libisch, A. V. Krasheninnikov, M. Schleberger, S. Facko, A. G. Borisov, A. Arnau, and F. Aumayr, “Ultrafast electronic response of graphene to a strong and localized electric field,” *Nat. Commun.* **7**, 13948 (2016).
- ¹³P. P. Michałowski, W. Kaszub, I. Pasternak, and W. Strupiński, “Graphene enhanced secondary ion mass spectrometry (GESIMS),” *Sci. Rep.* **7**, 7479 (2017).
- ¹⁴S. V. Verkhoturov, M. J. Eller, R. D. Rickman, S. Della-Negra, and E. A. Schweikert, “Single impacts of C_{60} on solids: Emission of electrons, ions and prospects for surface mapping,” *J. Phys. Chem. C* **114**(12), 5637–5644 (2010).
- ¹⁵M. J. Eller, S. V. Verkhoturov, S. Della-Negra, and E. A. Schweikert, “SIMS instrumentation and methodology for mapping of co-localized molecules,” *Rev. Sci. Instrum.* **84**(10), 103706-1–103706-7 (2013).
- ¹⁶R. D. Rickman, S. V. Verkhoturov, E. S. Parilis, and E. A. Schweikert, “Simultaneous ejection of two molecular ions from keV gold atomic and polyatomic projectile impacts,” *Phys. Rev. Lett.* **92**, 047601 (2004).
- ¹⁷See https://www.tedpella.com/Support_Films_html/Graphene-TEM-Support-Film.htm for information about graphene layers placed on a lacey carbon structures.

- ¹⁸B. J. Garrison and Z. Postawa, "Molecular dynamics simulations, the theoretical partner to dynamic cluster SIMS experiments," in *ToF-SIMS—Surface Analysis by Mass Spectrometry*, 2nd ed., edited by J. C. Vickerman and D. Briggs (IMP&Surface Spectra, Ltd., Chichester, Manchester, 2013), pp. 151–192, and references therein.
- ¹⁹S. J. Stuart, A. B. Tutein, and J. A. Harrison, "A reactive potential for hydrocarbons with intermolecular interactions," *J. Chem. Phys.* **112**, 6472–6486 (2000).
- ²⁰L.-L. C. Liu, Y. Liu, S. V. Zybin, H. Sun, and W. A. Goddard, "ReaxFF-Ig: Correction of the ReaxFF reactive force field for London dispersion, with applications to the equations of state for energetic materials," *J. Phys. Chem. A* **115**, 11016–11022 (2011).
- ²¹G. Grochola, S. P. Russo, and I. K. Snook, "On fitting a gold embedded atom method potential using the force matching method," *J. Chem. Phys.* **123**, 204719 (2005).
- ²²J. F. Ziegler, J. P. Biersack, and U. Littmark, *The Stopping and Range of Ions in Matter* (Pergamon, New York, 1985).
- ²³Z. Postawa, B. Czerwinski, M. Szweczyk, E. J. Smiley, N. Winograd, and B. J. Garrison, *Anal. Chem.* **75**, 4402 (2003).
- ²⁴P. Sigmund, "Recollections of fifty years with sputtering," *Thin Solid Films* **520**, 6031–6049 (2012).
- ²⁵W. Eckstein, in *Sputtering by Particle Bombardment III*, edited by R. Behrisch and W. Eckstein (Springer-Verlag, Berlin, Heidelberg, 2007), and references therein.
- ²⁶Z. Postawa, B. Czerwinski, M. Szweczyk, E. J. Smiley, N. Winograd, and B. J. Garrison, *J. Phys. Chem. B* **108**, 7831 (2004).
- ²⁷T. J. Colla, R. Aderjan, R. Kissel, and H. M. Urbassek, "Sputtering of Au induced by 16 keV Au cluster bombardment: Spikes, craters, late emissions, fluctuations," *Phys. Rev. B* **62**, 8487–8493 (2000).
- ²⁸B. J. Garrison, Z. Postawa, K. E. Ryan, J. C. Vickerman, R. P. Webb, and N. Winograd, "Internal energy of molecules ejected due to energetic C₆₀ bombardment," *Anal. Chem.* **81**, 2260–2267 (2009).
- ²⁹M. Kerford and R. P. Webb, "Desorption of molecules by cluster impact: A preliminary molecular dynamics study," *Nucl. Instrum. Methods Phys. Res., Sect. B* **180**, 44 (2001).
- ³⁰R. P. Webb, "The computer simulation of energetic cluster–solid interactions," *Radiat. Eff. Defects Solids* **162**, 567 (2007).
- ³¹J. T. Tian, T. Zheng, J. Y. Yang, S. Y. Kong, J. M. Xue, Y. G. Wang, and K. Nordlund, "Capacity of graphite's layered structure to suppress the sputtering yield: A molecular dynamics study," *Appl. Surf. Sci.* **337**, 6 (2015).
- ³²M. L. Yu and N. D. Lang, "Mechanisms of atomic ion emission during sputtering," *Nucl. Instrum. Methods Phys. Res., Sect. B* **14**(4-6), 403–413 (1986).
- ³³Z. Sroubek, X. Chen, and J. A. Yarmoff, "Ion formation and kinetic electron emission during the impact of slow atomic metal particles on metal surfaces," *Phys. Rev. B* **73**(4), 045427 (2006).
- ³⁴J. D. Watts and R. J. Bartlett, "A theoretical study of linear carbon cluster monoanions, C_n⁻, and dianions, n (n = 2–10)," *J. Chem. Phys.* **97**, 3445–3457 (1992).
- ³⁵A. Bekkerman, B. Tsipinyuk, A. Budrevich, and E. Kolodney, "Direct experimental evidence for the thermal nature of delayed electron emission from a superhot C₆₀ molecule," *J. Chem. Phys.* **108**, 5165 (1998).
- ³⁶B. Czerwinski, L. Rzeznik, R. Paruch, B. J. Garrison, and Z. Postawa, "Effect of impact angle and projectile size on sputtering efficiency of solid benzene investigated by molecular dynamics simulations," *Nucl. Instrum. Methods Phys. Res., Sect. B* **289**, 1578 (2011).
- ³⁷D. Brenes, Z. Postawa, A. Wucher, P. Blenkinsopp, B. Garrison, and N. Winograd, "Fluid flow and effusive desorption: Dominant mechanisms of energy dissipation after energetic cluster bombardment of molecular solids," *J. Phys. Chem. Lett.* **2**, 2009 (2011).
- ³⁸B. J. Garrison, A. Delcorte, and K. D. Krantzman, "Molecule liftoff from surfaces," *Acc. Chem. Res.* **33**, 69–77 (2000).
- ³⁹A. Delcorte and B. J. Garrison, "Kiloelectronvolt argon-induced molecular desorption from a bulk polystyrene solid," *J. Phys. Chem. B* **108**, 15652–15661 (2004).
- ⁴⁰Z. Postawa, B. Czerwinski, N. Winograd, and B. J. Garrison, "Microscopic insights into the sputtering of thin organic films on Ag{111} induced by C₆₀ and Ga bombardment," *J. Phys. Chem. B* **109**, 11973–11979 (2005).
- ⁴¹M. Golunski, S. V. Verkhoturov, D. S. Verkhoturov, E. A. Schweikert, and Z. Postawa, "Effect of substrate thickness on ejection of phenylalanine molecules adsorbed on free-standing graphene bombarded by 10 keV C₆₀," *Nucl. Instrum. Methods Phys. Res., Sect. B* **393**, 13 (2017).
- ⁴²S. E. Maksimov, S. V. Verkhoturov, V. V. Solomko, and N. Kh. Dzhemilev, "Kinetic-energy release distributions and stability of niobium-carbon clusters sputtered from the surface of niobium carbide by xenon ions," *J. Surf. Invest.: X-Ray, Synchrotron Neutron Tech.* **7**, 996–1000 (2013).
- ⁴³J. D. DeBord, S. V. Verkhoturov, L. M. Perez, S. W. North, M. B. Hall, and E. A. Schweikert, "Measuring the internal energies of species emitted from hypervelocity nanoparticle impacts on surfaces using recalibrated benzylpyridinium probe ions," *J. Chem. Phys.* **138**, 214301 (2013).
- ⁴⁴F. Li, X. Jiang, J. Zhao, and S. Zhang, "Graphene oxide: A promising nanomaterial for energy and environmental applications," *Nano Energy* **16**, 488–515 (2015).
- ⁴⁵O. Jankovský, M. Nováček, J. Luxa, D. Sedmidubský, V. Fila, M. Pumera, and Z. Sofer, "A new member of the graphene family: Graphene acid," *Chem. - Eur. J.* **22**, 17416–17424 (2016).
- ⁴⁶I. A. Vacchi, C. Spinato, J. Raya, A. Bianco, and C. Ménard-Moyon, "Chemical reactivity of graphene oxide towards amines elucidated by solid-state NMR," *Nanoscale* **8**, 13714–13721 (2016).
- ⁴⁷See https://www.tedpella.com/Support_Films_html/Graphene-TEM-Support-Film.htm#anchor21822-5 for information about free standing 2-layer GO film.
- ⁴⁸X. Pu, G. Yang, and C. Yu, "Liquid-type cathode enabled by 3D sponge-like carbon nanotubes for high energy density and long cycling life of Li-S batteries," *Adv. Mater.* **26**, 7456–7461 (2014).
- ⁴⁹Y. Kanai, V. R. Khalap, P. G. Collins, and J. C. Grossman, "Atomistic oxidation mechanism of a carbon nanotube in nitric acid," *Phys. Rev. Lett.* **104**, 066401 (2010).
- ⁵⁰A. Wucher and A. Duvenbeck, "Kinetic excitation of metallic solids: Progress towards a microscopic model," *Nucl. Instrum. Methods Phys. Res., Sect. B* **269**, 1655–1660 (2011).
- ⁵¹B. Weidtmann, S. Hanke, A. Duvenbeck, and A. Wucher, "Computer simulation of cluster impact induced electronic excitation of solids," *Nucl. Instrum. Methods Phys. Res., Sect. B* **303**, 51–54 (2013).
- ⁵²V. V. Pogosov and V. I. Reva, "Energetics of charged metal clusters containing vacancies," *J. Chem. Phys.* **148**, 044105 (2018).
- ⁵³H. Haberland, *Clusters of Atoms and Molecules: Theory, Experiment, and Clusters of Atoms* (Springer-Verlag, Berlin, Heidelberg, 1994), pp. 217–220.
- ⁵⁴N. Kh. Dzhemilev, A. M. Goldenberg, I. V. Veriovkina, and S. V. Verkhoturov, "Fragmentation of cluster ions in SIMS: Cluster distributions over lifetime, excitation energy and kinetic energy release," *Nucl. Instrum. Methods Phys. Res., Sect. B* **114**, 245–251 (1996).
- ⁵⁵C. Bréchnignac, P. Cahuzac, F. Carlier, and J. Leygnier, "Photoionization of mass-selected K_n⁺ ions: A test for the ionization scaling law," *Phys. Rev. Lett.* **63**, 1368–1371 (1989).
- ⁵⁶M. J. Eller, C.-K. Liang, S. Della-Negra, A. B. Clubb, H. Kim, A. E. Young, and E. A. Schweikert, "Hypervelocity nanoparticle impacts on free-standing graphene: A sui generis mode of sputtering," *J. Chem. Phys.* **142**, 044308 (2015).
- ⁵⁷R. Zan, Q. M. Ramasse, U. Bangert, and K. S. Novoselov, "Graphene reknits its holes," *Nano Lett.* **12**, 3936–3940 (2012).
- ⁵⁸B. M. Smirnov, "Clusters in external fields," in *Cluster Processes in Gases and Plasmas* (WILEY-VCH Verlag GmbH & Co., 2010).
- ⁵⁹C. Mansilla and T. Wirtz, "Storing matter: A new analytical technique developed to improve the sensitivity and the quantification during SIMS analyses," *Surf. Interface Anal.* **42**, 1135–1139 (2010).
- ⁶⁰A. Wucher, "Molecular ionization probability in cluster-SIMS," *J. Vac. Sci. Technol., B* **36**, 03F123 (2018).

Article 6

*Mechanisms of particle ejection from free-standing two-layered graphene stimulated by keV argon gas cluster projectile bombardment –
Molecular dynamics study*

Gołuński M., Hrabar S. & Postawa Z.

Surface and Coatings Technology 391, 125683 (2020)

doi:[10.1016/j.surfcoat.2020.125683](https://doi.org/10.1016/j.surfcoat.2020.125683)

Reproduced under the terms of the Creative Commons CC-BY license, which permits unrestricted use, distribution, and reproduction in any medium, provided the original work is properly cited.



Mechanisms of particle ejection from free-standing two-layered graphene stimulated by keV argon gas cluster projectile bombardment – Molecular dynamics study

M. Gołński*, S. Hrabar, Z. Postawa

Institute of Physics, Jagiellonian University, ul. Lojasiewicza 11, 30-348 Krakow, Poland

ARTICLE INFO

Keywords:
Graphene
Argon cluster
Molecular dynamics
SIMS

ABSTRACT

Molecular dynamics computer simulations are employed to investigate processes leading to particle ejection from free-standing two-layered graphene irradiated by keV argon gas cluster projectiles. The effect of the primary kinetic energy and the projectile size on the ejection process is investigated. It has been found that both these parameters have a pronounced influence on the emission of particles. The interaction between argon projectiles and graphene is strong regardless of graphene's minimal thickness. A significant portion of the primary kinetic energy is deposited into the sample. Part of this energy is used for particle emission, which is substantial. As a result, circular nanopores of various dimensions are created depending on the bombardment conditions. A major part of the deposited energy is also dispersed in a form of acoustic waves. Different mechanisms leading to particle ejection and defect formation are identified depending on the projectile energy per atom. The implications of the results to a novel analytical approach in Secondary Ion Mass Spectrometry based on ultrathin free-standing graphene substrates and a transmission geometry are discussed.

1. Introduction

Two-dimensional crystals have been a subject of extensive studies for some time due to their unique properties [1]. One of the most inspiring 2D materials is graphene. Due to its exceptional electric properties, high intrinsic strength, and stiffness, this material entered many fields of engineering, for example electronics, composite materials, and photovoltaics, just to name a few [2,3]. Despite the already conducted extensive studies, still much effort must be spent to better understand various aspects of graphene and graphene-like materials [4].

There are numerous methods used for graphene preparation, characterization, or alteration. Some of them are relying on ion beam bombardment [5]. Two of the less apparent forms of using the ion beam are cleaning the graphene surface from contaminations and uplifting of deposited material for further chemical analysis. Kim et al. considered the cleaning of suspended graphene with argon clusters [6], while few others worked on the subject of using these projectiles for cleaning of graphene supported on the surface [7–10]. Verkhoturov et al. proposed to use free-standing graphene as a substrate for chemical analysis by Secondary Ion Mass Spectrometry (SIMS). In this approach, a so-called “transmission geometry” is used in which the analysed organic material

is deposited on one side of the ultrathin substrate, while another side is bombarded by cluster projectiles [11,12]. It is argued that such geometry can be particularly attractive for the analysis of ultra-small amounts of organic material, molecular nano-objects, and supramolecular assemblies [11,12].

Cluster ion beams are a natural choice to uplift the organic molecules. Impacts of these projectiles lead to more gentle, collective movement of the substrate and analysed material, which favours the emission of intact molecules [13,14]. Although one of the most successful clusters used in organic SIMS is C₆₀ fullerene [15], there is a significant movement towards larger clusters, such as argon gas clusters consisting of hundreds or even thousands of atoms [16–18]. Bombardment of free-standing graphene by C₆₀ projectiles has already been investigated [11,19–24]. However, there is no analogous work available for larger clusters, even though these projectiles are more optimal for the analysis of materials consisting of large organic molecules [13,14]. As a result, not much is known about processes that will lead to a material ejection in this case. Most of the existing theoretical works on the projectile-graphene interaction focuses on the ion beam-induced creation of defects in graphene [25,26]. Much less is known about processes that cause removal of carbon atoms from this material,

Abbreviations: MD, molecular dynamics; SIMS, Secondary Ion Mass Spectrometry

* Corresponding author at: ul. Lojasiewicza 11, 30-348 Krakow, Poland.

E-mail addresses: mikolaj.golunski@gmail.com (M. Gołński), sviatoslav.hrabar@doctoral.uj.edu.pl (S. Hrabar), zbigniew.postawa@uj.edu.pl (Z. Postawa).

<https://doi.org/10.1016/j.surfcoat.2020.125683>

Received 17 November 2019; Received in revised form 21 February 2020; Accepted 23 March 2020

Available online 25 March 2020

0257-8972/ © 2020 The Authors. Published by Elsevier B.V. This is an open access article under the CC BY license (<http://creativecommons.org/licenses/by/4.0/>).

leading to creation of defects, particularly when large cluster projectiles are used. The objective of this paper is, therefore, to describe the dynamics of the energetic argon gas cluster bombardment of free-standing graphene. The results are used to provide insight into phenomena leading to the ejection of atoms from the bombarded system.

2. Computer model

The molecular dynamics (MD) computer simulations are used to model cluster bombardment. Briefly, the movement of particles is determined by integrating Hamilton's equations of motion. The forces between carbon atoms in the system are described by the Charge Implicit ReaxFF (CI-ReaxFF) force field [27], which allows for the creation and breaking of covalent bonds. While preserving the accuracy of the original ReaxFF potential, this force field is several times faster and has an appropriate repulsive wall to describe high energy collisions properly. Forces between argon atoms and between argon and carbon atoms are described by the Lenard-Jones potential [28] splined with KrC potential [29] for high energy collisions. A more detailed description of the MD method can be found elsewhere [30]. The gas clusters consisting of 60, 100, 366, and 1000 argon atoms are chosen as projectiles. These clusters have diameters of approximately 1.4 nm, 1.6 nm, 3 nm, and 4 nm, respectively. The kinetic energy and number of argon atoms in the projectile cluster are changed to investigate the effect of these parameters on the particle ejection process. Impacts of Ar_{60} , Ar_{100} , Ar_{366} , and Ar_{1000} projectiles with kinetic energy between 1 and 40 keV are investigated. All impacts occur along the surface normal. The shape and size of the samples are chosen based on visual observations of energy transfer pathways stimulated by the impacts of argon clusters. As a result, cylindrical samples are used. For Ar_{60} , Ar_{100} , and Ar_{366} projectiles samples have a diameter of 40 nm. Substrates with a diameter of 80 nm are used for the Ar_{1000} projectile. Samples consist of a double layer of graphene with a highly oriented pyrolytic graphite structure. They contain 92,126 and 368,564 atoms, respectively. Rigid and stochastic regions are used to simulate the thermal bath that keeps the sample at the required temperature, to prevent reflection of pressure waves from the boundaries of the system, and to maintain the shape of the sample [30,31]. The simulations are run at a target temperature of 0 K. Most simulations extend up to 10 ps, which is long enough to achieve saturation in the ejection yield versus time dependence. Only simulations for Ar_{1000} with kinetic energy below 15 keV are run for 80 ps to investigate the massive deformation of graphene, which occurs in these systems over a prolonged time. Twenty-five impact points randomly selected near the centre of the sample are chosen for each combination of projectile size and primary kinetic energy to achieve statistically reliable data. Simulations are performed with the large-scale atomic/molecular massively parallel simulator code (LAMMPS) [32], which has been modified to describe sputtering conditions better. In principle, particles ejected in the direction of the primary beam (the transmission direction) and in the opposite direction (the reflection direction) are collected. However, as emission in the reflection direction is minimal, only the data for the transmission direction are presented in this paper.

3. Results and discussion

Dependence of the total sputtering yield and of the fraction of projectile atoms penetrating through the sample on the primary kinetic energy is presented in Fig. 1. The yield initially increases with kinetic energy but saturates for higher energies in the investigated range for the same projectile. For each projectile, there is a minimum kinetic energy required to eject substrate particles or to perforate graphene. These energies are presented in Table 1. Threshold energy shifts towards larger values with the projectile size. Furthermore, the ejection of graphene atoms requires higher kinetic energy than the emission of argon atoms. The latter is an indicator of graphene perforation.

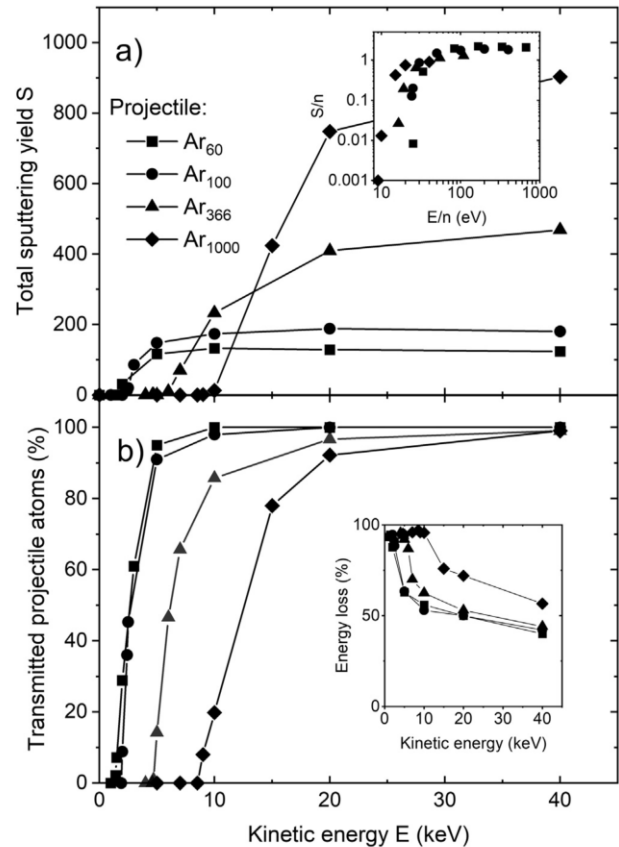


Fig. 1. The effect of the projectile kinetic energy E and size n on a) sputtering yield S , and b) fraction of transmitted projectile atoms for various Ar clusters. The inset to panel a) shows the data normalized to the number of projectile atoms. The inset to panel b) shows the fraction of the primary kinetic energy lost by the projectile.

Table 1

Values of the threshold energy E_{th} , threshold energy per atom E_{th}/n , threshold momentum (M_{th}), and threshold projected momentum M_{pth} for substrate particle emission ($_s$) and graphene perforation ($_p$).

	Ar_{60}	Ar_{100}	Ar_{366}	Ar_{1000}
$E_{th,s}$ (keV)	1.5	2.4	5.0	10.0
$E_{th,p}$ (keV)	1.4	2.0	4.7	9.0
$E_{th,s}/n$ (eV)	25	24	13	10
$E_{th,p}/n$ (eV)	23	20	12	9
$M_{th,s}$ ($kg \cdot m/s$) $\cdot 10^{-19}$	0.6	1.0	2.8	6.5
$M_{th,p}$ ($kg \cdot m/s$) $\cdot 10^{-19}$	0.6	0.9	2.7	6.2
$M_{pth,s}$ ($kg \cdot m/s/m^2$) $\cdot 10^2$	4.0	5.0	3.9	5.2
$M_{pth,p}$ ($kg \cdot m/s/m^2$) $\cdot 10^2$	3.9	4.6	3.8	4.9

Difference between these two thresholds increases with the projectile size. This means that it is easier for a large projectile to penetrate graphene without emission of carbon atoms.

It has been shown that the relation between the sputtering yield S and parameters of the cluster projectiles can be significantly simplified if the data are presented in a special form [33–35]. Such representation, sometimes called “universal”, is shown in the inset to Fig. 1a [33,34]. Indeed, at the high E/n region, data points for all projectiles are located at the same line, and the dependence between S/n and E/n is linear, where E is the projectile's kinetic energy, and n is the number of projectile atoms. At low E/n value, the data points cannot be placed on a single line, and the S/n vs E/n dependence becomes nonlinear, as reported previously [33,34]. The onset of the nonlinear region depends

strongly on the cluster size, shifting it to the lower kinetic energy per atom as the size of the cluster projectile increases. The same trend has been observed previously [33,34]. Our results indicate that the universal representation implemented for the sputtering of thick samples is valid also for systems with limited dimensionality. Popok et al. [35] proposed another approach aimed at simplifying the relation between projectile range and projectile parameters. In this approach, the effect of projectile size and its kinetic energy was unified by using the projectile momentum [35]. The effect of the application of all these approaches to our threshold energy data is shown in Table 1. It is evident that expressing the ejection onsets by the projected momentum seems to be the most universal. The projected momentum is calculated by dividing the projectile momentum by the area of the projectile's projection on the graphene surface, as proposed in Ref. [35].

The yield of ejected carbon atoms increases with the projectile size when the primary kinetic energy is constant. There is a significant particle emission from the bombarded sample, especially for large high-energy projectiles. Almost all projectile atoms penetrate through an ultrathin sample. Only below approximately 5 keV for Ar₆₀, Ar₁₀₀, 10 keV for Ar₃₆₆, and 15 keV for Ar₁₀₀₀ penetration efficiencies are significantly reduced, as shown in Fig. 1b. It is evident that a significant fraction of the primary kinetic energy is lost by a projectile regardless of the minimum thickness of the sample, as indicated by the data presented in the inset to Fig. 1b. For instance, for 10 keV projectiles, more than half of the primary kinetic energy is lost when penetrating through graphene layers. This fraction decreases as the kinetic energy increases for a given projectile size. It also increases as the projectile size decreases for a given primary kinetic energy, particularly at low kinetic energy. It is interesting to note that the projectile loses its kinetic energy even in cases where no ejection of substrate atoms occurs. This observation indicates that graphene sheets consume a part of the primary kinetic energy.

The primary kinetic energy also influences the relative contribution of various species in the ejected plum, as presented in Fig. 2. Numbers in the bottom-right corners of individual spectra indicate the kinetic energy per projectile atom, which is proposed as the universal metric to characterize ejection phenomena stimulated by cluster projectile

impacts [33,34]. This quantity is proportional to a square of the projectile velocity. For energetic projectiles, mainly carbon monomers populate the plum. The most abundant ejection shifts to larger fragments with a decrease of the projectile energy per atom. At the same time, a relative ejection of carbon monomers decreases. At certain conditions, carbon trimers are the most abundant species in the ejected flux, as seen, for instance, for 20 and 40 keV Ar₁₀₀₀ projectiles (20 and 40 eV/n respectively). For these impacts, the emission of carbon monomers is almost absent. This is a surprising observation, as in a typical sputtering experiment the emission of monomers is a dominant channel of particle removal [36]. Based on the similarities in the mass spectra, we divide all investigated impacts into three categories, as indicated in Fig. 2. Impacts leading to the significant ejection of carbon monomers are classified as category A. This category contains impacts of the projectiles with the largest kinetic energy per atom used in our study. Impacts leading to a dominant emission of larger fragments are marked as category B. This category includes medium energy impacts. Finally, impacts resulting in no emission of substrate particles are grouped in category C. This category contains impacts of the projectiles with the lowest kinetic energy per atom investigated in our study.

Differences in the particle emission process caused by impacts assigned to categories A, B, and C are even more pronounced in velocity distributions of the ejecta. In Fig. 3, we present velocity distributions of C, C₂, and C₃ fragments ejected from graphene in the transmission direction. The spectra are normalized to their maxima, because in the following reasoning we will be interested only in their shape. For category A impacts, the ejecta have broad velocity distributions. The shape and the peak position of spectra for each fragment type are different. Carbon monomers are, on average, the fastest-moving particles. Larger fragments move with lower velocity, which is typical behaviour observed for sputtering experiments [36]. Much more interesting are the velocity spectra of particles ejected by impacts classified as category B. These spectra are narrower than earlier distributions. Surprisingly, they have almost identical shapes for all three types of the emitted species at the same impact conditions. Moreover, the velocity corresponding to the most abundant emission correlates with the initial velocity of a projectile. These features are different from a typical

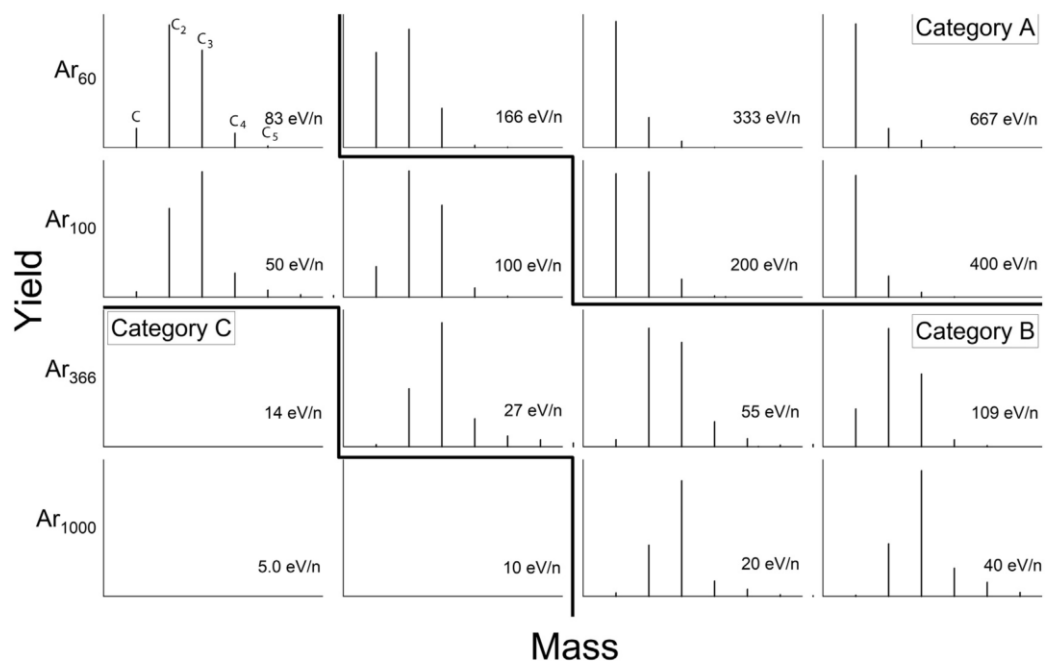


Fig. 2. Mass spectra of particles ejected in the transmission direction for 16 impact conditions corresponding to 4 projectile sizes and 4 primary kinetic energies. Graphs are grouped into three categories A, B, and C based on similarities of the spectra features (see text). Projectile atoms are not shown.

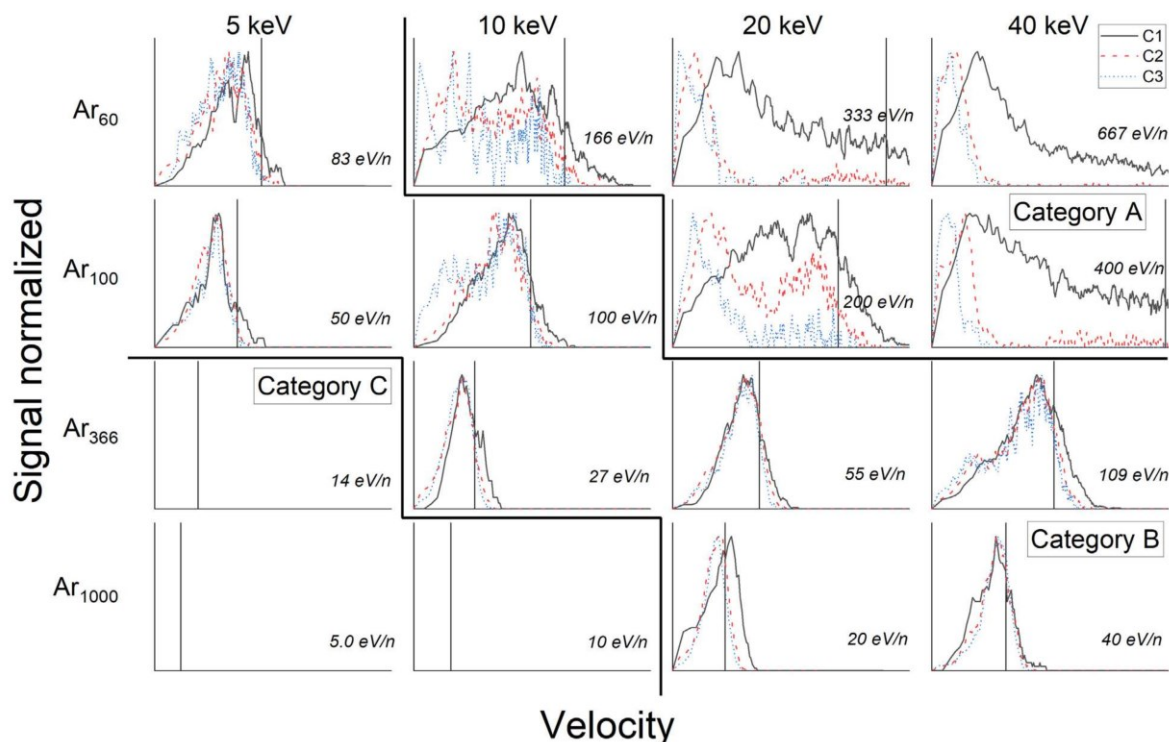


Fig. 3. Velocity distributions of 16 incidence conditions corresponding to different projectiles and primary kinetic energies. Different lines show velocities distributions of emitted C atoms (black solid line), C dimers (red dashed line), and C trimers (blue dotted line). Vertical lines denote the initial velocity of a projectile. All spectra are normalized to their maxima. Initial projectile velocity for the 40 keV Ar₆₀ impact is outside of the velocity scale. Numbers at the bottom right corner of each spectrum depict the kinetic energy per projectile atom. (For interpretation of the references to colour in this figure legend, the reader is referred to the web version of this article.)

sputtering experiment, where the shape of the velocity spectra does not depend on the primary kinetic energy, at least in the linear cascade regime, and are usually different for various ejected species [36]. These differences can be expected, as there is no time and space for the linear collision cascade to develop in our samples. Nevertheless, the ejection of various fragments with the same velocity spectra is still puzzling. There are no velocity distributions in Fig. 3 for the impacts of category C, as no particles are ejected in this case.

The temporal evolution of studied systems is investigated to identify processes responsible for the particle ejection and explain the observed

trends. The results are shown in Figs. 4, 5, 6, 7, and 8, as well as in Animations 1, 2, 3, and 4. An example of temporal snapshots for category A impacts is shown in Fig. 4, and in Animation 1. The data are obtained for 40 keV Ar₆₀ projectile, which is the fastest projectile investigated in our study. The integrity of the projectile is compromised almost immediately after it passes through the graphene. However, during the impact, the projectile atoms stay together and interact collectively with the sample. After the collision, all projectile atoms penetrate through the substrate. The ejection of both projectile and substrate atoms is forward directed. Only a few substrate atoms are emitted

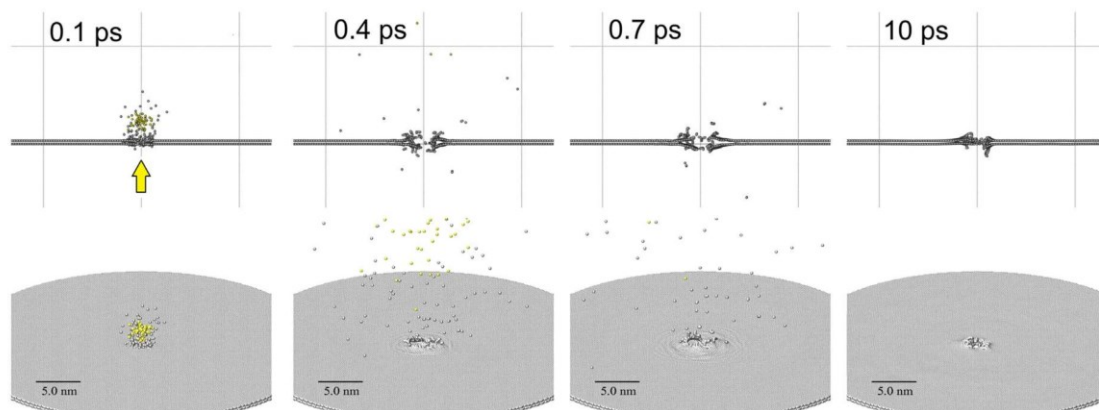


Fig. 4. Temporal snapshots from the simulation of a 40 keV Ar₆₀ impact at graphene. The top row contains side views of the system obtained at various moments given by the values at the top left corners. The lower row contains perspective view of the same system. For a side view only 2 nm thick slice through the centre of the sample is shown. Carbon atoms are depicted as grey balls while argon atoms are yellow. Thin lines in the background denote the distance of 10 nm. Arrow indicates the direction of an incoming projectile. (For interpretation of the references to colour in this figure legend, the reader is referred to the web version of this article.)

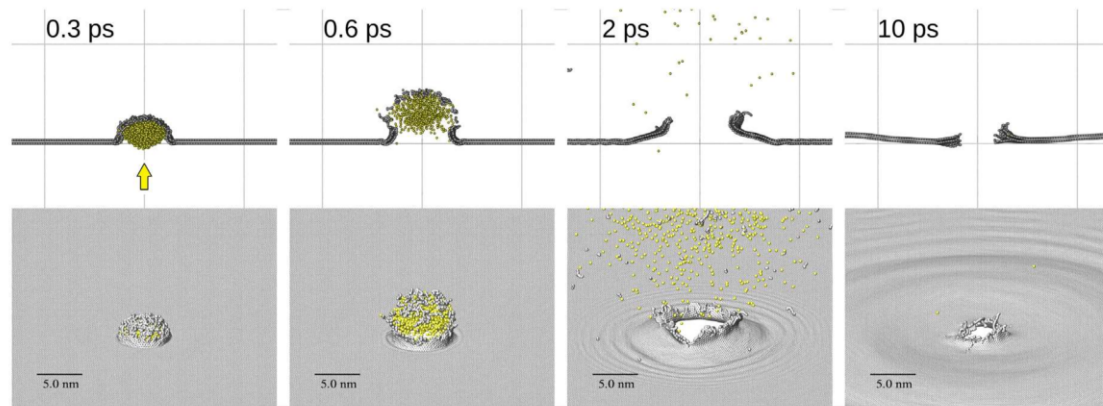


Fig. 5. Temporal snapshots from the simulation of a 40 keV Ar_{1000} impact at graphene. A detailed description of the content of the figure is provided in Fig. 4.

in the reflection direction. Atom removal leads to a formation of initially almost circular nanopore. Zhao et al. have found that energetic clusters can be used to fabricate nanopores in graphene in a controlled way by varying the properties of the incident beam [20,37]. They have found that impact energy of 11.4 eV per projectile atom is needed to create a nanopore in a single layer of graphene when bombarded with C_{60} projectile at normal incidence [20,37]. This value is smaller than the threshold energy for the nanopore formation by Ar_{60} projectiles, as shown in Table 1. This difference is expected, as Ar_{60} has a different mass than C_{60} , and two-layered graphene is bombarded in our case.

The structure of a newly created nanopore is dynamic. We observe, for instance, that new bonds are created in this area. The radicals created by the impact are highly reactive and tend to form new bonds instantly. Some of these bonds are also formed between carbon atoms located in different layers. Again, similar behaviour was reported for C_{60} bombardment of graphene [20,37], and C_{60} and Ar_n bombardment of fullerite [38]. These new bonds lead not only to a hardening of the rim but also to a partial self-healing of the created nanopore.

As already discussed, a significant fraction of the primary kinetic energy is transferred to the sample. Most of this energy is carried away by circular acoustic waves that propagate outward from the point of impact. For the Ar_{60} bombardment, these waves have a maximum amplitude of approximately 0.1 nm. The process is very effective as graphene planes can efficiently transfer kinetic energy. It has been shown, for instance, that this property is responsible for an unusually small sputtering yield observed from pyrolytic graphite bombarded by C_{60} [39].

The analysis of Animation 1 indicates that two processes lead to the emission of carbon particles. Initially, carbon atoms are ejected by a

direct interaction with a projectile. Because the projectile is energetic, the collisions are violent, and a lot of energy is transferred between Ar and C atoms. Original bonds between carbon atoms are easily broken, which leads predominantly to the emission of monomers. The presence of a conglomerate of Ar and C atoms at a distance of ~ 1.5 nm from the graphene already at 100 fs, as seen in Fig. 4, indicates that most of the carbon atoms ejected in this phase have high velocities. The second process leading to particle ejection occurs later and may last for several picoseconds. The rim is energized during projectile penetration. Some of this energy can be used to eject carbon particles. These particles are ejected along various polar angles with lower kinetic energy than atoms emitted by a direct interaction with the projectile. However, there is also a significant vertical and radial movement in this area. The vertical movement initially leads to a temporary separation of the layers near the rim area. It has been shown that this process can be used to stimulate efficient emission of intact organic molecules from layers deposited on graphene substrate [12,24]. Later, the vertical movement combines with correlated radial displacements of C atoms around the rupture and is transformed into collective movements, which develop wave-like vertical oscillations and radial planar compressions. A similar phenomenon also has been observed on graphite and graphene surfaces bombarded by C_{60} [12,21,40,42]. Approximately 20% of the primary kinetic energy transferred from the projectile to the sample is carried away by ejected substrate atoms for a 40 keV Ar_{60} bombardment. The remaining part is carried away by outwardly propagating waves.

The projectile has a lower kinetic energy per atom during category B impacts as compared to the category A bombardment, as shown in Fig. 3. It means that it moves slower. Examples of category B impacts are presented in Fig. 5 (Animation 2) and in Fig. 6 for a 40 keV Ar_{1000}

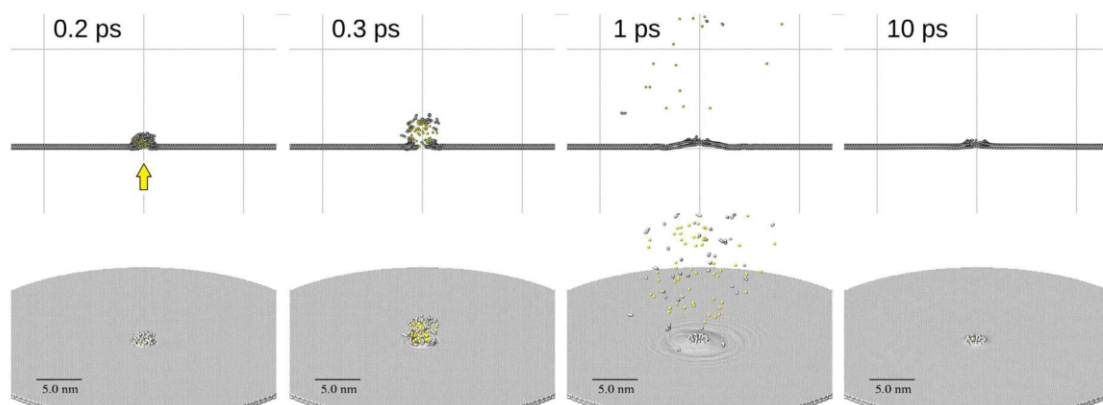


Fig. 6. Temporal snapshots from the simulation of a 5 keV Ar_{60} impact at graphene. A detailed description of the content of the figure is provided in Fig. 4.

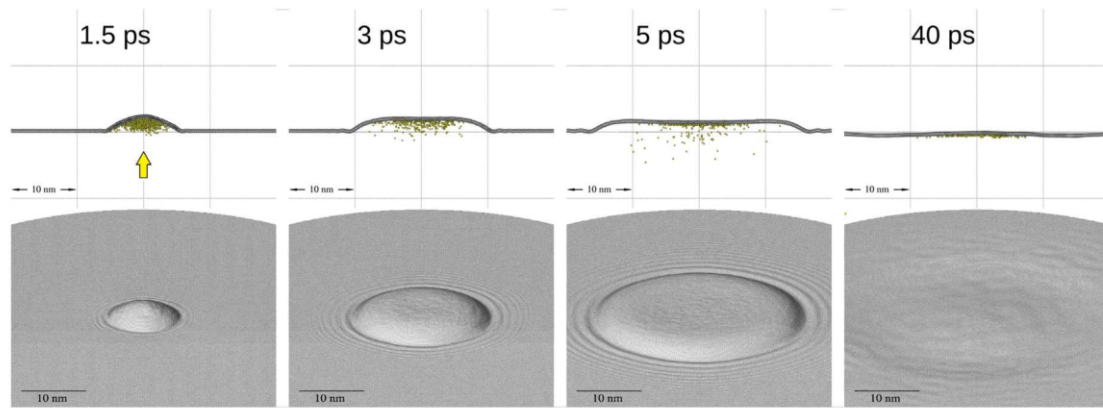


Fig. 7. Temporal snapshots from the simulation of a 5 keV Ar_{1000} impact at graphene. A detailed description of the content of the figure is provided in Fig. 4.

and 5 keV Ar_{60} , respectively. Just like in the case of category A impacts, projectiles are being compressed and flattened. However, the extent of flattening is more significant now. After approximately 0.2 ps for 5 keV Ar_{60} and 0.4 ps for 40 keV Ar_{1000} graphene becomes perforated. A large pore is formed for Ar_{1000} . However, even for 5 keV Ar_{60} projectiles, the orifice has a larger diameter as compared to the 40 keV Ar_{60} impact, as the 5 keV Ar_{60} projectile expands laterally before penetrating through the graphene layers. As shown in Figs. 5 and 6, and in Animation 2, carbon atoms located initially directly above the impinging projectile are removed collectively from the sample. They remain in almost original lattice, as they are entrained as one entity by Ar projectiles. Consequently, these atoms have similar velocities as the propagating clusters. This velocity is lower than the initial projectile velocity because a part of the primary kinetic energy is already consumed to perforate graphene. Carbon atoms entrained by the projectile are separated later when the projectile disintegrates, forming various fragments. However, they preserve their velocities. This observation explains why these particles have similar velocity distributions. Furthermore, the process is gentle and spatially correlated. Consequently, not only monomers but mostly larger fragments of the original lattice survive the ejection process. As a result, the peak in the mass spectra shifts towards larger fragments as compared to the mass spectra of category A impacts. The effect becomes more pronounced for larger projectiles. These observations account for the main features of the data shown in Figs. 2 and 3. Just like in the case of category A impacts, a fraction of the primary kinetic energy is deposited in graphene sheets, which leads to a formation of acoustic waves. Because the projectile is moving slower, there is more time for interactions between projectile atoms and atoms residing near the rim of the formed nanopore. More

energy is transferred from the projectile to the sample. However, there is also more time to drain this energy away from the nanopore. Simulations indicate that this process is fast. Consequently, more acoustic waves with higher amplitudes are created, but the density of the deposited energy near the rim area is small. As a result, the rim is less energized, fewer carbon particles are emitted from this area, and carbon entrainment becomes the primary mechanism of particle ejection.

Finally, the impacts of category C should be discussed. These impacts do not lead to carbon ejection from the sample. However, graphene is still disturbed. In fact, the substrate can be more significantly altered than in previously discussed cases for the impacts of large projectiles. Our simulations identify two possible scenarios. In the first case, both the projectile momentum and its kinetic energy are not sufficient to perforate the sample. This scenario is illustrated in Fig. 7 and in Animation 3 for 5 keV Ar_{1000} . For these impact conditions, the projectile is almost entirely decelerated. During deceleration, projectile flattens significantly spreading its atoms over a wide area below the graphene. Most of the primary kinetic energy is transferred to the sample, as shown in Fig. 1. This energy is used predominantly to deform the sample and to create acoustic waves. As a result, the graphene surface bulges out in the direction of the primary beam over a large area, and numerous acoustic waves propagate outwards. Finally, the projectile atoms become back-reflected, but their kinetic energy is small. The deposited energy is carried away from the impact area and its density is not sufficient to stimulate the ejection of carbon from graphene. After the deposited energy is dispersed in graphene, the system returns to its initial shape.

In the second scenario, the momentum of the projectile is sufficient

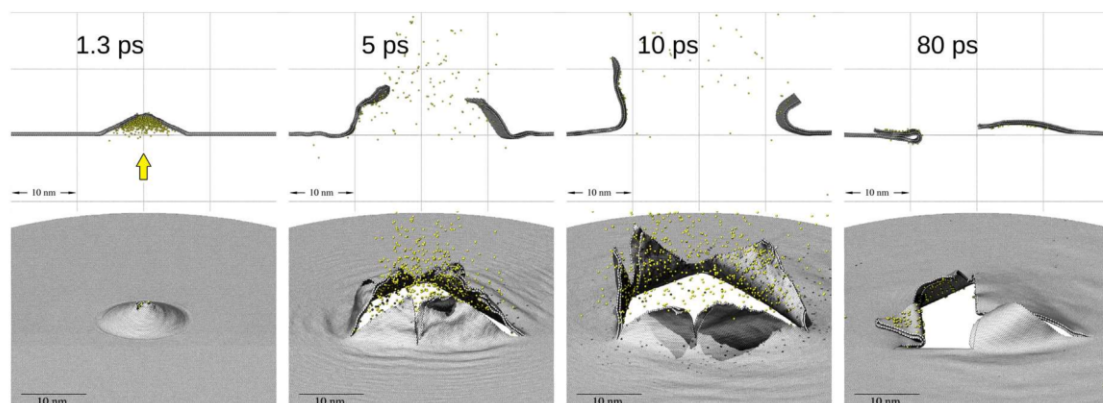


Fig. 8. Temporal snapshots from the simulation of a 10 keV Ar_{1000} impact at graphene. A detailed description of the content of the figure is provided in Fig. 4.

to break graphene, but the deposited density of the primary kinetic energy is still not enough to eject carbon atoms. This scenario is illustrated in Fig. 8 and in Animation 4 for a 10 keV Ar₁₀₀₀ impact. After the impact of a massive projectile, the graphene substrate begins to deform conically, just like it did in the earlier case. Graphene begins to buckle out. Again, the projectile decelerates and flattens over a large area. However, now its momentum is sufficient to rip the sample. A small rupture is formed initially, but soon radial cracks along crystallographic directions occur, which propagate quickly. Graphene layers unfold in a petal-like form. Five triangular-shaped petals fold at their bases. The system opens like a flower. The opening is vast, with dimensions significantly exceeding the projectile diameter. Argon atoms easily move through this opening. Individual petals move out. Some of them are even placed for a short moment on the graphene surface. Even in these extreme conditions, the structure does not break. Instead, the elastic strain forces the petals to move back into the opening. Even at the end of our simulation (80 ps) there is still kinetic energy in the petal movement. The formation of petal-like structures has also been shown in experiments with a supersonic micro-particle bombardment of multilayer graphene [43]. It is fascinating to note that even argon cluster projectiles can stimulate the same effects as orders of magnitude larger micro-projectiles. As indicated by Figs. 7 and 8, the processes stimulated by category C impacts are much more prolonged in time, as compared to scenarios present during category A and B impacts.

4. Conclusions

We presented the results of computer simulations investigating the bombardment of two-layered free-standing graphene by argon cluster projectiles with various kinetic energy and size. For most of the impacts considered, there is a substantial emission of carbon from graphene. Even though graphene is a very thin material, it absorbs a lot of the projectile's kinetic energy. Based on the differences in the ejecta, we divided impacts into three categories. Impacts with high kinetic energy per atom are described as category A. These impacts result in the ejection of high amounts of atomic carbon due to direct collisions with a projectile followed by emission from the energized rim of the rupture in graphene. Medium kinetic energy per atom impacts are classified as category B. In these impacts, the projectile gently pushes material out from graphene, resulting in the ejection of larger graphene fragments, especially C₃ particles. Finally, low-kinetic energy per atom impacts are described as category C. Such impacts do not lead to any carbon ejection even if they result in piercing the graphene layers. These impacts may, however, significantly modify a structure of graphene, especially for massive and large projectiles. In this case, the formation of large petal-like defects is observed. Similar structures have been already observed in experiments with micro-sized projectiles of comparable velocity and multilayer graphene targets [43].

It has been proposed that C₆₀ projectiles can be used for a controlled perforation of graphene. In principle, also Ar clusters could be used for the same purpose as there is a definite relation between Ar cluster size and dimension of the nanopore created by its impact. From a practical point, however, it is currently not possible to make an ion beam composed of Ar clusters of the same size. Due to technical reasons, Ar ion beams always contain a distribution of Ar clusters with different sizes. As a result, only limited control of the pore sizes can be achieved with these projectiles.

Finally, a few comments can be made about the applicability of Ar cluster projectiles and ultrathin graphene substrates for SIMS analysis of organic overlayers in transmission geometry. Studies with C₆₀ projectiles have shown that intact organic molecules are emitted by the unfolding of the topmost graphene layer. In this case, the graphene sheet acts as a catapult that can gently hurl molecules into the vacuum. There is a considerable amount of energy associated with this movement, which means that even very large molecules can be uplifted. During argon cluster bombardment, there is more energy in this

motion, and the movement extends to a much higher lateral distance from the point of impact. Consequently, a larger number of adsorbed molecules could be ejected by a single projectile impact, making analysis of small amounts of organic material even more viable.

Supplementary data to this article can be found online at <https://doi.org/10.1016/j.surfcoat.2020.125683>.

Author statement

Mikołaj Gołuński: Conceptualization, Methodology, Validation, Formal analysis, Investigation, Data Curation, Writing - Original Draft, Writing - Review & Editing, Project administration, Funding acquisition.

Sviatoslav Hrabar: Data Curation, Visualization.

Zbigniew Postawa: Conceptualization, Software, Validation, Investigation, Resources, Writing - Review & Editing, Supervision, Funding acquisition.

Declaration of competing interest

The authors declare that they have no known competing financial interests or personal relationships that could have appeared to influence the work reported in this paper.

Acknowledgements

This work was supported by the National Science Centre, Poland grant numbers: 2016/23/N/ST4/00971 and 2015/19/B/ST4/01892. MD simulations were performed at the PLGrid Infrastructure, Poland.

References

- [1] I. Lyuksyutov, A.G. Naumovets, V. Pokrovsky, Introduction, in: I. Lyuksyutov, A.G. Naumovets, V. Pokrovsky (Eds.), *Two-dimensional Crystals*, Academic Press, 1992, pp. 11–14.
- [2] A.K. Geim, K.S. Novoselov, *Nat. Mater.* 6 (2007) 183–191.
- [3] F. Bonaccorso, L. Colombo, G. Yu, M. Stoller, V. Tozzini, A.C. Ferrari, R.S. Ruoff, V. Pellegrini, *Science* 347 (2015) 1246501.
- [4] A.C. Ferrari, F. Bonaccorso, V. Fal'ko, K.S. Novoselov, S. Roche, P. Boggild, S. Borini, F.H. Koppens, V. Palermo, N. Pugno, J.A. Garrido, R. Sordan, A. Bianco, L. Ballerini, M. Prato, E. Lidorikis, J. Kivioja, C. Marinelli, T. Ryhanen, A. Morpurgo, J.N. Coleman, V. Nicolosi, L. Colombo, A. Fert, M. Garcia-Hernandez, A. Bachtold, G.F. Schneider, F. Guinea, C. Dekker, M. Barbone, Z. Sun, C. Galiotis, A.N. Grigorenko, G. Konstantatos, A. Kis, M. Katsnelson, L. Vandersypen, A. Loiseau, V. Morandi, D. Neumaier, E. Treossi, V. Pellegrini, M. Polini, A. Tredicucci, G.M. Williams, B.H. Hong, J.H. Ahn, J.M. Kim, H. Zirath, B.J. van Wees, H. van der Zant, L. Occhipinti, A. Di Matteo, I.A. Kinloch, T. Seyller, E. Quesnel, X. Feng, K. Teo, N. Rupesinghe, P. Hakonen, S.R. Neil, Q. Tannock, T. Lofwander, J. Kinaret, *Nanoscale* 7 (2015) 4598–4810.
- [5] S. Shukla, S.-Y. Kang, S. Saxena, *Appl. Phys. Rev.* 6 (2019) 021311.
- [6] S. Kim, A.V. Ievlev, J. Jakowski, I.V. Vlasiouk, X.H. Sang, C. Brown, O. Dyck, R.R. Unocic, S.V. Kalinin, A. Belianinov, B.G. Sumpter, S. Jesse, O.S. Ovchinnikova, *Carbon* 131 (2018) 142–148.
- [7] B.J. Tyler, B. Brennan, H. Stec, T. Patel, L. Hao, I.S. Gilmore, A.J. Pollard, *J. Phys. Chem. C* 119 (2015) 17836–17841.
- [8] K. Mochiji, N. Inui, R. Asa, K. Moritani, *E-Journal of Surface Science and Nanotechnology* 13 (2015) 167–173.
- [9] A.Y. Galashev, *Comput. Mater. Sci.* 98 (2015) 123–128.
- [10] K. Moritani, S. Houzumi, K. Takeshima, N. Toyoda, K. Mochiji, *J. Phys. Chem. C* 112 (2008) 11357–11362.
- [11] S. Geng, S.V. Verkhoturov, M.J. Eller, S. Della-Negra, E.A. Schweikert, *J. Chem. Phys.* 146 (2017) 054305.
- [12] S.V. Verkhoturov, M. Gołuński, D.S. Verkhoturov, B. Czerwinski, M.J. Eller, S. Geng, Z. Postawa, E.A. Schweikert, *J. Chem. Phys.* 150 (2019) 160901.
- [13] S. Fearn, *Mater. Sci. Technol.* 31 (2015) 148–161.
- [14] N. Winograd, Gas cluster ion beams for secondary ion mass spectrometry, in: P.W. Bohn, J.E. Pemberton (Eds.), *Annual Review of Analytical Chemistry*, 11 2018, pp. 29–48.
- [15] D. Weibel, S. Wong, N. Lockyer, P. Blenkinsopp, R. Hill, J.C. Vickerman, *Anal. Chem.* 75 (2003) 1754–1764.
- [16] S. Rabbani, A.M. Barber, J.S. Fletcher, N.P. Lockyer, J.C. Vickerman, *Anal. Chem.* 83 (2011) 3793–3800.
- [17] S.J. Lee, C.M. Choi, B.K. Min, J.Y. Baek, J.Y. Eo, M.C. Choi, *Bull. Kor. Chem. Soc.* 40 (2019) 877–881.
- [18] T.B. Angerer, P. Blenkinsopp, J.S. Fletcher, *Int. J. Mass Spectrom.* 377 (2015)

- 591–598.
- [19] S.V. Verkhoturov, S. Geng, B. Czerwiński, A.E. Young, A. Delcorte, E.A. Schweikert, *J. Chem. Phys.* 143 (2015) 2–7.
- [20] S. Zhao, J. Xue, L. Liang, Y. Wang, S. Yan, *J. Phys. Chem. C* 116 (2012) 11776–11782.
- [21] M. Gołuński, Z. Postawa, *Acta Phys. Pol. A* 132 (2017) 222–224.
- [22] M. Gołuński, S.V. Verkhoturov, D.S. Verkhoturov, E.A. Schweikert, Z. Postawa, *Nucl. Instrum. Methods Phys. Res., Sect. B* 393 (2017) 13–16.
- [23] Z.C. Xu, W.R. Zhong, *Appl. Phys. Lett.* 104 (2014) 261907.
- [24] S.V. Verkhoturov, M. Gołuński, D.S. Verkhoturov, S. Geng, Z. Postawa, E.A. Schweikert, *J. Chem. Phys.* 148 (2018) 144309.
- [25] O. Lehtinen, J. Kotakoski, A.V. Krashennnikov, J. Keinonen, *Nanotechnology* 22 (2011) 175306.
- [26] O. Lehtinen, J. Kotakoski, A.V. Krashennnikov, A. Tolvanen, K. Nordlund, J. Keinonen, *Phys. Rev. B* 81 (2010) 153401.
- [27] M. Kanski, D. Maciazek, Z. Postawa, C.M. Ashraf, A.C.T. van Duin, B.J. Garrison, *J. Phys. Chem. Lett.* 9 (2018) 359–363.
- [28] R.A. Aziz, M.J. Slaman, *Mol. Phys.* 58 (1986) 679–697.
- [29] W.D. Wilson, L.G. Haggmark, J.P. Biersack, *Phys. Rev. B* 15 (1977) 2458–2468.
- [30] B.J. Garrison, Z. Postawa, *Mass Spectrom. Rev.* 27 (2008) 289–315.
- [31] Z. Postawa, B. Czerwiński, M. Szewczyk, E.J. Smiley, N. Winograd, B.J. Garrison, *J. Phys. Chem. B* 108 (2004) 7831–7838.
- [32] S. Plimpton, *J. Comput. Phys.* 117 (1995) 1–19.
- [33] C. Anders, H.M. Urbassek, R.E. Johnson, *Phys. Rev. B* 70 (2004) 155404:1–6.
- [34] A. Delcorte, B.J. Garrison, K. Hamraoui, *Anal. Chem.* 81 (2009) 6676–6686.
- [35] V.N. Popok, J. Samela, K. Nordlund, E.E.B. Campbell, *Phys. Rev. B* 82 (2010) 201403–1 - 201403-4.
- [36] W.O. Hofer, *Top. Appl. Phys.* 64 (1991) 15–90.
- [37] W.S. Li, L. Liang, S.J. Zhao, S. Zhang, J.M. Xue, *J. Appl. Phys.* 114 (2013) 234304.
- [38] B. Czerwiński, A. Delcorte, *J. Phys. Chem. C* 117 (7) (2013) 3595–3604.
- [39] J. Tian, T. Zheng, J. Yang, S. Kong, J. Xue, Y. Wang, K. Nordlund, *Appl. Surf. Sci.* 337 (2015) 6–11.
- [40] R.P. Webb, *Radiat. Eff. Defects Solids* 162 (2007) 567–572.
- [41] M. Gołuński, Z. Postawa, *J. Vac. Sci. Technol., B: Nanotechnol. Microelectron.* 36 (2018) 03F112.
- [42] J.H. Lee, P.E. Loya, J. Lou, E.L. Thomas, *Science* 346 (2014) 1092–1096.

Article 7

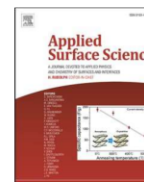
Mechanisms of Molecular Emission from Phenylalanine Monolayer Deposited on Free-standing Graphene Bombarded by C₆₀ Projectiles

Gołuński M., Hrabar S. & Postawa Z.

Applied Surface Science 539, 148259 (2021)

doi:[10.1016/j.apsusc.2020.148259](https://doi.org/10.1016/j.apsusc.2020.148259)

Reproduced with permission of Elsevier.



Mechanisms of molecular emission from phenylalanine monolayer deposited on free-standing graphene bombarded by C₆₀ projectiles

Mikołaj Gołuński, Sviatoslav Hrabar, Zbigniew Postawa*

Smoluchowski Institute of Physics, Jagiellonian University, ul. Lojasiewicza 11, 30-348 Krakow, Poland

ARTICLE INFO

Keywords:

MD simulations
SIMS
Graphene
Organic overlayer
Sputtering
C60

ABSTRACT

The Molecular Dynamics (MD) computer simulations are used to gain insight into the mechanism of molecular ejection from a monolayer of phenylalanine (C₉H₁₁NO₂) molecules deposited on free-standing two-layer graphene. The system is bombarded with C₆₀ projectiles with different kinetic energy and angle of incidence. Mass spectra, sputtering yields, and angular distributions of emitted particles are recorded in two bombardment geometries, in which the projectile hits the sample from above and below.

The sputtering yields increase with the primary kinetic energy. There is an optimal angle of incidence for each kinetic energy, leading to the most effective molecular emission. The value of this angle increases with kinetic energy. The interplay between the area energized by the impinging projectile, the energy back-reflection, and molecular fragmentation determines the shape of the yield dependence on the angle of incidence. The bombardment geometry has little effect on the efficiency of molecular emission. Generally, organic molecules are emitted by interaction with the projectile and/or a graphene substrate. The main factor affecting the relative contribution of each of these interactions is whether graphene is punctured. The implications of current results for the potential use of graphene supports in Secondary Ion Mass Spectrometry are discussed.

1. Introduction

In recent years, cluster ion beams have attracted increasing experimental and theoretical attention due to their ability to increase the ejection of large intact organic molecules and reduce the accumulation of chemical damage in Secondary Ion Mass Spectrometry (SIMS) [1–4]. The use of cluster projectiles enabled three-dimensional depth profiling of organic and biological systems, exposing this technique to the universe of new possibilities. One of the most successful clusters used in organic SIMS is C₆₀ fullerene [5]. In standard SIMS geometry, the detector is on the same side of the target as the ion gun. Usually, metals or semiconductors are used to support the investigated material. Recently, a novel SIMS configuration has been proposed, using transmission orientation in combination with free-standing graphene support [6]. In this orientation, the analyzed organic material is deposited on one side of the ultra-thin substrate, while cluster projectiles bombard another side. The use of ultra-thin support allows for minimizing interference between substrate and analyte signals. The formation of negative molecular ions is also increased by two orders of magnitude due to the

presence of graphene [7–9]. It was therefore argued that such geometry could be particularly attractive for studying isolated small nano-objects and supramolecular assemblies [6–10].

There is an extensive database of theoretical studies aimed at determining processes leading to the emission of molecules deposited on thick substrates [1,11–19]. In particular, it was found that various processes are responsible for molecular ejection, depending on whether the projectile is atomic or cluster [1]. For atomic projectiles, the development of a linear collision cascade leads to particle emission [20]. Simultaneous interactions with many ejecting substrate atoms are necessary to stimulate the uplifting of large organic molecules having multiple contact points with the surface [12]. The probability that monoatomic projectiles will generate a time and space-correlated ejection of a sufficient number of substrate atoms to displace a large organic molecule sharply decreases as the number of these contact points increases. As a result, these projectiles are not optimal for the uplifting of large intact molecules.

Much better are cluster projectiles. The impact of these projectiles leads to the development of a non-linear collision cascade and the

* Corresponding author.

E-mail addresses: mikolaj.golunski@doctoral.if.uj.edu.pl (M. Gołuński), sviatoslav.hrabar@doctoral.uj.edu.pl (S. Hrabar), zbigniew.postawa@uj.edu.pl (Z. Postawa).

<https://doi.org/10.1016/j.apsusc.2020.148259>

Received 21 May 2020; Received in revised form 15 October 2020; Accepted 22 October 2020

Available online 28 October 2020

0169-4332/© 2020 Elsevier B.V. All rights reserved.

unfolding of the topmost layers in a time and space correlated manner [21–23]. The formation of a crater is one of the consequences of this action. Another consequence is the ejection of organic molecules by the collective processes [14,15]. For large gas cluster projectiles, the molecules can also be entrained in a stream of projectile atoms reflected from the substrate [17–19]. This process is particularly effective in the case of off-normal impacts of projectiles consisting of thousands of weakly bonded atoms. It should be noted that simulations of bulk phenylalanine sample bombardment with large gas clusters confirm the “gas-flow” mechanic with the emission of intact molecules mainly from the rim of the crater [24]. Finally, small, weakly bound molecules can be uplifted from the substrate by interacting with circular acoustic waves [13,16]. Such waves can be generated by cluster impacts on the surface of materials with a membrane-like structure, like graphite.

Although the molecular emission from the organic overlayers deposited on thick substrates is well documented, much less is known about the processes leading to molecular emission from two-dimensional (2D) substrates. Processes generated in such substrates must be different due to their limited vertical dimensions, which does not allow for the development of a full collision cascade. Several simulations have been performed on the C_{60} bombardment of clean graphene [6,25–31]. So far, only a few simulations of the C_{60} bombardment of organic molecules deposited on free-standing graphene have been performed [8,9,32]. All these simulations are performed for impacts in transmission geometry. Moreover, they are limited to the normal incidence and minimal range of incident kinetic energy. There is no simulation studying molecular emission from graphene bombarded by cluster projectiles in standard sputtering configuration, in which both the ion gun and the detector are on the same side of the substrate. The purpose of this article is to investigate the processes that lead to the ejection of organic molecules deposited on ultrathin free-standing graphene utilizing a wide range of projectile kinetic energies and impact angles. Molecular emission stimulated by projectile impacts conducted in the novel transmission configuration and standard sputtering setup is investigated to identify and explain differences in mechanisms of molecular emission in these two systems. The implications of the results for the potential use of graphene support in Secondary Ion Mass Spectrometry are discussed.

2. Material and methods

The molecular dynamics (MD) computer simulations are used to model cluster bombardment. Briefly, the movement of particles is determined by integrating Hamilton’s equations of motion. The forces between carbon atoms in the system are described by the ReaxFF-1g force field [33], which allows for the formation and breaking of covalent bonds. This potential is splined at short distances with a Ziegler-Biersack-Littmark (ZBL) potential [34] to describe high-energy collisions adequately. We have decided to use the ReaxFF-1g potential as it was made for modeling energetic collisions. It should be pointed out, however, that a Reax potential parametrized to describe the amino acids is also published [35]. This potential was parametrized to describe low-energy processes. Therefore, it should be supplemented with a repulsive wall to accurately describe interatomic collisions at short distances (high-energy collisions). We have run a series of trial simulations with both potentials and found out that in our system, the results are similar. We have already published a few studies aimed to investigate various aspects of the particle emission from clean graphene and graphene covered with phenylalanine molecules using the Reax-1g potential [25,26,32]. Therefore, this force-field will be used in this manuscript to allow for a direct comparison of the current and previously published data. However, it should be stressed that parametrization developed for amino acids should be used in sputtering studies, where low-energy collisions are responsible for particle emission. Such a situation will occur, for example, during cluster bombardment of bulk phenylalanine systems. In this case, a full collision cascade will develop inside a thick

sample, and the particles emitted into the vacuum will originate from a low-energy tail of this cascade [20]. Electronic stopping was disregarded as in the case of the investigated sample and energies the nuclear stopping is much more prevalent than electronic processes [34]. A more detailed description of the MD method can be found elsewhere [1].

The shape and size of the samples are selected on the basis of visual observations of energy transfer pathways stimulated by C_{60} impacts [25,26]. As a result, cylindrical samples with a diameter of 40 nm are used. We observe that for the smaller sample (35 nm), the sample size affects the results. On the other hand, using a sample with a diameter of 45 nm makes the simulations more computationally intensive, with no added benefit. The samples consist of a double layer of graphene with a highly oriented pyrolytic graphite structure. We produced a HOPG structure by creating ideal graphene sheets in AB stacking and minimizing their energy. We confirmed the structure by visual inspection of a stable graphene sample. The whole sample consists of a single graphene “crystal”. We used a double layer of graphene due to our previous collaboration with an experimental group that operated on such a system and required a theoretical analysis of their experimental outcomes [6–10]. Therefore, our current results can be related to these studies. Moreover, such substrates can be easily purchased, giving opportunities for other experimenters to verify our work. A monolayer of phenylalanine molecules ($C_9H_{11}NO_2$) is deposited on graphene. Molecules were first placed on the graphene surface in an orderly fashion with an experimental density of Phe monolayer [36]. Then their positions have been randomized, and the energy of the whole sample has been minimized through prolonged simulation with no constraints. Phenylalanine was chosen because it is an essential amino acid that enables research into the system of interest to the bio-SIMS community. The molecule is also relatively simple, which reduces the computational cost of calculations. The thickness of the organic monolayer (without graphene) is about 1 nm. The samples are bombarded by C_{60} projectiles directed at the graphene substrate (transmission geometry) or the organic layer (sputtering geometry), as shown in Fig. 1. A wide range of kinetic energies (0.5–40 keV) and the incidence angles (0° – 80°) of the projectile are used to investigate the influence of these parameters on the particle ejection process. The angle of incidence is defined between the direction of the initial projectile motion and the normal vector of the sample plane. Organic particles ejected from both sides of the sample are collected. However, there is almost no emission of organic material into the “substrate side” of the graphene sheet, even with impacts conducted in sputtering geometry (Fig. 1). Therefore, only the emission of particles on the “organic side” of the sample is discussed later in the paper.

Rigid and stochastic regions are used to simulate a thermal bath that maintains the sample at the required temperature, to prevent reflection

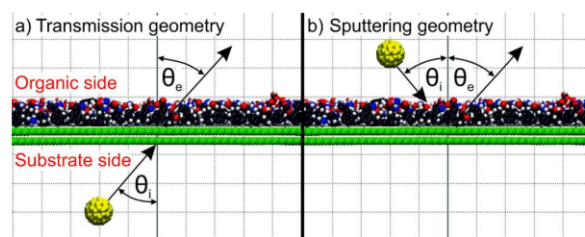


Fig. 1. Schematic diagram of systems used to model C_{60} bombardment of phenylalanine monolayer deposited on free-standing graphene in a) transmission and b) sputtering geometry. C_{60} projectile atoms are yellow, graphene atoms are green, while atoms of organic molecules are expressed by following colours: carbon is black, nitrogen is blue, oxygen is red, hydrogen is grey. The arrows indicate the directions of the projectile impact and the emission of material from the sample. The polar emission angle and the angle of projectile incidence are marked by θ_e and θ_i , respectively. The polar angles larger than zero are referred to as “off-normal polar angles”. (For interpretation of the references to colour in this figure legend, the reader is referred to the web version of this article.)

of pressure waves from the boundaries of the system, and to maintain the shape of the sample [23]. These boundaries are proposed originally for 3D solids, and their application to 2D systems is not apparent. To test the applicability of such an approach, we performed calculations for a series of 10 keV C_{60} impacts at a clean 2-layer graphene substrate that was 8 times larger (320 nm diameter) than the original system used in our study. This system's size was large enough to ensure that even the quickest disturbances induced by the projectile impact did not reach the system's boundaries within the time needed to complete the emission of all particles. As a result, there is no effect of the rigid and stochastic boundaries on the sputtering yield in such a system. Within the statistical accuracy of our results, we do not see any difference in the sputtering yields calculated on both systems, which proves the applicability of the adopted approach to 2D systems, at least for analysis of the particle ejection process. The simulations are run at a target temperature of 0 K. They extend to 20 ps for impacts with kinetic energy below 15 keV, and 40 ps otherwise. This time is sufficient to achieve saturation of the ejection yield versus time dependence. For each set of conditions, nine impacts are simulated at randomly selected points located near the center of the sample to obtain statistically reliable data. Simulations are performed with the large-scale atomic/molecular massively parallel simulator code (LAMMPS) [37] that has been modified to model sputtering conditions more efficiently.

3. Results

We start by examining the effect of primary kinetic energy and the angle of incidence on the movement of the C_{60} projectile atoms. Such knowledge is useful for determining graphene piercing conditions and the efficiency of the primary energy deposition process. The number of projectile atoms penetrating and back-reflecting from the sample and the fraction of the primary kinetic energy lost by these atoms during interaction with the bombarded system is presented in Fig. 2. Let's start by examining the effect of projectile kinetic energy for impacts along normal to the surface. For kinetic energy less than or equal to 1 keV, none of the projectile atoms penetrate the sample. However, even if the sample is not ruptured, the projectile loses a significant portion of its primary kinetic energy. For example, for kinetic energy below 5 keV, almost all energy is transferred from the projectile to the bombarded system. Also, the number of back-reflected projectile atoms is minimal, which indicates that most of the projectiles are trapped at the sample. The transmitted projectile atoms emerge for 2 keV C_{60} impacts, which indicates that the sample is ruptured. The number of transmitted projectile atoms increases as the primary kinetic energy increases until all projectile atoms pass through the sample. At the same time, a smaller portion of the projectile kinetic energy is deposited in the sample. For example, almost 90% of the impact energy is deposited in the system by 5 keV C_{60} . This value drops to just 40% for the system bombarded by 40 keV projectile. There is no difference in the efficiency of the energy deposition process for impacts conducted in transmission and sputtering configuration. However, the number of transmitted projectile atoms is sensitive to bombardment geometry, especially near the energy needed to pierce the sample. Fewer projectile atoms pass through the sample during impacts that occur near surface normal in sputtering configuration than transmission geometry.

The angle of incidence also has an apparent effect on the number of transmitted and back-reflected projectile atoms and the amount of energy transferred from the projectile to the system. The number of transmitted projectile atoms decreases as the angle of incidence increases when the kinetic energy of the projectile is constant. Most of the atoms that do not penetrate the sample are back-reflected, especially for off-normal impacts. Projectile atoms can also be trapped inside the sample. The probability of this process increases with the increase of the angle of incidence and reduction of kinetic energy. For each primary kinetic energy, there is a critical angle when none of the projectile atoms penetrate the sample. The value of this angle increases with the primary

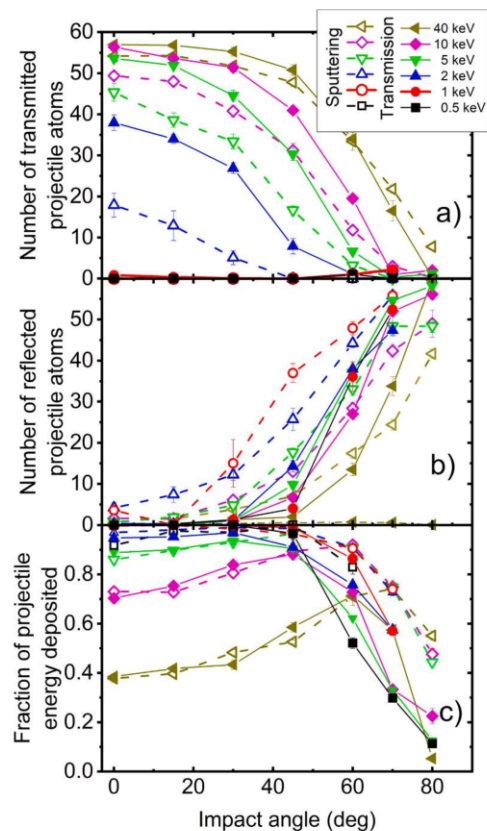


Fig. 2. Dependence of the number of projectile atoms a) transmitted through the sample and b) reflected from the sample and c) a fraction of the projectile's primary kinetic energy deposited in the sample on the kinetic energy and angle of incidence of C_{60} projectile bombarding the sample in sputtering (open symbols and dashed lines) and transmission geometry (full symbols and solid lines). Vertical lines with whiskers denote error bars resulting from multiple impacts simulated for each set of initial conditions, as described in Section 2.

kinetic energy. The angle of incidence also affects the efficiency of energy losses. This effect is especially visible in the case of high energy impacts. Initially, this amount increases with the angle of incidence, as shown in Fig. 2c. In the end, however, the amount of energy transferred to the system decreases as more energy is back-reflected. The shape of the dependence of the number of transmitted projectile atoms on the angle of incidence is similar for transmission and sputtering geometry. Impact geometry also has little effect on the amount of energy loss, at least for angles of incidence below 60°. At larger angles, more energy is transferred to the sample during impacts in the sputtering geometry.

Knowledge about what happens to projectile atoms provides useful information about the behavior of the bombarded system. However, for the potential use of graphene in SIMS, knowledge about the emission of organic molecules is much more important. The mass spectra of the particles emitted from the phenylalanine overlayer bombarded with 0.5 keV, 10 keV, and 40 keV C_{60} projectiles at normal incidence are presented in Fig. 3. The spectra only show particles ejected from the organic overlayer, i.e., both the projectile and graphene atoms are eliminated from this figure. The peak corresponding to the intact phenylalanine molecules occurs in all spectra. The height of this peak is comparable in almost all cases presented in Fig. 3. Only for 0.5 keV C_{60} impact, conducted in sputtering configuration, the emission of intact molecules hardly exists. However, this behavior is expected because this projectile has very low kinetic energy. The presence of strong emission of intact molecules for 0.5 keV C_{60} bombardment in transmission geometry is much more mysterious. For all presented impacts, the emission of intact

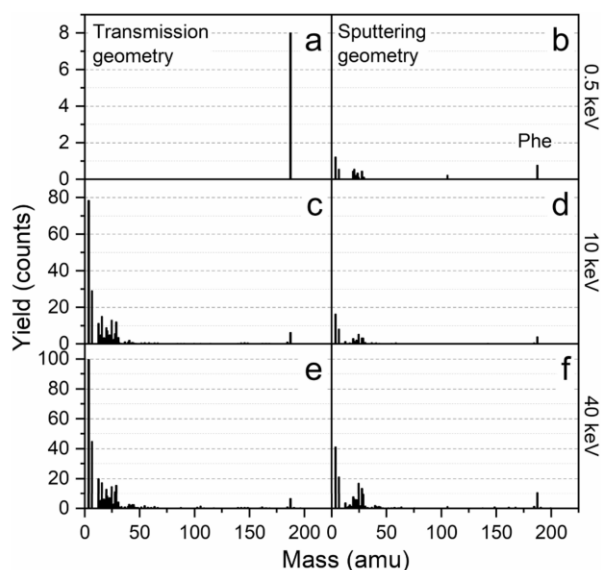


Fig. 3. Mass spectra of particles emitted from the phenylalanine (Phe) overlayer by a, b) 0.5 keV, c, d) 10 keV and e, f) 40 keV C_{60} projectile impacts in transmission (left panel) and sputtering (right panel) geometry. In all cases projectiles arrive at the sample along the surface normal. Dashed lines in the background are for reference only.

molecules is accompanied by the ejection of molecular fragments. The most abundant are H atoms, followed by H_2 , C_2 , O, and C.

Analysis of the mass spectra allows determining how the projectile properties affect the degree of fragmentation and emission efficiency of the analyzed molecules. This knowledge is necessary, for example, to find optimal ion-beam settings leading to the most efficient emission of intact molecules. Having a strong signal of the intact molecule is a significant concern for SIMS. The impact of the primary kinetic energy and angle of incidence on the number of ejected intact phenylalanine molecules and their fragments is presented in Fig. 4. Data for molecular fragments are expressed in molecular equivalents. In this representation, the given point represents the total mass of all emitted fragments divided by the mass of the intact phenylalanine molecule. The shapes of all graphs are similar. For each primary kinetic energy, there is a specific local angle of impact that leads to the most abundant ejection of particles, which we call an optimal impact angle θ_e^{opt} . The value of this angle depends on the primary kinetic energy and impact configuration, as shown in the insets. For 0.5 keV C_{60} impacts conducted in transmission

configuration, the strongest ejection occurs when the sample is bombarded along a surface normal. In this case, the yield monotonically decreases as the angle of incidence increases. The most abundant emission shifts towards higher angles of incidence as the primary kinetic energy increases (see insets to Fig. 4). On the other hand, for sputtering geometry, the maximum emission always occurs at the off-normal angles of incidence. Similar behavior is observed for molecular fragments. The number of fragments decreases as the kinetic energy of the projectile decreases, which is anticipated because collisions become more gentle for projectiles with lower energy.

The results presented in Fig. 4 lead to two unexpected conclusions. First, fragmentation of the molecules is more critical in transmission than in sputtering geometry. The basic process leading to the formation of fragments are direct collisions with projectile atoms [3,11,14,38]. More energetic collisions should occur in sputtering geometry, where the projectile collides with an organic overlayer, still having its original kinetic energy. For transmission geometry, a significant part of the kinetic energy is lost during graphene perforation [26]. As a result, less energetic collisions should occur between the projectile and organic molecules, which should lead to less fragmentation. This behavior clearly does not take place. It is also surprising that there is no gain in the material emission yield when transmission geometry is used instead of a standard sputtering configuration. One of the reasons for proposing this innovative configuration was the expectation that the projectile bombarding the sample from below would lead to a stronger emission of organic material. In this arrangement, the projectile momentum is transferred directly to the molecules of the organic layer, and the molecules eject directly towards the detector. In the sputtering configuration, the projectile momentum transferred to organic molecules must first be reverted. One would expect this process to be less effective. Contrary to these expectations, molecular yields are comparable in both geometries. Only when the sample is not ruptured, the emission of intact molecules is higher in transmission geometry.

The ejection yield is one of the key parameters for the efficient detection of the analyzed material. However, the directionality of emission is also important. The kinetic energy integrated polar angle distributions of intact molecules ejected by projectile impacts are shown in Fig. 5. The data in this figure are also azimuthally integrated and peak-normalized. Only for 0.5 keV and 1 keV projectile impacts conducted in the transmission configuration intact molecules are ejected near the surface normal. For all other impacts, the most effective ejection of these species occurs at the off-normal polar angles, usually around 50° .

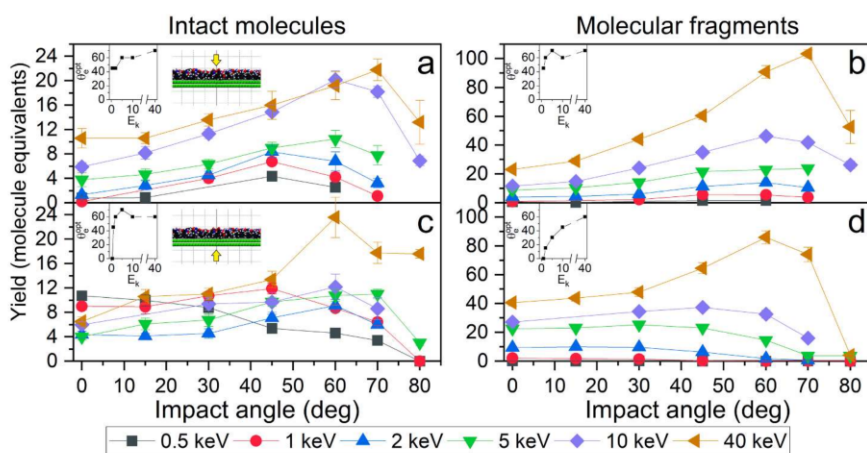


Fig. 4. Dependence of the yield on intact molecules (a, c) and molecular fragments (b, d) on the kinetic energy and angle of incidence of C_{60} projectiles. The particles are emitted from a monolayer of phenylalanine molecules deposited on graphene bombarded by C_{60} projectiles from above (a, b) and below (c, d), as indicated by the yellow arrows in the insets. The inset diagrams represent the dependence of the polar angle leading to the most efficient emission, θ_e^{opt} , on the projectile kinetic energy E_k . (For interpretation of the references to colour in this figure legend, the reader is referred to the web version of this article.)

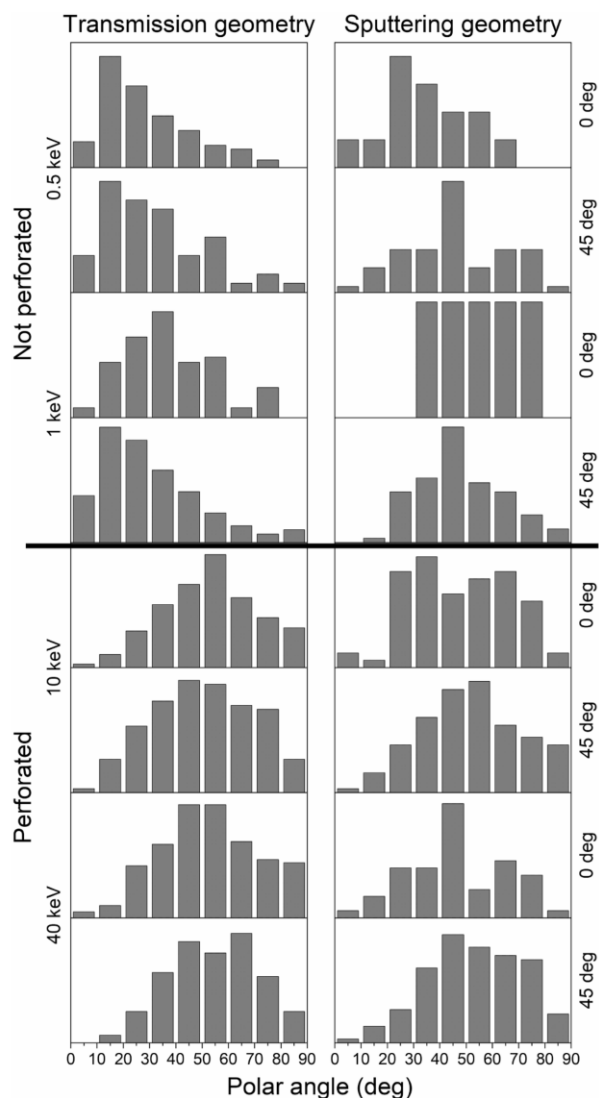
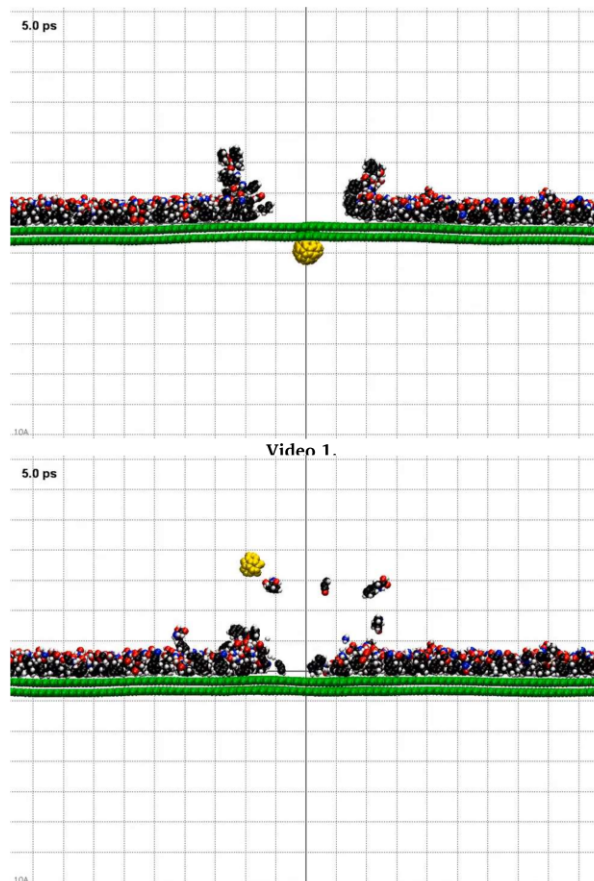


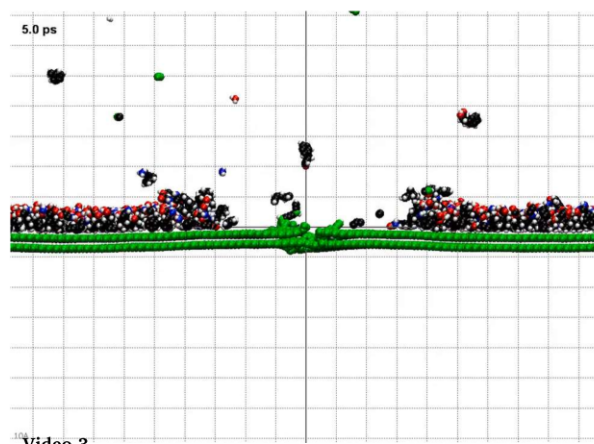
Fig. 5. Peak-normalized angular distributions of intact phenylalanine molecules ejected after C_{60} impacts with a different kinetic energy and angle of incidence.

4. Discussion

Processes responsible for the particle ejection should be delineated to explain observed trends. This task can be accomplished by performing a mechanistic analysis of energy transfer pathways, tracking the temporal evolution of the system. Such an evolution is shown in Fig. 6 for the impacts of 0.5 and 10 keV C_{60} projectiles along the surface normal. These two energies are selected to represent low- and high-energy impacts, i.e., impacts that do not cause perforation of the sample or lead to a puncture. These impacts are also visualized in Animations 1, 2, 3, and 4. Analysis of this data indicates that the main factor differentiating the mechanisms of molecular ejection is whether the sample has been punctured or not.



Video 2.



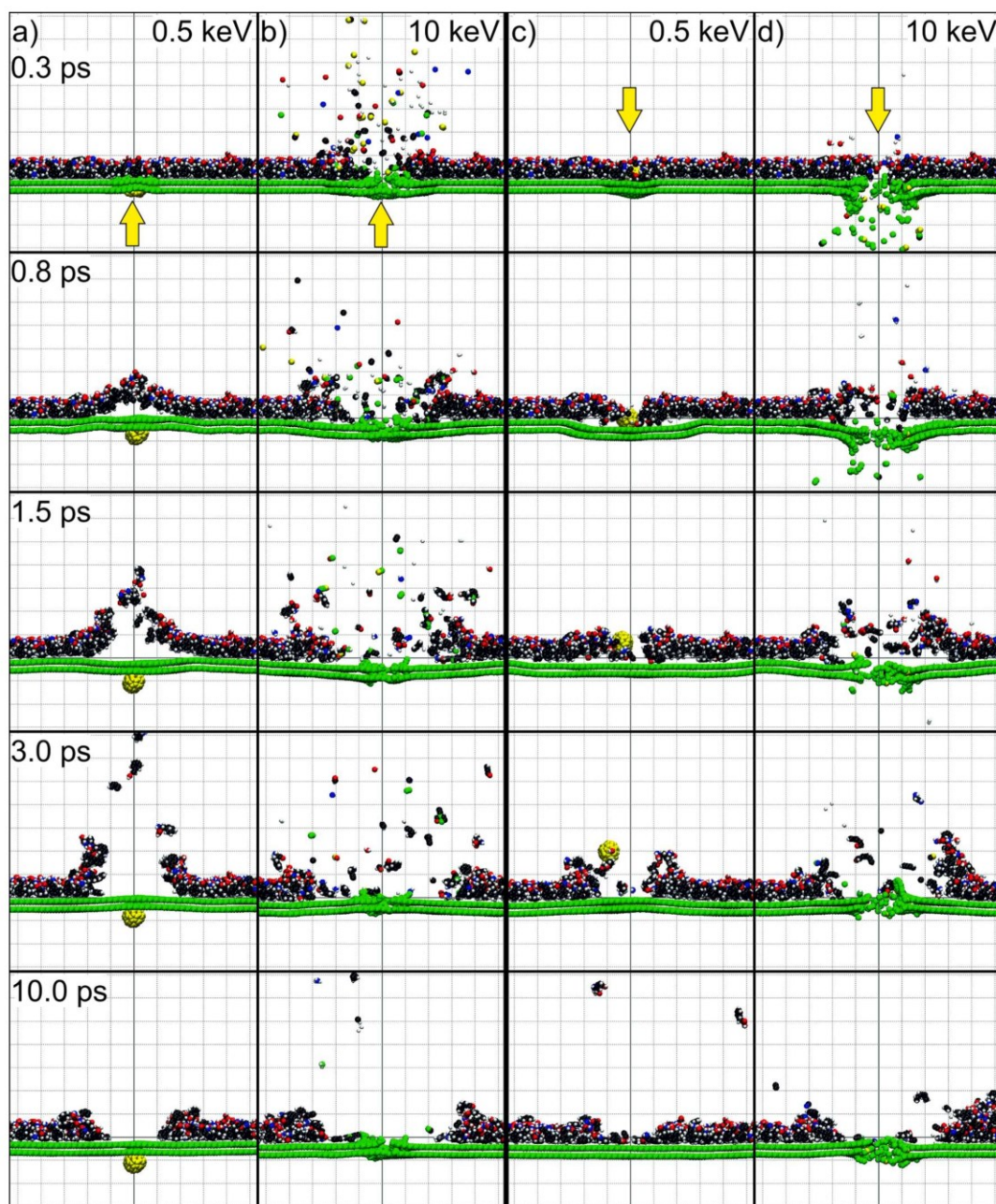
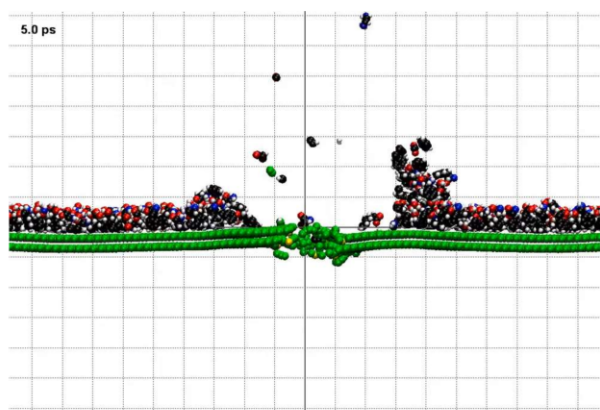


Fig. 6. Temporal snapshots from the simulation of 0.5 keV and 10 keV C_{60} impacts of C_{60} projectile along the surface normal at phenylalanine monolayer deposited on free-standing graphene. Only 2 nm wide slice through the centre of the sample is shown. Thin lines in the background denote the distance of 1 nm. The yellow arrows indicate directions of the projectile impact. (For interpretation of the references to colour in this figure legend, the reader is referred to the web version of this article.)



Video 4. Examples of impact scenarios in cases where the substrate is not perforated are shown in Fig. 6a and c for 0.5 keV C_{60} bombardment conducted in transmission and sputtering geometry, respectively. These impacts are also visualized in Animations 1 and 3. In both cases, the integrity of the projectile is not compromised upon the impact. It interacts with a surrounding environment as one object, though its structure can get disturbed after impact, especially during high-angle impacts. For transmission geometry, the projectile collides directly only with the graphene substrate. Graphene sheets bulge out along the direction of the primary beam, pushing organic molecules up. The process is delicate and spatially correlated. As a result, molecular fragmentation is minimal. About 0.6 ps after impact, a portion of the organic layer near the impact point detaches from the substrate. About 0.8 ps, the projectile stops completely, and graphene layers begin to return to their original shape. However, molecules previously energized by graphene deformation are no longer in contact with the substrate. They continue to move up. These molecules are only bound to the sample by intermolecular forces. These forces are too weak to prevent molecules from leaving the sample. The ejected molecules move mainly in directions close to the normal to the surface. Finally, small circular acoustic waves are generated in the substrate. They propagate away from the point of impact energizing molecules further away. However, the energy of these waves is too low to uplift phenylalanine molecules. Eventually, all movement in the system disappears, and the projectile remains trapped at the bottom of the graphene substrate.

For bombardment conducted in sputtering geometry, the projectile comes from above the sample. First, it interacts with the molecules of the organic layer, pushing them aside. Also, in this case, the projectile is not destroyed and transfers its kinetic energy to neighboring molecules in a delicate way. However, now its kinetic energy is higher than during impacts in transmission geometry, where some of the projectile energy was absorbed by graphene. As a consequence, molecular fragmentation, although small, is more pronounced than in the case of bombardment in transmission geometry, as shown in Fig. 3. After passing through the overlayer, C_{60} comes in contact with graphene, pushing it down. Initially, the organic overlayer remains flat. As a result, the gap between the molecules and the substrate is formed near the point of impact. At about 0.7 ps, the organic molecules begin to follow the downward motion of graphene. The movement of the molecules is slow. At about 1.1 ps, deformed graphene begins to straighten under the influence of elastic strain forces. However, it must take another 1 ps before the molecules start moving up. In the meanwhile, acoustic waves are generated in graphene. These waves dissipate the deposited energy from the impact zone. The straightening layers of graphene act like a catapult trying to throw molecules into a vacuum. However, most of the energy deposited in the impact zone is already taken away by the waves. As a result, the sputtering yield is very low, as shown in Fig. 3. Intact molecules are emitted at off-normal polar angles because they have already

obtained some transverse momentum when the projectile has penetrated the layer. Eventually, the emission of particles stops.

Different ejection scenarios occur in cases where the kinetic energy of the projectile is sufficient to pierce the sample. Examples of such impact scenarios are shown in Fig. 6b and d for 10 keV C_{60} bombardment carried out in transmission and sputtering geometry, respectively. These impacts are also visualized in Animations 2 and 4. For the high-energy bombardment, differences between impacts conducted in transmission and sputtering geometry are much smaller than in cases where the sample was not perforated. After the projectile impact, the sample is quickly perforated, and an almost circular rupture forms in the sample. For transmission geometry, the projectile breaks down when it collides with graphene. It is no longer a single object. Instead, it creates a conglomerate of smaller particles moving independently. This conglomerate also contains particles ejected from the graphene substrate. All these particles move with high kinetic energy. Their movement is no longer correlated spatially and temporally. They collide with organic molecules located near the point of impact, shattering them into pieces. As a result, all molecules located within a circular zone with a diameter of approximately 2 nm, centered at the projectile point of impact, are destroyed. The emission of organic particles starts already at 0.1 ps. Initially, only molecular fragments are emitted as a result of direct interaction with the energetic projectile, and substrate particles are emitted. Most of these fragments move in a direction close to the normal to the surface.

For sputtering geometry, the projectile first collides with the organic overlayer. Its kinetic energy is higher than in the case of the transmission configuration, in which part of the energy is consumed for graphene perforation. However, projectile integrity is not yet compromised by contact with the organic layer. The projectile disintegrates only after hitting graphene. For now, it still interacts with organic molecules as a single large object. Although the projectile kinetic energy is high, the collisions between projectile and organic molecules are spatially and temporally correlated. As a result, they are more gentle, and fewer molecules are destroyed. Thus, the difference in the projectile integrity during interaction with the sample is responsible for the smaller fragmentation observed in sputtering than transmission geometry, which was unexpected.

For both incidence geometries, the transmitted and knocked-on atoms carry some of the projectile kinetic energy. Another part of this energy is deposited in graphene near the rupture rim. Graphene sheets start to move vigorously in this area. An energized zone is also created in the organic overlayer. It undergoes lateral expansion. An almost planar pressure wave is generated in the organic layer, which leads to the collective movement of phenylalanine molecules. The pressure wave also relocates organic molecules away from the point of impact, forcing some of them to pile up. As a result, these particles form a circular rim around the zone cleared of molecules, and the disturbed area of the organic overlayer extends far beyond the area of the crack formed in graphene. The weak binding of phenylalanine molecules to the graphene substrate and inside the overlayer facilitates this phenomenon.

The critical process that regulates the abundance of the ejecta is the separation of the molecular layer from graphene. The downward movement of graphene leads to this separation. For transmission geometry, radial compression of the molecular layer pushes the graphene membrane down. For sputtering configuration, graphene is pushed down mainly by interaction with the incoming projectile. The propagation of the pressure pulse in the organic layer in combination with layer/substrate separation leads to the bending of the organic layer upwards and the emission of molecules. This emission is additionally stimulated by correlated interaction with the graphene substrate. Membrane atoms interact with atoms of phenylalanine molecules and transfer the momenta to them. In this way, the molecules eject without destruction. In other words, the membrane acts like a trampoline for molecules [8,9]. The energetics of the above processes is similar in both tested impact geometries. Accordingly, particle emission is comparable

in both cases.

The temporal evolution of the system bombarded by 0.5 keV and 10 keV C_{60} impacts at 45° is shown in Fig. 7. It is also visualized in Animations 5, 6, 7, and 8. A comparison of these data with the data shown in Figs. 2 and 6 leads to the conclusion that three factors should be considered in order to accurately describe changes in molecular emission due to the change of the angle of incidence. The first factor is related to the area of the sample excited by the projectile. As the angle of incidence increases, the projectile can move a longer path inside the organic layer. As a consequence, it can collide with a more significant number of organic molecules and uplift them. This phenomenon enhances molecular emission and is essential for low-energy impacts, non-

performing the sample, conducted in sputtering geometry. It is also crucial for high-energy impacts rupturing the sample. It is not essential for low-energy impacts in the transmission configuration because the projectile cannot immerse in the organic layer. The second factor is related to the component of the projectile momentum perpendicular to the sample and projectile back-reflection process. For off-normal impacts, this component is reduced. Moreover, an increasing part of projectile kinetic energy is carried by back-reflected projectile atoms for off-normal impacts, as shown in Fig. 2. Consequently, less energy is available to stimulate molecular emissions. This phenomenon reduces molecular emission. The third process is related to molecular fragmentation. In cases where an increase in the angle of incidence

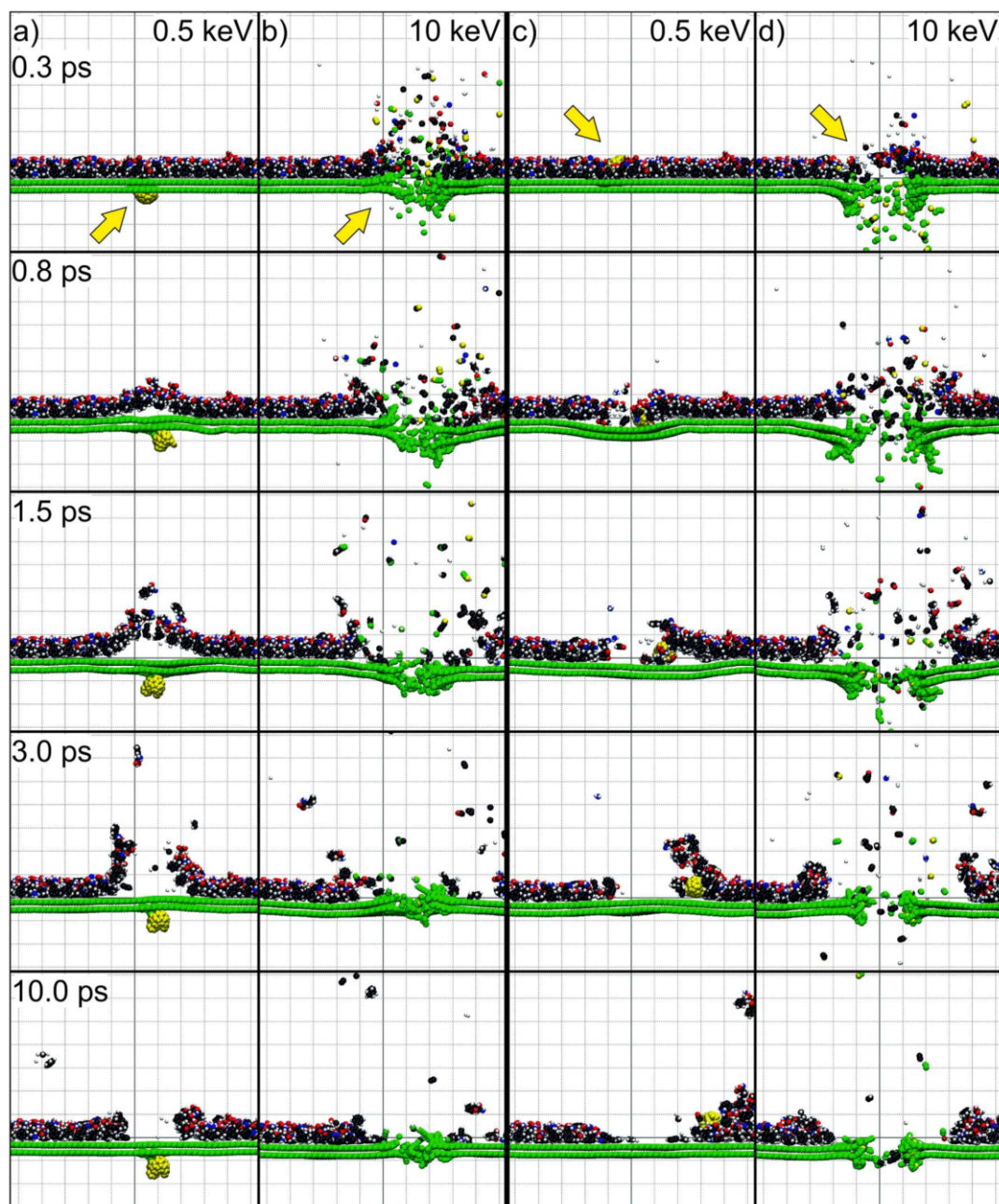
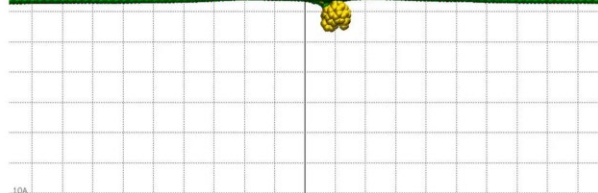
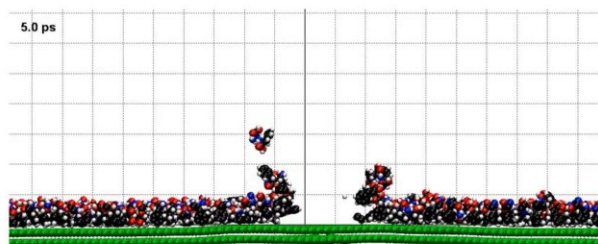
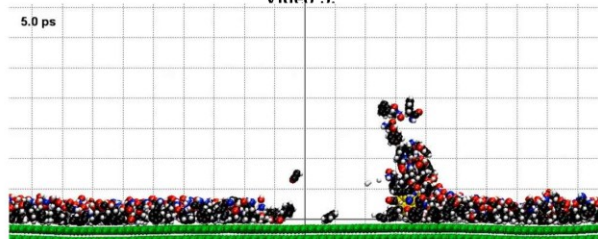


Fig. 7. Temporal snapshots from the simulation of 0.5 keV and 10 keV C_{60} impacts at phenylalanine monolayer deposited on free-standing graphene at 45° incidence angle. A detailed description of the content of the figure is provided in Fig. 6.

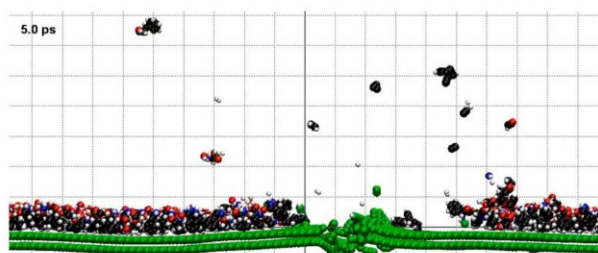
makes collisions less energetic, fewer molecules are fragmented. As a result, the yield of intact molecules increases at the expense of the yield of molecular fragments. This situation can occur because, in the case of off-normal impacts, some of the energy is reflected back.



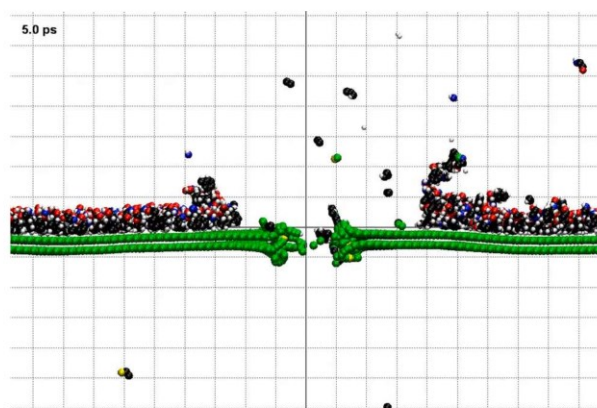
Video 5.



Video 6.



Video 7.



Video 8. The interplay of the processes described above determines the shape of the yield versus impact angle dependence. For example, for high-energy impacts, the first process initially dominates, and the signals of intact molecules and fragments increase. At a certain angle of incidence, the decrease in the energy available for the molecular emission overweighs the increase in the emission area and the signal decreases. An increase of the projectile kinetic energy reduces the impact of energy back-reflection, as seen in Fig. 2, and consequently, shifts the angle corresponding to the maximum signal to a higher value. The influence of the third process is especially visible in the case of high-energy impacts at high impact angles in transmission geometry. It is, for example, responsible for keeping strong molecular emission for 40 keV C_{60} impacts at 80° . For low-energy impacts, the fragmentation is already minimal. For low-energy impacts conducted in transmission geometry, the influence of the first process is also minimal. In this case, the projectile just bounces off graphene and has no contact with the organic layer. Consequently, the signal decreases as the angle of incidence increases because less energy is available to bulge the substrate and stimulate molecular ejection. It is noteworthy that in the case of low-energy impacts in transmission geometry, only the momentum component perpendicular to the sample appears to be responsible for molecular ejection. This conclusion is based on the observation that even in the case of off-normal impacts, intact molecules are still ejected close to the surface normal, as shown in Fig. 7a.

The data presented in Fig. 2 indicate that the bombardment process in transmission and sputtering geometry may not be symmetrical. The difference between these two impact geometries becomes especially visible in the case of impacts with kinetic energy close to the threshold energy needed to rupture the sample. The results obtained on a clean two-layer graphene system bombarded with C_{60} projectiles at normal incidence show that about 63%, 46%, and 20% of the projectile kinetic energy is deposited in this sample by 5 keV, 10 keV, and 40 keV C_{60} , respectively [26]. After conversion into energy units, the energy deposited in the sample is 3.1 keV, 4.5 keV, and 8 keV, respectively. The data presented in Fig. 2c indicate that the analogous values obtained for the current system are approximately 85%, 70%, and 35% or 4.3 keV, 7 keV, and 14 keV. A comparison of these numbers indicates that graphene is the main absorber of deposited energy, especially during low-energy impacts. In transmission geometry, the projectile collides with graphene with original kinetic energy. The energy of the projectile in contact with graphene in sputtering geometry is lower because some of the energy is already lost in the organic overlayer. As a result, fewer projectile atoms have a chance to penetrate through graphene in sputtering setup than in transmission geometry. For high-energy impacts, projectile atoms coming into contact with graphene in transmission and sputtering geometry also have different kinetic energy. In this case, however, the projectiles have excess kinetic energy, which makes it possible to penetrate the sample, regardless of impact geometry.

5. Conclusions

The effect of the kinetic energy, angle of incidence, and geometry of the projectile impact on the efficiency of particle ejection from phenylalanine monolayer deposited on free-standing graphene is investigated. It has been found that the signal increases with the primary kinetic energy. However, more energetic impacts also lead to more significant molecular fragmentation. For a given kinetic energy, there is a specific angle of incidence, which leads to the most efficient molecular emission. This angle increases with the increase of the projectile kinetic energy. The interplay of three factors determines the shape of the relationship between the yield and the angle of incidence. The first factor is related to the area of the sample energized by the projectile. With the increase of the angle of incidence, the projectile may travel a longer path inside the organic layer or energize a larger area of a graphene substrate. Consequently, it can collide with and uplift a larger number of phenylalanine molecules. The second factor is related to the component of the projectile momentum perpendicular to the sample and the process of projectile back-reflection. For off-normal impacts, this component is reduced, and an increasing part of projectile kinetic energy is dissipated by the back-reflected projectile atoms. Consequently, less energy is available to stimulate molecular emissions. The third factor is related to molecular fragmentation. In cases where the increase of the incidence angle makes collisions less energetic, fewer molecules are fragmented. As a result, the yield of intact molecules may increase at the expense of the yield of molecular fragments.

The mechanism of molecular emission from phenylalanine monolayer deposited on free-standing graphene bombarded by keV C_{60} projectile bombardment are delineated. In general, molecules are emitted by interaction with the projectile atoms and graphene substrate. The main factor influencing the relative contribution of each of these two phenomena is whether graphene is punctured. In the case that graphene is not punctured and the projectile arrives from below the sample (transmission geometry), the direct interaction between the substrate and adsorbed molecules is the only process that leads to particle emission. The projectile interacts directly only with graphene, leading to its deformation. The kinetic energy accumulated in this deformation is subsequently transferred to the molecules. The ejection of intact molecules is significant in this case, and the molecules are emitted near the surface normal. If a projectile bombards the organic side of the sample (sputtering geometry), the direct energy transfer between the projectile and the organic molecules is entirely responsible for molecular emission. Graphene plays the role of a non-penetrable membrane, redirecting projectile momentum upwards. Also, in this case, mainly intact molecules are emitted, but the emission is very low. Impact geometry has a significant impact on the effectiveness of molecular emission for bombardment along the surface normal. A robust molecular signal is present in transmission geometry, while the emission is very low for the sputtering configuration. However, this difference decreases with the angle of incidence, and, for example, at 45° , the yields measured in transmission and sputtering geometries are comparable.

In the event of impacts leading to the sample perforation, organic particles are emitted through the joint action of projectile atoms and a graphene substrate. The projectile kinetic energy deposited in graphene leads to the ejection of substrate atoms and deformations of graphene, especially near the rupture. The first phenomenon leads to the creation of a hole in the substrate and fragmentation of molecules colliding with these particles. Graphene bending acts like a trampoline and ejects weakly bound molecules, especially in transmission geometry. Graphene movement also leads to the temporary separation of the molecular layer from the substrate. Direct collisions between projectile atoms and the organic molecules cause a molecular fragmentation and emission of fragments. However, some of the energy deposited in the organic overlayer also leads to the formation of a planar pressure pulse. This pulse propagates in the overlayer and accelerates the molecules sideways. The process is not very energetic. However, in combination with

the temporary separation of molecules from the substrate due to the bending of graphene, it also leads to the emission of molecules. The flux of particles ejected in directions close to the surface normal consists mainly of molecular fragments, while intact molecules are emitted predominantly at off-normal angles. Impact geometry does not affect the efficiency of molecular ejection. We do not see molecular emission stimulated by interaction with the acoustic waves generated in graphene by the projectile impact.

Finally, a few comments on the possibilities of using graphene substrates for SIMS analysis are given. Previous studies have shown that the presence of graphene can increase the efficiency of negative organic ion formation by 2 orders of magnitude [8]. This observation is the basis of the suggestion that graphene would be an excellent substrate for studying isolated small nano-objects and supramolecular assemblies. The proposed mechanisms of ionization involve the tunneling of electrons from the vibrationally excited area around the rupture to the molecules, and/or a direct proton transfer exchange. If someone would only be interested in achieving strong emission of intact neutral molecules, as, in the case of Secondary Neutral Mass Spectrometry (SNMS), the most preferable would be the application of transmission geometry in combination with C_{60} impacts that do not lead to sample perforation. In this case, molecular emission is strong, and there is no chemical damage build up in the bombarded sample. However, SIMS does not register neutral particles, but ions. The probability of ionization will be minimal for low-energy impacts. Higher kinetic energies are needed to ensure effective ionization [8]. Our results indicate that high-energy C_{60} bombardment at off-normal angles is the most preferred configuration for such analyzes because it leads to both high emission and ionization. Our data also show that molecular emission is comparable in transmission and sputtering geometries. This is an important observation because the latter configuration is used in almost all SIMS and other experimental systems using ion beams to analyze and modify materials. As a result, no modification of the experimental system is needed to implement graphene substrates.

CRediT authorship contribution statement

Mikołaj Goluński: Conceptualization, Formal analysis, Investigation, Methodology, Writing - review & editing, Software, Visualization. **Sviatoslav Hrabar:** Formal analysis, Writing - review & editing, Validation. **Zbigniew Postawa:** Writing - original draft, Supervision.

Declaration of Competing Interest

The authors declare that they have no known competing financial interests or personal relationships that could have appeared to influence the work reported in this paper.

Acknowledgments

The authors gratefully acknowledge financial support from the Polish National Science Center, Programs Nos. 2016/23/N/ST4/00971 and 2019/33/B/ST4/01778. This research was supported in part by PLGrid Infrastructure.

References

- [1] B.J. Garrison, Z. Postawa, Computational view of surface based organic mass spectrometry, *Mass Spectrom. Rev.* 27 (2008) 289–315, and references therein.
- [2] N. Winograd, The Development of Secondary Ion Mass Spectrometry (SIMS) for Imaging, in: M.L. Gross, R.M. Caprioli (Eds.), *The Encyclopedia of Mass Spectrometry*, Elsevier, Boston, 2016, pp. 103–112.
- [3] A. Delcorte, B.J. Garrison, K. Hamraoui, Dynamics of molecular impacts on soft materials: from fullerenes to organic nanodrops, *Anal. Chem.* 81 (2009) 6676–6686.
- [4] J.S. Fletcher, Latest applications of 3D ToF-SIMS bio-imaging, *Biointerphases* 10 (2015) 018902.

- [5] D. Weibel, S. Wong, N. Lockyer, P. Blenkinsopp, R. Hill, J.C. Vickerman, A C_{60} primary ion beam system for time of flight secondary ion mass spectrometry: its development and secondary ion yield characteristics, *Anal. Chem.* 75 (2003) 1754–1764.
- [6] S.V. Verkhovurov, S. Geng, B. Czerwinski, A.E. Young, A. Delcorte, E.A. Schweikert, Single impacts of keV fullerene ions on free standing graphene: emission of ions and electrons from confined volume, *J. Chem. Phys.* 143 (2015) 164302.
- [7] S.V. Verkhovurov, B. Czerwinski, D.S. Verkhovurov, S. Geng, A. Delcorte, E. A. Schweikert, Ejection-ionization of molecules from free standing graphene, *J. Chem. Phys.* 146 (2017) 084308.
- [8] S.V. Verkhovurov, M. Goluński, D.S. Verkhovurov, S. Geng, Z. Postawa, E. A. Schweikert, “Trampoline” ejection of organic molecules from graphene and graphite via keV cluster ions impacts, *J. Chem. Phys.* 148 (2018) 144309.
- [9] S.V. Verkhovurov, M. Goluński, D.S. Verkhovurov, B. Czerwinski, M.J. Eller, S. Geng, Z. Postawa, E.A. Schweikert, Hypervelocity cluster ion impacts on free standing graphene: experiment, theory and applications - perspective, *J. Chem. Phys.* 150 (2019) 160901–160916, and references therein.
- [10] S. Geng, S.V. Verkhovurov, M.J. Eller, A.B. Clubb, E.A. Schweikert, Characterization of individual free-standing nano-objects by cluster SIMS in transmission, *J. Vac. Sci. Technol. C* 34 (2016) 03H117.
- [11] R. Chatterjee, Z. Postawa, N. Winograd, B.J. Garrison, Molecular dynamics simulation study of molecular ejection mechanisms: KeV particle bombardment of $C_6H_6/Ag\{111\}$, *J. Phys. Chem. B* 103 (1999) 151–163.
- [12] B.J. Garrison, A. Delcorte, K.D. Krantzman, Molecule liftoff from surfaces, *Accounts Chem. Res.* 33 (2000) 69–77, and references therein.
- [13] M. Kerford, R.P. Webb, Desorption of molecules by cluster impact. A preliminary molecular dynamics study, *Nucl. Instrum. Methods Phys. Res. Sect. B: Beam Interactions Mater. Atoms* 180 (2001) 44–52.
- [14] Z. Postawa, Sputtering simulations of organic overlayers on metal substrates by monoatomic and clusters projectiles, *Appl. Surf. Sci.* 231 (2004) 22–28.
- [15] Z. Postawa, B. Czerwinski, N. Winograd, B.J. Garrison, Microscopic insights into the sputtering of thin organic films on $Ag\{111\}$ induced by C_{60} and Ga bombardment, *J. Phys. Chem. B* 109 (2005) 11973–11979.
- [16] R.P. Webb, The computer simulation of energetic cluster-solid interactions, *Radiat. Eff. Defects Solids* 162 (2007) 567–572.
- [17] L. Rzeźnik, B. Czerwinski, B.J. Garrison, N. Winograd, Z. Postawa, Microscopic insight into the sputtering of thin polystyrene films on $Ag\{111\}$ induced by large and slow Ar clusters, *J. Phys. Chem. C* 112 (2008) 521–531.
- [18] L. Rzeźnik, B. Czerwinski, B.J. Garrison, N. Winograd, Z. Postawa, Molecular dynamics simulations of sputtering of organic overlayers by slow, large clusters, *Appl. Surf. Sci.* 255 (2008) 841–843.
- [19] B. Czerwinski, L. Rzeźnik, R. Paruch, B.J. Garrison, Z. Postawa, Effect of impact angle and projectile size on sputtering efficiency of solid benzene investigated by molecular dynamics simulations, *Nucl. Instrum. Methods B* 269 (2011) 1578–1581.
- [20] P. Sigmund, Theory of sputtering. I. Sputtering yield of amorphous and polycrystalline targets, *Phys. Rev.* 184 (1969) 383–416.
- [21] C. Anders, H.M. Urbassek, Cluster-size dependence of ranges of 100eV/atom Au_n clusters, *Nucl. Instrum. Methods B* 228 (2005) 57–63.
- [22] J. Samela, K. Nordlund, Atomistic simulation of the transition from atomistic to macroscopic cratering, *Phys. Rev. Lett.* 101 (027601) (2008) 027601–027604.
- [23] Z. Postawa, B. Czerwinski, M. Szweczyk, E.J. Smiley, N. Winograd, B.J. Garrison, Enhancement of sputtering yields due to C_{60} versus Ga bombardment of $Ag\{111\}$ as explored by molecular dynamics simulations, *Anal. Chem.* 75 (2003) 4402–4407.
- [24] C. Mucksch, C. Anders, H. Gnaser, H.M. Urbassek, Dynamics of L-phenylalanine sputtering by argon cluster bombardment, *J. Phys. Chem. C* 118 (2014) 7962–7970.
- [25] M. Goluński, Z. Postawa, Effect of sample thickness on carbon ejection from ultrathin graphite bombarded by keV C-60, *Acta Phys. Pol.* 132 (2017) 222–224.
- [26] M. Goluński, Z. Postawa, Effect of kinetic energy and impact angle on carbon ejection from a free-standing graphene bombarded by kilo-electron-volt C-60, *J. Vac. Sci. Technol. C* 36 (2018) 03F112.
- [27] S.J. Zhao, J.M. Xue, L. Liang, Y.G. Wang, S. Yan, Drilling nanopores in graphene with clusters: a molecular dynamics study, *J. Phys. Chem. C* 116 (2012) 11776–11782.
- [28] Z.C. Xu, W.R. Zhong, Probability of self-healing in damaged graphene bombarded by fullerene, *Appl. Phys. Lett.* 104 (2014) 261907.
- [29] J. Luo, T.H. Gao, L. Li, Q. Xie, Z. Tian, Q. Chen, Y.C. Liang, Formation of defects during fullerene bombardment and repair of vacancy defects in graphene, *J. Mater. Sci.* 54 (2019) 14431–14439.
- [30] Z.C. Xu, J.L. Wen, W.R. Zhong, L. Wei, Statistical law of high-energy fullerene and its derivatives passing through graphene, *Commun. Theor. Phys.* 65 (2016) 361–365.
- [31] A.V. Krashennnikov, F. Banhart, Engineering of nanostructured carbon materials with electron or ion beams, *Nat. Mater.* 6 (2007) 723–733.
- [32] M. Goluński, S.V. Verkhovurov, D.S. Verkhovurov, E.A. Schweikert, Z. Postawa, Effect of substrate thickness on ejection of phenylalanine molecules adsorbed on free-standing graphene bombarded by 10 keV C-60, *Nucl. Instrum. Methods B* 393 (2017) 13–16.
- [33] L.C. Liu, Y. Liu, S.V. Zybin, H. Sun, W.A. Goddard, ReaxFF-Ig: correction of the ReaxFF reactive force field for London dispersion, with applications to the equations of state for energetic materials, *J. Phys. Chem. A* 115 (2011) 11016–11022.
- [34] J.F. Ziegler, J.P. Biersack, U. Littmark, *The Stopping and Range of Ions in Matter*, Pergamon, New York, 1985.
- [35] S. Monti, A.C.T. van Duin, S.-Y. Kim, V. Barone, Exploration of the conformational and reactive dynamics of glycine and diglycine on TiO_2 : computational investigations in the gas phase and in solution, *J. Phys. Chem. C* 116 (2012) 5141–5150.
- [36] A.D. Petelska, M. Naumowicz, Z.A. Figaszewski, The equilibrium of phosphatidylcholine-amino acid system in monolayer at the air/water interface, *Cell Biochem. Biophys.* 60 (2011) 155–160.
- [37] S. Plimpton, Fast parallel algorithms for short-range molecular-dynamics, *J. Comput. Phys.* 117 (1995) 1–19.
- [38] A. Delcorte, B.J. Garrison, keV fullerene interaction with hydrocarbon targets: projectile penetration, damage creation and removal, *Nucl. Instrum. Methods B* 255 (2007) 223–228.

ADDITIONAL ACHIEVEMENTS

Below I present my co-authored articles that are out of scope for the thesis, conferences I gave talks at, projects I was involved in, and scholarships and awards I was granted during the time of PhD studies.

Published articles not related to the thesis

1. Kruszelnicki J., Goluński M., Ciochoń P., Noya M., Villarejo E.P. & Żyra J. SME segmentation and regional development agencies' innovation support measures. *Regional Studies, Regional Science* **7**, 511-531, doi:[10.1080/21681376.2020.1811753](https://doi.org/10.1080/21681376.2020.1811753) (2020).
2. Guo W., Kański M., Liu W., Goluński M., Zhou Y., Wang Y., Cheng C., Du Y., Postawa Z., Wei W. & Zhu Z. Three-Dimensional Mass Spectrometric Imaging of Biological Structures Using a Vacuum Compatible Microfluidic Device. *Analytical Chemistry* **92**, 13785-13793, doi:[10.1021/acs.analchem.0c02204](https://doi.org/10.1021/acs.analchem.0c02204) (2020).
3. Kański M., Maciążek D., Goluński M. & Postawa Z. Sputtering of octatetraene by 15 keV C₆₀ projectiles: Comparison of reactive interatomic potentials. *Nuclear Instruments and Methods in Physics Research Section B: Beam Interactions with Materials and Atoms* **393**, 29-33, doi:[10.1016/j.nimb.2016.10.023](https://doi.org/10.1016/j.nimb.2016.10.023) (2016).

Conference talks

1. 23rd International Workshop on Inelastic Ion-Surface Collisions IISC-23, 17-22.11.2019, Matsue, Japan
Molecular Dynamics of Organic Monolayer on Free-Standing Graphene Bombarded with keV C₆₀ Clusters in Transmission Direction
2. 18th European Conference on Applications of Surface and Interface Analysis ECASIA2019, 15-20.09.2019, Dresden, Germany
Hypervelocity cluster ion impacts on free-standing graphene
3. 21st International Conference Surface Modification of Materials by Ion Beams SMMIB2019, 25-30.08.2019, Tomsk, Russia
Molecular Dynamics of free-standing graphene bombarded with keV Ar_n clusters
4. SIMS Europe 2018, 16-18.09.2018, Münster, Germany
Molecular Dynamics of Thin Organic Layer Deposited on Free-Standing Graphene Bombarded with keV C₆₀ Projectiles
5. 14th International Conference on Computer Simulation of Radiation Effects in Solids COSIRES 2018, 18-22.06.2018, Shanghai, China
Molecular Dynamics of Thin Organic Layer Deposited on Free-Standing Graphene Bombarded with keV C₆₀ Projectiles
6. 21st International Conference on Secondary Ion Mass Spectrometry, 10-15.09.2017, Kraków, Poland
Computer Modelling of Free-Standing Graphene Bombarded with keV C₆₀ Projectiles

7. 13th International Conference on Computer Simulation of Radiation Effects in Solids “COSIRES 2016”, 19-24.06.2016, Loughborough, UK

Computer Modelling of Ejection of Phenylalanine Molecules Deposited on Free-Standing Graphene by keV C₆₀ Projectiles

8. XI-th International Conference on Ion Implantation and Other Applications of Ions and Electrons “ION 2016”, 13-16.06.2016, Kazimierz Dolny, Poland

Computer Modelling of Ejection of Phenylalanine Molecules Deposited on Free-Standing Graphene by keV C₆₀ Projectiles

Projects, scholarships, and awards

- Research project lead in PRELUDIUM grant no. 2016/23/N/ST4/00971 from Polish National Science Center (Jagiellonian University, 2017-2021)
- Co-coordinator in OaSIS project no. 777443 from European Union Horizon 2020 (Cracow University of Technology, 2018-2020)
- Research project assistant in OPUS grant no. 2015/19/B/ST4/01892 from Polish National Science Center (Jagiellonian University, 2016-2018)
- Research project assistant in OPUS grant no. 2013/09/B/ST4/00094 from Polish National Science Center (Jagiellonian University, 2015-2016)

- PhD scholarship (Jagiellonian University, 2015-2021)
- Jagiellonian Interdisciplinary PhD Programme Scholarship (Jagiellonian University, 2018-2020)
- Rector scholarship for the best PhD students (Jagiellonian University, 2017/2018)

- 2nd place in national robotics contest KrakRobot (Jagiellonian University, 2016)

LICENSES AND PERMISSIONS

In this part, I present permissions for reproducing the articles and figures included in the thesis. Proper attributions are given in the figures' descriptions or before the reprint of the specific articles in the appendix titled "Reprints of publications".



All figures that do not have a remark quoting their copyright, as well as the rest of the thesis, are created by myself under the Creative Commons Attribution-Share Alike 4.0 International license, which allows free use, distribution, and creation of derivatives, so long as the license is unchanged and clearly noted, and the original author is attributed – and if you alter, transform, or build upon this work, you may distribute the resulting work only under the same license as this one. (<https://creativecommons.org/licenses/by-sa/4.0>)



RightsLink®



Home



Help



Email Support



Sign in



Create Account

Microscopic Insights into the Sputtering of Ag{111} Induced by C60 and Ga Bombardment



Author: Zbigniew Postawa, Bartłomiej Czerwinski, Marek Szewczyk, et al

Publication: The Journal of Physical Chemistry B

Publisher: American Chemical Society

Date: Jun 1, 2004

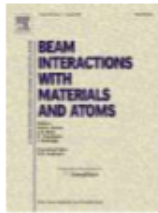
Copyright © 2004, American Chemical Society

PERMISSION/LICENSE IS GRANTED FOR YOUR ORDER AT NO CHARGE

This type of permission/license, instead of the standard Terms & Conditions, is sent to you because no fee is being charged for your order. Please note the following:

- Permission is granted for your request in both print and electronic formats, and translations.
 - If figures and/or tables were requested, they may be adapted or used in part.
 - Please print this page for your records and send a copy of it to your publisher/graduate school.
 - Appropriate credit for the requested material should be given as follows: "Reprinted (adapted) with permission from (COMPLETE REFERENCE CITATION). Copyright (YEAR) American Chemical Society." Insert appropriate information in place of the capitalized words.
 - One-time permission is granted only for the use specified in your request. No additional uses are granted (such as derivative works or other editions). For any other uses, please submit a new request.
- If credit is given to another source for the material you requested, permission must be obtained from that source.

[BACK](#)[CLOSE WINDOW](#)



Effect of substrate thickness on ejection of phenylalanine molecules adsorbed on free-standing graphene bombarded by 10keV C60

Author: M. Golunski,S.V. Verkhoturov,D.S. Verkhoturov,E.A. Schweikert,Z. Postawa

Publication:

Nuclear Instruments and Methods in Physics Research Section B: Beam Interactions with Materials and Atoms

Publisher: Elsevier

Date: 15 February 2017

© 2016 Elsevier B.V. All rights reserved.

Journal Author Rights

Please note that, as the author of this Elsevier article, you retain the right to include it in a thesis or dissertation, provided it is not published commercially. Permission is not required, but please ensure that you reference the journal as the original source. For more information on this and on your other retained rights, please visit: <https://www.elsevier.com/about/our-business/policies/copyright#Author-rights>

BACK

CLOSE WINDOW

AIP PUBLISHING LICENSE TERMS AND CONDITIONS

Apr 09, 2021

This Agreement between Mr. Mikołaj Gołuński ("You") and AIP Publishing ("AIP Publishing") consists of your license details and the terms and conditions provided by AIP Publishing and Copyright Clearance Center.

License Number	5044720542109
License date	Apr 09, 2021
Licensed Content Publisher	American Vacuum Society
Licensed Content Publication	Journal of Vacuum Science & Technology B
Licensed Content Title	Effect of kinetic energy and impact angle on carbon ejection from a free-standing graphene bombarded by kilo-electron-volt C60
Licensed Content Author	Mikolaj Golunski, Zbigniew Postawa
Licensed Content Date	May 1, 2018
Licensed Content Volume	36
Licensed Content Issue	3
Type of Use	Thesis/Dissertation

09.04.2021,

Requestor type	Author (original article)
Format	Print and electronic
Portion	Excerpt (> 800 words)
Will you be translating?	No
Title	Study of the emission of organic material from a free-standing graphene substrate by keV cluster bombardment
Institution name	Jagiellonian University
Expected presentation date	May 2021
Portions	Whole article as a part of my PhD thesis
Requestor Location	Mr. Mikołaj Gołuński ul. Łojasiewicza 11 Kraków, 30-348 Poland Attn: Mr. Mikołaj Gołuński
Total	0.00 USD

Terms and Conditions

American Vacuum Society -- Terms and Conditions: Permissions Uses

American Vacuum Society ("AVS") hereby grants to you the non-exclusive right and license to use and/or distribute the Material according to the use specified in your order, on a one-time basis, for the specified term, with a maximum distribution equal to the number that you have ordered. Any links or other content accompanying the Material are not the subject of this license.

1. You agree to include the following copyright and permission notice with the

09.04.2021,

reproduction of the Material: "Reprinted with permission from [FULL CITATION]. Copyright [PUBLICATION YEAR], American Vacuum Society." For an article, the copyright and permission notice must be printed on the first page of the article or book chapter. For photographs, covers, or tables, the copyright and permission notice may appear with the Material, in a footnote, or in the reference list.

2. If you have licensed reuse of a figure, photograph, cover, or table, it is your responsibility to ensure that the material is original to AVS and does not contain the copyright of another entity, and that the copyright notice of the figure, photograph, cover, or table does not indicate that it was reprinted by AVS, with permission, from another source. Under no circumstances does AVS, purport or intend to grant permission to reuse material to which it does not hold copyright.
3. You may not alter or modify the Material in any manner. You may translate the Material into another language only if you have licensed translation rights. You may not use the Material for promotional purposes. AVS reserves all rights not specifically granted herein.
4. The foregoing license shall not take effect unless and until AVS or its agent, Copyright Clearance Center, receives the Payment in accordance with Copyright Clearance Center Billing and Payment Terms and Conditions, which are incorporated herein by reference.
5. AVS or the Copyright Clearance Center may, within two business days of granting this license, revoke the license for any reason whatsoever, with a full refund payable to you. Should you violate the terms of this license at any time, AVS, American Vacuum Society, or Copyright Clearance Center may revoke the license with no refund to you. Notice of such revocation will be made using the contact information provided by you. Failure to receive such notice will not nullify the revocation.
6. AVS makes no representations or warranties with respect to the Material. You agree to indemnify and hold harmless AVS, American Vacuum Society, and their officers, directors, employees or agents from and against any and all claims arising out of your use of the Material other than as specifically authorized herein.
7. The permission granted herein is personal to you and is not transferable or assignable without the prior written permission of AVS. This license may not be amended except in a writing signed by the party to be charged.
8. If purchase orders, acknowledgments or check endorsements are issued on any forms containing terms and conditions which are inconsistent with these provisions, such inconsistent terms and conditions shall be of no force and effect. This document, including the CCC Billing and Payment Terms and Conditions, shall be the entire agreement between the parties relating to the subject matter hereof.

This Agreement shall be governed by and construed in accordance with the laws of the State of New York. Both parties hereby submit to the jurisdiction of the courts of New York County for purposes of resolving any disputes that may arise hereunder.

Questions? customercare@copyright.com or +1-855-239-3415 (toll free in the US) or +1-978-646-2777.

AIP PUBLISHING LICENSE TERMS AND CONDITIONS

Apr 09, 2021

This Agreement between Mr. Mikołaj Gołuński ("You") and AIP Publishing ("AIP Publishing") consists of your license details and the terms and conditions provided by AIP Publishing and Copyright Clearance Center.

License Number	5044730020522
License date	Apr 09, 2021
Licensed Content Publisher	AIP Publishing
Licensed Content Publication	Journal of Chemical Physics
Licensed Content Title	"Trampoline" ejection of organic molecules from graphene and graphite via keV cluster ions impacts
Licensed Content Author	Stanislav V. Verkhoturov, Mikołaj Gołuński, Dmitriy S. Verkhoturov, et al
Licensed Content Date	Apr 14, 2018
Licensed Content Volume	148
Licensed Content Issue	14
Type of Use	Thesis/Dissertation
Requestor type	Author (original article)

09.04.2021,

Format	Print and electronic
Portion	Excerpt (> 800 words)
Will you be translating?	No
Title	Study of the emission of organic material from a free-standing graphene substrate by keV cluster bombardment
Institution name	Jagiellonian University
Expected presentation date	May 2021
Portions	Whole article
Requestor Location	Mr. Mikołaj Gołuński ul. Łojasiewicza 11 Kraków, 30-348 Poland Attn: Mr. Mikołaj Gołuński
Total	0.00 USD

Terms and Conditions

AIP Publishing -- Terms and Conditions: Permissions Uses

AIP Publishing hereby grants to you the non-exclusive right and license to use and/or distribute the Material according to the use specified in your order, on a one-time basis, for the specified term, with a maximum distribution equal to the number that you have ordered. Any links or other content accompanying the Material are not the subject of this license.

1. You agree to include the following copyright and permission notice with the reproduction of the Material: "Reprinted from [FULL CITATION], with the permission of AIP Publishing." For an article, the credit line and permission notice must be printed on the first page of the article or book chapter. For photographs, covers, or tables, the notice may appear with the Material, in a footnote, or in the reference list.
2. If you have licensed reuse of a figure, photograph, cover, or table, it is your

09.04.2021,

responsibility to ensure that the material is original to AIP Publishing and does not contain the copyright of another entity, and that the copyright notice of the figure, photograph, cover, or table does not indicate that it was reprinted by AIP Publishing, with permission, from another source. Under no circumstances does AIP Publishing purport or intend to grant permission to reuse material to which it does not hold appropriate rights.

You may not alter or modify the Material in any manner. You may translate the Material into another language only if you have licensed translation rights. You may not use the Material for promotional purposes.

3. The foregoing license shall not take effect unless and until AIP Publishing or its agent, Copyright Clearance Center, receives the Payment in accordance with Copyright Clearance Center Billing and Payment Terms and Conditions, which are incorporated herein by reference.
4. AIP Publishing or Copyright Clearance Center may, within two business days of granting this license, revoke the license for any reason whatsoever, with a full refund payable to you. Should you violate the terms of this license at any time, AIP Publishing, or Copyright Clearance Center may revoke the license with no refund to you. Notice of such revocation will be made using the contact information provided by you. Failure to receive such notice will not nullify the revocation.
5. AIP Publishing makes no representations or warranties with respect to the Material. You agree to indemnify and hold harmless AIP Publishing, and their officers, directors, employees or agents from and against any and all claims arising out of your use of the Material other than as specifically authorized herein.
6. The permission granted herein is personal to you and is not transferable or assignable without the prior written permission of AIP Publishing. This license may not be amended except in a writing signed by the party to be charged.
7. If purchase orders, acknowledgments or check endorsements are issued on any forms containing terms and conditions which are inconsistent with these provisions, such inconsistent terms and conditions shall be of no force and effect. This document, including the CCC Billing and Payment Terms and Conditions, shall be the entire agreement between the parties relating to the subject matter hereof.

This Agreement shall be governed by and construed in accordance with the laws of the State of New York. Both parties hereby submit to the jurisdiction of the courts of New York County for purposes of resolving any disputes that may arise hereunder.

V1.2

Questions? customercare@copyright.com or +1-855-239-3415 (toll free in the US) or +1-978-646-2777.

AIP PUBLISHING LICENSE TERMS AND CONDITIONS

Apr 09, 2021

This Agreement between Mr. Mikołaj Gołuński ("You") and AIP Publishing ("AIP Publishing") consists of your license details and the terms and conditions provided by AIP Publishing and Copyright Clearance Center.

License Number	5044730224721
License date	Apr 09, 2021
Licensed Content Publisher	AIP Publishing
Licensed Content Publication	Journal of Chemical Physics
Licensed Content Title	Hypervelocity cluster ion impacts on free standing graphene: Experiment, theory, and applications
Licensed Content Author	Stanislav V. Verkhoturov, Mikołaj Gołuński, Dmitriy S. Verkhoturov, et al
Licensed Content Date	Apr 28, 2019
Licensed Content Volume	150
Licensed Content Issue	16
Type of Use	Thesis/Dissertation
Requestor type	Author (original article)

09.04.2021,

Format	Print and electronic
Portion	Excerpt (> 800 words)
Will you be translating?	No
Title	Study of the emission of organic material from a free-standing graphene substrate by keV cluster bombardment
Institution name	Jagiellonian University
Expected presentation date	May 2021
Portions	Whole article
Requestor Location	Mr. Mikołaj Gołuński ul. Łojasiewicza 11 Kraków, 30-348 Poland Attn: Mr. Mikołaj Gołuński
Total	0.00 USD

Terms and Conditions

AIP Publishing -- Terms and Conditions: Permissions Uses

AIP Publishing hereby grants to you the non-exclusive right and license to use and/or distribute the Material according to the use specified in your order, on a one-time basis, for the specified term, with a maximum distribution equal to the number that you have ordered. Any links or other content accompanying the Material are not the subject of this license.

1. You agree to include the following copyright and permission notice with the reproduction of the Material: "Reprinted from [FULL CITATION], with the permission of AIP Publishing." For an article, the credit line and permission notice must be printed on the first page of the article or book chapter. For photographs, covers, or tables, the notice may appear with the Material, in a footnote, or in the reference list.
2. If you have licensed reuse of a figure, photograph, cover, or table, it is your

09.04.2021,

responsibility to ensure that the material is original to AIP Publishing and does not contain the copyright of another entity, and that the copyright notice of the figure, photograph, cover, or table does not indicate that it was reprinted by AIP Publishing, with permission, from another source. Under no circumstances does AIP Publishing purport or intend to grant permission to reuse material to which it does not hold appropriate rights.

You may not alter or modify the Material in any manner. You may translate the Material into another language only if you have licensed translation rights. You may not use the Material for promotional purposes.

3. The foregoing license shall not take effect unless and until AIP Publishing or its agent, Copyright Clearance Center, receives the Payment in accordance with Copyright Clearance Center Billing and Payment Terms and Conditions, which are incorporated herein by reference.
4. AIP Publishing or Copyright Clearance Center may, within two business days of granting this license, revoke the license for any reason whatsoever, with a full refund payable to you. Should you violate the terms of this license at any time, AIP Publishing, or Copyright Clearance Center may revoke the license with no refund to you. Notice of such revocation will be made using the contact information provided by you. Failure to receive such notice will not nullify the revocation.
5. AIP Publishing makes no representations or warranties with respect to the Material. You agree to indemnify and hold harmless AIP Publishing, and their officers, directors, employees or agents from and against any and all claims arising out of your use of the Material other than as specifically authorized herein.
6. The permission granted herein is personal to you and is not transferable or assignable without the prior written permission of AIP Publishing. This license may not be amended except in a writing signed by the party to be charged.
7. If purchase orders, acknowledgments or check endorsements are issued on any forms containing terms and conditions which are inconsistent with these provisions, such inconsistent terms and conditions shall be of no force and effect. This document, including the CCC Billing and Payment Terms and Conditions, shall be the entire agreement between the parties relating to the subject matter hereof.

This Agreement shall be governed by and construed in accordance with the laws of the State of New York. Both parties hereby submit to the jurisdiction of the courts of New York County for purposes of resolving any disputes that may arise hereunder.

V1.2

Questions? customercare@copyright.com or +1-855-239-3415 (toll free in the US) or +1-978-646-2777.



Mechanisms of molecular emission from phenylalanine monolayer deposited on free-standing graphene bombarded by C60 projectiles

Author: Mikołaj Gołuński, Sviatoslav Hrabar, Zbigniew Postawa

Publication: Applied Surface Science

Publisher: Elsevier

Date: 15 February 2021

© 2020 Elsevier B.V. All rights reserved.

Journal Author Rights

Please note that, as the author of this Elsevier article, you retain the right to include it in a thesis or dissertation, provided it is not published commercially. Permission is not required, but please ensure that you reference the journal as the original source. For more information on this and on your other retained rights, please visit: <https://www.elsevier.com/about/our-business/policies/copyright#Author-rights>

BACK

CLOSE WINDOW